TLR7 as a therapeutic target for pancreatic ductal adenocarcinoma and cancer-associated cachexia

By:
Katherine A. Michaelis

A DISSERTATION

Presented to the Program of Physiology and Pharmacology and
Oregon Health & Science University
School of Medicine
in partial fulfillment of
the requirements for the degree of

Doctor of Philosophy

April 2019

Acknowledgments

When reflecting on my path in science and graduate school, I am overwhelmed with gratitude for the brilliant, hardworking, and giving people I have had the chance to work alongside and learn from. It would be impossible to name them all and describe their contributions without doubling the length of this thesis, but described below are just a few.

First, I am grateful for the mentorship of my advisor, Dan Marks, whose knowledge, wisdom, and guidance have been invaluable assets in my development as a scientist. When I first started at OHSU as an MD/PhD student interested in medical oncology, I initially thought that my research focus would be in cancer biology. However, with Dan, I've gotten to perform research that has indelibly shaped my perspective about oncology and provided meaning to many of experiences I've already had in medicine. Within the first days of medical school, my class embarked upon the deeply personal experience of working with the person our instructors explained would be our "first patient": someone who chose to donate their body to medical education after death. My team did not know much about our first patient's identity or story; all we were told was that he had passed away from cancer. However, what became clear over the ensuing weeks was that the suffering our donor had endured as a cancer patient was far more than just his tumor burden would suggest. His dignified, tall frame was rendered impossibly gaunt and frail, his musculature weakened and wasted away, his body war-torn and wounded from his battles with this cruel disease. A few months later, I saw Dan speak for the first time on his research in our MD/PhD journal club. Finally, I was able to understand and put a name to the

other condition my first patient suffered from: cachexia. I was fascinated by the notion that understanding how the body responds to malignancy in disorders like cachexia could alleviate much of the suffering cancer patients cope with, and extend survival in the process. The very next summer, I took the opportunity to rotate with Dan's research group, and it was an easy choice to continue there for my graduate studies. Despite the veritable plethora of hats Dan wears in his career, he always makes the time to sit down with each of his trainees and talk about interesting literature, new results, and experimental strategy. I have barged into his office many a time with exciting or bizarre data, and his interpretations and scientific musings proved unfailingly helpful in these moments. I am lucky to have spent graduate school with a mentor who not only fosters growth and leadership in trainees, but also provides everything from experimental troubleshooting and thoughtful paper edits to entertaining stories and helpful career advice. His unique perspective and knowledge are well-known and respected throughout our MD/PhD program, and I'm honored by the opportunity to have learned from him throughout these years. I hope to continue my focus on cancer as a systemic disorder throughout my career, and am thankful for the way Dan has shaped my thinking both clinically and scientifically.

As everyone in research knows, science is a team sport. Luckily for me, I have had a team of exceptional talent and wisdom during my graduate studies. Whether it was Pete Levasseur's unbeatable molecular biology skills served with a side of distinctly New England humor, Xinxia Zhu's passion for research and boundless skill in all things mouse work, or Stephanie Krasnow's thoughtful and knowledgeable scientific guidance, I knew I was going to be in good hands from the time I first rotated in the Marks lab. A couple of years later, we were joined by Mason Norgard, whose enthusiasm, skilled lab hands, and dedication have been invaluable in countless studies since. But among the best features of the Marks lab is our small army of MD/PhD

students to celebrate and commiserate with – Kevin Burfeind, Brennan Olson, and John Butler have all added levity, knowledge, and camaraderie to my time spent in grad school. I am also thankful for our most recent additions, Abby Buenafe and Sherif Abdelhamad, whose kindness and scientific acumen are much appreciated resources to everyone who works with them.

Outside of my immediate lab group, I owe a debt of gratitude to many investigators at OHSU and beyond. My excellent advisory committee (Virginia Brooks, David Jacoby, Peter Kurre, Terry Morgan, and Philip Streeter) consistently provided knowledge, encouragement, and helpful feedback throughout my time in graduate school. I am also grateful to Mara Sherman, who is joining my committee for my defense and contributing her expertise to the evaluation of this body of work. Among my team of mentors at OHSU, Dr. Jacoby in particular has been terrific in providing everything from hilarious stories and scientific guidance to emergency coffee and moral support, and I am fortunate to have benefitted from his presence over the years. I am also grateful for Terry Morgan, who has always made the time to look at histology slides with me, has expertly fielded all manner of pathology questions from me, and whose enthusiasm and insight are always appreciated. In addition, I was fortunate to receive funding from the OHSU TL1 training program, which provided me with excellent mentorship and training in the area of clinical and translational research. Next, I am thankful to Lisa Coussens, who generously permitted me the opportunity to collaborate with her lab to learn more about the intricacies of tumor immunology and gain access to exciting new technologies in tumor biology analytics. The entire Coussens lab has been outstandingly helpful, especially Shannon Liudahl, Sam Sivagnanam, Courtney Betts, William Larson, and Teresa Beechwood. Their knowledge and guidance augmented my project's depth as well as my own understanding of the tumor biology field. Lastly, I am thankful for the support

and community provided by the Brenden-Colson Center for Pancreatic Care, and for the faculty, students, staff, and patients who contribute to pancreatic cancer research at OHSU.

Going back further, my current career would have been impossible without the guidance of many mentors along the way, and this list is by no means exhaustive. One of my earliest inspirations was Kristen Donley, my high school AP Biology teacher, whose lively teaching and passion for science helped solidify my decision to pursue further studies in molecular and cell biology. Not long after, I had my first true research experience with Dr. Maggie Wierman, a physician scientist who instilled in me a passion for endocrinology, translational research, and medicine. Between my undergraduate studies and starting at OHSU, I had the fortune of working with Dr. Clyde Wright, another physician scientist whose fantastic mentorship, dedication, and encouragement helped me immeasurably as I chose to pursue training as an MD/PhD. I am also grateful for all of the countless other role models, mentors, mentees, and colleagues I have had over these years in research.

However, the greatest luck I have had in my life is my family and friends. This is for my mother, whose compassion, insight, humor, fierce loyalty, and strength are a consistent force of positivity. This is for my father, who not only has an admirably encyclopedic knowledge of everything from engineering to history, but whose thoughtful guidance and sense of humor have never failed to brighten my days. I am also lucky to have two great siblings: my older brother James, whose brilliance, kindness, and hard work are an inspiration, and my younger brother Matthew, whose lightning-fast wit, sarcasm, creativity, and intellect are a force to be reckoned with. Next, I am thankful for my wonderfully supportive partner, Ryan, who manages to make me happy even on bad data days, and whose companionship, encouragement, humor, and perspective have been invaluable throughout the time I've known him. Though I moved to

Oregon knowing no one in the state, I was fortunate to meet many amazing people at OHSU in medical school, graduate school, and the MD/PhD program. These friendships have not only been essential for surviving school, but they have filled my years here with great conversations, laughter, and countless memories of adventures and misadventures alike. To all of my friends, especially Anjali, Flo, Leah, Elizabeth, Nat, Hannah, and Sarah: thank you for being there and making the most of this experience together.

Abstract

Pancreatic ductal adenocarcinoma (PDAC) is among the deadliest of malignancies, with a dismal survival rate and limited treatment options. Advances in therapeutic modalities are urgently needed not only to successfully restrain tumor growth, but to address the underlying physiological aberrations that drive significant morbidity and mortality in PDAC. Specifically, no therapies exist to treat cachexia, a complex metabolic and behavioral syndrome that is present in up to 85% of patients with PDAC. To address this therapeutic gap, I performed three main studies detailed over the course of this dissertation. First, we established a novel model of pancreatic cancer cachexia using transplantation mouse models. Using epithelial cells transplanted from $KRAS^{LSL.G12D/+}$ $TP53^{LSL.R172H/+}$ Pdx-Cre (KPC) mice into the pancreas of immunocompetent syngeneic recipient mice, we demonstrated key behavioral, physiological, and molecular manifestations of cachexia were reliably induced in conjunction with PDAC lesion development. Next, I used mouse models to determine whether the immune-enhancing agent R848, an agonist of Toll-like receptor 7 (TLR7), could be delivered in a manner to overcome sickness responses and allow safe therapeutic use during cancer. This study revealed that sickness responses to TLR7 stimulation undergo tachyphylaxis using a daily systemic dosing schedule, likely via induction of immune tolerance. Finally, I applied the optimized R848 dosing strategy to our model of PDAC and cancer-associated cachexia to determine effects on tumor response and cachexia status. This revealed that for a majority of epithelial clones, R848 results in stromal TLR7-dependent anti-tumor responses, reduced cachexia manifestations, and extended survival. Overall, these studies show that when delivered appropriately, immune enhancing agents such as R848 could provide demonstrable benefit in the context of PDAC and cancer-associated cachexia.

Graphical abstract

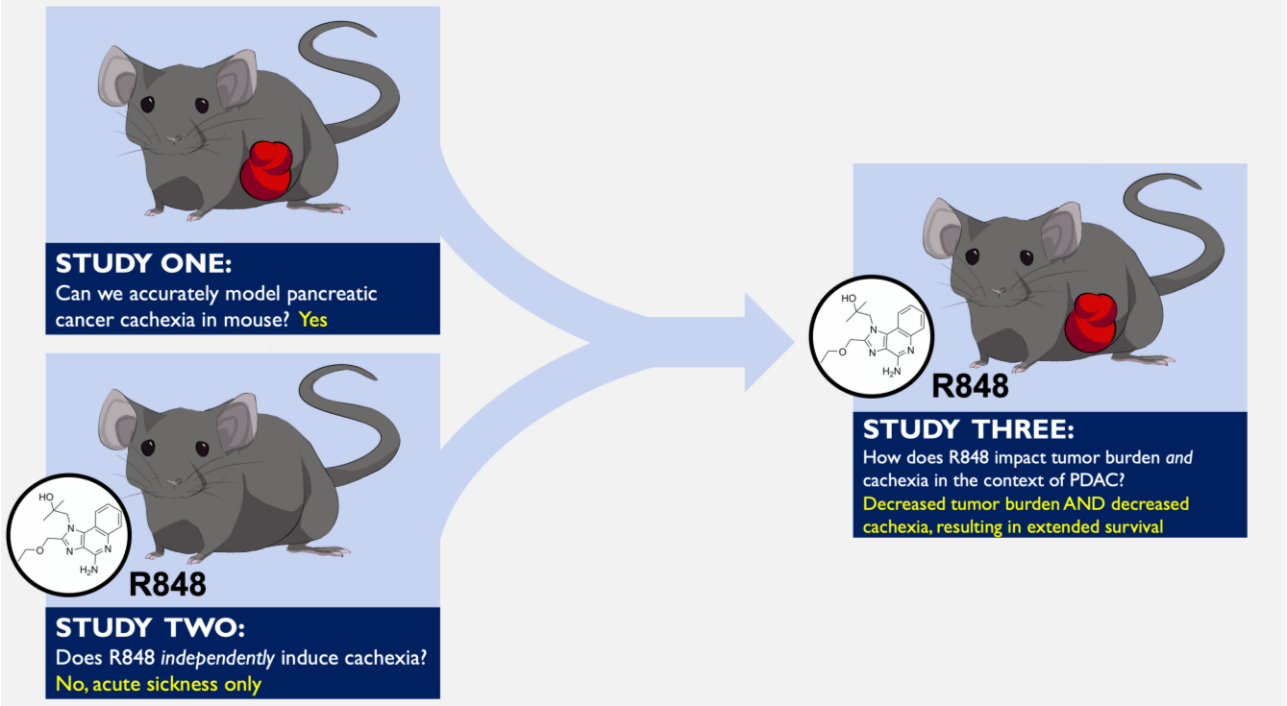

List of Abbreviations

Cachexia and related terminology:

ECOG	Eastern Oncology Cooperative Group score
PS	Performance status
CT	Computed tomography
MRI	Magnetic resonance imaging
NMR	Nuclear magnetic resonance relaxometry
LBM	Lean body mass
LMA	Locomotor activity
MBH	Mediobasal hypothalamus
ARC	Arcuate nucleus of the hypothalamus
PVN	Periventricular nucleus of the hypothalamus
BBB	Blood-brain barrier
HPA	Hypothalamic-pituitary-adrenal
HPG	Hypothalamic-pituitary-gonadal
MED	Minimum effective dose
MTD	Maximum tolerable dose

Pancreatic cancer types, therapies, and cell subsets:

PDAC	Pancreatic ductal adenocarcinoma
PanIN	Pancreatic intraepithelial neoplasia
IPMN	Intraductal papillary mucinous neoplasm
KPC	LSL-$Kras^{+/G12D}$ LSL-$Trp53^{+/R172H}$ *Pdx1-Cre*
FOLFIRINOX	Folinic acid, 5-flurouracil, irinotecan, oxaliplatin
R848	(Also referred to as Resiquimod)
VEH	Vehicle
mIHC	Multiplex immunohistochemistry
ROI	Region of interest
TAM	Tumor-associated macrophage
PSC	Pancreatic stellate cell
CAF	Cancer-associated fibroblast
TIL	Tumor infiltrating lymphocyte
Th1	T helper 1
Th2	T helper 2

Genes and proteins:

CD11b	Integrin alpha M
CD11c	Integrin, alpha X (complement component 3 receptor 4 subunit)

CD19	Cluster of differentiation 19
CD3	Cluster of differentiation 3
CD4	T-cell surface glycoprotein CD4
CD45	Protein tyrosine phosphatase, receptor type, C
CD8a	Cluster of differentiation 8a
F4/80	EGF-like module-containing mucin-like hormone receptor-like 1
FOXP3	Forkhead box P3
Ly6C	Lymphocyte antigen 6 complex, locus C1
Ly6G	Lymphocyte antigen 6 complex locus G6D
MHCI	MHC class II antigen
NK1.1I	Killer cell lectin-like receptor subfamily B, member 1
B220	Protein tyrosine phosphatase receptor type C isoform B220
BTK	Bruton's tyrosine kinase
CD206	Cluster of differentiation 206
CD86	Cluster of differentiation 86
CSF1R	Colony stimulating factor 1 receptor
EOMES	Eomesodermin
FOXP3	Forkhead box P3
GATA3	Gata binding protein 3
GDF15	Growth and differentiation factor 15
GZMB	Granzyme B
Ki-67	Marker of proliferation Ki-67
PANCK	Pancytokeratin
PDL-1	Programmed death-ligand 1
PD-1	Programmed death 1
RORγt	RAR-related orphan receptor gamma
TCF1	Transcription factor T cell factor 1
TIM3	T-cell immunoglobulin and mucin-domain containing 3
Mafbx	Muscle atrophy F-box
Murf1	Muscle ring finger 1
Foxo1	Forkhead box O1
Bnip3	BCL2 Interacting Protein 3
Ctsl1	Cathespin L1
Gabarapl	GABA Type A Receptor Associated Protein Like
Il1b	Interleukin-1 beta
Il1r1	Interleukin 1 receptor type 1
Selp	P-selectin
Tlr7	Toll-like receptor 7
Ccl2	C-C motif chemokine ligand 2
Cxcl10	C-X-C motif chemokine 10
Icam1	Intercellular adhesion molecule 1
Apcs	Amyloid P component, serum
Crp	C-reactive protein
Orm1	Orosomucoid 1
Lcn2	Lipocalin 2
Ifna	Interferon alpha-1
18s	18s ribosomal subunit

Table of Contents

INTRODUCTION

I. Pancreatic cancer: clinical management, mechanisms, and therapeutic approaches

> *"It lives desperately, inventively, fiercely, territorially, cannily, and defensively--at times, as if teaching us how to survive. To confront cancer is to encounter a parallel species, one perhaps more adapted to survival than even we are."*
>
> — Siddhartha Mukherjee, *The Emperor of All Maladies*

Currently the 4th leading cause of cancer mortality in developed nations, pancreatic cancer is projected to result in 56,770 new cases and 45,750 deaths in the United States in 2019. In the absence of improved therapies, pancreatic cancer is expected to rise to the 2nd leading cause of cancer-related mortality by 2030[1]. Owing to both the frequently advanced stage of disease at the time of diagnosis and a lack of effective medical therapies, the estimated 5-year survival of pancreatic cancer is as low as 8%. Though pancreatic cancer comes in many forms, the most common and most deadly is pancreatic ductal adenocarcinoma (PDAC), a malignancy of the exocrine pancreas which accounts for roughly 93% of diagnoses. The median survival of patients diagnosed with locally advanced PDAC is 6-9 months, and for the 52% of patients whose disease is metastatic at the time of diagnosis, estimated survival is a mere 3 months [2]. These grim statistics speak to the urgent need to improve understanding of the mechanistic underpinnings of this illness, and to expand therapeutic options to extend and improve the lives of patients diagnosed with PDAC. In this chapter, I will review PDAC epidemiology and risk factors, current standards of care, key mechanisms of disease, and new approaches for the treatment of PDAC.

Epidemiology, patient characteristics, and risk factors

An estimated 367,000 new cases of pancreatic cancer were diagnosed worldwide in the year 2015, a number which has steadily risen since the 1970s [3]. Pancreatic cancer most commonly occurs over the age of 50, with a majority of patients in their 60s and 70s at time of diagnosis. Men are at slightly elevated risk relative to women, accounting for an estimated 52% of cases. Lifestyle factors that have been linked to development of pancreatic cancer include smoking, smokeless tobacco products, sedentary lifestyle, heavy alcohol consumption, and diets high in saturated fat [2]. Other patient characteristics that are documented to increase pancreatic cancer risk include obesity, diabetes, and chronic pancreatitis [4-6]. Diabetes bears a complicated relationship with pancreatic cancer, as it can be both a risk factor and a sign of PDAC depending on context. Type 1 diabetics have a 2-fold relative risk of PDAC compared with healthy controls, while type 2 diabetics are estimated to have a 1.8-fold relative risk of diagnosis [7,8]. However, it should be emphasized that the majority of the aforementioned risk factors are so common that they typically do not warrant screening for pancreatic cancer. The exception is a specific category of diabetes: new onset diabetes is relatively uncommon in patients greater than 50 years of age, and may be due to an underlying malignancy [9]. The type of diabetes associated with pancreatic masses is classified as diabetes type 3c (pancreatogenic). It can also occur in the context of cystic fibrosis, chronic pancreatitis, and surgical resection. Heredity is another important factor, given that an estimated 10% of PDAC cases have a family history of pancreatic cancer [10]. Known risk alleles include mutations in BRCA1, BRCA2, MLH1, CDKN2A, ATM, STK11, and PALB2 [2]. Other diagnoses associated with pancreatic cancer include Peutz-Jeghers syndrome, hereditary pancreatitis, Lynch syndrome, cystic fibrosis, and Li-Fraumeni syndrome. Patients with elevated risk on the basis of family history or genetic factors are highly recommended for screening and prevention programs, which have demonstrated an early detection benefit in this population [11].

Next, I will review current clinical management guidelines from the 2018 National Comprehensive Cancer Network for diagnosis and staging, surgical management, medical management, and radiotherapeutic management of pancreatic cancer. [12]

Diagnosis and staging

Though pancreatic cancer has many therapeutic challenges, one of the most significant is late diagnosis. Few effective biomarkers exist for pancreatic cancer, and none to date have been successful in picking up early disease with sufficient sensitivity and specificity to apply to a general patient population. While patients typically have a large variety of symptoms and signs for months leading up to their official diagnosis, the majority of these (pain, fatigue, unexplained weight loss, decreased appetite, and digestive symptoms) occur in numerous illnesses and are not specific to pancreatic cancer. Diagnosis usually occurs following the onset of more definitive signs, including jaundice, pancreatitis, or imaging studies (ultrasound or CT) revealing a mass.

Ideally, patients should be referred to a multidisciplinary team at a high-volume center for next stages of workup. The first crucial piece of diagnostic information is a high-quality pancreas protocol abdominal CT, which delineates the tumor's relation to key vascular structures. The CT imaging study is used to determine whether disease is surgically resectable, borderline resectable, locally advanced, or metastatic. At diagnosis, approximately 10-20% of patients have resectable disease, 30-40% have locally advanced disease, and 50-60% have metastatic disease. A tissue biopsy to confirm PDAC is then performed by ERCP or EUS-guided fine-needle aspiration (FNA). Biopsies can also prove beneficial in the context of neoadjuvant therapy, where they can provide information to optimize selection of chemotherapy.

Treatment modalities and factors influencing clinical decision-making

For patients with resectable disease, the path is surgery with or without neoadjuvant therapy, followed by adjuvant chemotherapy or chemoradiation. The goal for patients with borderline resectable disease is to downstage the tumor using neoadjuvant chemotherapy or radiation, such that they move fully into the resectable category. For patients who are unable to obtain a successful resection, including most locally advanced and all metastatic patients, clinical management is performed primarily in the medical oncology setting. While the standard of care for *all* patients with pancreatic adenocarcinoma is to enroll in a clinical trial, common strategies for surgical, medical, and radiotherapeutic disease management are summarized below.

Surgery

Following a pancreas protocol CT staging of disease, patients are evaluated for the possibility of surgery primarily on the basis of the tumor's relationship to major local vasculature. Surgery represents the only option for potentially curing a patient with pancreatic cancer, but is only an option for roughly 15-20% of patients. The surgical candidate for PDAC have tumors with no arterial contact with the celiac axis, superior mesenteric artery, or common hepatic artery, and less than 180 degrees of contact with the superior mesenteric vein, portal vein, or inferior vena cava. Patients with minor deviations from these criteria can sometimes be accommodated with vascular reconstruction procedures, or they can be classified as having potentially resectable disease. When possible, the goals of surgical management in PDAC include resection of the primary tumor and regional lymph nodes. Strategies in the surgical arena include the Whipple procedure for masses located in the head of the pancreas, and distal pancreatectomy for masses located in the body or tail.

Radiation

The role of radiation therapy in management of PDAC is two-fold. First, it can be used in the neoadjuvant setting, particularly in locally advanced disease, to radiate areas around vasculature and attempt to make removal of the tumor more feasible. Second, it can be used in the adjuvant setting, especially in the context of patients who are at a high risk for local recurrence. This group can include patients who had positive resection margins or metastatic spread to local lymph nodes. Radiation therapy can also be used in locally advanced disease, in which the goal is typically to prevent or delay local progression, particularly any associated pain and obstruction. Finally, radiation therapy can be used in a palliative capacity for patients with metastatic disease. The goal in this context is similar to that of locally advanced disease, and is primarily to relieve pain and obstruction secondary to tumor growth. Radiation is commonly used in the context of patients who cannot tolerate chemotherapy due to poor performance status or serious comorbidities. Ideally, however, it is combined with a chemotherapy regimen based on the patient and the extent of their illness, as described in the section below.

Chemotherapy

Regardless of the stage of pancreatic cancer, chemotherapy is a crucial element of treatment. Chemotherapy can be delivered prior to surgery in the neoadjuvant setting, particularly for patients whose tumors are borderline resectable, to improve the likelihood of a successful resection with negative margins. However, the most common scenarios are to receive chemotherapy either in the post-surgical adjuvant setting, or in the absence of surgery. Even with "complete" surgical resection, 80% of patients go on to develop recurrent disease, making chemotherapy necessary. One of the most key determinants of chemotherapy selection is the performance status of a patient, a feature that will be discussed at length in the following chapter

(*Cachexia as an unmet need in the treatment of pancreatic cancer*). The Eastern Cooperative Oncology Group, or ECOG, score is a measure of a patient's "performance status", or ability to function in their daily lives. This score is scaled from 0-5, in which a 0 is assigned to asymptomatic patients, 1 is assigned for symptomatic but ambulatory patients, 2 is assigned to symptomatic patients who are <50% in bed during the day, 3 is assigned to symptomatic patients who are >50% in bed during the day, 4 is assigned to patients who are completely bedbound, and 5 is assigned in the case of death. Performance status is tightly linked to risk of adverse events and a patient's ability to tolerate chemotherapy, and is therefore always considered when navigating treatment choices during PDAC. As previously stated, the standard of care is to enroll patients in a clinical trial, but commonly used regimens are summarized here.

For patients with ECOG performance status 0-1, FOLFIRINOX and modified FOLFIRINOX provide the best outcome and longest median survival in both surgically resected and metastatic disease. FOLFIRINOX is a 4-drug regimen consisting of 5-flurouracil, leucovorin, irinotecan, and oxaliplatin, with modified regimens involving differential timing and dosing of the same medications. In the context of surgically resected PDAC, a recent clinical trial demonstrated that patients receiving FOLFIRINOX had a median survival of 54.4 months, a marked improvement over the 34.8 month median survival observed with gemcitabine [13]. Furthermore, in patients with an ECOG performance status of 0-1, a large clinical trial demonstrated that patients on FOLFIRINOX had an overall survival of 11.1 months, compared to 6.8 months in the gemcitabine group [14]. However, only an estimated 2.9% of PDAC patients carry an ECOG score of 0, and 39.1% an ECOG score of 1 [15]. For the other 58% of patients, FOLFIRINOX is unfortunately not an option because of the dire lack of therapies to address performance status in pancreatic cancer. For these patients, options typically include a combination of gemcitabine and albumin-bound paclitaxel.

Other regimens in use for patients with poor performance status include gemcitabine with capecitabine, capecitabine monotherapy, and 5-fluorouracil with leucovorin.

Unlike other arenas of oncology, success in targeted and personalized medicine for PDAC has made only an incremental difference for patient outcomes. A small number of mutations have been found to be targetable in clinical trials, including BRCA1, BRCA2, and PALB2, which can be targeted with the addition of cisplatin. Particularly for patients with Lynch syndrome, who have inherited deficits in DNA mismatch repair genes, microsatellite instability may be unusually high and permit successful use of drugs such as checkpoint inhibitors. For most patients with PDAC, FDA-approved immunotherapy strategies have not shown substantial benefit. However, immune based mechanisms are still highly targetable and an expanding domain of investigation, and much more research is needed.

Investigational therapies

With current outcomes of chemotherapy unable to meet the needs of a majority of patients, new therapies are in urgent demand. A noteworthy feature of PDAC is its abundant desmoplastic stroma, a feature that results in an extremely high interstitial pressure and physical barricade against the distribution of chemotherapy into the tumor [16]. One constituent of the stroma extracellular matrix of PDAC is hyaluronan, which can be extremely abundant in the tumors of a subset of patients. Peghyaluronidase alfa (PEGPH20) is a pegylated recombinant human hyaluronidase that has shown benefit in patients with high levels of tumor hyaluronic acid, but only in combination with gemcitabine and nab-paclitaxel [17].

Another commonly cited challenge in the treatment of PDAC is its profoundly immunosuppressive tumor microenvironment. There is a relative lack of immune cell infiltrate in PDAC lesions, including tumor-infiltrating cytotoxic T cells. One approach to modify this feature is pegilodecakin, a PEGylated form of recombinant IL-10 that alleviates T cell exhaustion and is currently in Phase III trials for PDAC (NCT02923921) [18]. Another promising strategy is GVAX, a GM-CSF-secreting allogenic pancreatic tumor cell line vaccine that improves intratumoral T cell infiltration and germinal center formation [19]. Other immune pathways under various stages of therapeutic development include CSF1R, CCL2/CCR2, CXCR4, TGFβ, and CD47 [20]. Unfortunately, a variety of previously-promising therapies such as ibrutinib (an inhibitor of Bruton tyrosine kinase), palbociclib (an inhibitor of CDK4/6), and MM-141 (an inhibitor of IGF1R), have all been abandoned due to unsuccessful clinical trials, highlighting the need for novel therapeutics targeting pathways in PDAC.

Molecular and cell biology of pancreatic cancer: roles of the tumor microenvironment

As knowledge has accumulated on the origin and progression of pancreatic cancer, it has become clear that a large variety of cell types contribute to the unique biology of this disease. These layers of complexity are crucial not only in understanding how PDAC itself is formed, but they inform therapeutic design by delineating the multifactorial barriers to successful anti-tumor responses. This next section will therefore briefly overview pancreatic cancer at two levels: first, the neoplastic cell itself, and second, the cell types collectively composing the tumor microenvironment. The tumor microenvironment will be further subdivided into the constituents of a) pancreatic host cells including pancreatic stellate cells, cancer-associated fibroblasts, and neurons; and b) immune cells of both innate and adaptive lineages.

Neoplastic cells in PDAC

Like most types of cancer, PDAC is thought to undergo carcinogenesis in a multi-stage progression from precursor lesion to malignancy. The majority of fulminant PDAC arises from a type of precursor lesion known as pancreatic intraepithelial neoplasia (PanIN), but it may also arise from other precursor lesions including intraductal papillary mucinous neoplasms (IPMN) [21]. A molecular hallmark of PDAC carcinogenesis is the presence of constitutively activating mutations in the KRAS GTPase, which can be found in greater than 90% of lesions. Other genetic foci that facilitate transition to malignancy in PDAC are *TP53, MYC, CDKN2A/p16,* and *SMAD4,* mutations of which can be found in 50-80% of cases [2]. Currently, none of these key genetic drivers of carcinogenesis and tumor progression are considered therapeutic targets, though this remains an active area of investigation.

To uncover novel epithelial cell-intrinsic targets and decipher targetable pathways in PDAC, multiple molecular classification models of pancreatic cancer subsets have been proposed in recent years that are stratified by unique transcriptional profiles. Moffitt's classification system defines two types of epithelial categories, classical and basal-like, the latter of which portends poor survival [22]. Meanwhile, the Collisson classifiers include three epithelial subtypes of classical, quasi-mesenchymal, and exocrine-like, based on surgically microdissected samples [23]. Lastly, the Bailey subtypes include squamous, pancreatic progenitor, immunogenic, and aberrantly differentiated endocrine exocrine (ADEX), however, these were not separated for stromal and epithelial compartments and do not purely reflect changes to neoplastic cells [24]. Further investigations of these molecular classification systems could provide benefit in therapeutic design by defining master regulators of tumor progression and providing personalized recommendations for a patient's tumor subtype.

Pancreatic stellate cells and cancer-associated fibroblasts

A number of elements present in the normal pancreas are crucial in the process of carcinogenesis and tumor progression. One of the most noteworthy is the pancreatic stellate cell, a myofibroblast-like cell residing in the exocrine pancreas. These cells remain in a quiescent state during times of health, and can be distinguished by their intracellular lipid droplets, vitamin A storage, and expression of the markers GFAP, desmin, nestin, and vimentin [25]. Pancreatic stellate cells serve a crucial role in tissue remodeling and homeostasis, whereby they play a role in tissue architecture and response to injury [26]. However, during times of inflammatory stress such as pancreatitis, pancreatic stellate cells undergo a process of activation that results in increased proliferation, migration, and extracellular matrix deposition.

Ultimately, it is thought that pancreatic stellate cells are the primary origin of cancer-associated fibroblasts in PDAC, a cell population known to contribute to the complexity of disease pathogenesis and progression in multiple ways [27]. First, these cells are responsible for production of a large variety of extracellular matrix components such as hyaluronic acid that increase tumor interstitial pressure and serve as a physical barrier to treatment [16]. Second, pancreatic stellate cells enable the growth and development of neoplastic cells. These mechanisms include provision of soluble secretome components that promote PDAC anabolism, as well as release of metabolic precursors such as alanine [28,29].

Next, cancer-associated fibroblasts may be crucial for the immunosuppressive phenotype of PDAC, and are therefore an important target for enabling successful immunotherapy. Cancer associated fibroblasts exist in multiple forms in PDAC, including a myofibroblastic form expressing high levels of alpha-smooth muscle actin, and an inflammatory form that produces

high levels of cytokines such as IL-6 [30]. Differentiation of these populations may be mediated by IL-1-dependent JAK/STAT signaling, which promotes an inflammatory phenotype, and TGF-β, which promotes a myofibroblastic phenotype [31]. Interestingly, cancer-associated fibroblasts may be therapeutically reprogrammed with the vitamin D receptor ligand calcipotriol, which promotes reversion to a quiescent state [30]. However, it must be emphasized that the cancer-associated fibroblast may serve a protective role as well: global deletion of stroma with systemic ganciclovir, or the inhibition of the sonic hedgehog (Shh) signaling pathway, results in severe cachexia and accelerated mortality [32-34]. This important cell type is therefore an interesting target not only from the perspective of tumor progression, but also chemotherapy delivery and the modulation of cachexia phenotypes in PDAC.

Pancreatic neuronal cells

Neurons are another key constituent of the normal pancreas that play a contributory role to the development and progression of PDAC. The pancreas is a richly innervated organ, a feature that allows communication with the central nervous system and is crucial in maintaining nutritional homeostasis. Afferent signaling from the pancreas is transduced by vagal and spinal pathways, consisting of small myelinated and unmyelinated fibers that transmit mechanosensory and nociceptive signals via the nodose ganglia (vagal) and T6-L2 dorsal root ganglia (spinal) [35]. The pancreas is also innervated both parasympathetic and sympathetic efferent neurons, with the former mediated by the dorsal motor nucleus of the vagus, and the latter mediated by sympathetic preganglionic neurons of the upper lumbar and lower thoracic segments of the spinal cord [36]. In the context of PDAC, perineural invasion is a negative prognostic factor that affects a majority of patients, both contributing to the severe pain syndrome associated with PDAC, tumor inflammatory signaling, and infiltration of adjacent tissues [37]. An interesting pair of recent studies

shows that the balance of sympathetic and parasympathetic input to the pancreatic neoplastic niche can contribute to disease progression in PDAC. First, it was found that in the LSL-Kras$^{+/G12D}$ LSL-Trp53$^{+/R172H}$ *Pdx1-Cre* (KPC) genetically engineered mouse model of pancreatic cancer, subdiaphragmatic vagotomy accelerated carcinogenesis, whereas the muscarinic agonist bethanechol ablated this effect [38]. Indeed, these studies demonstrated that cholinergic signaling both suppresses tumorigenesis and extends survival in mice with established PDAC. Concurrently, a second study found that catecholamine activity downstream of chronic restraint stress or isoproterenol promoted ADRB2-dependent acceleration of PDAC development in the KPC mouse [39]. These studies implicated pancreatic innervation as a multifactorial driver of pancreatic cancer, both through neural signaling inputs and through inflammatory changes to the tumor microenvironment. Intriguingly, nerves also act as a relay between the central nervous system and the pancreas during cancer, which is an unexplored potential mechanism of PDAC-associated cachexia.

Tumor immune microenvironment in PDAC

The immune landscape of pancreatic cancer consists of regulatory T cells, myeloid-derived suppressor cells, tumor-associated macrophages, and mast cells [40]. The functional phenotype of these cells is characteristically immunosuppressive. With high levels of anti-inflammatory cytokines TGFβ, IL10, CXCR4, and CXCL10 in the tumor microenvironment, as well as frequent expression of the T cell inhibitory signal PDL-1 on neoplastic cells, anti-tumor responses by tumor infiltrating lymphocytes (TIL) are functionally repressed. The myeloid derived suppressor cell is a multipotent progenitor cell that is released from the bone marrow at times of stress, and instead of differentiating into a granulocyte, macrophage, or dendritic cell, it proliferates at sites of damage and has an immunoregulatory function. Myeloid dysfunction is a common feature of

PDAC, with tumor associated macrophages and myeloid derived suppressor cells taking on an early inflammation-resolving phenotype that promotes T helper 2 and T regulatory cell polarization [41]. Indeed, relatively higher levels of myeloid inflammation correlates with a worsened prognosis in pancreatic cancer, an effect that is thought to be driven by a decreased ability to mount an anti-tumor immune response [42].

When examining the unifying characteristics of the rare patients who are long-term survivors of PDAC, tumor immune cell features are among the most important predictors. In one study, patients with an average survival of 6 years post-diagnosis had relatively more intratumoral CD8+ T cells and greater T cell repertoire polyclonality compared with short-term survivors [43]. Furthermore, patients with a lower prevalence of circulating monocytes have longer survival in PDAC, which may be due to how CCR2+ monocytes can be recruited to PDAC lesions and promote local immunosuppressive signaling [44]. These findings underscore that the immunosuppressive tumor microenvironment is a robust avenue for therapeutic discovery in PDAC. Some proposed targets to modify the innate immune component of the tumor microenvironment are GM-CSF, CSF1R, CCR2, STAT3, and RAGE [45]. Meanwhile, strategies to modify adaptive immunity include tumor vaccines such as GVAX, as well as the targets PDL1, CTLA4, PD1, TGFβR1, and IL10 [45]. Together, these agents aim to reverse immunosuppressive signaling in PDAC, mitigate cytotoxic T cell exclusion, and promote the development of adaptive anti-tumor immunity.

The other half of the equation

Given the level of complexity and nuance intrinsic to the tumor in pancreatic ductal adenocarcinoma, continued studies will be necessary to refine the physician's armamentarium

and expand mechanistic knowledge of the tumor intrinsic aspects of PDAC. These factors include improved chemotherapies, enhanced integration of radiation therapy, and the introduction of successful immunotherapies and targeted therapies to target the tumor and its associated microenvironment. Further research into neoplastic cells, tumor stroma components, and the tumor immune microenvironment will be crucial for these goals. However, it is important not to lose sight of the other half of the equation: the impact of cancer on a patient's body. In the next chapter, I will discuss how cachexia, a complex metabolic and behavioral disorder ubiquitous among PDAC patients, is a core aspect of disease pathogenesis, a driver of cancer-associated morbidity, and a necessary therapeutic target in pancreatic cancer.

II. Cachexia as an unmet need in the treatment of pancreatic cancer

> *"It is said that if you know your enemies and know yourself, you will not be imperiled in a hundred battles; if you do not know your enemies but do know yourself, you will win one and lose one; if you do not know your enemies nor yourself, you will be imperiled in every single battle."*
>
> —Sun Tzu, *The Art of War*

Though it is well-known that PDAC is an especially challenging malignancy to treat from the tumor biology perspective alone, an equally pressing challenge is how PDAC changes systemic physiology. For nearly all patients with PDAC, the foremost of these systemic changes is a condition known as cachexia. Cachexia is a serious and often fatal disorder associated with a variety of chronic diseases including cancer, AIDS, cystic fibrosis, heart failure, renal failure, and rheumatoid arthritis. In all of these diverse conditions, cachexia brings forth a complex set of metabolic and behavioral derangements including anorexia, sickness behaviors such as lethargy and fatigue, increased basal metabolic rate, and preferential loss of lean mass. Despite cachexia's substantial contribution to both morbidity and mortality, there are no effective therapies. This is particularly pertinent in PDAC, where cachexia is an important determinant of patient prognosis. Not only does cachexia cause sweeping changes to systemic physiology that accelerate mortality, it also results in decreased ability to tolerate treatments such as chemotherapy and surgery. To address the unmet need for an effective therapy for cachexia, many current hypotheses investigate the idea that tumors directly signal to muscle, resulting in its catabolism. This focus can help

explain muscle wasting, but it does not shed light on other key manifestations of this fundamentally multisystem disorder. For example, a growing body of evidence indicates that inflammatory signaling from the periphery is detected and transduced into a central nervous system response, which alters metabolic, endocrine, and behavioral neuronal activity and results in the systemic manifestations of cachexia. These systems are all impacted in the case of pancreatic cancer and result in decreased quality and quantity of life. However, no therapy has yet succeeded in alleviating this urgent therapeutic need.

Epidemiologic studies indicate PDAC is the among the most cachexia-associated malignancies, with an estimated frequency as high as 85% [46]. While cachexia is often viewed as a quality of life issue by many healthcare providers, it must be underscored that cachexia itself can accelerate disease progression, limit therapeutic options, and can be the direct cause of patient mortality [47]. Indeed, multiple studies have found that performance status, sarcopenia, and cachexia status are among the most consistently important determinants of survival duration in pancreatic cancer [48-52]. In addition, cachexia and sarcopenia are associated with increased therapy-associated toxicity, higher risk of post-operative infections, and prolonged hospitalization. [49,50,53-59]. This effect is further illustrated by a 2010 clinical trial for advanced pancreatic cancer: a stratification analysis of patients with ECOG performance status score of 0 versus 2 revealed a survival difference of 5.5 months [60]. For reference, the survival advantage of FOLFIRINOX over gemcitabine in the setting of advanced cancer is estimated at 4.3 months. In other words, if a therapy existed that fully palliated cancer-associated cachexia, these clinical trial data indicate that it would extend survival of patients receiving the standard of care more than any existing drug on the market.

Despite these facts, cachexia remains a misunderstood and under-addressed entity. A common misconception among healthcare providers is that weight loss in the oncology setting is merely due to a lack of food intake, whether from pain, chemotherapy side effects, or depression. However, it should be noted that even in the presence of anorexia, patients with pancreatic cancer have a paradoxically increased resting metabolic rate , such that caloric deficits can exceed 1200kcal per day [61]. Furthermore, it is important to note that cachexia is often a presenting sign of cancer that occurs prior to therapeutic intervention which is not remedied by nutritional supplementation. Patients with cachexia experience disproportionately weight loss compared with their degree of anorexia, and unlike simple starvation, it is due to loss from both fat and lean mass compartments [62]. In the context of pancreatic cancer, both the exclusive wasting of muscle and combined wasting of muscle and fat portend a worsened diagnosis [63]. Another important misconception among healthcare providers is that obese individuals cannot be cachectic. This has been a particularly harmful assumption in light of the high number of patients with pancreatic cancer who are overweight or obese at the time of diagnosis. Sarcopenic obesity is an extremely common entity, with an estimated prevalence of 13-25% among pancreatic cancer patients, and it is associated with decreased overall survival [64].

To delve into the idea of why cachexia is especially crucial in PDAC, it is illustrative to examine the concept of the therapeutic window. Particularly for drugs like cytotoxic chemotherapies, dose selection is a careful balance of efficacy and tolerability. Choosing a dose that is too low results in inadequate disease response, whereas a dose that is too high results in toxicities. The therapeutic window is delineated by two borders: the minimum effective dose (MED) and the maximum tolerable dose (MTD). As covered in the previous chapter, chemotherapy is an integral part of treatment for pancreatic cancer regardless of grade and stage.

Furthermore, the choice of chemotherapy regimen depends heavily on the patient's performance status. The reason for this becomes readily apparent in light of the therapeutic window, as illustrated in the graphs below. As the relative burden of cachexia increases, the ability to tolerate chemotherapy-related toxicity decreases, and more drug-related adverse events are likely to occur due to the relatively weakened state at baseline. Therefore, the dose-toxicity curve is shifted in the context of cachexia such that lower amounts of chemotherapy result in a higher rate of adverse events, and the maximum tolerable dose is significantly lower:

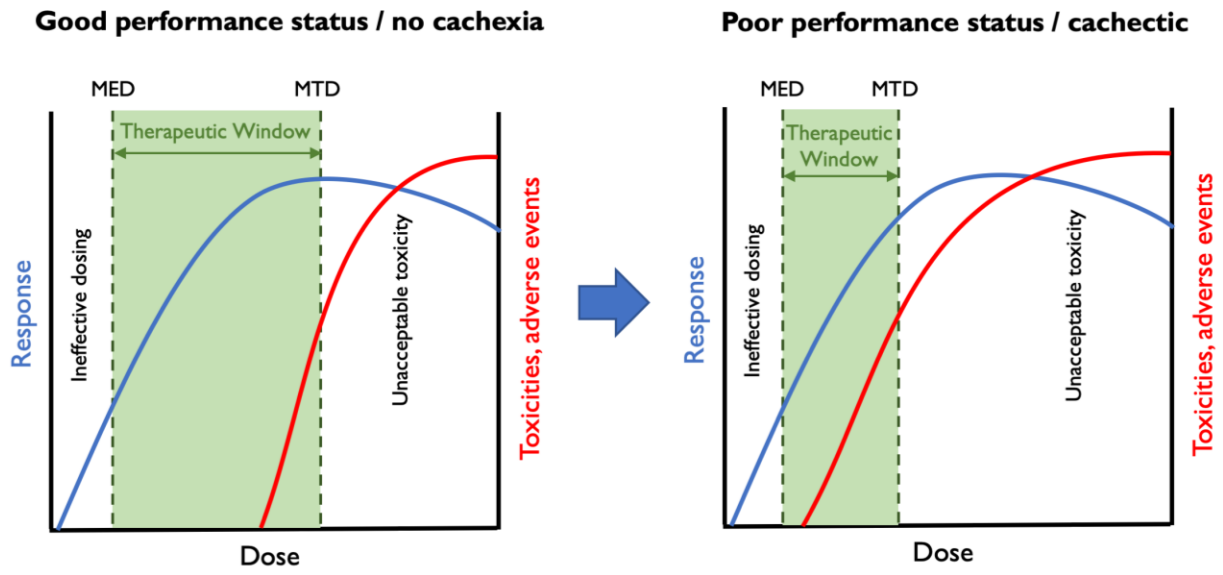

In this sense, it can be readily appreciated that cachexia results in two major harms to patient outcomes in pancreatic cancer. First, cachexia is independently associated with an increased risk of morbidity and mortality, as well as a decreased quality of life. Second, cachexia limits the ability to provide sufficient therapeutic dosing to achieve adequate tumor responses. Because of the direct and intersectional contributions of cachexia to outcomes in pancreatic cancer, it is beneficial to think about therapeutic design as an interaction of tumor and host.

In a systems-based framework, outcomes from a therapy can be thought of as a relationship between the effects on primary disease state and the effects on systemic physiology (e.g. cachexia status). As one example, the outcome of survival duration following a cancer diagnosis can be described in a regression model as follows:

$$\hat{y} = b_0 - b_1 x_1 - b_2 x_2 - b_3 x_1 x_2$$

where $\hat{y}$ is the predicted duration of survival, b_0 is the baseline expected survival for the patient prior to their cancer diagnosis, x_1 is the severity of tumor features, x_2 is the severity of systemic cancer effects such as cachexia, and $x_1 x_2$ is the interaction between tumor and host features. In this case, b_1 describes how a therapy modifies tumor burden, b_2 describes how a therapy modifies systemic aspects of cancer such as cachexia, and b_3 describes how a therapy modifies the interaction between tumor burden and systemic effects. In many cases, the therapeutic modifier effects can differ tremendously between tumor and system. For example, chemotherapies with excellent antineoplastic activity but an unfavorable toxicity profile may strongly reduce tumor burden ($b_1 \ll 1$), but severely compromise systemic health and exacerbate cachexia ($b_2 \gg 1$), or worsen the impact systemic effects exert at a given level of tumor burden ($b_3 \gg 1$). In this situation, the would-be survival benefit of tumor burden reduction may be entirely negated or outweighed by the negative effects on systemic physiology. Other trends become apparent looking at this relation that are relatively unexplored in oncology. Namely, a therapy that does not impact tumor burden whatsoever ($b_1 = 1$) could still exert a survival benefit if it either decreases cachexia ($b_2 < 1$) or decreases the impact of cachexia on survival at a given level of tumor burden ($b_3 < 1$). Using a systems-based philosophy, the ideal therapeutic regimen will have neutral ($b_x = 1$) or beneficial ($b_x < 1$) impacts on all of these three variables. There is therefore a need to assess the therapeutic impact on all of these variables in the preclinical setting, since any of them could theoretically result in improvements or harms to patient survival.

Therefore, one of the most effective steps scientists and clinicians can take to improve outcomes in pancreatic cancer is to consider the other half of the equation: how therapies could be used to reduce cachexia and systemic illness. Not only would successful cachexia therapies result in a wider therapeutic window for patients with low performance status, but they would also *independently* extend survival and quality of life for patients. With this in mind, I will next discuss current mechanistic understanding and therapeutic approaches to cachexia.

III. Mechanisms and treatment of cachexia

> *"The flesh is consumed and becomes water… the abdomen fills with water, the feet and legs swell, the shoulders, clavicles, chest, and thighs melt away… The illness is fatal.".*
>
> —Hippocrates, *Affections XXII*

With the abundant evidence proving cachexia is a key determinant of prognosis in pancreatic cancer, it is clear that better cachexia therapies are among the most important steps we can take to improve PDAC outcomes. However, owing to the complexity of cachexia as an illness, no treatment to date has been fully effective. Recent discoveries about the mechanistic basis of this syndrome may soon provide much-needed targeted interventions, and further research into the mechanisms of cachexia is certain to advance therapeutic design efforts. One key challenge of cachexia resides with its multisystemic nature. Unlike focusing on a single entity such as a tumor, cachexia is a systemic physiology problem that requires careful consideration of many concurrent processes and organ systems. Within this systemic physiology problem is a network of regulatory nodes, including the central nervous system, the immune system, and the tumor. Furthermore, cachexia's pathogenesis involves key recipient nodes, including tissues like muscle and fat that undergo catabolism during disease. Cachexia may potentially be resolved by targeting the signaling within any key regulatory node, or by interfering with signals acting upon recipient nodes. In this chapter, I will highlight mechanisms of cachexia from two fundamental angles: the central nervous system and muscle. Next, I will describe the current state of treatment for cachexia, along with promising new therapies under development.

Adapted from Seminars in Cell and Developmental Biology, June 2016

The central role of hypothalamic inflammation in the acute illness response and cachexia

Kevin G. Burfeind* and Katherine A. Michaelis*, Daniel L. Marks
** Authors contributed equally to this work*

Abstract

When challenged with a variety of inflammatory threats, multiple systems across the body undergo physiological responses to promote defense and survival. The constellation of fever, anorexia, and fatigue is known as the acute illness response, and represents an adaptive behavioral and physiological reaction to stimuli such as infection. On the other end of the spectrum, cachexia is a deadly and clinically challenging syndrome involving anorexia, fatigue, and muscle wasting. Both of these processes are governed by inflammatory mediators including cytokines, chemokines, and immune cells. Though the effects of cachexia can be partially explained by direct effects of disease processes on wasting tissues, a growing body of evidence shows the central nervous system (CNS) also plays an essential mechanistic role in cachexia. In the context of inflammatory stress, the hypothalamus integrates signals from peripheral systems, which it translates into neuroendocrine perturbations, altered neuronal signaling, and global metabolic derangements. Therefore, this review will discuss how hypothalamic inflammation is an essential driver of both the acute illness response and cachexia, and why this organ is uniquely

equipped to generate and maintain chronic inflammation. First, the review will focus on the role of the hypothalamus in acute responses to dietary and infectious stimuli. Next, it will discuss the role of cytokines in driving homeostatic disequilibrium, resulting in muscle wasting, anorexia, and weight loss. Finally, it will address mechanisms and mediators of chronic hypothalamic inflammation, including endothelial cells, chemokines, and peripheral leukocytes.

Introduction

Sickness behaviors and their associated metabolic responses are among the most ubiquitous and readily identifiable aspects of acute and chronic illness. In the context of acute threats, the onset of fever, anorexia, lethargy, and catabolism of lean body tissues all evolved as important defenses to promote survival. However, with chronic and ongoing inflammation, these same defenses prove to be a double-edged sword, leading to neurodegeneration, psychiatric conditions, and cachexia. Cachexia is an important predictor of morbidity and mortality in a diverse array of conditions ranging from infectious disease to cancer. Though a large body of work has focused on the direct interaction of cytokines and inflammatory mediators with muscle tissue in the development of cachexia, these direct effects do not account for all aspects of body mass alterations in acute and chronic illness. An increasing body of work suggests the central nervous system (CNS) is a key mechanistic force in the pathogenesis of cachexia by sensing inflammation, integrating information from peripheral organ systems, and evoking downstream changes in body mass and metabolism.

Decades of investigation provide ample evidence that the CNS functions as both a receiver and amplifier of peripheral inflammatory insults, thereby orchestrating a behavioral and metabolic program that leads to wasting and debilitation if prolonged. As a demonstration of

neuronal signaling leading to amplified response to inflammation, intracerebroventricular (ICV) injection of pro-inflammatory cytokines potently induces anorexia, lethargy, and catabolism at doses far below the threshold for response with peripheral injection [65-68]. Collectively, existing data support a model wherein peripheral inflammatory insults are amplified and modified within the mediobasal hypothalamus (MBH), creating a paracrine inflammatory milieu that in turn initiates and sustains alterations in the activity of neuronal populations that regulate appetite and metabolism. The attenuated blood brain barrier (BBB) and dynamic regulation of vascular access found in this region is undoubtedly one of the reasons this brain area is highly sensitive to a number of metabolic and inflammatory signaling molecules [69]. This review will focus on recent insights in how stimuli of hypothalamic inflammation, including dietary, infectious, and neoplastic sources, are sensed in the CNS and translated peripherally into illness responses and cachexia.

Central nervous system control of body mass and energy homeostasis

Within the MBH, there are several neuronal populations in various nuclei responsible for regulation of appetite, body mass, and energy homeostasis. These populations include anorexigenic and orexigenic neuronal subsets, which decrease and increase appetite and food intake respectively. Key anorexigenic populations include pro-opiomelanocortin (POMC) and cocaine and amphetamine regulated transcript (CART) expressing neurons [70]. POMC is a precursor polypeptide that can be differentially processed for production of αMSH, ACTH, and opioid peptides β-endorphin and [met]enkephalin [71]. POMC neurons release the anorexic neurotransmitter αMSH, which binds to type 4 melanocortin receptors (MC_4R) in a number of downstream sites in the brain to decrease appetite and energy storage. CART is a neuropeptide first discovered as a transcriptional target of cocaine and amphetamine exposure, but was

subsequently found to act as an endogenous psychostimulant that increases locomotor activity and decreases food intake [72]. Conversely, two key orexigenic populations include neurons expressing agouti-related peptide (AgRP) and neuropeptide Y (NPY). AgRP was first characterized because of a curious connection between pigmentation and metabolic phenotypes, both of which act through melanocortin receptors: mice carrying the dominant *Agouti* allele known as lethal yellow not only demonstrate a yellow pigmentation, but are profoundly obese [73]. Further characterization determined that the counter-regulatory neuropeptide AgRP functions as an antagonist of the MCR4 receptor and AgRP neurons directly inhibit POMC neuronal activity, producing increased appetite and energy storage [74,75]. NPY was first identified as a neuropeptide structurally and biologically similar to the intestinal peptide YY (PYY), and is a potent orexigen in the brain and autonomic nervous system [76,77]. Both anorexigenic and orexigenic neuronal circuitry are affected by physiologic cues and by pathophysiologic signals such as cytokines and pathogen-associated molecular patterns (PAMPs) [78]. Therefore, the MBH is a key central target of cytokine signaling and provides an important primary neuronal substrate linking inflammation to muscle catabolism, anorexia, and other sickness responses [79-83].

The brain-muscle axis: a model for hypothalamic mechanisms of illness responses and cachexia

In states of illness, the body initiates several processes to mobilize energy stores and provide anabolic building blocks for the acute phase response. While these processes are integral to normal immune physiology, they can result in pathologic homeostatic disequilibrium, where the body assumes a state of energy wasting. As a result, tissue breakdown occurs in organs important to activities of daily living. Muscle is an abundant source of amino acids, and often the main target of pathologic tissue breakdown in disease. Selective catabolism of skeletal muscle is

one of the hallmarks of cachexia. It is well known that prolonged systemic inflammation causes skeletal muscle breakdown [84-86]. While much of the literature has focused on catabolic pathways within muscle itself, a growing body of evidence indicates the CNS is a key mediator in this process [87-89]. In particular, the hypothalamic-pituitary (HPA) axis promotes catabolism of carbohydrates, lipids, and proteins in peripheral tissue in response to cytokines that enter the CNS. As a result, adipose tissue undergoes lipolysis, and proteolysis occurs in skeletal muscle [89]. However, skeletal muscle proteolysis occurs selectively over lipolysis in states of neuroinflammation [90].

Skeletal muscle catabolism is mediated by hypothalamic cytokines

A series of studies demonstrate that through the actions of the prototypical inflammatory cytokine IL-1β, a cascade of signaling is initiated in the hypothalamus, resulting in both local and systemic changes in gene expression, protein synthesis, and neuroendocrine signaling [87,88,90,91]. In a rodent model of cancer cachexia, hypothalamic expression of IL-1β mRNA was increased. When IL-1β was administered ICV, animals experienced profound muscle wasting. Importantly, this effect did not occur when IL-1β was administered IP [90], supporting the hypothesis that central, rather than peripheral inflammation is the main instigator of muscle catabolism in this model of cachexia.

While hypothalamic IL-1β alone can induce muscle atrophy [90], other pro-inflammatory cytokines are implicated in this process. However, there is conflicting evidence regarding the significance of these cytokines, and additional research is needed to fully elucidate their mechanisms [91]. For example, IL-6 is well established as an important mediator in muscle metabolism [92,93] but its role within the hypothalamus is not well known. Although systemic

inflammation increases levels of IL-6 in the hypothalamus in concordance with altered energy homeostasis [94], the effect of ICV IL-6 on skeletal muscle has not been examined. Furthermore, TNFα can directly induce skeletal muscle catabolism [95-97] and produces anorexia when administered centrally [98,99], yet ICV administration of TNFα in rodents does not induce skeletal muscle thermogenesis [98]. However, follow-up studies are lacking, and thus the roles of hypothalamic TNFα, IL-6, or other proinflammatory cytokines in skeletal muscle catabolism remain largely unknown. As such, this remains an important area of research in the pathophysiology of cachexia.

Role of neuroendocrine modulation of muscle mass

Following the onset of hypothalamic inflammation, a neuroendocrine signaling cascade is initiated, including marked activation of the HPA axis [69]. These neuroendocrine mediators can act directly on skeletal muscle, or act on other organs to amplify the inflammatory signal. It is also likely that CNS mediated activation of the sympathetic nervous system contributes to the disordered muscle metabolism in cachexia, including inhibition of protein synthesis as well as proteolysis within skeletal muscle and myofibril breakdown [90]. Endogenous glucocorticoids such as cortisol (or corticosterone in rodents) are important in their ability to modify metabolism of fats, carbohydrates, and proteins, as well as exert control over immune response in times of stress. The chief regulation of glucocorticoid release in humans is at the level of the hypothalamus and pituitary, which produce corticotrophin releasing hormone (CRH) and adrenocorticotrophic hormone (ACTH) respectively. CRH, manufactured in the paraventricular nucleus (PVN) of the hypothalamus, provides the initiating signal of the HPA axis by promoting release of ACTH from corticotroph cells of the anterior pituitary. Direct stimulation by ACTH causes production and release of cortisol from the zona fasiculata of the adrenal cortex [100]. Broadly speaking, stress is the

key activator of the HPA axis. This system is widely evolutionarily conserved as a method of mounting a defense against stressors including infection and starvation, largely by shifting targets of anabolism and catabolism. While the immune system must undergo tremendous anabolism during stress, with increased production of granulocytes and acute phase proteins, other systems must undergo catabolism in order to provide a supply of biomolecules and energy, particularly in the face of stress-induced anorexia. Skeletal muscle is a major site of protein storage, and serves as a primary target of glucocorticoids. Thus, upon HPA axis activation, skeletal muscle undergoes catabolism to increase plasma levels of free amino acids [90]. These amino acids can be used either for production of proteins such as acute phase reactants, or can enter as Krebs cycle intermediates and serve as gluconeogenic substrates in the liver [101]. This process is mediated by proteosomal degradation of muscle protein, with E3 ubiquitin ligases, Muscle Atrophy F-box (MAFBx), and Muscle Specific Ring Finger Protein 1 (MuRF1) playing key roles [102,103].

In the early phases of acute illness, the catabolism of skeletal muscle provides an important energy substrate upon which other defenses can be built. However, when inflammation persists in the context of subacute and chronic disease, this mobilization of protein from skeletal muscle leads to substantial atrophy and functional impairment. The clinical archetype of "matchstick limbs" seen in Cushing's disease, a syndrome resulting from ACTH-secreting pituitary adenomas, serves as a classic illustration of skeletal muscle derangements evoked by the HPA axis [104]. However, Cushing's disease is only one of many conditions known to cause neuroendocrine muscle wasting. Compelling evidence demonstrates that the CNS invokes peripheral muscle wasting via the HPA axis in both cancer and diabetes, with hypothesized roles in numerous other chronic illnesses [91,105]. As such, the CNS not only is tied to the global metabolic dysregulation and

behavioral aspects of the illness response, but it is also able to employ neuroendocrine signaling to invoke an indirect pathway of disease-mediated skeletal muscle atrophy.

Mechanisms of hypothalamic inflammation in metabolic derangements: insights from high fat diet and obesity

Consistent with a wide variety of other pathologies, hypothalamic inflammation occurs in both acute and chronic stages. In both instances, the hypothalamus acts in a feed-forward loop to propagate inflammatory responses in the periphery, including changes in behavior and metabolism. To understand how signals arising from the periphery can induce disordered systemic metabolism via a hypothalamic relay, it is illustrative to examine obesity as a systemic inflammatory disorder. In particular, exposure to high fat diet (HFD) is widely studied as a cause of hypothalamic inflammation that in turn leads to significant alterations in body mass regulation and energy homeostasis. Specifically, HFD exposure causes acute inflammation and gliosis in the MBH, which alters metabolic signaling in this part of the brain [106]. HFD exposure therefore represents one of several acute inflammatory insults capable of inducing global metabolic derangements via hypothalamic signaling.

Multiple forms of dietary stressors have been investigated for their ability to induce hypothalamic inflammation and downstream alterations in metabolism, including high sucrose diet, high polyunsaturated fatty acid diet, and high saturated fat diet [107,108]. Though all of these diets are capable of producing obesity in experimental models, hypothalamic inflammation and gliosis only consistently ensues in the context of high saturated fat diets. These CNS manifestations substantially precede the onset of overt changes in weight and body mass, occurring within 1-4 days of the onset of a high saturated fat diet [106,109]. A key site of inflammation

is the arcuate nucleus, where HFD produces reactive gliosis, increased expression of inflammatory genes IL-1β, IL-6, and TNFα, astrocyte injury, and eventually POMC neuronal injury [106,110]. Further studies indicate that, similarly to peripheral macrophages, microglia of the MBH exhibit an M1-dominant inflammatory response in the presence of saturated fatty acids [110].

To date, studies investigating the mechanisms of HFD-induced hypothalamic inflammatory changes have identified two main pathways: NF-κB signaling and endoplasmic reticulum stress. The hypothalamus demonstrates a different pattern of NF-κB activity compared to peripheral systems, including higher expression of both IKKβ and NF-κB inhibitory protein IκBα, with an overall suppression of NF-κB activity [111]. However, with HFD exposure, this dynamic is altered to significantly increase NF-κB activity in the MBH. Forced suppression of NF-κB signaling via MBH-targeted IKKβ knockout results in decreased dietary intake, while MBH-targeted constitutive NF-κB activation results in central insulin and leptin resistance. This same study identified hypothalamic endoplasmic reticulum stress as both an upstream inducer and downstream event of NF-κB signaling [111]. Further studies confirm the importance of NF-κB to hypothalamic energy homeostasis. In both leptin deficient and diet-induced obese (DIO) mice, pharmacologic and genetic inhibition of IKKβ/NF-κB signaling in the arcuate nucleus results in improvements in glucose tolerance and hypothalamic insulin signaling, as well as increasing energy expenditure [112].

The importance of hypothalamic inflammation rests primarily with the fact that the hypothalamus is a central regulator of whole-body metabolism, which produces substantial downstream consequences. Central administration of the saturated fat palmitic acid not only induces a program of hypothalamic inflammation, including increased local expression of

cytokines IL-6, IL-1β, and TNFα, but it also leads to decreases in leptin-induced mRNA expression related to gluconeogenesis, glucose transport, and lipogenesis in the liver [113]. These peripheral pathological outcomes are abrogated by reduction of hypothalamic inflammation. For example, hypothalamus-specific inhibition of Toll-like receptor 4 (TLR4) and TNFα both result in improved insulin sensitivity in the liver, resulting in decreases in hepatic steatosis and gluconeogenesis [114]. However, TLR4-mediated and TNFα -mediated hypothalamic signaling lead to divergent downstream consequences, with only TLR4 signaling inhibition leading to loss of body mass.

Overall, these findings demonstrate that hypothalamic inflammation results as a consequence of high exposure to saturated fat, and through inflammatory changes and recruitment of glial cell populations is able to alter both peripheral metabolism and behavior. As such, HFD models provide a compelling example of how peripherally derived inflammatory stimuli can induce systemically significant pathophysiological changes in the hypothalamus. In contrast to infectious and neoplastic sources of inflammation, however, HFD eventually produces changes which inhibit anorexigenic POMC and CART neurons, while increasing expression of orexigenic NPY and AgRP. Therefore, hypothalamic inflammation is a potent inducer of peripheral pathophysiological states, the manifestations of which vary substantially with the type and duration of inflammatory stimulus. Through what is in many ways a similar mechanism, other inflammatory insults of the hypothalamus provoke the familiar anorexia, fever, and weight loss known collectively as the acute illness response.

Hypothalamic inflammation and the acute illness response

The most commonly experienced cause of the acute illness response is logically that which the system directly evolved to combat: the immediate threat of infection. The quintessential traits

of acute inflammation and sickness were described as early as Roman antiquity; however, many molecular mechanisms linking inflammation to sickness behavior remain incompletely understood. Even though it is clear that acute inflammation resulting from infection can be deadly, as in sepsis, it is also increasingly clear that acute phase responses are essential to survival. Thus, a significant and growing body of work has focused on understanding the peripheral and central mediators of the response to acute infection, and determining whether each individual step of the process is beneficial or deleterious. The hypothalamus is a vital component of the system responsible for sensing and responding to infectious stimuli, serving as an upstream effector of fever, mobilization of energy stores, and initiation of sickness-associated behaviors. As such, research has focused on two arms of this system: first, how the hypothalamus responds to infectious stimuli on a molecular and signaling level, and second, how hypothalamic sensing of threats leads to downstream manifestations of sickness.

In its role as a sensor of acute infectious stimuli, the hypothalamus employs a diverse array of danger and pathogen associated molecular pattern (DAMP and PAMP) receptors, as well as being robustly responsive to cytokines and chemokines. Peripheral or central injection of viral or bacterial PAMPs or pro-inflammatory cytokines produces neuronal activation in several brain regions, particularly in nuclei that make up the MBH and its associated vascular structures, collectively known as the median eminence [115-117]. Within this region, two key appetite regulating populations of centrally projecting neurons alter their roles as effectors during inflammatory responses: the anorexigenic POMC and CART, and the orexigenic AgRP and NPY.

Much of the current understanding of acute hypothalamic inflammation derives from experiments using lipopolysaccharide (LPS), a PAMP isolated from the outer membrane of gram-

negative bacteria. LPS binds to TLR4 to induce canonical NF-κB signaling, which alters gene transcription to produce a myriad of cytokines, chemokines, and stress response proteins. Both ICV and IP LPS produce acute sickness responses, suggesting it can act through direct interactions with the hypothalamus as well as indirect pathways from the periphery (although with far greater potency after direct CNS administration). Upon exposure to LPS, animals develop sickness-associated anorexia, and orexigenic signaling via NPY decreases at the transcriptional level [118,119]. Similarly, AgRP secretion is decreased following LPS exposure, even though its mRNA levels are increased [81]. Conversely, the appetite inhibiting pathways are activated following LPS exposure. With acute LPS stimulation, POMC neurons are activated, and MC4R and POMC mRNA levels increase [120,121]. Accordingly, both pharmacologic inhibition of MC4R signaling with AgRP, and repression of POMC neuron activation both abrogate the anorexia response following LPS exposure [121-123].

Similar to HFD exposure, the molecular mechanism of LPS-induced hypothalamic inflammation involves NF-κB signaling via TLR4 and endoplasmic reticulum stress [124]. Specifically, TLR4, MyD88, and CD14 are critical to the initiation of sickness behaviors: mice with genetic deletion of any of these proteins demonstrate reduced anorexia in response to IP LPS compared to wild type [118,125]. Fever, anorexia, and hypothalamic inflammation responses to LPS exposure involve the signaling intermediate atypical protein kinase C, whereas hypoactivity and weight loss seem to be mediated by separate pathways [126]. Additionally, inducible nitric oxide synthase (iNOS) is induced by LPS exposure in the MBH, where nitric oxide inhibits orexigenic neurons via a STAT dependent mechanism independent of prostaglandin synthesis [127,128]. Obviously, these are important but not exclusive molecular signaling pathways whereby PAMP exposure is translated into behavior, nor is the MBH the only brain region involved. Indeed, it is clear that the

brainstem has both redundant and exclusive roles relative to the MBH (for example), but discussion of the entirety of the CNS response to inflammation is beyond the scope of this review.

Though a large body of work has focused exclusively on LPS as an instigator of hypothalamic inflammation of infectious etiologies, viral proteins and nucleic acids are less explored, yet potent inducers of central inflammation. In a study by Jang et al, viral and bacterial components, Tat and LPS respectively, were compared in their effects on hypothalamic inflammation and resultant sickness behavior. Following IP exposure to Tat or LPS, NF-κB was acutely activated in the MBH, which induced hypothalamic production of the pro-inflammatory cytokines IL-1β, IL-6, and TNFα. In corticotroph AtT20 cells, NF-κB served as a transcriptional regulator of increased POMC expression following exposure to LPS, Tat, and pro-inflammatory cytokines IL-1β and TNFα. Hypothalamic injection of LPS or Tat both caused a significant reduction in food intake and body weight. However, these effects were prevented by blockade of NF-κB signaling via IKK inhibitory peptide, as well as by blockade of melanocortin signaling via administration of AgRP. Furthermore, specific IKKβ knockout in POMC neurons attenuated anorexia following LPS and Tat exposure. Hypothalamic NF-κB was also activated by high doses of ICV leptin and serves as a transcriptional regulator of leptin-stimulated POMC expression, suggesting NF-κB is common signaling pathway for all three stimuli [121]. In addition to viral proteins, the viral double stranded RNA mimetic poly I:C causes fever, malaise, anorexia, and hypoactivity [129-131]. While the fever induced by poly I:C depends partially on IL-1β and IFNα, the mechanism of viral induction of sickness behavior is not yet fully understood – however, this PAMP clearly promotes inflammatory signaling and HPA axis activation at the level of the hypothalamus [129,132,133].

Importantly, the hypothalamus regulates exposure to inflammatory stimuli differently from peripheral sites of surveillance. While LPS priming decreases the magnitude of cytokine release in the hypothalamus in subsequent LPS exposures, it has the opposite effect in the spleen, where increased levels of IL-1β and IL-1R are induced by repeated exposures [134]. Furthermore, IP LPS exposure time-dependently increases STAT3 phosphorylation in both the hypothalamus and liver, but the hypothalamus demonstrates a relatively more acute and transient signaling response compared to the liver [135]. Most intriguing of all is the recent discovery that microglia have a distinct ontogeny from the peripheral immune system, which may explain why it differs in its responses to inflammatory events [136]. Despite the long-held assumption that microglia originate in bone marrow, akin to other monocytes, fate mapping demonstrates that microglia are seeded from the embryonic yolk sac and remain as a self-sustaining population throughout life. While other tissue macrophages arise from this same embryonic event, the key difference is that only the peripheral tissues continue to recruit from hematopoietic stem cells of the bone marrow [137]. Microglia may recruit from the peripheral monocyte pool during times of profound pathology, such as major insults to the BBB, but they remain an isolated and self-renewing population in most physiological states. This discovery is important, as the distinct lineage of microglia suggests they are likely to have distinct molecular signaling pathways to detect and propagate inflammation. These combined data suggest acute hypothalamic inflammation is a process robustly induced by a variety of stimuli, proceeds through distinct signaling modalities compared to peripheral tissues, and requires a combination of signal initiation and signal propagation events. A variety of signaling mediators and anatomical considerations make hypothalamic inflammation a particularly unique and a targetable niche of acute sickness responses and cachexia alike.

The role of cytokines in acute hypothalamic inflammation and cachexia

While cytokines are key signaling mediators in normal immune responses, high levels are damaging and can lead to sustained inflammation with many detrimental effects. In cancer, higher levels of cytokines correlate with poorer outcomes [138]**.** Furthermore, elevated circulating levels of TNFα and IL-6 in cardiac cachexia are the strongest predictor for pathological weight loss [139,140]. While cytokines have significant effector functions in various organs including muscle [141], it is their action in the CNS, specifically the hypothalamus, that is the primary driver of the behavioral features of cachexia [142]. In spite of the presence of the mostly impermeable BBB, there are several ways cytokines can enter the brain from the circulation. First, since circumventricular organs lack a BBB, most cytokines can enter the hypothalamus by volume diffusion [143]. In addition, some cytokines, including IL-6 [144], TNFα [145], and IL-1β [146], can cross through various transporter systems. Lastly, circumventricular organs and the choroid plexus contain macrophage-like cells that express TLRs, allowing cytokines to exert their functions without entering the brain parenchyma [147]. Dozens of different cytokines have been implicated in cachexia. However, in the hypothalamus, the most robust data supports roles for TNFα and IL-1β in cachexia and sickness behavior [148,149].

TNFα

Although TNFα has direct effects on various target tissues [148,150,151], its most potent actions in regard to cachexia occur in the hypothalamus. Within the hypothalamus, the actions of TNFα alone lead to anorexia, thermogenesis, and increased respiratory rate [98,152,153]. Exposure of ventromedial hypothalamic slice cultures to TNFα causes decreased firing rate of neurons in that nucleus [154]. In rodents, ICV injection of TNFα leads to decreased food intake and increased respiratory quotient [153]. These symptoms correlate with increased expression of mediators of the

JAK/STAT signaling pathway within the hypothalamus, indicating this signaling mechanism is an important mediator in sickness behavior. Furthermore, ICV injection of TNFα leads to reduced food intake and weight loss. In addition to the JAK/STAT signaling pathway, it also was determined that TNFα signaling within the hypothalamus leads to increased thermogenesis in brown adipose tissue via β-adrenergic signaling [98]. Further studies are necessary to determine the specificity of different TNFα signaling pathways within the hypothalamus in cachexia.

IL-1β

IL-1β is established as one of the primary molecules in neuroimmune signaling**.** While IL-1β can act on numerous different types of cultured cells found within the brain, functional IL-1 receptors are primarily localized to endothelial cells and certain neuronal populations, including those within the ARC [155]. It is well documented that systemic inflammation increases IL-1β activity in the hypothalamus [90,156,157]**.** IP injection of LPS induced increased IL-1β expression in endothelial cells of the PVN [156]. Furthermore, IL-1β is an important cytokine in the hypothalamic relay leading to skeletal muscle catabolism [90]. In rodents, chronic ICV administration of IL-1β induces skeletal muscle wasting [90]. In the same study, development of carcinoma-induced cachexia was associated with increased hypothalamic IL-1β expression. In addition, knockout of endothelial IL-1 receptor attenuated expression of IL-1β, TNF-α, and IL-6 mRNA in the brain in a mouse model of chronic stress [158].

From acute to chronic: how hypothalamic inflammation contributes to transition from sickness to cachexia

Although IL-1β and TNFα potently induce acute anorexia, animals rapidly desensitize to continuous ICV administration [159-162]. This tachyphylaxis indicates these cytokines are not sufficient to produce sustained catabolism, suggesting other mediators are necessary to maintain

and amplify the inflammatory signal. While the mechanism of chronic hypothalamic inflammation in cachexia is not fully understood, several candidates have been identified. The cytokine leukemia inhibitory factor (LIF) is expressed in the ARC, and can induce anorexia in inflammatory disease [66,163,164]. In contrast to IL-1β and TNFα, chronic administration of LIF does not induce tachyphylaxis [165-167]. However, the neuroinflammatory actions of LIF appear to overlap with IL-1β synergistically, suggesting that it may be a secondary amplifier of inflammatory response rather than the sole mediator of chronic hypothalamic inflammation [168].

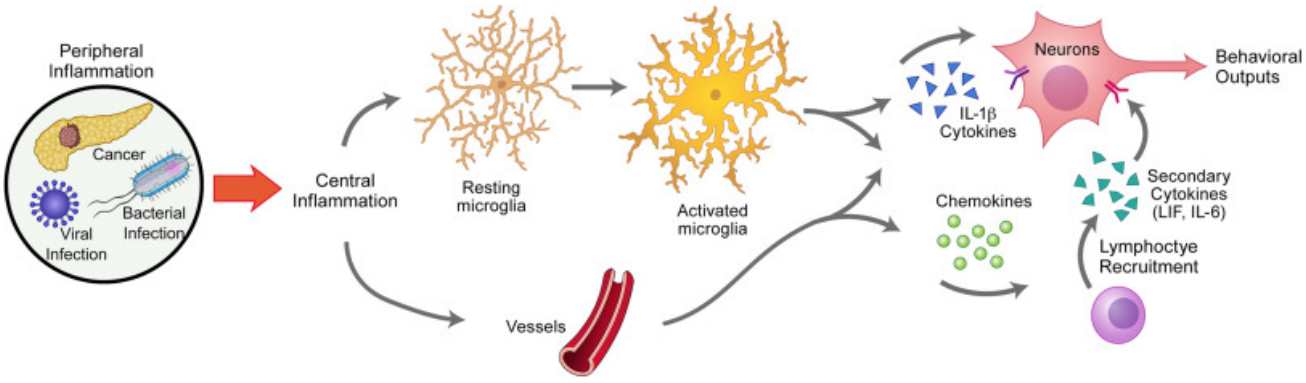

Fig. 1. Initiation, amplification, and perpetuation of hypothalamic inflammation.

Repeated CNS exposure to primary inflammatory cytokines results in tachyphylaxis; therefore, additional pathophysiological steps must be involved to maintain chronic inflammation in cachexia. Upon entering the CNS, cytokines bind to PAMP receptors and activate numerous types of cells, including glia and hypothalamic vascular endothelial cells. Microglia are recruited and activated by PAMPs, which results in increased release of cytokines and chemokines. Endothelial cell activation in vasculature results in secretion of IL-1β and additional cytokines, chemokine secretion, and expression of cell adhesion molecules. Chemokines and adhesion molecules in turn recruit leukocytes from the periphery. These cells secrete secondary cytokines, such as IL-6 and LIF. These pathways ultimately converge on neurons to elicit neuroendocrine, metabolic, and behavioral changes.

While most studies focus on the altered signaling of neurons within the hypothalamus in producing sickness response, an emerging body of evidence suggests non-neuronal cells play an important role in the transition from acute to chronic inflammation in the CNS in cachexia. In particular, activation of hypothalamic microglia and endothelium, followed by secondary recruitment of peripheral leukocytes, may lead to the observable changes in neuronal activity (Figure 1). Specifically, cytokines initiate a cascade involving endothelial activation, followed by increased expression of cell adhesion molecules, secretion of chemokines, and recruitment of peripheral leukocytes. While the role of these mediators in the hypothalamus is not well known, they represent an important area for future research in the field of cachexia.

A reactive endothelium and leukocyte recruitment: new frontiers in neuroinflammatory mechanisms of cachexia

When crossing from the periphery to the CNS, cytokines and other inflammatory molecules first encounter endothelial cells, which express high levels of cytokine receptors. This interaction leads to secretion of additional cytokines, expression of selectins, production of chemokines, and peripheral lymphocyte recruitment. While the role of these mediators has not been studied extensively in the hypothalamus specifically, there is evidence to suggest they play a key role in the sequelae of cachexia (discussed further below). Further studies are necessary to determine possible variations in these immune response proteins within the hypothalamus. Furthermore, these mediators have not yet been targeted in the context of cachexia, presenting an unexplored opportunity for therapeutic intervention.

An activated endothelium

Upon exposure to inflammatory products, vascular endothelial cells enhance their primary role in the circulatory system by activating pathways designed to combat pathogens. Endothelial cells express TLRs that serve as activation switches in response to a variety of DAMPs and PAMPs, leading to several phenotypic changes. Upon activation, inter-epithelial junctions are downregulated, allowing for immune cells to access tissue and fight pathogens. Furthermore, endothelial cells can produce cytokines and molecules such as metalloproteinases that are directly toxic to pathogens, as well as adhesion molecules to promote leukocyte migration and extravasation. In the CNS, neuroinflammation activates endothelial cells and other cells associated with the BBB. If the neuroinflammation persists, this can cause BBB breakdown, which is associated with several pathologies such as Alzheimer's disease [169], Parkinson's disease [170], vascular dementia [171], stroke [172], and multiple sclerosis [173].

Cytokines and the hypothalamic endothelium

All of the major cytokines involved in cachexia play a role in activating endothelial cells. It is well known that increased expression of cytokines selectively occurs within endothelial cells of circumventricular organs of the hypothalamus during systemic inflammation [147,156,157]. For example, injection of LPS leads to increased expression of IL-1β in endothelial cells of the hypothalamus [157]. This induces the production of numerous immune response elements, including cytokines, adhesion molecules, matrix metalloproteinases, and coagulation factors [174]. In addition, IL-1β activates cyclooxygenase in cerebral endothelium, leading to production of the pyrogenic arachidonic acid metabolite prostaglandin E2 [175]. Furthermore, upon exposure to LPS, IL-1β is a key mediator to microglial production of the vasodilator and neuromodulator nitric oxide, via increased biosynthesis of iNOS [176].

Additional cytokines play important roles in endothelial activation as well. In cerebral microvascular endothelial cells, TNFα exposure induces Rho activation and myosin light chain phosphorylation, leading to a gradual increase in permeability and loss of endothelial junctions [177]. IL-6 is produced locally by brain endothelium upon LPS injection [178] and can be further induced by IL-1β [179]. Lastly, although it does not cross the BBB [180], TGF-β accumulates in cerebral endothelium [181] and is reported to increase BBB permeability during inflammation [182].

While endothelial activation in response to cytokines is not exclusive to the hypothalamus, the circumventricular structures - including the MBH - make this organ uniquely equipped to sense, amplify, and respond to inflammatory molecules. First, the MBH is a highly vascularized structure lacking a BBB, containing mainly fenestrated capillaries, which provides circulating materials direct access to the parenchyma. Second, due to its adjacency to the third ventricle, the MBH is in direct contact with the CSF, furthering its exposure to circulating solutes within the CNS. Third, within the ependymal lining of the third ventricle are specialized cells called tanycytes. These cells are found exclusively within the ventricular lining of the hypothalamus, and extend processes deep into the parenchyma [183]. Although relatively little is known about tanycytes, evidence suggests they are heavily involved in energy homeostasis and hypothalamic neuroendocrine signaling [184]. However, the role of these cells in cachexia has not been investigated. Lastly, as described previously, the hypothalamus is the feeding center of the CNS, and many of these areas, including the PVN and ARC, express receptors for these cytokines [155,185-187].

Extensive vasculature and ample access to cytokine exposure make the hypothalamus an ideal location for signal amplification via endothelial signaling. Furthermore, in response to cytokines, cell adhesion molecules are upregulated and chemokines are secreted, subsequently leading to peripheral immune cell infiltration. All of these factors make the hypothalamus prone to perpetuation of inflammation, which is critical for development of cachexia.

Cell Adhesion Molecules

Endothelial adhesion molecules function to tether circulating leukocytes to vascular endothelium, as well as facilitate rolling and migration into tissue. There are several different adhesion molecules expressed on leukocytes and endothelial cells, which fall into two broad categories: selectins, which are expressed on endothelial cells (with the exception of L-selectin) and integrins, which are expressed on leukocytes [188].

Cellular adhesion molecules have very low levels of basal expression and are only upregulated in inflammatory conditions [189]. While expression of these molecules is necessary for an appropriate immune response, they can be markers of pathologic inflammation. Increased expression of adhesion molecules is reported in numerous systemic inflammatory diseases, such as atherosclerosis [190], heart failure [191] inflammatory bowel disease [192], allergy [193], renal disease [194], COPD [195], and cancer [196]. While the role of adhesion molecules in local immune responses has been studied extensively in nearly every condition that causes cachexia, their role in the pathophysiology of sickness behavior and cachexia itself is less well known. In patients with cancer cachexia, P-selectin polymorphisms are predictive of increased muscle wasting [197]. In an accompanying rodent model of cachexia, the P-selectin gene was a top early-induced gene [197]. Furthermore, a follow-up study found P-selectin polymorphisms were associated with increased

risk of developing cachexia in pancreatic cancer patients [198]. These studies assessed the role of P-selectin in skeletal muscle, rather than the CNS. No studies have investigated the expression and function of P-selectin or other adhesion molecules within the hypothalamus in cachexia. However, these adhesion molecules are highly upregulated in other portions of the brain during acute and chronic inflammation [199-201]. Furthermore, in rodent models of liver inflammation, cellular adhesion molecules within the CNS are implicated as important mediators of sickness behavior [200-202]. Liver disease is often associated with high plasma concentrations cytokines and endotoxins, which results in increased expression of cellular adhesion molecules, chemokines, and subsequent leukocyte recruitment. Kerfoot et al. reported that in mice with cholestatic inflammatory liver disease, there were increased levels of endothelial adhesion molecule VCAM-1. This correlated with increased levels of monocytes within brain parenchyma. Furthermore, blockade of leukocyte trafficking molecules α-4 integrin and P-selectin abolished this effect [200]. In a follow-up study administration of the same blocking antibody combination resulted in a decrease in sickness behavior, quantified by social interaction, in mice with inflammatory liver disease [201].

These results, along with substantial evidence indicating adhesion molecules play a prominent role in other neuroinflammtory diseases such as multiple sclerosis [203], Alzheimer's disease [204], and stroke [205], make it reasonable to suspect these molecules are important in the pathophysiology of cachexia. Furthermore, viral models of cachexia suggest leukocyte recruitment into the CNS, which is mediated by chemokines and adhesion molecules, also has an important role in sickness behavior [206,207] (see Section 5.2.3).

Chemokines

Chemokines are small proteins that attract and activate immune cells. They are involved in virtually all pathologies with an inflammatory component. While their role in the immune response is well known, it was only recently discovered that they are prominent mediators of CNS response to stress. In the CNS, chemokine receptors are upregulated on astrocytes [208], microglia [209], and neurons [210] during neuroinflammation. In states of stress, hypothalamic chemokines play an important role in the pathophysiology of cachexia [211]. ICV administration of numerous chemokines into the rat brain, including IL-8/CXCL8, IP-10/CXCL10, CCL2 and RANTES/CCL5, decreases short-term food intake [212]. During states of stress, these chemokines are expressed mainly in circumventricular organs [211]. Furthermore, CXCL8 expression in the PVN is implicated in signaling of stress hormones, such as ACTH and CRH [213].

Various chemokines cause a leukocyte response in the CNS via migration from the periphery into the brain parenchyma. While the role of these molecules in the hypothalamus in cachexia is not yet known, previous studies show they are important in endothelial activation and maintenance of neuroinflammation. For example, Wu et al. showed that genetic deletion of CCR2 in mice prevented endothelial activation and leukocyte recruitment into the CNS after ICV LPS injection [214]. Similarly, when CCR2 is knocked out of microglia, monocyte infiltration into the CNS is decreased during systemic inflammation. This subsequently results in decreased sickness behavior, at least as measured by diminished social interaction [201].

Furthermore, CXCL10 is associated with T-cell responses, and regulates the migration of T-cells into the brain parenchyma in response to various neuroinflammatory states [206,215]. It is induced by IFN-Y [207] and in the CNS is expressed almost exclusively in astrocytes [207,216]. While the

role of CXCL10 in the hypothalamus has not been studied, mice infected IP with the parasite *Trypanosoma brucei* showed increased CXCL10 expression in the hypothalamus [217]. Furthermore, mice with global CXCL10 deletion show decreased mortality in lymphocytic choriomeningitis virus (LCMV) infection, a viral model of cachexia [206,207]. However, these knockout studies did not assess hypothalamic infiltration or sickness behavior. Future studies should investigate whether CCR2 or other chemokine knockouts can attenuate additional inflammation or alleviate cachexia symptoms.

High levels of chemokines within the brain, along with increased expression of adhesion molecules on endothelial cells suggest a mechanism of recruiting peripheral cells into the CNS during neuroinflammation and a potential role for these cells in cachexia. While the role of peripheral leukocytes has not been studied in most forms of cachexia, for over 20 years immunologists have been studying a murine model of viral CNS infection that induces profound wasting. This wasting is mediated almost entirely by infiltration of peripheral lymphocytes into the CNS. As described in the following section, this model presents a powerful means for investigating the role of leukocytes in viral cachexia, and a framework for studying these cells in other causes of sickness behavior.

Leukocyte recruitment

While leukocyte trafficking into the CNS is evident in several neurological diseases that result in cachexia, their role in the pathophysiology of hypothalamus mediated sickness behavior is unknown. However, studies of LCMV infection demonstrate that peripheral leukocytes enter the CNS and play an important role in maintaining cachexia [218-220]. T-cells release a number of cytokines capable of producing an illness response when injected centrally, including IL-6 and LIF

[221,222]. In animals inoculated ICV with LCMV, anorexia and lethargy are maintained by MHC II restricted CD4+ cells [218]. Mice treated with anti-CD8 antibodies or HLA Class I knockout then infected with LCMV experienced nonlethal chronic wasting, losing approximately 25% of their body weight over the course of 32 days before recovering [218].

While the LCMV model is used extensively from the immunology standpoint to study persistent infections, it has rarely been used to study cachexia [220,223]. Kampershroer and Quinn infected CD8+ T-cell deficient mice with LCMV via ICV inoculation and found that wasting was dependent on IFN-γ and IL-1, with IL-6 contributing to symptoms [223]. However, in contrast to previous cachexia literature, wasting was not dependent on TNFα. In a recent study, Stamm et al. injected WT mice with LCMV virus IV at different doses and sought to identify dose effects and further characterize mediators of wasting. The authors found a positive correlation between weight loss and viral dose, but were unable to attenuate symptoms with IFN-γ or IL-1 blockade [220]. Nevertheless, these studies show the LCMV model is a potent inducer of cachexia and these intriguing results suggest it can be a means of making new discoveries in the mechanisms and treatment of cachexia.

Future studies are needed to determine whether lymphocyte recruitment in LCMV models is a byproduct of elevated numbers of lymphocytes recruited systemically to fight infection, or a mediator of hypothalamic inflammation and an integral part of the mechanism of cachexia. In addition to LCMV, other mouse models of sickness behavior demonstrate that systemic inflammation induces leukocyte recruitment in the CNS. In models of inflammatory liver disease, monocytes were found in various regions of the brain and produced TNFα, amplifying the neuroinflammatory response [200,201]. Blocking entry of these molecules to the CNS attenuated

sickness behavior. In contrast to LCMV studies, the leukocyte population entering the CNS was almost exclusively monocytes. Unfortunately, the hypothalamus was not assessed as a potential location for leukocyte recruitment. Future studies are needed to investigate whether monocytes play a role in the hypothalamus in inflammatory liver disease.

Lastly, in a rodent model of chronic stress, monocytes were reported to infiltrate the CNS, including the PVN [158,224]. Future studies will be necessary to assess whether leukocyte recruitment is specific to the hypothalamus and determine the characteristics and effector functions of these cells.

Recent studies demonstrate that peripheral leukocytes enter the brain in cachexia and play a role in the neuroinflammatory response that causes sickness behavior. In addition to the studies mentioned above, studies in cancer immunology have shown that leukocytes play an important role in modulating inflammatory immune response in the brain [225]. However, the specificity and characteristics of these cells have yet to be fully elucidated. Further studies are needed to determine if these cells enter the hypothalamus, and the role of their effector functions.

Concluding remarks on central nervous system

Whether in the context of acute or chronic inflammatory insults, a growing body of evidence implicates the hypothalamus as a driving force in the pathophysiology of the acute illness response and cachexia. The hypothalamus orchestrates orexigenic and anorexigenic drives in both physiological and pathophysiological states. A variety of dietary stressors, infectious stimuli, and chronic illnesses are able to alter the behavior of these cell populations. Anatomical considerations such as the attenuated BBB of the median eminence allow direct sensing of

DAMPs and PAMPS, as well as indirect sensing of threats via peripheral immune responses giving rise to cytokines. Hypothalamic exposure to any of numerous inflammatory stimuli triggers an acute illness response, caused by IL-1β and TNF-α, leading to fever, lethargy, anorexia, and weight loss. These molecules act acutely by binding to receptors on circumventricular neuronal populations, such as POMC and AgRP, triggering a feed-forward loop involving skeletal muscle catabolism and lipolysis. While cytokines are important mediators of acute illness responses, their effects are rapidly attenuated and undergo tachyphylaxis over time, implicating additional mediators in chronic hypothalamic inflammation. The key paracrine and autocrine signaling pathways local to the hypothalamic neurons and glia remain yet to be fully elucidated, but the recent discovery of the separate ontogeny of microglia from peripheral immune cells provides an exciting opportunity for understanding how inflammation differs in the CNS. Furthermore, cytokines can also act on endothelial cells within the rich capillary supply of the hypothalamus, leading to further production of cytokines, increased expression of cell adhesion molecules such as selectins and integrins, and secretion of chemokines. Subsequently, peripheral leukocytes are recruited into the CNS, where they secrete cytokines and amplify neuroinflammation. While LCMV and chronic liver inflammation rodent models provide insight on the role of peripheral leukocytes in cachexia, no studies have addressed their function within the hypothalamus. Further studies and characterization are needed to determine whether these cells enter the MBH or adjacent structures in states of inflammation. Even though many unknowns persist, one thing remains clear: the hypothalamus is crucial in both the acute sickness response and cachexia, and an improved understanding of its role in these processes could prove essential in uncovering the elusive therapeutic solution for these conditions.

Mechanisms of cachexia: muscle

Perhaps the best understood aspect of cachexia, and certainly the most studied, is muscle wasting. As one of the most vivid and definitional parts of the cachexia disease process, muscle wasting and sarcopenia are vitally important disease manifestations to focus on because of their direct link to multiple aspects of patient prognosis. Muscle atrophy in cachexia is due to a combination of impaired myogenesis and increased muscular catabolism [226,227]. One of the earliest pieces of evidence that cachexia is an independent target for cancer survival was a 2010 report on blockade of the activin IIB receptor. While this therapy has no benefit toward tumor burden, it extended survival of animals in a muscle-specific mechanism by decreasing activation of the ubiquitin-proteosome system and induction of atrophic genes [228]. Many aspects of muscle wasting are derived from inflammatory signals, as illustrated by the higher levels of circulating TNF, IL-1β, LIF, and IL-6 observed in sarcopenia [229,230] Among these, IL-6 is a particularly robust driver of muscle wasting via its actions on STAT3 signaling [231]. In addition, elevated levels of TGFβ superfamily cytokines such as myostatin, GDF11, GDF15, and activins are found during cancer cachexia and are directly linked to muscle catabolism [232]. Importantly, not all drivers of muscle wasting in cachexia are due to inflammatory mediators acting directly on muscle: the central nervous system is also able to mediate muscle wasting during cachexia by activation of the hypothalamic-pituitary-adrenal axis [90]. Lastly, it is important to consider that chemotherapy itself can result in muscular catabolism, likely by a combination of direct cytotoxicity to muscle and increased production of inflammatory mediators [233].

Downstream of these diverse activators of catabolism, the myoblast responds with activation of both ubiquitin-proteosome and autophagy systems. E3 ubiquitin ligases such as *Murf1* and *Mafbx* are commonly upregulated in mouse models of cachexia, under the control of

the transcription factors *Foxo1* and *Foxo3* [102,234]. In addition to this system, *Foxo* proteins regulate induction of the autophagy system, which can further contribute to muscle breakdown [235]. Key dysregulated targets of the autophagy system in muscle include beclin 1, autophagy protein 5, and MAPILC3B [236]. Other regulatory pathways of muscle include AKT, angiotensin II, and C/EBPβ [237]. Activation of these combined molecular pathways result in proteolysis of muscle, and when coupled to loss of muscle regenerative signals, the net result is muscle atrophy. A large amount of work still needs to be done in the clinical arena to identify key drivers of muscle catabolism in patient populations, as well as to define effective targets for restoration of muscular homeostasis during cachexia.

Treatment of cachexia

Given the multiple systems involved in cachexia, treatment remains exceptionally challenging. At this time, the only FDA-indicated therapy for cachexia is megestrol acetate (17α-(acetyloxy)-6-methylpregna-4,6-diene-3,20-dione), a synthetic progesterone derivative. While mesgestrol acetate first gained FDA approval for treatment of breast cancer and endometrial carcinoma, clinical observation demonstrated that high doses of the drug were also capable of inducing weight gain and enhancing appetite.[238] In 1993, further studies led to megestrol acetate's FDA approval for use in cachexia, a wasting condition associated with diverse chronic illnesses including cancer, HIV, COPD, heart disease, and kidney failure. Though many new agents have been investigated in the treatment of cachexia, megestrol acetate remains the mainstay of cachexia therapy in current medical practice. Many of the effects of megestrol acetate are dose-dependent. At low doses, it acts on the pituitary to reduce intrinsic gonadotropin levels, making it useful as a component of hormonal contraception or as a treatment for breast and endometrial cancer.[239] However, at high doses, it acts as a potent orexigenic agent, capable of inducing weight

gain and increased appetite in the context of severe and chronic illness.[240] Unfortunately, megesterol acetate has not shown to be effective in treating any of the most serious aspects of cachexia, namely lean mass wasting and associated risk of increased mortality, and it also is associated with an increased risk of thromboembolic events and death [241]. In a similar vein, corticosteroids can be used to improve appetite and sense of well-being in the short term, but should generally be avoided because of harmful side effects including myopathy [242].

Newer agents in cachexia include ghrelin and ghrelin mimetics, which target the growth hormone secretagogue receptor to result in appetite stimulation and improved anabolism [243]. The most successful drug in this class thus far is anamorelin, which has demonstrated benefit toward lean body mass in two clinical trials of non-small cell lung carcinoma [244,245]. Among the most exciting targets in recent years is GDF15, a TGFβ superfamily cytokine which targets the brainstem-restricted receptor GFRAL. GDF15 is released in response to tissue damage and malignancy, resulting in anorexia dependent on GFRAL-expressing neurons of the area postrema [246]. Given that GDF15 is also associated with PDAC tumorigenesis, inhibition of this molecule may provide multimodal benefit during pancreatic cancer [247]. Other strategies include the anabolic-catabolic transforming agent espindolol, a dual beta blocker and 5-HT1α agonist. In a phase II trial of patients with lung or colorectal cancer, espindolol was associated with increased lean and total mass, as well as improvements in handgrip strength [248]. Because inflammatory mediators are thought to play a role in cachexia's initiation and maintenance, targeted biologics and anti-inflammatories are another set of heavily investigated agents in cachexia. However, these have not demonstrated benefit in clinical trials thus far – indeed, three separate trials on TNF inhibitors failed to show benefit on any aspect of cachexia [249-251]. Similarly, clinical trials of anti-inflammatories such as NSAIDs, thalidomide, and omega-3 fatty acids have not yielded

improvements in cachexia status [46]. Overall, while there are promising therapies in the pipeline for the treatment of cachexia, the fact remains that there are no effective FDA-approved therapies at this juncture. At this juncture, further research is urgently needed to elucidate mechanisms and identify viable targets for targeting cancer-associated cachexia.

IV. Working hypothesis and experimental outline

In order to extend and improve the lives of patients with pancreatic cancer, novel approaches are needed to target the malignancy and to ameliorate cachexia. In my own approach to this problem, I framed this as an extension of the concept of the therapeutic window. Disease-intrinsic limitations on the therapeutic window in pancreatic cancer include both tumor burden and cachexia. To extend survival in PDAC, one can target either or both of these two factors using a systems-integrated approach. With this in mind, my experiments aimed to establish and test a PDAC model in which tumor effects and systemic effects could both be assessed as primary outcomes. **I hypothesized that PDAC can be accurately modeled in mice, that TLR7 agonists can be delivered in a tolerable manner in healthy animals, and that TLR7 agonists can improve tumor burden and cachexia status in murine models of PDAC.** To investigate these hypotheses, my findings are delineated in three stages:

1) **Establish a reliable mouse model of pancreatic cancer cachexia**

   The first task was to implement and characterize a murine model of cachexia with pancreatic cancer as a primary etiology. For this, I used an epithelial clone derived from the $Kras^{LSL.G12D/+}$ $p53^{LSL.R172H/+}$ $Pdx\text{-}Cre^{tg/+}$ (KPC) genetically engineered mouse model of PDAC [252]. This model was characterized using three routes of administration (subcutaneous, intraperitoneal, and orthotopic). We assessed a wide variety of manifestations that occur in patients with cachexia, ranging from behavior to molecular physiology. In both intraperitoneal and orthotopic routes, we found that implanted KPC-

derived epithelial cells consistently produce pancreatic masses resulting in hypophagia, weight loss, decreased locomotor activity, muscle wasting, adipose tissue wasting, and endocrine changes consistent with cachexia.

2) **Elucidate mechanisms and tolerability of the TLR7/8 agonist R848**

In the second study, I sought out to understand the full behavioral and molecular kinetics of R848, a Toll-like receptor 7 (TLR7) agonist with potential for treating PDAC. In this study, we found that R848's mechanisms in the CNS are attributable to effects on microglia, the resident immune cell of the brain. Chronic treatment was associated with attenuation of sickness responses, indicating that R848 can be tolerable if delivered appropriately. Further, we unveiled that molecular and behavioral tachyphylaxis to continued R848 appears to induce immune tolerance to other canonical innate inflammatory signals such as lipopolysaccharide.

3) **Explore effects of R848 on PDAC tumor response and cancer cachexia**

After firmly establishing a murine model of pancreatic cancer associated cachexia and the safety of R848, I evaluated R848 in the context of PDAC-associated cachexia. In this framework, both tumor response and systemic responses (e.g. cachexia) are weighted as equally important primary determinants of therapeutic outcome. These studies revealed that R848 induces immune-mediated anti-tumor responses while also alleviating cachexia manifestations, setting it apart from many traditional chemotherapies. To maximize experimental rigor and gauge the translational relevance of TLR7 agonists in PDAC, these studies compared multiple clones of KPC-derived epithelial cells and integrated patient data on tumor gene expression.

V. Establishment and characterization of a novel murine model of pancreatic cancer cachexia

Katherine A. Michaelis, Xinxia Zhu, Kevin G. Burfeind, Stephanie M. Krasnow, Peter R. Levasseur, Terry K. Morgan, Daniel L. Marks

Adapted from the Journal of Cachexia, Sarcopenia, and Muscle, October 2017 [253]

Abstract:

Background: Cachexia is a complex metabolic and behavioral syndrome lacking effective therapies. Pancreatic ductal adenocarcinoma (PDAC) is one of the most important conditions associated with cachexia, with greater than 80% of PDAC patients suffering from the condition. To establish the cardinal features of a murine model of PDAC-associated cachexia, we characterized the effects of implanting a pancreatic tumor cell line from a syngeneic C57BL/6 $KRAS^{LSL.G12D/+}$ $P53^{R172H/+}$ Pdx-$Cre^{+/+}$ (KPC) mouse.

Methods: Male and female C57BL/6 mice were inoculated subcutaneously, intraperitoneally, or orthotopically with KPC tumor cells. We performed rigorous phenotypic, metabolic, and behavioral analysis of animals over the course of tumor development.

Results: All routes of administration produced rapidly growing tumors histologically consistent with moderate to poorly differentiated PDAC. The phenotype of this model was dependent on route of administration, with orthotopic and intraperitoneal implantation inducing more severe cachexia than subcutaneous implantation. KPC tumor growth decreased food intake, decreased adiposity and lean body mass, and decreased locomotor activity. Muscle catabolism was observed in both skeletal and cardiac muscle, but the dominant catabolic pathway differed between these tissues. The wasting syndrome in this model was accompanied by hypothalamic inflammation,

progressively decreasing brown and white adipose tissue uncoupling protein 1 (*Ucp1*) expression, and increased peripheral inflammation. Hematologic and endocrine abnormalities included neutrophil-dominant leukocytosis and anemia, and decreased serum testosterone.

Conclusions: Syngeneic KPC allografts are a robust model for studying cachexia that recapitulate key features of the PDAC disease process and induce a wide array of cachexia manifestations. This model is therefore ideally suited for future studies exploring the physiological systems involved in cachexia and for preclinical studies of novel therapies.

Background

Among the direst complications of chronic disease, cachexia is a multisystemic syndrome involving metabolic derangements, lean mass catabolism, and behavioral changes including anorexia and fatigue [62,142]. Cachexia's impact extends beyond its widespread harm to quality of life, and it is estimated to be the direct cause of death in 20-30% of all cancer patients [254,255]. In addition, cachexia contributes to cancer-associated morbidity by weakening patients to the point they cannot tolerate chemotherapy or surgery [256-258]. Despite the widespread need for improved cachexia therapies, there remain very few treatments for this condition [238,240]. To design a therapy that addresses the root causes and manifestations of cachexia, it will be necessary to expand upon understanding cachexia pathophysiology through preclinical modeling. Because cachexia is by definition linked to its underlying disease processes, we sought to create a model fulfilling three criteria: 1) the underlying disease process is known to cause cachexia in humans, 2) the disease process and resultant cachexia can be induced reproducibly and consistently in a model organism, and 3) the model recapitulates a maximal number of the systems and processes implicated in cachexia.

With these criteria in mind, an ideal pathophysiological framework for cachexia research is pancreatic ductal adenocarcinoma (PDAC). Among all forms of malignancy, PDAC is among the most highly associated with cachexia, with an estimated 83% of patients suffering from the condition [259-261]. Furthermore, up to 20% of cancer patients die directly from cachexia, and many more become unable to tolerate chemotherapy regimens or surgery specifically because of decreased performance status associated with cachexia [262-267]. Murine cachexia research has historically focused on four models: Lewis lung carcinoma (LLC), C26 colorectal adenocarcinoma (C26), patient-derived tumor xenografts (PDX), and genetically engineered mouse models (GEMMs). While these models provided a majority of the current understanding of cachexia, recent studies have highlighted the need for expanding upon and rigorously characterizing experimental methods for studying cachexia. For these reasons, we aimed to generate and establish the cardinal features of a PDAC cell line-induced, syngeneic, immunocompetent murine cachexia model.

To examine PDAC cachexia, we selected a cell line isolated from the PDAC lesion of a C57BL/6 mouse genetically modified to conditionally express $KRAS^{G12D}$ and the point mutant $p53^{R172H}$ under a pancreas-specific Pdx1 Cre driver (KPC) [268]. KPC is one of the best-established murine models of PDAC, recapitulating a common oncogenic mutation in PDAC combined with a common tumor suppressor mutation event associated with progression from PanIN III lesions to fulminant PDAC [269]. Using this cell line as a syngeneic KPC allograft, we tested the effects of three different routes of administration: subcutaneous (SQ), intraperitoneal (IP), and orthotopic (OT) pancreatic implantation. Animals were assessed for changes in body composition such as lean mass loss, fat mass loss, muscular atrophy, and neuroendocrine disturbances. In addition, animals were monitored for behaviors including food intake and locomotor activity. Finally, site-specific

manifestations of cachexia were assessed throughout a variety of tissues, including the central nervous system, fast-twitch and slow-twitch fiber enriched skeletal muscle groups, heart, liver, brown and white adipose tissue, and blood.

Results

KPC allografts result in anorexia and body composition changes consistent with cachexia

KPC allografts lead to sickness behaviors, weight loss, and mortality, consistent with both PDAC and cachexia. The trajectory of illness follows a staged and reproducible series of manifestations, with onset of anorexia at 5-8 days and mortality at 11-14 days post-inoculation (Figure 1). All three routes of implantation resulted in rapid tumor growth without evidence of graft rejection. Despite being a robust route of administration for other models of cancer cachexia, subcutaneous implantation of KPC typically reaches tumor burden endpoint (tumor volume in excess of 10% of body weight) prior to the onset of late-stage cachexia (Figure 1a). Although this was a consistent finding in younger animals, we did see an exception in an older female cohort, in which subcutaneous tumor implantation resulted in relative decreases in cumulative food intake in the final 7 days from 1454 ± 24 mg/g body weight in controls to 1011 ± 14 mg/g body weight in tumor-bearing animals ($p < 0.0001$, n=4/group). Simultaneously, tumor-bearing animals gained weight overall due to tumor progression ($F(1,60) = 67.15$, $p < 0.0001$, n = 4/group) (Supplemental Figure 1). In contrast, intraperitoneal tumor growth in males consistently resulted in anorexia within 8 days, with relative reductions in cumulative food intake over the final 6 days from 663.8 ± 21.8 mg / g body weight in controls to 434.0 ± 35.2 mg/g body weight in tumor-bearing animals ($p < 0.001$, n=4-5/group), despite unchanging total body weight (Figure 1b). In females, intraperitoneal tumor growth resulted in anorexia within nine days, and reduced food intake over the final five days

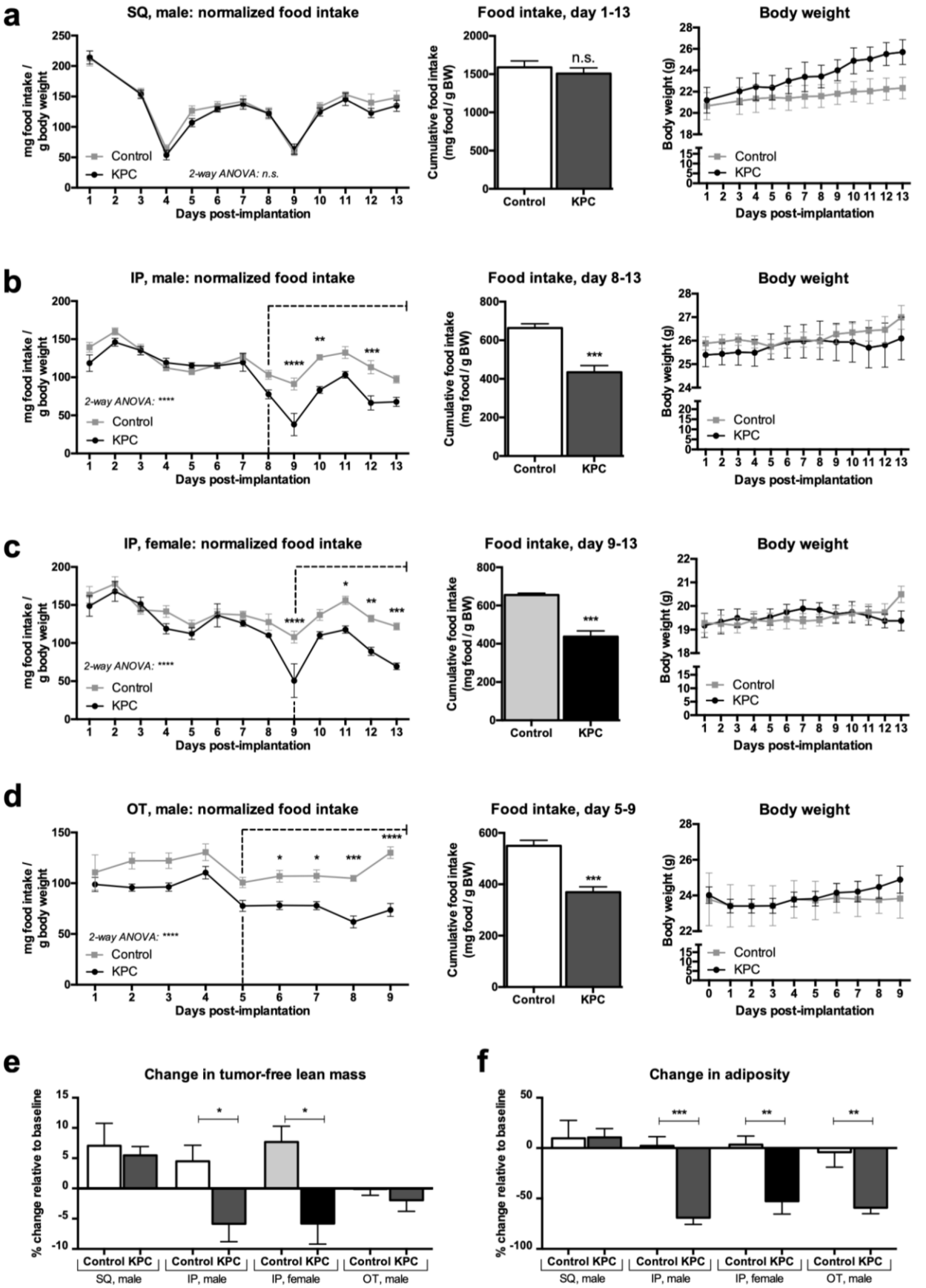
a
SQ, male: normalized food intake
mg food intake / g body weight
Control
KPC
2-way ANOVA: n.s.
Days post-implantation
Food intake, day 1-13
Cumulative food intake (mg food / g BW)
n.s.
Control
KPC
Body weight
Body weight (g)
Control
KPC
Days post-implantation
b
IP, male: normalized food intake
2-way ANOVA: ****
Food intake, day 8-13
***
Body weight
c
IP, female: normalized food intake
2-way ANOVA: ****
Food intake, day 9-13
***
Body weight
d
OT, male: normalized food intake
2-way ANOVA: ****
Food intake, day 5-9
***
Body weight
e
Change in tumor-free lean mass
% change relative to baseline
Control KPC
SQ, male
IP, male
IP, female
OT, male
f
Change in adiposity

Fig. 1: *Food intake, body weight, and body composition changes in KPC-induced cachexia.*

Dotted line demarcates cachexia stage as defined by continued presence of anorexia. Food intake throughout post-implantation phase, cumulative food intake during cachexia phase, and body weight over post-implantation phase in (a) subcutaneous, (b) intraperitoneal with male subjects, (c) intraperitoneal with female subjects, and (d) orthotopic routes of administration. Body composition changes were characterized with regard to lean mass (e) and adiposity (f). *, P<0.05; **, P<0.01; ***, P<0.001; ****, P<0.0001.

---

from 655.2 ± 9.2 mg/g body weight in controls to 437.4 ± 30.3 mg/g body weight in tumor-bearing animals ($p < 0.0001$, n=5/group), despite stable total body weight (Figure 1c). Similarly, orthotopic tumor growth resulted in a reduction in cumulative food intake over the final 5 days from 549.7 ± 21.3 mg/g body weight in controls to 369.4 ± 20.6 mg/g body weight in tumor-bearing animals ($p < 0.001$, n=5/group), without a change in total body weight (Figure 1d). The anorexia resulting from intraperitoneal and orthotopic tumor implantation typically exceeds that seen in subcutaneous tumor implantation, both in time of onset and degree of severity.

Given that KPC-engrafted animals gain weight from tumor growth while losing weight from tissue catabolism, NMR body composition analysis was used to determine the degree of lean and adipose tissue loss. The tumor-free lean mass is defined as the lean mass measurement on NMR minus the tumor mass on necropsy, given that PDAC tumor volume is detected as lean mass on NMR. While control male mice gained 4.5 ± 2.7% lean mass over the course of 13 days, male mice implanted IP with KPC lost 5.9 ± 3.0% tumor-free lean mass ($p < 0.05$, n=4-5/group, Figure 1e). Similarly, control female mice gained 7.7 ± 2.6% lean mass over the course of 13 days, while female mice implanted IP with KPC lost 5.8 ± 3.4% tumor-free lean mass ($p < 0.05$, n=5/group,

Figure 1e). In addition to lean mass wasting, KPC produces marked adipose tissue wasting. Control male mice gained 2.2 ± 9.0% fat mass over the course of 13 days, whereas male mice implanted IP with KPC lost 69.0 ± 6.6% fat mass ($p < 0.0001$, n=4-5/group, Figure 1f). Control female mice gained 3.5 ± 8.4% fat mass over the course of 13 days, while female mice implanted IP with KPC lost 52.6 ± 12.8% fat mass ($p < 0.01$, n=5/group, Figure 1f). Overall, wasting in the KPC model is observed in both lean and adipose tissue compartments, and does not significantly differ between sexes.

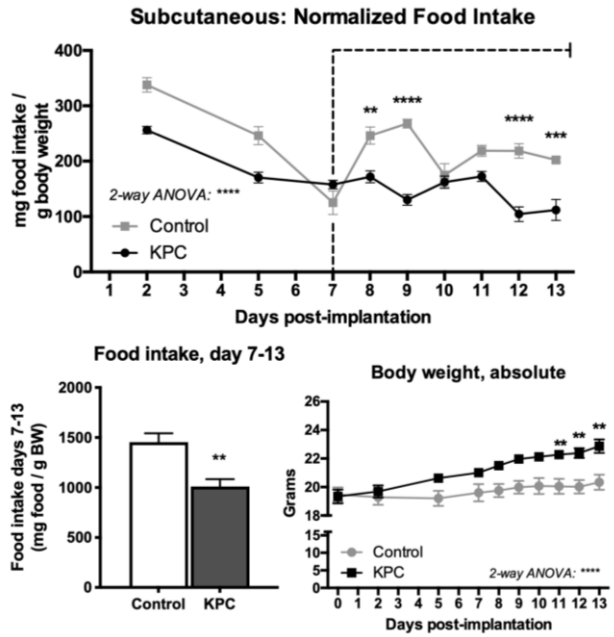

Fig. S1: *Food intake and body weight changes in an older female cohort demonstrating subcutaneous KPC-induced cachexia.*

Dotted line demarcates cachexia stage as defined by continued presence of anorexia. Food intake throughout post-implantation phase, cumulative intake during cachexia phase, and body weight over post-implantation phase in subcutaneous routes of administration in a 4-month old female cohort. *, P<0.05; **, P<0.01; *** P<0.001; ****, P<0.0001.

Decreased locomotor activity is an early and consistent feature of KPC-induced cachexia

Fatigue and lethargy are among the most significant and least therapeutically addressed manifestations of cachexia, and it is therefore important that cachexia models recapitulate these traits. Indeed, decreased locomotor activity (LMA) is an early manifestation of KPC-induced cachexia. Analyses of LMA were subdivided into 12h light and dark cycles, corresponding to sleep

and wake cycles respectively. In KPC-engrafted males, the cumulative sum of average wake cycle counts per hour during anorexia-defined cachexia decreased from 788 ± 26 to 458 ± 42 in tumor-bearing animals relative to controls (p = 0.0002, n=4-5/group, Figure 2a), with no changes in sleep cycle LMA. In KPC-engrafted females, the cumulative sum of average wake cycle counts/hour during anorexia-defined cachexia decreased from 707 ± 55 to 370 ± 37 in tumor bearing animals relative to controls (p = 0.001, n=5/group, Figure 2c). In addition, KPC-engrafted females exhibited decreased LMA during sleep cycle, with a decrease from 373 ± 27 to 266 ± 23 in tumor-bearing animals relative to controls (p = 0.02, n=5/group, Figure 2d). The onset of activity loss is sexually dimorphic: females decrease LMA within 7-8 days of tumor growth, whereas males do

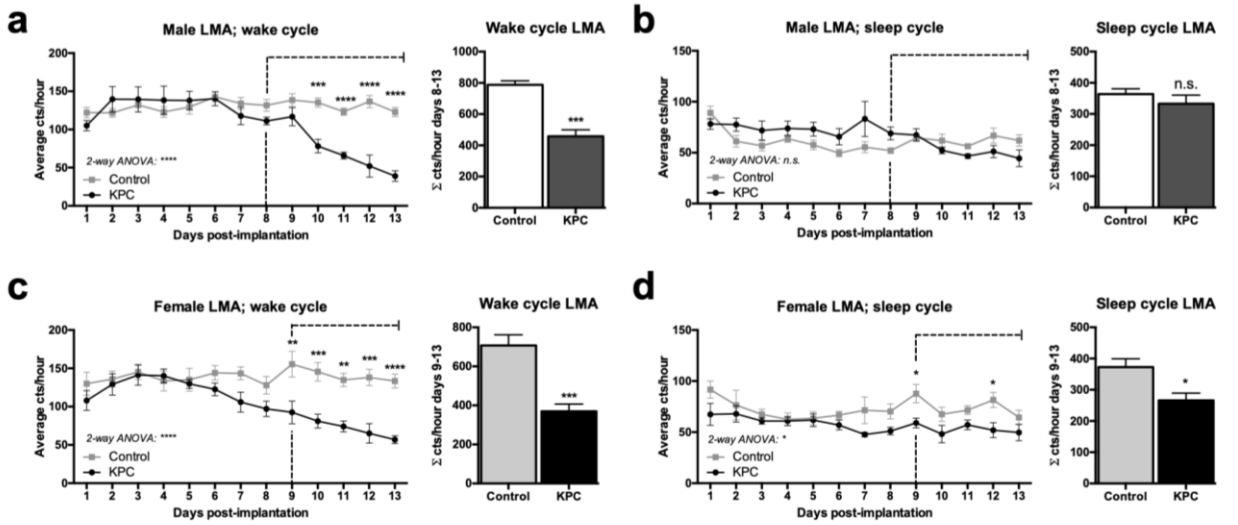

Fig. 2: *KPC engraftment progressively decreases locomotor activity (LMA) in both sexes.*
Locomotor activity in average counts/hour, with cumulative sum of counts/hour during anorexia-defined cachexia stage. Dotted line demarcates the onset of anorexia. (a) Wake cycle LMA in counts per hour in males and wake cycle cumulative counts/hour during anorexia stage, (b) Sleep cycle LMA in counts per hour in males and sleep cycle cumulative counts/hour during anorexia stage, (c) Wake cycle LMA in counts per hour in females and wake cycle cumulative counts/hour during anorexia stage, (d) Sleep cycle LMA in counts per hour in females and sleep cycle cumulative counts/hour during anorexia stage.

not exhibit significant losses in LMA until 9-10 days of tumor growth. Furthermore, only females demonstrate a decrease in sleep cycle LMA. It is important to note that in females, a decrease in LMA is the first measurable behavioral change in KPC-induced cachexia and precedes anorexia by up to 2 days. In contrast, males demonstrate a simultaneous onset of anorexia and decreased LMA.

KPC allograft gross and microscopic features

The three routes of administration each resulted in distinct patterns of tumor growth, with particularly strong differences between the subcutaneous group versus the intraperitoneal and orthotopic groups. Subcutaneously implanted KPC cells formed only primary tumor masses isolated to the site of injection, with well-defined borders. Orthotopic KPC implants into the pancreas show ragged infiltration and patchy gross morphology. This type of intraperitoneal transplantation did not lead to seeding of other peritoneal surfaces, or metastases to other organs. In contrast, intraperitoneal implantation of KPC led to multifocal tumor growth on peritoneal surfaces, but with the majority of tumor growth localized to the pancreas. Hemorrhagic ascites were variably present in intraperitoneal and orthotopic tumor models. Interestingly, tumor growth was sexually dimorphic, with males developing larger tumor masses than female animals (Supplemental Figure 2).

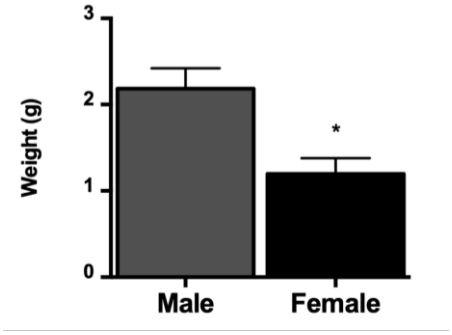

Fig. S2: *Tumor burden at necropsy in male and female animals.*

Total tumor weight at time of end-stage cachexia in males and females in the same experiment implanted with intraperitoneal KPC. *, $p<0.05$

Histologic sections strengthened these gross observations. The PDAC was moderate to poorly differentiated with conspicuous mitotic figures and coagulative tumor cell necrosis. In the subcutaneous allografts, tumor cells were arranged in nodules with well-circumscribed borders. There was minimal desmoplastic change to the stroma and no conspicuous host inflammatory response (Figure 3). In contrast, the orthotopic and intraperitoneal allografts showed ragged tumor infiltration of the pancreas and a marked acute and chronic inflammatory host response. Because intraperitoneal administration reliably induces pancreatic tumor growth without requiring surgery, we chose to further characterize the intraperitoneal model using a systems-based approach.

Skeletal and cardiac muscle catabolism in KPC engrafted animals proceeds through distinct mechanisms and are not sexually dimorphic

Two key subsets of muscle tissue, skeletal and cardiac, were examined in KPC engrafted mice at end-stage cachexia. KPC tumor burden resulted in a progressive decrease in gastrocnemius weight, with no changes at day 5, a decrease from 5.23 ± 0.21 to 4.86 ± 0.13 mg/g initial body weight at day 7 ($p<0.05$, n=5/group), and a further decrease from 5.09 ± 0.17 to 4.15 ± 0.22 mg/g initial body weight at day 10 ($p<0.0001$, n=5/group) (Figure 4a). Late-stage KPC engrafted animals demonstrated a decrease in heart weight from 126.7 ± 3.0 to 95.7 ± 5.1 mg in males ($p<0.001$, n=4-5/group), and 96.9 ± 3.8 to 76.9 ± 2.1 mg in females ($p=0.0019$, n=5/group) (Figure 4b). In addition, animals sacrificed in mid-stage cachexia two days following the onset of anorexia demonstrate muscle loss in the fast-twitch fiber dominant muscles gastrocnemius, tibialis anterior, quadriceps, and to a lesser extent, the slow-twitch fiber dominant muscle soleus (Figure 4c). Skeletal muscle catabolism was driven by a combination of E3 ubiquitin ligase induction and autophagy, both of which increased in a time-dependent manner (Figure 4d). By

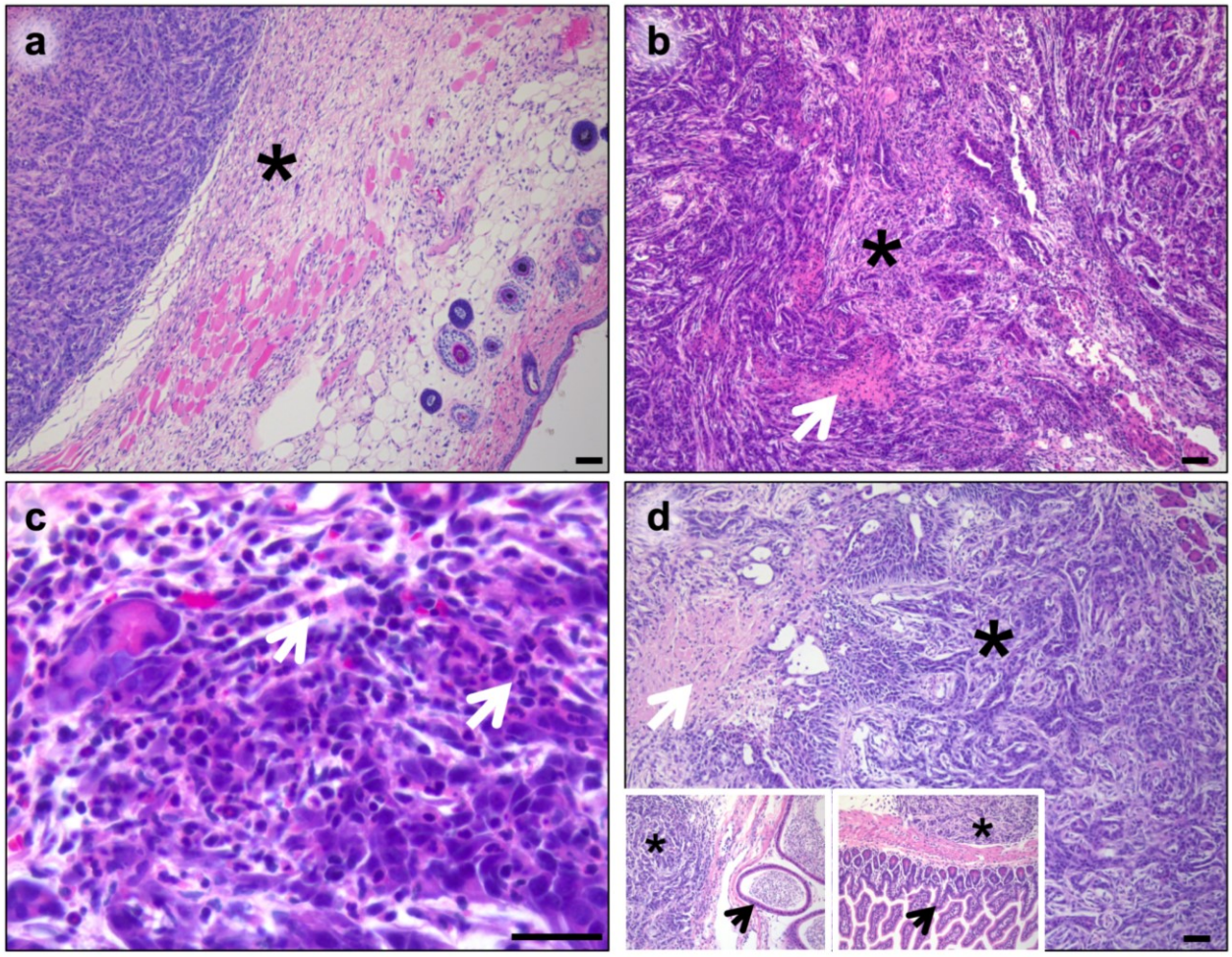

Fig. 3: *Histopathologic characteristics of KPC allografts.* (a) Subcutaneous implantation of KPC allographs shows well demarcated tumor nodule with minimal desmoplastic stroma (asterisk), no geographic necrosis, and no acute or chronic inflammation. (b) In contrast, orthotopic implantation into the pancreas leads to ragged infiltration of the organ with pronounced desmoplastic stroma, geographic necrosis (arrow) and acute inflammation (c). (d) Intraperitoneal implantation results in honing of tumor cells to the pancreas with similar histologic findings to orthotopic implantation. However, IP administration also seeds multiple peritoneal sites (e.g. epididymis and small bowel [insets]). Sections are stained with hematoxylin and eosin and photographed with 10x objective lens. Scale bar is 100um.

end stage, gastrocnemius catabolism in KPC-bearing animals versus controls coincided with a 21.2 ± 3.4 fold relative increase in gene expression of catabolic E3 ubiquitin ligase *Mafbx*, a 27.9 ± 9.2 fold increase in *Murf1*, a 4.80 ± 0.85 fold increase in *Foxo1*, a 5.39 ± 0.82 fold increase in autophagy gene *Bnip3,* a 4.82 ± 0.72 fold increase in *Ctsl,* a 7.8 ± 1.3 fold increase in *Gabarapl,* and a 7.5 ± 1.9 fold increase in adhesion molecule *Selp* ($p<0.01$ for all, n = 4/group) (Figure 4d). Cardiac atrophy in both sexes was accompanied by increased autophagy-related cardiac muscle gene expression of *Bnip3*, *Ctsl*, and *Gabarapl*, with relatively less induction of *Mafbx* and *Murf1* compared to skeletal muscle, and similar upregulation of *Selp* (Figure 4e) [88]. Gene expression analysis comparing gastrocnemius, tibialis anterior, and quadriceps with soleus demonstrated relative sparing of slow-twitch muscle from activation of the ubiquitin proteasome and autophagy catabolic pathways during mid-stage KPC cachexia (Figure 4f).

KPC engraftment results in hypothalamic inflammation and activation of the hypothalamic-pituitary-adrenal axis

A large body of evidence demonstrates that the hypothalamus is a critical driver of cachexia, transducing systemic inflammatory messages stemming from acute and chronic disease processes into a local and paracrine inflammatory response in the central nervous system [270-272]. Consistent with this evidence, KPC induces an array of genes responsive to inflammatory stimuli in the hypothalamus. Compared to controls, tumor-engrafted animals demonstrated a 3.39 ± 0.66 fold increase in *Il1β* ($p<0.001$), a 4.5 ± 1.1 fold increase in *Il4* ($p<0.01$), a 2.79 ± 0.11 fold increase in *Il1r1* ($p<0.0001$), a 43.1 ± 7.6 fold increase in *Selp* ($p<0.001$), a 2.63 ± 0.16 fold increase in *Arg1* ($p<0.01$), and a 1.56 ± 0.17 fold increase in *Nos2* ($p<0.01$) (n=6/group) (Figure 5a). However, there were no differences in hypothalamic gene expression of the gp130 cytokines *Il6* and *Lif*. The induction of inflammation is most pronounced in the hypothalamus and is not observed in other

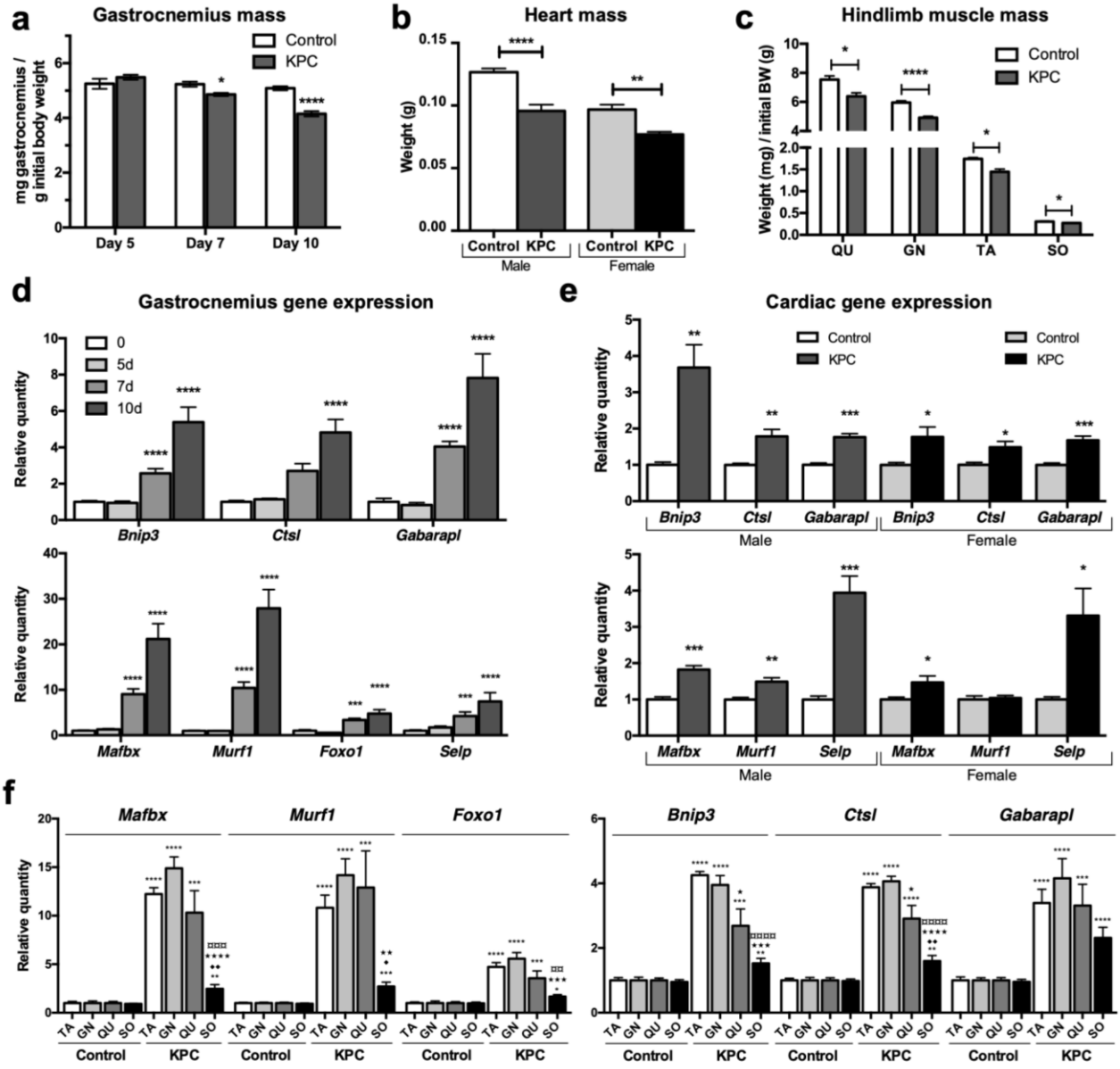

Fig. 4: *KPC engraftment results in catabolism and loss of skeletal and cardiac muscle.*

(a) Gastrocnemius mass in KPC and control animals sacrificed at designated timepoints. (b) Cardiac muscle at end-stage KPC cachexia in male and female animals. (c) Fast-twitch muscle groups gastrocnemius (GN), tibialis anterior (TA), quadriceps (QU), and soleus (SO) weights in control and KPC-engrafted animals during mid-stage cachexia. (d -f) Autophagy, ubiquitin proteasome pathway, and inflammatory gene expression gastrocnemius (d), cardiac muscle (e), and representative fast-twitch and slow-twitch muscles of the hindlimb (f). *, P<0.05; **, P<0.01; ***, P<0.001, **** P<0.0001; *, significantly different versus matched muscle control; ¤, significantly different versus KPC TA; ⋆, significantly different versus KPC GN; ⬥, significantly different versus KPC QU.

brain structures such as the cerebral cortex (Figure 5b). In alignment with previous findings that muscle atrophy during inflammatory stimuli is mediated by hypothalamic-pituitary-adrenal activation, end-stage KPC engrafted animals demonstrate a 1.77 ± 0.19 fold increase in hypothalamic expression of corticotropin-releasing hormone ($p<0.05$) (Figure 5c) [88,90].

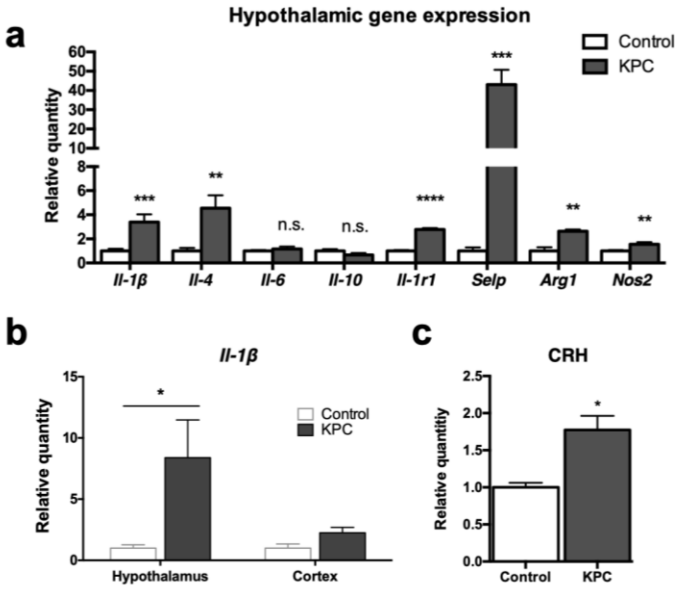

Fig. 5: *KPC induces hypothalamic inflammation and neuroendocrine alterations in the HPA axis.*

(a) Hypothalamic gene expression in tumor versus control, (b) Comparison of hypothalamic and cortical IL-1β gene expression, (c) hypothalamic CRH gene expression. *, P<0.05; **, P<0.01; ***, P<0.001; ****, P<0.0001.

.

KPC tumor progression induces loss of brown adipose tissue and WAT thermogenesis, accompanied by decreased core body temperature

An important mechanism seen in other subtypes of cancer cachexia, including LLC and C26 models, is energy loss through increased sympathetic nervous system outflow. In KPC engrafted animals, core body temperature remained relatively constant until end stage cachexia, with both light and dark cycle body temperature declining significantly in the last 2-3 days of illness (Figure 6a-b). End-stage cachexia was associated with severe depletion of brown adipose tissue (BAT) volume at necropsy (Supplemental Figure 3). Though BAT *Ucp1* expression did not differ significantly from controls at day 5, KPC-engrafted animals demonstrated a 52.27 ± 10.69%

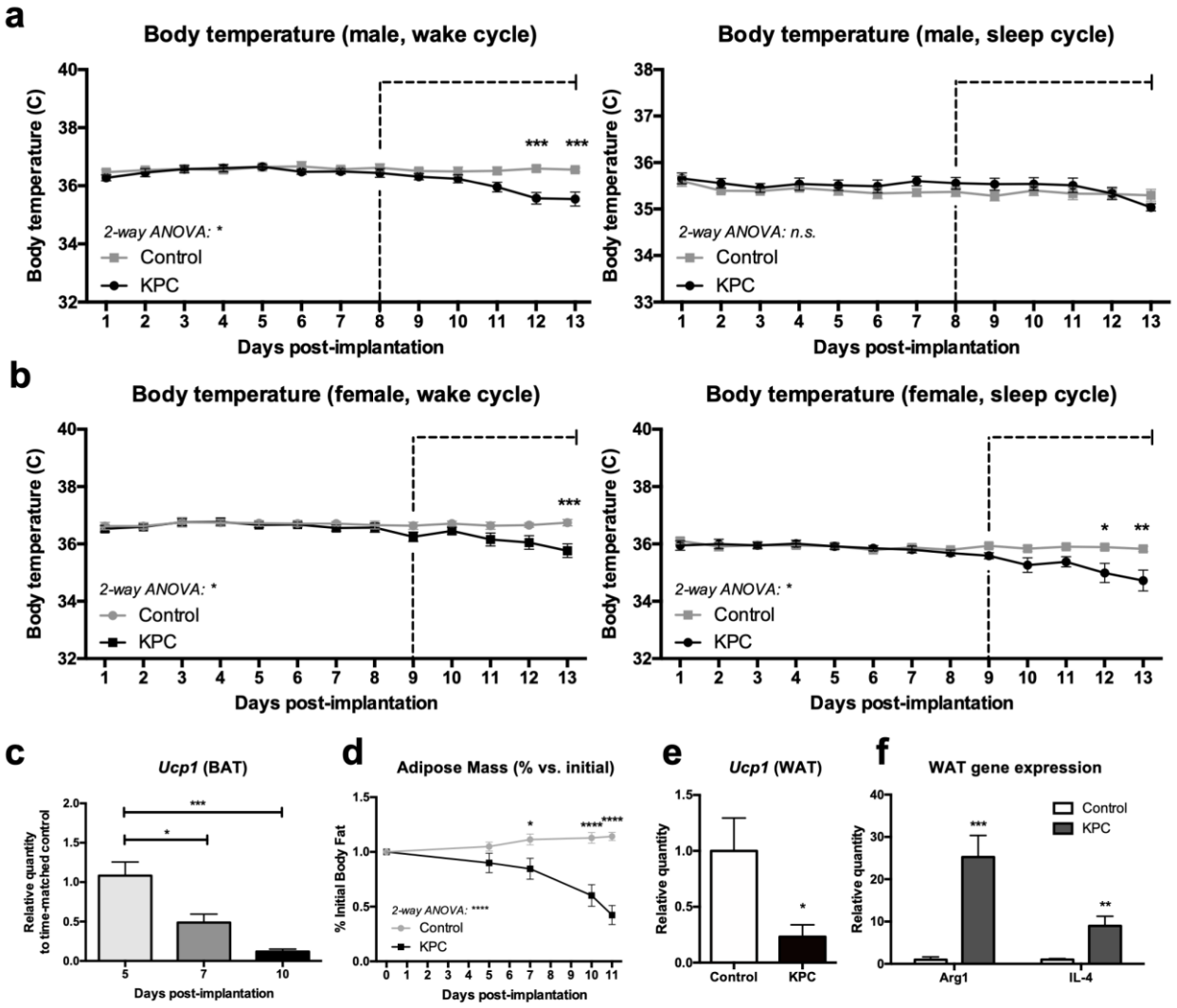

Fig. 6: *Body temperature decreases in conjunction with BAT and WAT UCP1 expression during KPC tumor progression, in conjunction with M2 macrophage activation in WAT*

(a) Core body temperature in wake and sleep cycles in KPC versus control males, (b) core body temperature in wake and sleep cycles in KPC versus control females, (c) BAT gene expression of *Ucp1* at 5, 7, and 10 days of KPC tumor progression relative to control, (d) longitudinal assessment of body fat mass by nuclear magnetic resonance imaging over the course of 0-11 days in KPC versus control animals, (e) WAT *Ucp1* expression at 10 days of KPC tumor progression versus control. (f) WAT *Arg1* and *Il4* expression at 10 days in KPC versus control. *, P<0.05; **, P<0.01; ***, P<0.001; ****, P<0.0001.

.

decrease at day 7 ($p<0.05$, n=5/group), and an 88.19 ± 0.03% decrease at day 10 ($p<0.0001$, n=5/group) (Figure 6c). Total adipose tissue in KPC-engrafted animals, however, underwent rapid loss over the course of the disease process, with significant changes detectable as early as 7 days ($p<0.0001$, n =5-7/group) (Figure 6d). White adipose tissue (WAT) demonstrated a 76.82 ± 10.73% decrease of *Ucp1* gene expression during end-stage illness ($p<0.05$, n=6/group) (Figure 6e). Loss of *Ucp1* in WAT from KPC-engrafted animals was accompanied by an increase in markers of alternatively activated macrophage infiltration, with a 8.98 ± 2.27 fold uprergulation of *Il4* ($p<0.01$, n=6/group) and a 25.24 ± 5.12 fold upregulation of *Arg1* ($p<0.001$, n=6/group) (Figure 6f).

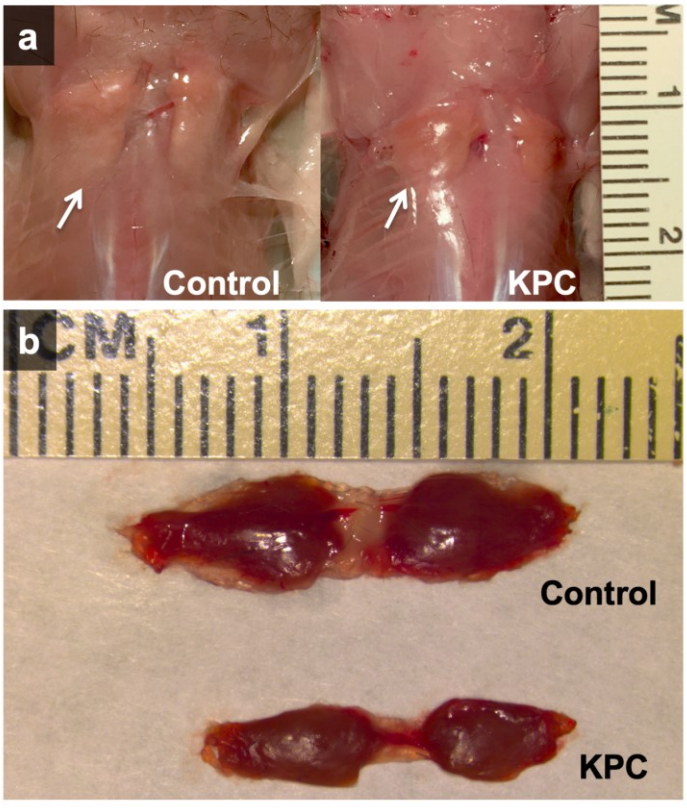

Fig. S3: *Gross appearance of BAT at necropsy.*
Representative photographs of interscapular brown adipose tissue in KPC-engrafted animals relative to controls. (a) Gross appearance of dorsum during end-stage cachexia; white arrow indicates brown adipose tissue. (b) Resected interscapular brown adipose tissue.

KPC allografts result in a systemic inflammatory response spanning multiple organ systems

The liver is extensively involved in systemic inflammatory responses to acute and chronic stimuli, contributing to cachexia by producing pro-inflammatory signals and consuming amino acids for acute phase protein synthesis. We specifically examined the acute phase proteins pentraxin 2/APCS, which in mice serves an analogous role to CRP in humans, and Orm1, which has recently been shown to have anorexigenic properties [267,273,274]. In males, KPC induced a 34.42 ± 6.89 fold increase in *Apcs* ($p < 0.001$, n=4-5/group) and a 6.61 ± 0.32 fold increase in *Orm1* relative to controls ($p<0.001$, n=4-5/group) (Figure 7a). In females, KPC induced a 8.07 ± 0.87 fold increase in *Apcs* ($p < 0.0001$, n=5/group) and a 5.30 ± 1.22 fold increase in *Orm1* ($p<0.01$, n=5/group) (Figure 7a). In addition to hepatic synthesis of acute phase proteins, the pro-inflammatory cytokine *Il-1β* was induced 5.76 ± 0.63 fold in KPC-engrafted males relative to controls ($p < 0.0001$, n=4-5/group) and 5.39 ± 0.77 fold in KPC-engrafted females relative to controls ($p < 0.001$, n=5/group) (Figure 7b). The spleens of KPC mice demonstrated consistent enlargement at necropsy, with an average weight of 183 ± 22 mg in tumor-bearing mice versus 70 ± 6 mg in controls ($p<0.05$, n=5/group) (Figure 7c).

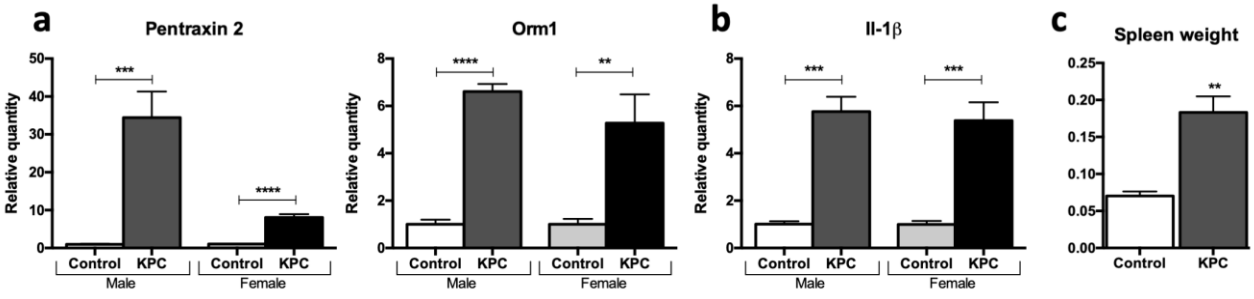

Fig. 7: *KPC tumor progression results in systemic inflammatory responses in hepatic tissue and spleen*
(a) Relative hepatic gene expression of acute phase proteins Pentraxin 2 (*Apcs*) and *Orm1* in control and KPC males and females (b) relative hepatic gene expression of *Il1β* in KPC males and females and, (c) spleen weight at necropsy in KPC versus control. *, P<0.05; **, P<0.01; ***, P<0.001; ****, P<0.0001.

KPC allografts result in anemia and neutrophil-dominant leukocytosis

One possible contributing mechanism of fatigue and cardiovascular strain in cancer cachexia is that chronic inflammation can result in anemia of chronic disease via liver and bone marrow signaling [275,276]. Consistent with a systemic inflammatory state, KPC tumor burden results in a marked neutrophil-dominant leukocytosis ($p<0.001$) with increases in other innate immune cells including monocytes ($p<0.01$) and eosinophils ($p<0.01$) (Supplemental Figure 4a). Other hematologic abnormalities included decreased hematocrit, erythrocytes, and platelets ($p<0.05$). Though baseline hematologic parameters were different between male and female animals, the observed anemia and leukocytosis in KPC-engrafted animals of both sexes was indistinguishable. (Supplemental Figure 4b).

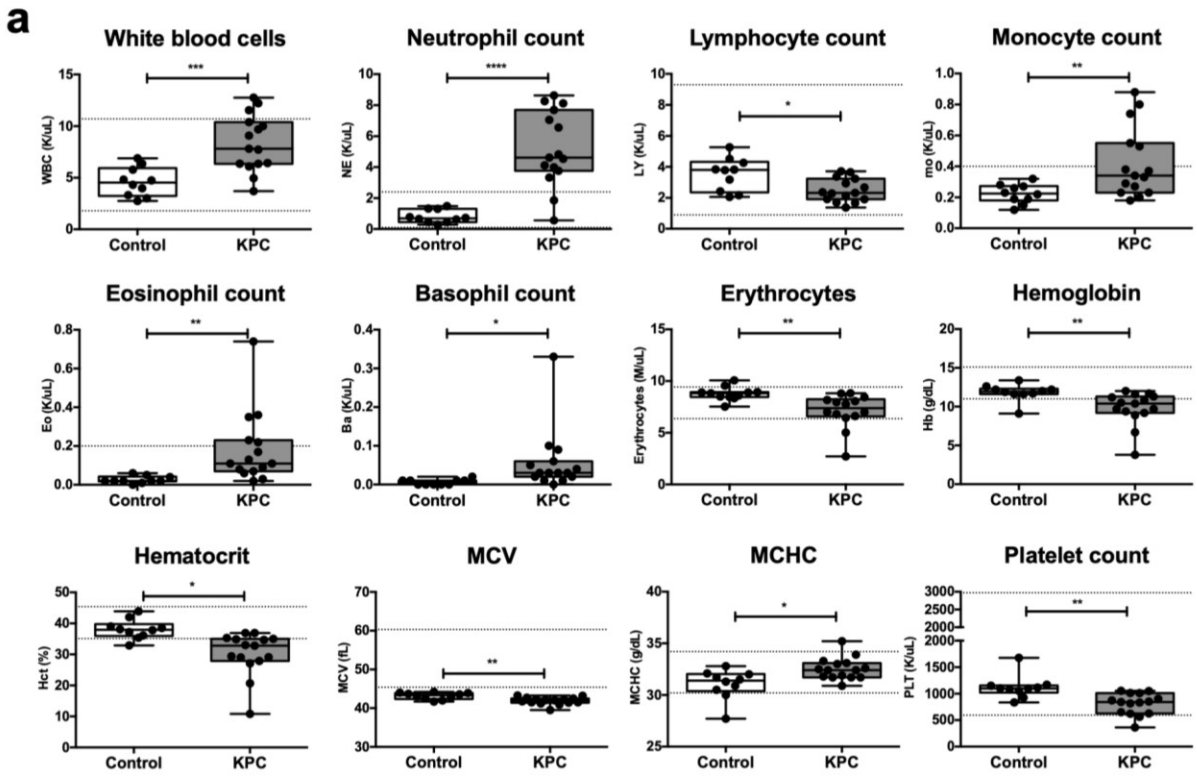

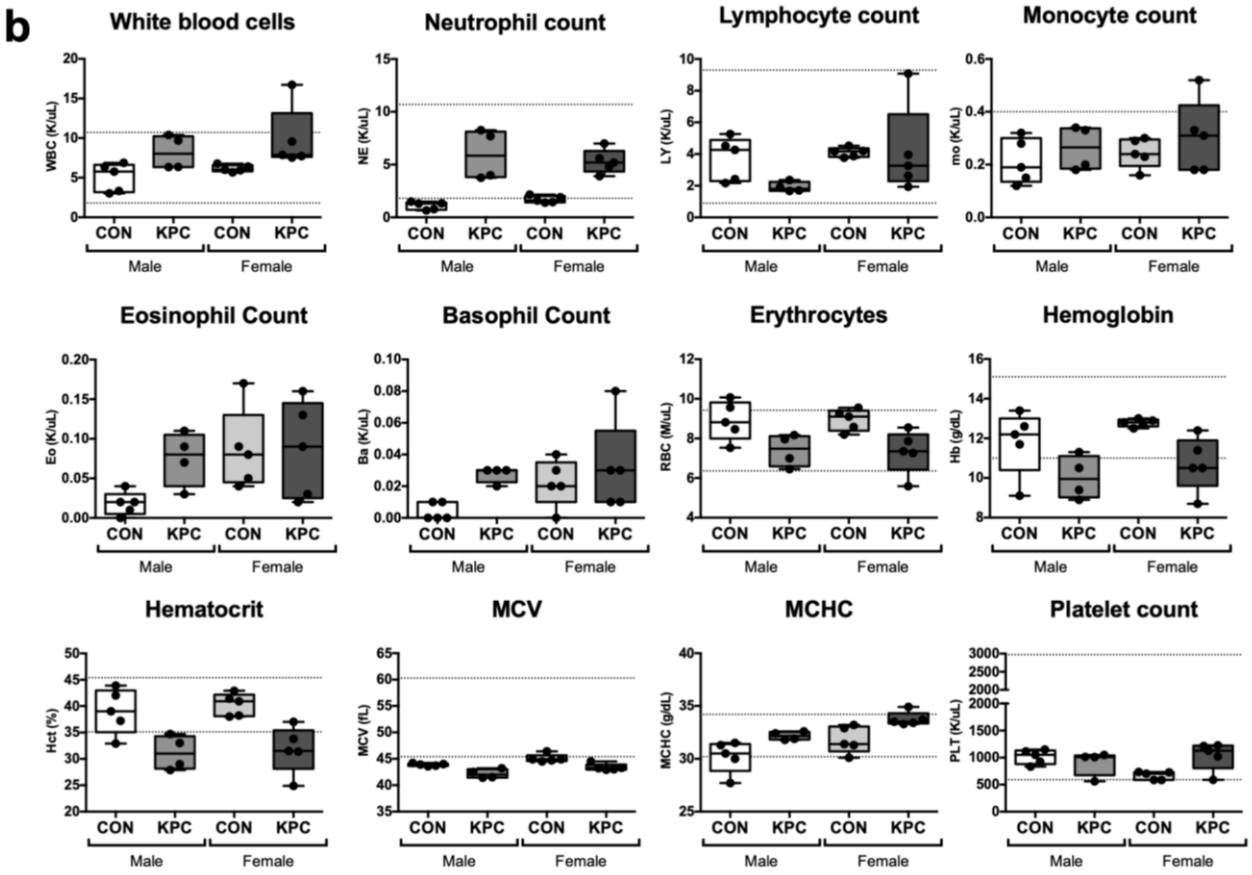

Fig. S4: *KPC engraftment results in hematologic changes including anemia and neutrophil-dominant leukocytosis.* (a) Complete blood count with differential during end-stage cachexia in males with IP KPC versus controls, and (b) complete blood count with differential during end-stage cachexia in males versus females with IP KPC. *, P<0.05; **, P<0.01; *** P<0.001.

KPC-induced cachexia is associated with severe loss of circulating testosterone, without other detectable endocrine changes

Cancer cachexia is associated with neuroendocrine dysregulation, particularly in the hypothalamic-pituitary-adrenal and hypothalamic-pituitary-gonadal axes [88,277,278]. KPC-engrafted males demonstrated marked hypogonadism, with a loss of greater than 97% of free testosterone relative to controls at time of sacrifice (p<0.01) (Figure 8a). While KPC-engrafted females also

demonstrated slight decreases in serum free testosterone, this difference did not reach statistical significance (p=0.13). Unlike testosterone, accurate assessment of serum estradiol concentrations requires simultaneous cycling of female animals, which was not implemented in this study. Importantly, blood glucose concentrations at time of sacrifice were not elevated in KPC-engrafted mice, demonstrating that tumor growth did not result in diminished insulin secretion or diabetes as a mechanism of wasting (Figure 8b).

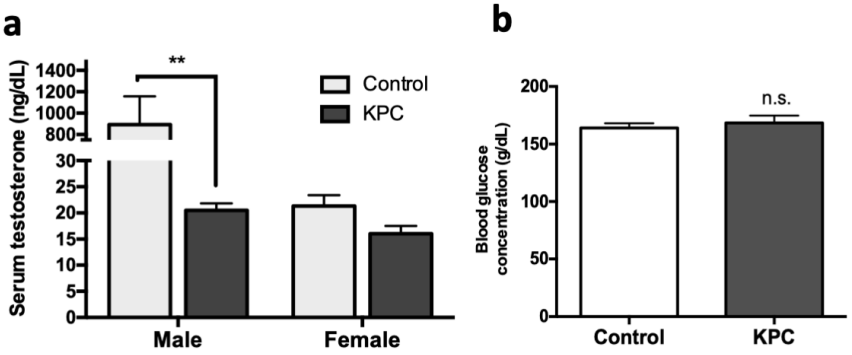

Fig. 8: *KPC tumor progression results in hypogonadism as manifested by decreased testosterone, without other endocrine changes including diabetes.*
(a) Serum free testosterone in male and female KPC animals relative to control (b) Blood glucose concentration at time of sacrifice in KPC and control. **, p<0.01

Discussion

A key rationale for characterization of the murine $KRAS^{LSL.G12D/+}$ $P53^{LSL.R172H/+}$ PDX-Cre^{+} (KPC) model in the context of cachexia is that pancreatic ductal adenocarcinoma (PDAC) is one of the most cachexia-associated forms of cancer, with greater than 80% of patients afflicted over the course of their illness. PDAC is also among the deadliest forms of cancer, with a 93% mortality rate in the 5 years following diagnosis [279-282]. Current approaches to treating PDAC include cytotoxic chemotherapy, ionizing radiation, and surgical resection [283,284]. One possible reason

these therapies are unsuccessful in achieving long-term survival is that they fail to treat cachexia, which is a key underlying cause of PDAC morbidity and mortality [259-261,285]. Even PDAC tumors of exceptionally small size are capable of inducing the widespread physiologic, metabolic, and behavioral changes that define cachexia [257,279,286]. Therefore, PDAC is a critical priority in cachexia research, and more effort must be directed toward elucidating molecular mechanisms and therapeutic targets in PDAC cachexia. Here, we demonstrate that syngeneic KPC allografts recapitulate key features of PDAC and induce a wide array of cachexia manifestations, including anorexia, decreased LMA, skeletal and cardiac muscle wasting, hypothalamic inflammation, and systemic inflammatory responses involving hematologic and endocrine perturbations. Overall, this is an accurate and reproducible model of PDAC-induced cachexia, and provides significant strengths relative to existing models.

In alignment with other cachexia models, we demonstrate muscle catabolism is a key aspect of KPC cachexia. Muscles with a high preponderance of fast-twitch fibers, including gastrocnemius, tibialis anterior, and quadriceps, were selected for skeletal muscle analysis because they are particularly susceptible to wasting in inflammatory states [90]. Indeed, KPC tumor growth induced tissue atrophy in all three of these muscle groups, corresponding to high expression levels of the ubiquitin ligases MAFBx and MuRF1 and their transcriptional inducer FOXO1. While there was also a minor decrease in the mass of soleus, a muscle enriched with type I slow-twitch fibers, the atrophy was of a lesser magnitude and corresponded to a blunted induction of catabolic gene programming relative to fast-twitch enriched muscles. Furthermore, the adhesion molecule P-selectin (SELP) was upregulated in fast-twitch skeletal muscle, consistent with previous findings in rats bearing MCA sarcoma [287]. We also found an increase in the expression of autophagy genes in skeletal muscle, corroborating previous clinical evidence

that this pathway of catabolism is a key contributor to lean tissue loss [288]. In addition to skeletal muscle, cardiac muscle is often profoundly catabolic and functionally compromised by cancer cachexia [289-291]. Cardiac dysfunction is independently associated with substantial morbidity and mortality in cachexia, and its mechanistic underpinnings are therefore an important topic of investigation. Cardiac muscle catabolism in cachexia has previously been linked to induction of autophagy, and variably to expression of atrophy-associated ubiquitin ligases [292,293]. Our data establish that the KPC model is similar to other cachexia models by producing skeletal muscle catabolism by E3 ubiquitin-ligase activation and cardiac muscle catabolism via autophagy, but that both pathways are active in both tissue subsets. The importance of autophagy to both skeletal and cardiac muscle in this model is in alignment with recent work demonstrating that megestrol acetate ameliorates lean mass loss in skeletal and cardiac muscle via inhibition of autophagy [294].

In addition to muscle wasting, these data establish that KPC is a highly inflammatory disease state spanning multiple systems. One key site of inflammation in this model is the liver. Our data demonstrate a robust and sexually dimorphic upregulation of pentraxin 2/APCS, the functional murine equivalent of CRP in human. CRP and APCS are induced in response to a variety of inflammatory stimuli primarily via IL-6, serving a key role in acute phase responses [273,274]. We also found that KPC increases hepatic expression of *Orm1*, another key acute phase reactant in both mouse and human known to serve numerous important roles in energy balance, immunity, and capillary barrier modulation. Furthermore, ORM1 is of metabolic and behavioral importance because it induces anorexia via leptin receptor signaling in the arcuate nucleus of the hypothalamus [267]. In mice, ORM1 is primarily synthesized by the liver and is the only ORM isoform induced in response to inflammatory stimuli. The induction of both *Apcs* and *Orm1*

indicates that KPC tumors induce a systemic inflammatory response and production of anorexigenic signaling proteins. Finally, we show that hepatic IL-1β is induced in both sexes during KPC tumor growth, thereby establishing that the liver is a key site of multimodal inflammatory signaling in this model. Interestingly, we observed an upregulation of SELP in functionally diverse tissues throughout the body, ranging from cardiac and skeletal muscle to the hypothalamus. This provides further mechanistic support to previous evidence that SELP polymorphisms are correlated with cachexia phenotype in clinical populations [198,287].

One key way in which the KPC model differs from existing cachexia models is that it does not induce *Ucp1* gene expression in BAT or WAT. Many studies have examined the role of increased sympathetic outflow in cachexia as a means of energy loss. The relevance of this mechanism is underscored by the ameliorative effects on sarcopenia and cachexia observed with the anabolic catabolic transforming agent espindolol, which acts as a nonspecific β-1 and β-2 adrenergic receptor antagonist [248,295]. Sympathetic outflow increases can manifest as "browning" of white adipose tissue or an increase of brown adipose tissue activity through increased expression of genes such as *Ucp1* [296,297]. UCP1 acts as an uncoupler of mitochondrial electron transport, which shifts adipocyte metabolism to increase thermogenesis while decreasing ATP synthesis, thereby increasing energy expenditure and lipid mobilization. The energy loss is not accompanied by increased core body temperature, even in thermoneutral conditions [296]. While we demonstrate a similar pattern to these prior experiments in regard to loss of body temperature in late stage cachexia, we found a loss in *Ucp1* in all adipose tissue rather than an increase. This may reflect that browning is a very early manifestation in cachexia that does not persist through end-stage disease, or that energy wasting via adipose tissue browning may not be a contributing factor in all etiologies of cachexia. The finding that the BAT was severely depleted at both mid- and late-

stage cachexia in this model argues for the former explanation, and suggests that sympathetic activation may occur early in the disease course. This model importantly demonstrates that loss of adipose tissue is an early and defining event in the progression of KPC cachexia, occurring simultaneously with or prior to muscle catabolism. This corroborates previous investigations in both patient populations and murine models demonstrating that altered fat metabolism is a widespread and potent contributor to cachexia pathophysiology.[141,298]

While commonly used preclinical murine models of cachexia such as LLC, C26, PDX, and GEMMs are clearly useful, each has substantial weaknesses. For example, implantation of LLC cells into syngeneic C57BL/6 mice provides a useful model for cachexia in lung cancer patients. However, this cell line was first isolated in 1951, and its wide use and inherent genomic instability has produced many distinctly heterogeneous subclones. As a result, LLC subclones range from highly cachexigenic to virtually unable to produce cachexia, and vary in the ability to induce WAT browning [297,299,300]. While C26 is also a very robust model, it is strongly dependent on IL-6 and LIF signaling in a mechanism that applies to some, but not all, cancer patients [301,302]. Corroborating this mechanism, IL-6 blocking therapies demonstrated clinical utility in a case series of cancer patients with extraordinarily high IL-6 levels [303,304]. However, given IL-6 is not elevated in all forms of cancer cachexia and therefore not a universal driver, other models are needed to investigate IL-6-independent mechanisms. Patient derived tumor xenografts are useful for their ability to test unique tumor cases, as well as investigate correlations between patient phenotype and murine cachexia outcomes, but require immunosuppression and are likely to lose a substantial proportion of signaling events due to the lack of species protein homology. Finally, GEMMs are variable with their time to spontaneous tumor formation and often demonstrate metabolic and behavioral abnormalities as a result of their genetic background. Further

information on these cachexia models and others not discussed here, including the rat models Yoshida ascites hepatoma (YAH-130) and Walker 256 carcinosarcoma (Walker 256), and the murine MAC 16 adenocarcinoma (MAC16), are detailed elsewhere in a recent review.[305]

In addition to the tumor-specific issues discussed above, the development of reliable preclinical models of cachexia is further hampered by the lack of standardization of key experimental details and measured outcomes. Therefore, recent efforts have focused on establishing standardized protocols for use of preclinical cachexia models and the characterization of their phenotypes, including a particularly robust study describing use and analysis of the C26 model [306]. Such details as the initial inoculum cell counts, site of implantation, and details of animal husbandry (e.g., diets, sex, housing conditions, etc.) do not follow general consensus guidelines, but these details are nonetheless critical to interpreting experimental outcomes. For example, despite the common rodent laboratory housing temperature at ~21˚C (room temperature), the thermoneutral zone of mice ranges from 26˚C during the active phase, to over 30˚C during the resting phase [307,308]. Housing in relatively cold environments, particularly when animals are individually housed (as is common for cachexia studies) leads to a variety of stress responses and overt changes in inflammation and immune function.[309] For example, mice demonstrate altered behavioral and immune responses to lipopolysaccharide, and have altered tumor growth and anti-tumor immune responses when housed in sub-thermoneutral environments [310,311]. For these reasons, the KPC model was characterized with cage temperatures measured at 26˚C and with adequate materials (nestlets) for thermoregulation. This combination avoids heat stress during the active phase, but facilitates normal immune function and minimizes stress [307-309]. Other environmental considerations in this study included a week long period of adaptation to novel environments and single housing prior to study initiation, regular handling in

advance of the study to reduce stress associated with investigator interactions, and multiple sources of enrichment known to reduce stress in lab animals (Enviro Dri, nestlets) [312]. Environmental design shortcomings of this study included that animals were individually housed in order to obtain individual LMA and food intake readings, despite the preference of mice to be group housed. However, group housed animals implanted with KPC did not demonstrate significant difference in onset to cachexia compared with singly housed animals, making it likely that this stressor was at most a minor contributor to the observed disease process (data not shown).

Another relatively understudied aspect of cachexia is sexual dimorphism. Clinical observations demonstrate that males are more adversely affected by cachexia than females, especially with regard to body weight, muscle mass, and muscle strength. Importantly, the rate of muscle wasting and weight loss correspond to survival in cancer patients [56,313], and males experience an increased degree of catabolism and an increased mortality risk in many different subsets of cancer [314-316]. In the C26 model of cancer cachexia, male mice experience greater body weight loss, loss of skeletal and cardiac muscle, and mortality compared to tumor-bearing females due to the protective effects of estrogen receptor signaling [292]. Our model demonstrates for the first time that LMA changes are sexually dimorphic, and in females are the first behavioral signal of cachexia onset. In contrast to other cachexia models including C26, KPC-engrafted female animals do not demonstrate protection against cardiac muscle wasting or autophagy, despite smaller overall tumor burden. Because estradiol is highly dynamic across the estrus cycle, and animals in this study were not simultaneously cycled, it was not possible to accurately assess whether hypogonadism could explain the relative lack of protection from cachexia in female KPC animals. Additional work will be necessary to determine whether hypogonadism or alternative

inflammatory signaling can explain the lack of protection from cardiac wasting in KPC-engrafted females compared with other cachexia models.

In sum, the syngeneic KPC graft model provides a platform for further in-depth investigations of cancer cachexia. Future experiments will be essential to examine these manifestations using a cancer cachexia staging approach, given that an ideal therapeutic for cancer cachexia will be administered alongside other disease interventions at an earlier stage of illness. A particularly useful framework for this is the International Consensus Criteria, such that the parameters described in this study will be examined during pre-cachexia, cachexia, and refractory cachexia stages [256]. Finally, this model will be of benefit for preclinical drug testing for both cachexia and PDAC interventions. Overall, this model adds substantially to experimental approaches to cancer cachexia with a specific focus on PDAC, and will serve as a valuable resource for a wide variety of basic and translational approaches in future studies.

Methods

Animals

Male and female C57BL/6J mice were obtained from The Jackson Laboratory (cat. #000664) and maintained in standard housing at 26°C and 12h light / 12h dark cycles. Animals were provided with *ad libitum* access to water and food (Purina rodent diet 5001; Purina Mills, St. Louis, MO, USA). In the week prior to tumor implantation, animals were transitioned to individual housing to acclimate to experimental conditions. Animal food intake and body weight were monitored daily immediately prior to lights out. All studies were conducted according to the National Institutes of Health Guide for the Care and Use of Laboratory Animals and approved by the Institutional Animal Care and Use Committee of Oregon Health & Science University.

Origin of cell lines; and tissue culture

The original KPC model expresses knock-in pancreas specific conditional alleles LSL-$KRAS^{G12D}$ and LSL-$TP53^{R172H}$ via the PDX-1-Cre driver. This model recapitulates PDAC tumor progression but is in a mixed 129/SvJae/C57BL/6 background. Therefore, the original KPC mouse was back-crossed into a C57BL/6 background for 9 generations and pancreatic tumors from these mice were harvested to produce primary epithelial KPC lines, which were kindly provided by Dr. Elizabeth Jaffee for use in these studies [268]. Cells were maintained in RPMI 1640 supplemented with 10% heat-inactivated FBS, 1% minimum essential medium non-essential amino acids, 1mM sodium pyruvate, and 50 U/mL penicillin/streptomycin (Gibco), with incubators maintained at 37°C and 5% CO_2.

Generation of PDAC models

C57BL/6 mice aged 7-12 weeks were inoculated subcutaneously, intraperitoneally, or orthotopically with an inoculum of 1 million to 5 million KPC tumor cells, while controls received heat-killed cells in the same volume. Subcutaneous implantation was performed with a 1mL injection of cell suspension in PBS into the interscapular subcutaneous space under brief isoflurane anesthesia. Intraperitoneal implantation was performed as a 1mL injection of cell suspension into the right iliac region, under brief isoflurane anesthesia. Orthotopic implantation was performed as previously described by injecting 3 million cells in 40 microliters into the tail of the pancreas, as defined by the pancreatic tissue immediately adjacent to the lower pole of the spleen, also under isoflurane anesthesia [317].

Nuclear magnetic resonance imaging

NMR measurements were taken at the beginning of the study for covariate adaptive randomization of tumor and sham groups to ensure equally distributed weight and body composition. Upon development of cachexia, mice were euthanized and subjected to repeat NMR body composition analysis. For serial measurements of adiposity, one cohort was subjected to NMR analysis at time points corresponding to no muscle catabolism, moderate muscle catabolism, and severe muscle catabolism (5d, 7d, 10d), and at time of sacrifice (11d).

Body temperature and locomotor activity measurement

Body temperature and voluntary home cage locomotor activity were measured via MiniMitter tracking devices (MiniMitter, Bend, OR, USA). Mice were implanted three days prior to tumor implantation with MiniMitter transponders in the intrascapular subcutaneous space. Using these devices, body temperature and movement counts in x-, y- and z-axes were recorded in 5 minute intervals (Vital View, MiniMitter).

Tissue collection and histology

At onset of cachexia or at pre-designated time points, animals were deeply anesthetized by ketamine cocktail. Formalin fixed paraffin-embedded histololgic sections were stained for hematoxylin and eosin. A surgical pathologist then reviewed them blinded to KPC administration group (e.g., SQ, OT, IP) and scored them as positive or negative for 1) ragged infiltration, 2) desmoplastic stromal response, and 3) host inflammatory response. Tumor, brain, gastrocnemius muscle, liver, blood, interscapular brown adipose tissue (BAT), and gonadal white adipose tissue (WAT) were harvested and stored in RNAlater (Ambion).

Quantitative qRT-PCR

RNA was extracted and purified with RNeasy Mini kits (Qiagen Inc.), then reverse transcribed into cDNA with a High Capacity cDNA Reverse Transcription Kit (Life Technologies). qRT-PCR was performed using TaqMan reagents and primer-probes (Applied Biotechnologies). Catabolism genes in muscle (muscle atrophy F-box, *Mafbx*; muscle ring finger 1, *MuRF1*; forkhead box O1, *Foxo1*), autophagy genes in heart (BCL2 Interacting Protein 3, *Bnip3*; cathespin L1, *Ctsl1*; GABA Type A Receptor Associated Protein Like, *Gabarapl*), inflammatory response genes in the brain (interleukin-1 beta, *Il-1β*; tumor necrosis factor α, *Tnfα*; interleukin 1 receptor type 1, *Il-1r1*; arginase 1, *Arg1*, nitric oxide synthase 2, *Nos2*; P-selectin, *Selp*; interleukin-6, *Il-6*, leukemia inhibitory factor, *Lif*), inflammatory response genes in liver (amyloid P component, serum, *Apcs;* orosomucoid 1, *Orm1, Il-1β*), and thermogenic and inflammatory genes in WAT and BAT (uncoupling protein 1, *Ucp1*; interleukin 4, *Il-4, Arg1*) were compared between tumor-bearing mice and tumor naïve controls by qRT-PCR and normalized to tissue-appropriate control genes (18S or beta actin).

Clinical assays

Whole blood counts with white blood cell differential were performed on EDTA-decoagulated samples obtained by cardiac puncture at time of necropsy using HemaVet 950 (Drew Scientific). Serum hormone assays were performed by the University of Virginia Ligand Assay and Analysis Core (URL: https://med.virginia.edu/research-in-reproduction/ligand-assay-analysis-core/). Testosterone was assayed in duplicate using IBL Mouse and Rat Testosterone Kit (catalog IB79174, range 10.0-1600ng/dL, and sensitivity 10ng/dL). Blood glucose was measured immediately prior to euthanasia with electronic glucometer (OneTouch Ultra).

Statistical Analysis

All reported studies are representative of 3 or more independent experiments, each with a minimum sample size of 4 per group. For comparison between tumor and control groups, data were assessed by student's *t* test or ANOVA (Prism 6.0, GraphPad Software). Longitudinal variables in each route of administration were binned into the categories of pre-cachexia and cachexia on the basis of anorexia. Cachexia is here defined as the interval beginning with two consecutive days with an average food intake difference greater than 10%, and pre-cachexia as the interval between implantation and cachexia onset. Post-hoc multiple comparisons tests were applied if a significant difference was present during the binned interval (pre-cachexia or cachexia). Bonferroni with baseline alpha = 0.05 was used for multiple comparison tests to determine at which time points the KPC and control groups were significantly different.

VI. Persistent Toll-like receptor 7 stimulation induces behavioral and molecular innate immune tolerance

Katherine A. Michaelis, Mason A. Norgard, Peter R. Levasseur, Brennan Olson, Kevin G. Burfeind, Abigail C. Buenafe, Xinxia Zhu, Sophia Jeng, Shannon McWeeney, Daniel L. Marks

Highlights

- Within the CNS, Toll-like receptor 7 (*Tlr7*) is most abundantly expressed in microglia
- Microglia produce abundant pro-inflammatory signals upon initial *Tlr7* stimulation
- In mice, the TLR7/8 agonist R848 results in dose-dependent acute sickness responses
- Microglia and mice undergo response tachyphylaxis with chronic *Tlr7* stimulation
- R848-induced tachyphylaxis results in heterologous desensitization to endotoxin

Abstract

Toll-like receptors 7 and 8 (TLR7 and TLR8) are endosomal pattern recognition receptors that detect a variety of single-stranded RNA species. While TLR7/8 agonists are a robust investigational therapeutic class, clinical utility of these agents is limited by sickness responses associated with treatment induction. To understand the kinetics and mechanism of these responses, we characterized the acute and chronic effects of TLR7 stimulation and its impact on the brain over time. Single-cell RNA-sequencing studies, RNAscope, and radiolabeled *in situ* hybridization demonstrate that central nervous system gene expression of TLR7 is exclusive to microglia. *In vitro* studies demonstrate that microglia are highly sensitive to TLR7 stimulation, and respond in a dose-dependent manner to the imidazoquinoline R848. *In vivo,* both intraperitoneal (IP) and intracerebroventricular (ICV) R848 induce acute sickness responses including hypophagia, weight loss, and decreased voluntary locomotor activity, associated with increased CNS pro-inflammatory gene expression and changes to glial morphology. However, chronic daily IP R848 resulted in rapid tachyphylaxis of behavioral and molecular manifestations of illness. In microglial *in vitro* assays, pro-inflammatory transcriptional responses rapidly diminished in the context of repeated R848. In addition to TLR7 desensitization, we found that microglia become partially refractory to lipopolysaccharide (LPS) following R848 pretreatment. Similarly, mice pre-treated with R848 demonstrate reduced sickness responses, hypothalamic inflammation, and hepatic inflammation in response to LPS. These data combined demonstrate that TLR7 stimulation induces acute behavioral and molecular evidence of sickness responses. Following prolonged dosing, R848 induces a refractory state to both TLR7 and TLR4 activation, consistent with induced immune tolerance.

Introduction

When challenged with signals indicating pathogenic threat or internal damage, multiple bodily systems mount responses aimed to eliminate the source of damage and restore homeostasis. First, the innate immune response is invoked by detection of a set of molecular motifs common to pathogens, such as components of viruses, bacteria, and fungi. At the same time immune cells traffic to the site of detected threats, and a coordinated set of behavioral and metabolic changes occurs to mitigate spread of pathogens, bolster the strength of immune responses, and provide raw materials for production of defense elements. Collectively, this phenomenon is termed the acute illness response, a highly evolutionarily conserved process that includes physiological and behavioral adaptations to stress [270]. Physiological responses to threat detection include fever, which inhibits pathogen replication, and muscle catabolism, which liberates amino acids for production of acute phase reactants and granulocytes. Behavioral responses include fatigue, anorexia, and decreased voluntary locomotor activity. In the short term, these processes are considered adaptive and promote survival in the face of threat and injury. However, crucial to the benefit of the acute sickness response is that it is self-limited in its nature – if prolonged, this process becomes highly deleterious to the survival of the organism.

Among the first lines of defense for pathogen response are pattern recognition receptors (PRRs), which include Toll-like receptors, NOD-like receptors, RIG-I-like receptors, and C-type lectin receptors [318]. Each of these receptors is uniquely targeted to a pathogen-associated molecular pattern (PAMP), macromolecular structures that are commonly conserved among microbial species and therefore suited for rapid detection. Upon a PRR binding its cognate ligand, an intracellular signaling cascade is triggered to induce transcriptional responses in innate immune signaling pathways, including NF-κB and IRF. The elicited transcriptional changes

promote rapid innate immune responses, and if the stimulus is significant enough in scale, initiates systemic changes including the acute illness response. Though the physiology downstream of many pattern recognition receptors is well characterized, the dynamics of other receptors remain relatively unexplored. Many cytokine receptors and pattern recognition receptors undergo physiological desensitization, also known as tachyphylaxis, upon repeated stimulation [319,320]. Conversely, certain specialized cytokines, such as leukemia inhibitory factor (LIF), are capable of producing sustained inflammatory signaling and behavioral sickness [66,165,167]. One relatively underexplored class of receptor in sickness are the endosomal innate immune receptors Toll-like receptors 7 and 8 (TLR7 and TLR8), both of which are activated by single-stranded RNA (ssRNA) and small molecule purine analogues (imidazoquinolines) [321]. These receptors are capable of detecting nucleic acid fragments from a large variety of viruses and bacteria, as well as endogenously produced small RNA species such as microRNA [322,323]. In mouse, TLR7 is expressed in myeloid and plasmacytoid dendritic cells, tissue resident macrophages, B cells, and T cells [324]. TLR8 demonstrates a predominantly monocytic and myeloid dendritic cell expression pattern; however, the murine form is not typically activated by human TLR8 pharmacologic agonists such as the imidazoquinoline R848 [325,326].

Both TLR7 and TLR8 are of considerable interest because of their dual potential for harm and benefit: they may directly contribute to the pathogenesis and progression of a number of diseases, but also are promising therapeutic targets. TLR7/8 are proposed as mechanistically important contributors to conditions including lupus and psoriasis, in which their inappropriate stimulation results in Th1 responses and autoimmunity [327,328]. Furthermore, TLR7 activation is proposed as a mediator of pancreatic tumorigenesis, neuronal apoptosis in states such as alcoholism and infection, and muscle cell death in cancer cachexia [329-331]. However, topical TLR7

agonists are in widespread clinical use for HPV-mediated genital warts, actinic keratosis, and basal cell carcinoma. These current uses represent a mere fraction of applications in which TLR7 agonists have therapeutic potential, with investigations underway for both single use and chronic use treatment paradigms. Because this class of receptor is associated with disease states, the fate of their use as therapeutic targets will depend heavily on whether TLR7/8 agonists are associated with sustained systemic harms and intolerable sickness-related side effects. Recent studies demonstrated that TLR7 stimulation is capable of inducing acute sickness responses, but more studies are necessary to investigate the mechanisms and determine whether negative responses are self-limited or sustained.

In this study, we aimed to investigate TLR7 agonists *in vivo* and *in vitro* to determine receptor localization within the central nervous system, and the physiological and molecular dynamics of pharmacologic stimulation of CNS immune cells. Because proposed uses of TLR7/8 agonists include both short-term and long-term treatment modalities, we used murine models to investigate acute and chronic effects of a therapeutically relevant dose of the imidazoquinoline TLR7/8 agonist R848. Key outcomes of these studies included determining the characteristics and chronicity of sickness responses to R848, the physiology and tissue-specific molecular outcomes of single and repeated dosing, and whether repeated dosing results in receptor desensitization. Lastly, we explored whether this desensitization is associated more broadly with immune tolerance, as assessed by responsiveness to the TLR4 agonist lipopolysaccharide.

Results

Central nervous system Tlr7 is most highly enriched in microglia

To understand which cells in the CNS are most likely to be primary recipients of TLR7-dependent signals, we combined RNA-seq, RNA-labeling techniques on murine brain tissue, and QPCR. A meta-analysis of single-cell RNA sequencing studies indicates that within the murine central nervous system under healthy conditions, *Tlr7* is highly expressed in microglia and CNS macrophages (Figure 1a). However, *Tlr7* is not commonly expressed in other cells of the CNS, including neurons, endothelial cells, astrocytes, and oligodendrocytes. Other innate immune receptors demonstrated variable degrees of expression in other CNS cell types, but were most consistently expressed in microglia. Certain innate immune receptors demonstrate unique central nervous system cell specificity, including high expression of *Tlr3* in astrocytes, and high expression of *Il1r1* in endothelial cells. Radiolabeled single probe *in situ* hybridization indicates that *Tlr7* is abundantly expressed throughout the murine CNS in cells morphologically consistent with microglia (Supplemental Figure 1). No differences in the distribution of *Tlr7* were observed with regard to brain region, with *Tlr7* positive cells uniformly present throughout the brain parenchyma. To expand upon this finding using microglial-specific labeling, brain sections from control or LPS-exposed animals were labeled using RNAscope with probes against *Tlr7* and the specific microglial marker *Tmem119* (Figure 1b, c, d). This assay again indicated that *Tlr7* expression is primarily restricted to microglia in all brain regions tested, and that *Tlr7* signal increases within microglia following inflammatory stimuli.

Next, we investigated whether *Tlr7* is differentially expressed in the brain following a variety of inflammatory stimuli. First, we compared astrocyte-dominant primary mixed glia with purified primary microglia for basal and LPS-stimulated expression of *Tlr7* (Figure 1e). In

agreement with our prior results, we found that *Tlr7* is predominantly expressed in microglia at baseline. Following LPS challenge, *Tlr7* expression underwent increases in microglia but not in primary mixed glia. To examine whether this difference is present *in vivo,* we used both pharmacologic and disease model sources of inflammatory stress to test CNS *Tlr7* expression. Because the hypothalamus serves a crucial role in processing and orchestrating the central response to inflammatory threats, we next examined *Tlr7* expression in both normal and inflamed states. In response to intracerebroventricular (ICV) TLR3 ligand Poly I:C, we observed increased hypothalamic gene expression of *Tlr7* (Figure 1f). Because one commonly proposed use of TLR agonists is cancer immunotherapy, we next queried the CNS levels of *Tlr7* in a murine model of pancreatic ductal adenocarcinoma (PDAC). In both sexes, PDAC resulted in increased hypothalamic *Tlr7* gene expression (Figure 1g). Overall, these studies indicated that *Tlr7* is broadly present in microglia at baseline, and undergoes increases in expression during acute and chronic inflammatory stress.

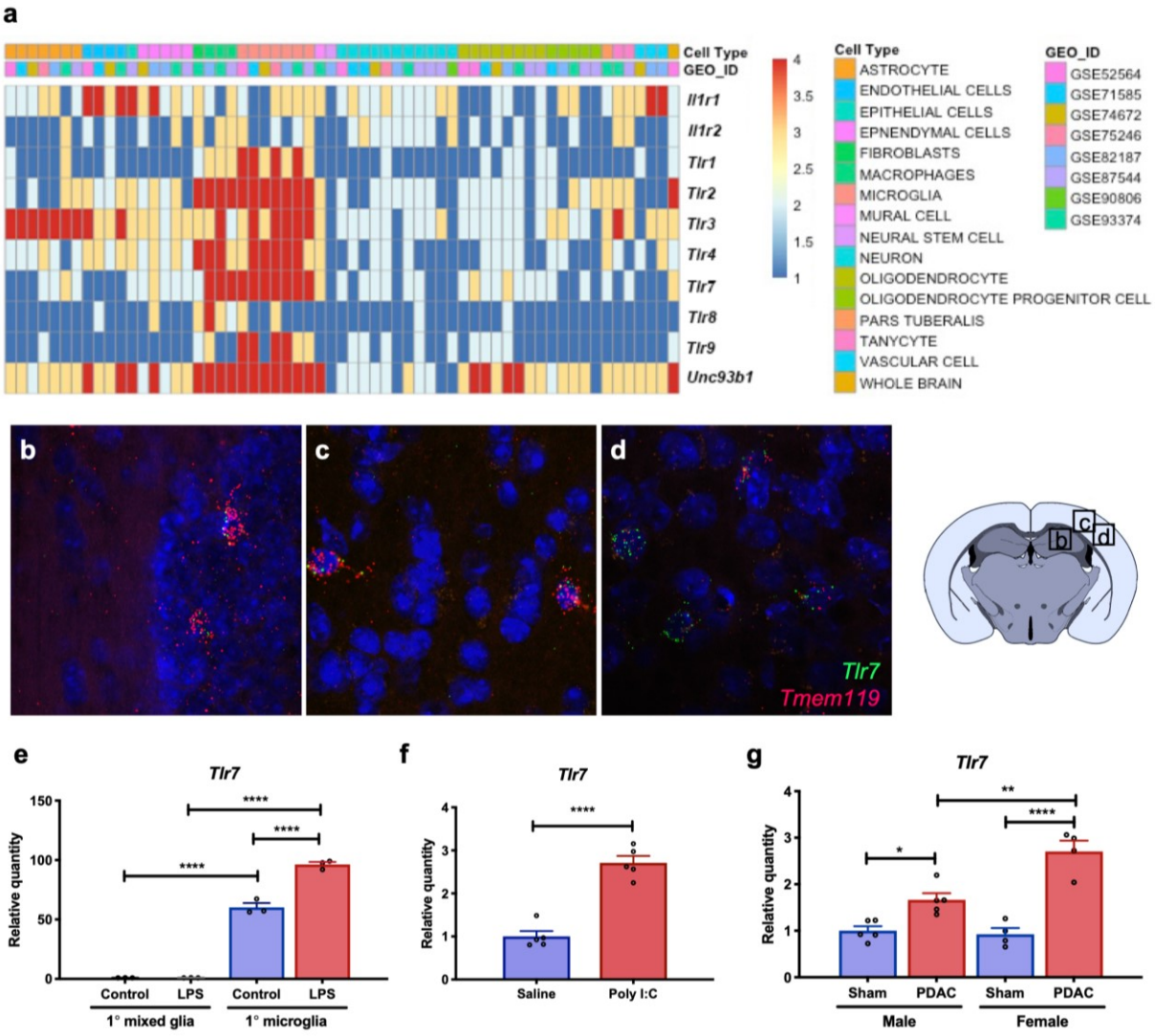

Figure 1. *Tlr7 is predominantly expressed in microglia, and is upregulated in the CNS following inflammatory stimuli*

(a) Meta-analysis of single cell RNA-seq datasets of the healthy CNS for key innate immune receptors and related proteins, stratified by GEO ID and cell type. RNAscope images for vehicle-treated hypothalamus (b), vehicle-treated cortex (c) and LPS-treated cortex (d) are shown for *Tlr7* and *Tmem119,* with DAPI stain to demarcate nuclei. A coronal section is shown to provide spatial context for RNAscope images 1b-1d. (e) *Tlr7* gene expression in astrocyte-dominant primary mixed glia cultures and primary microglial cultures exposed to vehicle or LPS (n=3/group). (f) *Tlr7* expression in hypothalamic homogenates following exposure to ICV saline or ICV poly I:C. (n=5/group) (g) Male versus female hypothalamic *Tlr7* expression in sham-operated and orthotopic pancreatic ductal adenocarcinoma (PDAC) (n=4-5/group). *, P<0.05; **, P<0.01; ****, P<0.0001.

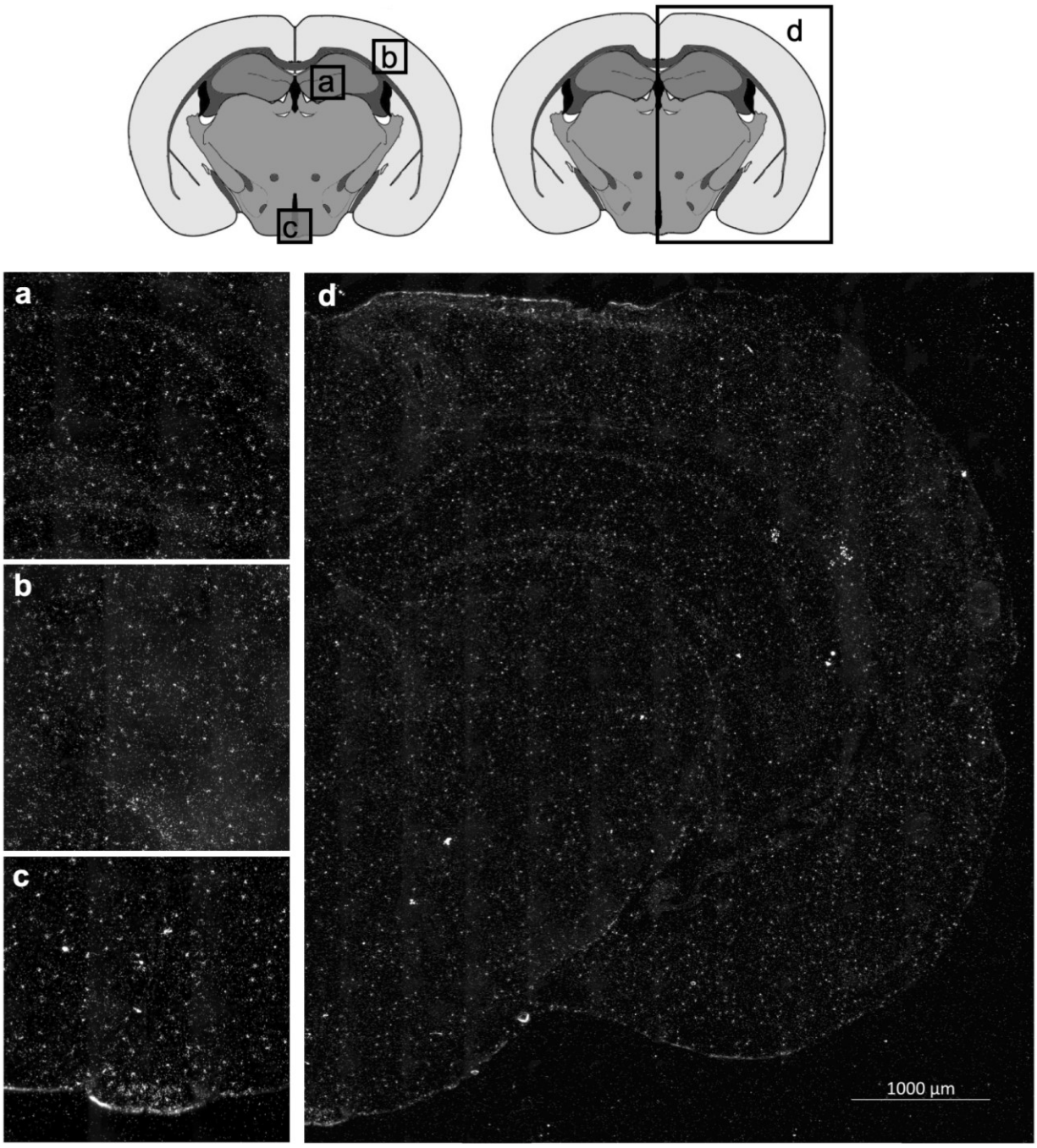

Figure S1. *Radiolabeled probe in situ hybridization of Tlr7 in the central nervous system*

Single-label in situ hybridization was used to label the distribution of *Tlr7* in the murine CNS during the inflammatory state of cancer cachexia. Imaging reveals silver grain clusters consistent with the size and distribution of microglia throughout the brain, including the hippocampus (a), cortex (b), and hypothalamus (c). A coronal hemibrain section in (d) reveals *Tlr7* is distributed throughout the brain parenchyma.

Microglia undergo pro-inflammatory responses following acute pharmacologic TLR7/8 stimulation

Given that we observed consistent and robust *Tlr7* expression in microglia but no other central nervous system cell types, we sought to explore the response to TLR7 stimulation specifically in microglia. To determine whether microglia are responsive to pharmacologic TLR7/8 stimulation, we exposed the immortalized microglial cell line SIM-A9 [332] to a variety of doses of the small molecule TLR7/8 agonist R848 ranging from 0.01ng/mL to 1mg/mL for 24 hours. R848 exposure resulted in robust increases in gene expression of *Ccl2*, *Cxcl10*, *Il1b*, *Il6*, *Nos2*, and *Tnfa,* including at doses in the low nanomolar range (Figure 2a). For assessing the kinetics of drug response, SIM-A9 was exposed to a time course of a constant 100ng/mL dose of the small molecule TLR7/8 agonist R848, indicating maximal pro-inflammatory gene expression responses from 8-12h post exposure (Figure 2b). In addition to these transcriptional changes, we found R848 rapidly induces intracellular TNF in a manner similar to LPS, with maximal responses observed at 6 hours post-exposure and tapering by 24-48 hours (Figure 2c).

Single-dose R848 results in acute sickness responses via both intraperitoneal and intracerebroventricular routes

Consistent with previous reports on TLR7 agonists in rat, both intraperitoneal (IP) and intracerebroventricular (ICV) administration of R848 resulted in acute sickness responses in mouse [333]. A dose response analysis was first performed via the IP route of administration,

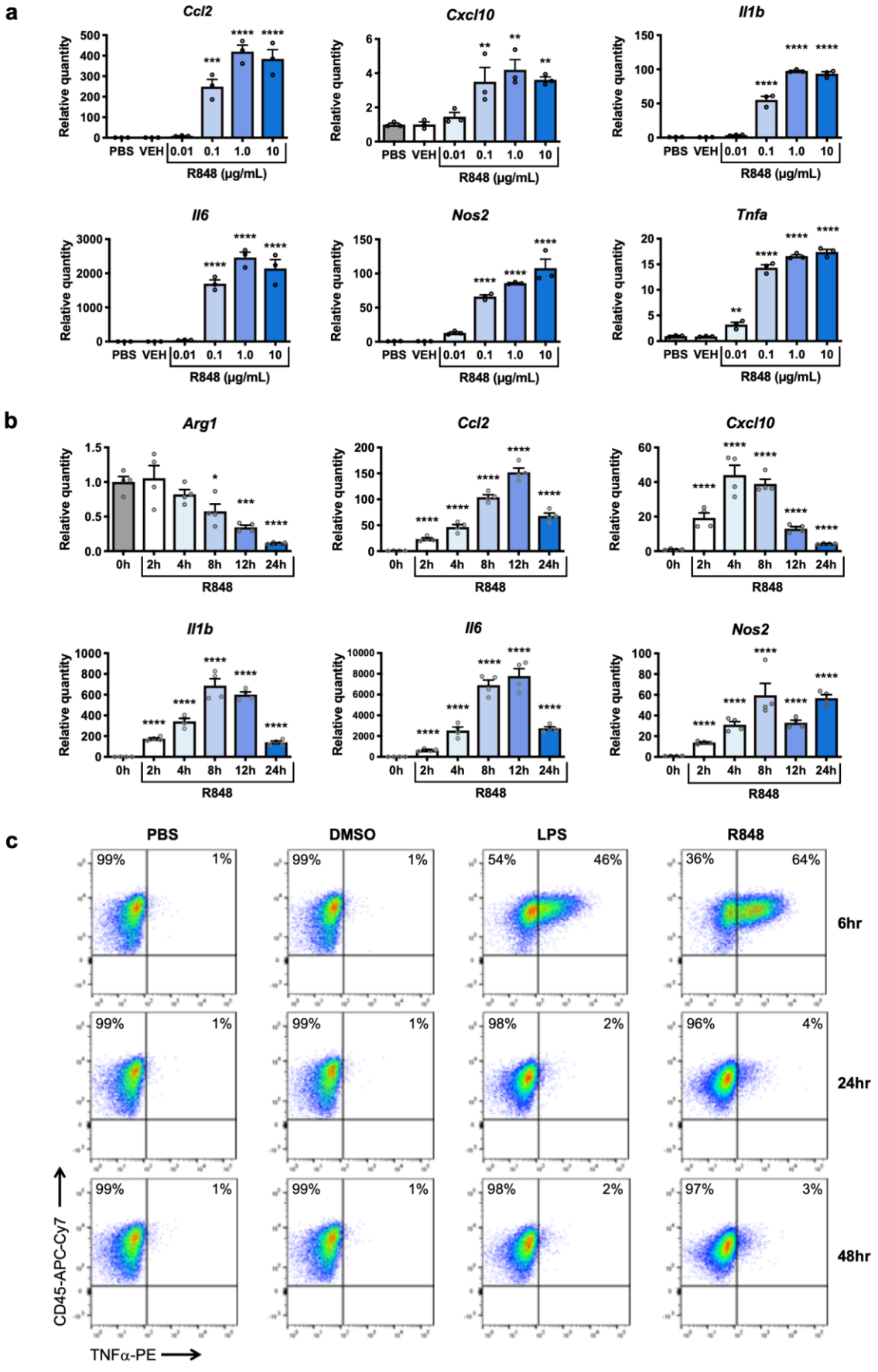
a
Ccl2
Cxcl10
Il1b
Il6
Nos2
Tnfa
Relative quantity
PBS VEH 0.01 0.1 1.0 10
R848 (μg/mL)
b
Arg1
Ccl2
Cxcl10
Il1b
Il6
Nos2
0h 2h 4h 8h 12h 24h
R848
c
PBS
DMSO
LPS
R848
99% 1%
99% 1%
54% 46%
36% 64%
6hr
99% 1%
99% 1%
98% 2%
96% 4%
24hr
99% 1%
99% 1%
98% 2%
97% 3%
48hr
CD45-APC-Cy7
TNFα-PE

Figure 2. *The TLR7/8 agonist R848 induces dose- and time-dependent changes in microglial gene and protein expression*

(a) The immortalized microglial cell line SIM-A9 was exposed to an escalating dose of R848 for 24h, then assessed for gene expression of downstream inflammatory response transcripts (n=3/group). (b) Using the lowest dose associated with transcriptional responses (100ng/mL), SIM-A9 were exposed for 2, 3, 8, 12, and 24h to R848 and assessed for transcription of cytokines, chemokines, and inflammatory response genes (n=4/group). (c) FACS plots quantifying intracellular TNFα in SIM-A9 following exposure to PBS (20μL), DMSO (0.1μL/mL), LPS (10ng/mL), or R848 (1μg/mL) for 6, 24, or 48 hours. *, P<0.05; **, P<0.01; ***, P<0.001; ****, P<0.0001.

---

showing that acute decreases in food intake occur in a dose dependent manner at doses as low as 1μg (Figure 3a). Concurrent with decreased food intake, subjects exposed to higher doses of IP R848 experienced weight loss 20-24h post-exposure (Figure 3b). To determine whether acute illness responses to R848 could be mediated independently within the CNS, two doses causing marginal or no sickness when given systemically (1μg and 100ng) were administered ICV. These doses both resulted in hypophagia and weight loss, demonstrating that the CNS alone can mediate TLR7-dependent illness responses (Figures 3c and 3d). In addition to decreased food intake and body weight, animals exhibited a brief increase in daytime body temperature following R848 administration, but subsequently exhibited decreased body temperature at night (Figure 3e). Importantly, TLR7KO and MyD88KO animals did not demonstrate changes in food intake or body weight in response to R848, demonstrating that associated sickness responses are mediated specifically through classical TLR7 signaling (Figure 3f).

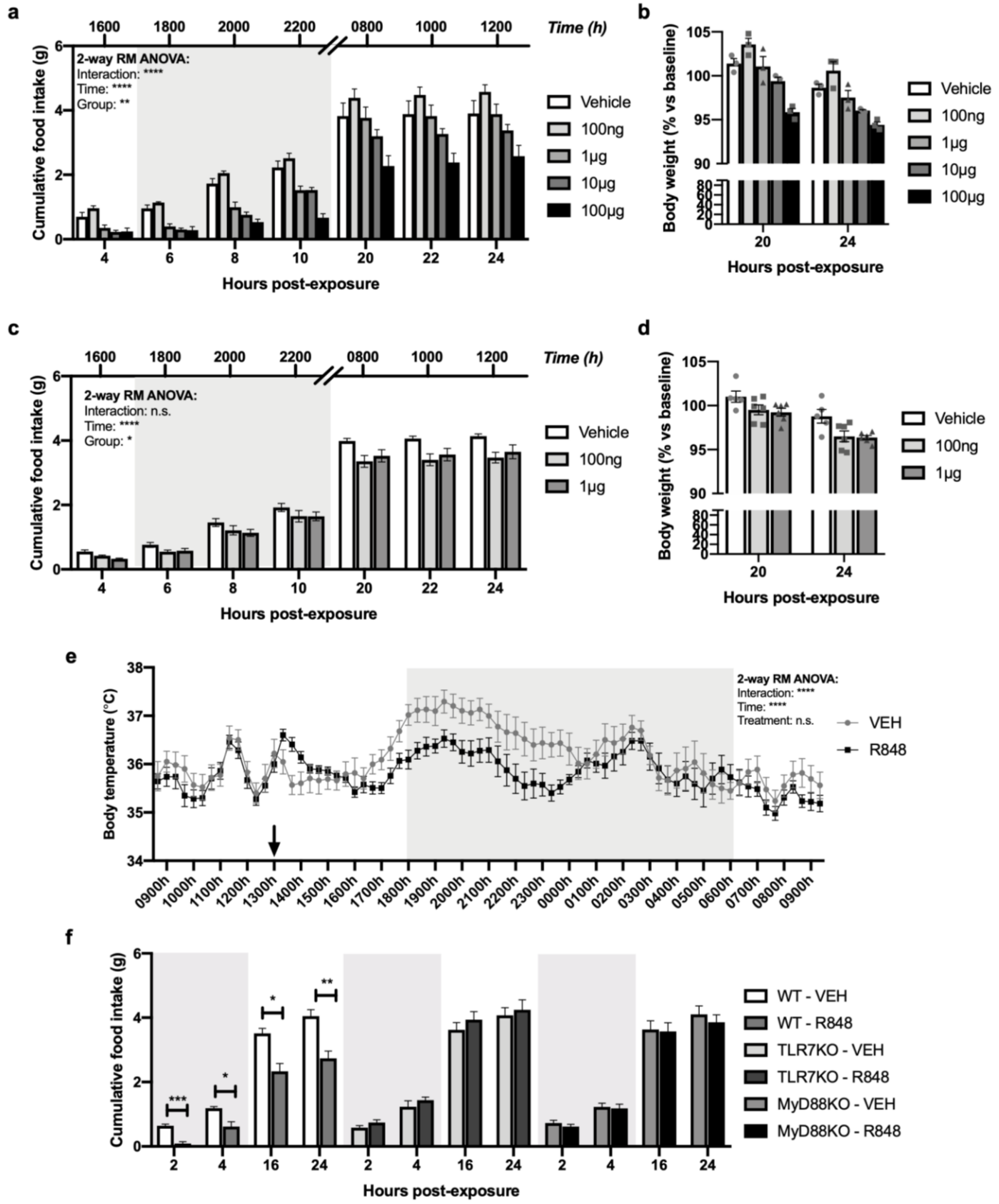
a
Time (h)
1600
1800
2000
2200
0800
1000
1200
Cumulative food intake (g)
2-way RM ANOVA:
Interaction: ****
Time: ****
Group: **
Vehicle
100ng
1µg
10µg
100µg
Hours post-exposure
b
Body weight (% vs baseline)
Vehicle
100ng
1µg
10µg
100µg
Hours post-exposure
c
Time (h)
Cumulative food intake (g)
2-way RM ANOVA:
Interaction: n.s.
Time: ****
Group: *
Vehicle
100ng
1µg
Hours post-exposure
d
Body weight (% vs baseline)
Vehicle
100ng
1µg
Hours post-exposure
e
Body temperature (°C)
2-way RM ANOVA:
Interaction: ****
Time: ****
Treatment: n.s.
VEH
R848
0900h
1000h
1100h
1200h
1300h
1400h
1500h
1600h
1700h
1800h
1900h
2000h
2100h
2200h
2300h
0000h
0100h
0200h
0300h
0400h
0500h
0600h
0700h
0800h
0900h
f
Cumulative food intake (g)
***
*
*
**
WT - VEH
WT - R848
TLR7KO - VEH
TLR7KO - R848
MyD88KO - VEH
MyD88KO - R848
Hours post-exposure

Figure 3. *R848 results in dose-dependent acute sickness responses when given by intraperitoneal or intracerebroventricular routes*

(a) Adult male C57BL6 mice were exposed IP to R848 in a doses ranging from 100ng to 100µg and monitored for food intake during a nocturnal feeding study (n=3/group). (b) Weight relative to baseline in mice exposed to 20 and 24h R848 IP, demonstrating weight loss at 10µg and 100µg. (c) The doses associated with least response peripherally were given by ICV injection to adult male C57BL6 mice and food intake was monitored via nocturnal feeding study (n=5-6/group). (d) Weight relative to baseline in mice exposed to 20 and 24h R848 ICV. (e) Body temperature in 20 minute intervals for mice injected with 10µg R848 IP at 1300h. (f) Food intake of WT, TLR7KO, and MyD88KO mice following 10µg R848 IP immediately prior to lights out and monitored over 24h. *, P<0.05; **, P<0.01; ***, P<0.001; ****, P<0.0001.

Chronic stimulation of TLR7 results in homologous desensitization and behavioral tachyphylaxis

Given that some proposed clinical uses of TLR7 agonists require chronic dosing regimens, animals were tested for the long-term physiological and molecular outcomes of chronic daily R848 use. Specifically, animals were tested for feeding behavior, locomotor activity, body weight homeostasis, and temperature over the course of extended intervals. As with before, the first dose of R848 resulted in acute sickness responses including hypophagia, decreased body weight, hypothermia, and decreased locomotor activity (Figure 4a, 4b). However, with subsequent doses of R848, animals demonstrated attenuated hypophagia and hypothermia, with no further decreases in body weight. Locomotor activity increased progressively over dark phases with continued daily dosing, but still remained slightly decreased in early phases of the night as long as 5-6 days later (Figure 4c).

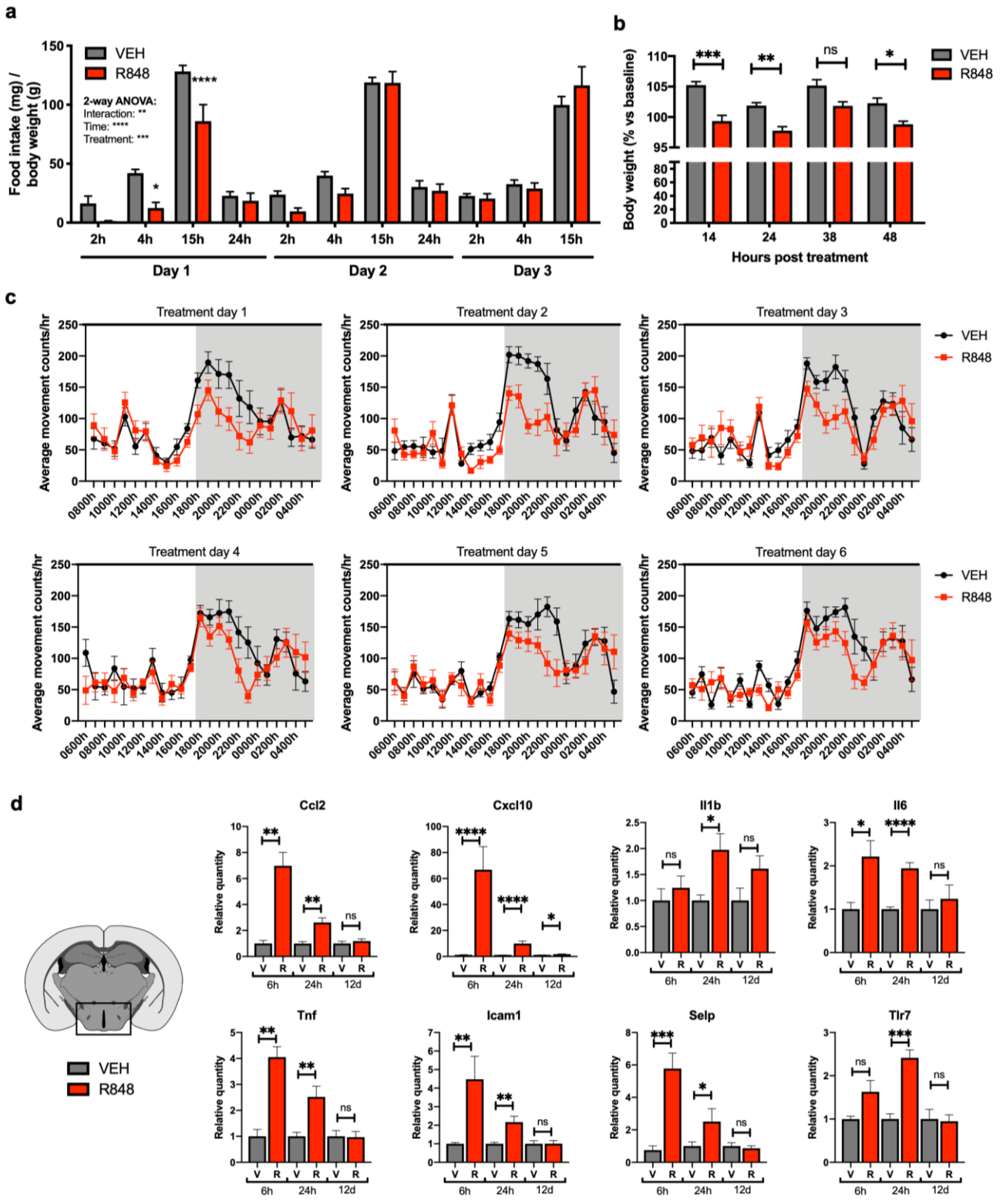
a
Food intake (mg) / body weight (g)
VEH
R848
2-way ANOVA:
Interaction: **
Time: ****
Treatment: ***
2h
4h
15h
24h
Day 1
Day 2
Day 3
b
Body weight (% vs baseline)
Hours post treatment
c
Treatment day 1
Treatment day 2
Treatment day 3
Treatment day 4
Treatment day 5
Treatment day 6
Average movement counts/hr
d
Ccl2
Cxcl10
Il1b
Il6
Tnf
Icam1
Selp
Tlr7
Relative quantity
6h
24h
12d

Figure 4. *Chronic R848 stimulation results in behavioral and molecular tachyphylaxis*
(a-b) Adult male C57BL6 mice were exposed IP to 10μg R848 or vehicle (VEH) for three consecutive days, and monitored for acute sickness responses. (a) Food intake at 2h, 4h, 15h, and 24h over 3 days of treatment (n=8/group). (b) Food intake at 14h, 24h, 36h, and 48h post-treatment. (c) Locomotor activity in average counts/hour for mice treated from 1200h-1300h daily with IP VEH or R848 over 6 days (n=9-10/group). (d) Hypothalamic gene expression of a variety of pro-inflammatory cytokines, chemokines, adhesion molecules, and *Tlr7*, following an acute 24h dose and 12 daily doses of 10μg R848 (n=5/group). *, P<0.05; **, P<0.01; ***, P<0.001; ****, P<0.0001.

To explore the molecular kinetics of this response in a key region of the brain associated with sickness responses, hypothalamic samples were queried for gene expression at 6 and 24 hours following a single dose of 10μg IP R848, and at 12 days on a daily dosing regimen of 10μg IP R848 (Figure 4d). Within 6 hours, increases were observed in *Ccl2, Cxcl10, Il6, Tnf, Icam1,* and *Selp*. These transcripts remained persistently elevated at 24 hours, and in addition, we observed induction of *Il1b* and *Tlr7*. However, following 12 doses of daily R848, all transcripts other than *Cxcl10* had fully returned to baseline expression levels, providing molecular evidence of tachyphylaxis.

Acute and chronic R848 exposure results in morphological changes to glia

In addition to the expected inflammatory gene expression downstream of TLR7 ligation, previous studies implicated TLR7 agonists in neuronal apoptosis, astrogliosis, and microgliosis [334]. To investigate this, we performed immunofluorescence immunohistochemistry on brain sections in control conditions and with R848 for acute (24 hour, single dose) and chronic (10 days, daily treatment) intervals (Figure 5 and Figure S2). Changes to microglia were apparent from even a

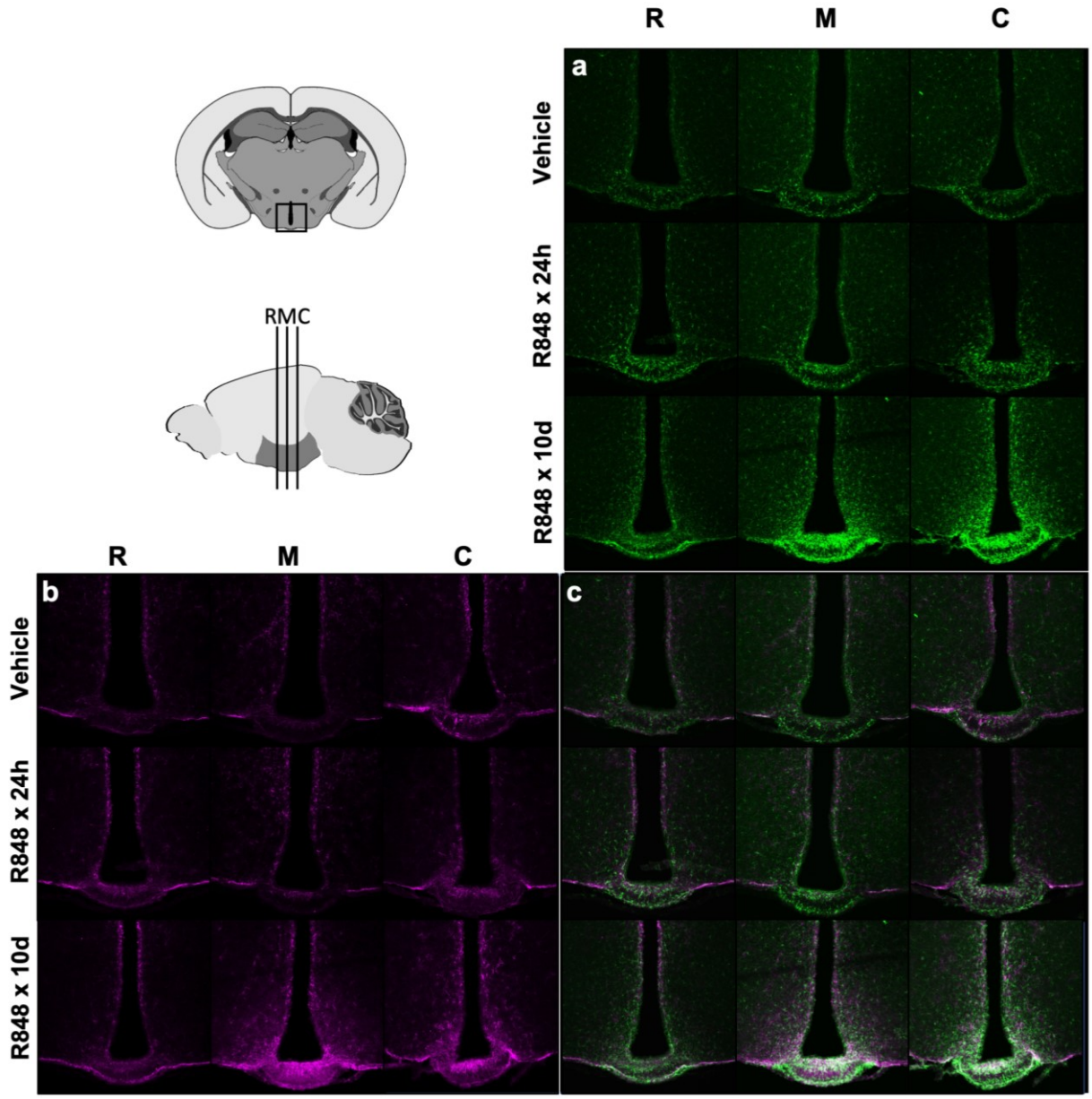

Figure 5. *Glial adaptations to acute and chronic TLR7 stimulation*

Representative confocal microscopy images of the mediobasal hypothalamus following IP vehicle treatment, 24 hours following a single IP dose of 10µg R848, and 24 hours following 10 doses of daily 10µg R848. Images are displayed from rostral (R), middle (M), and caudal (C) coronal sections of the mediobasal hypothalamus. (a) Iba-1 in green to mark microglia and macrophages, (b) GFAP in magenta to denote astrocytes, and (c) overlay of Iba-1 with GFAP. Progressive changes to GFAP signal can be observed from acute to chronic treatment intervals, with Iba1 signal location and density markedly different by day 10 of R848 treatment.

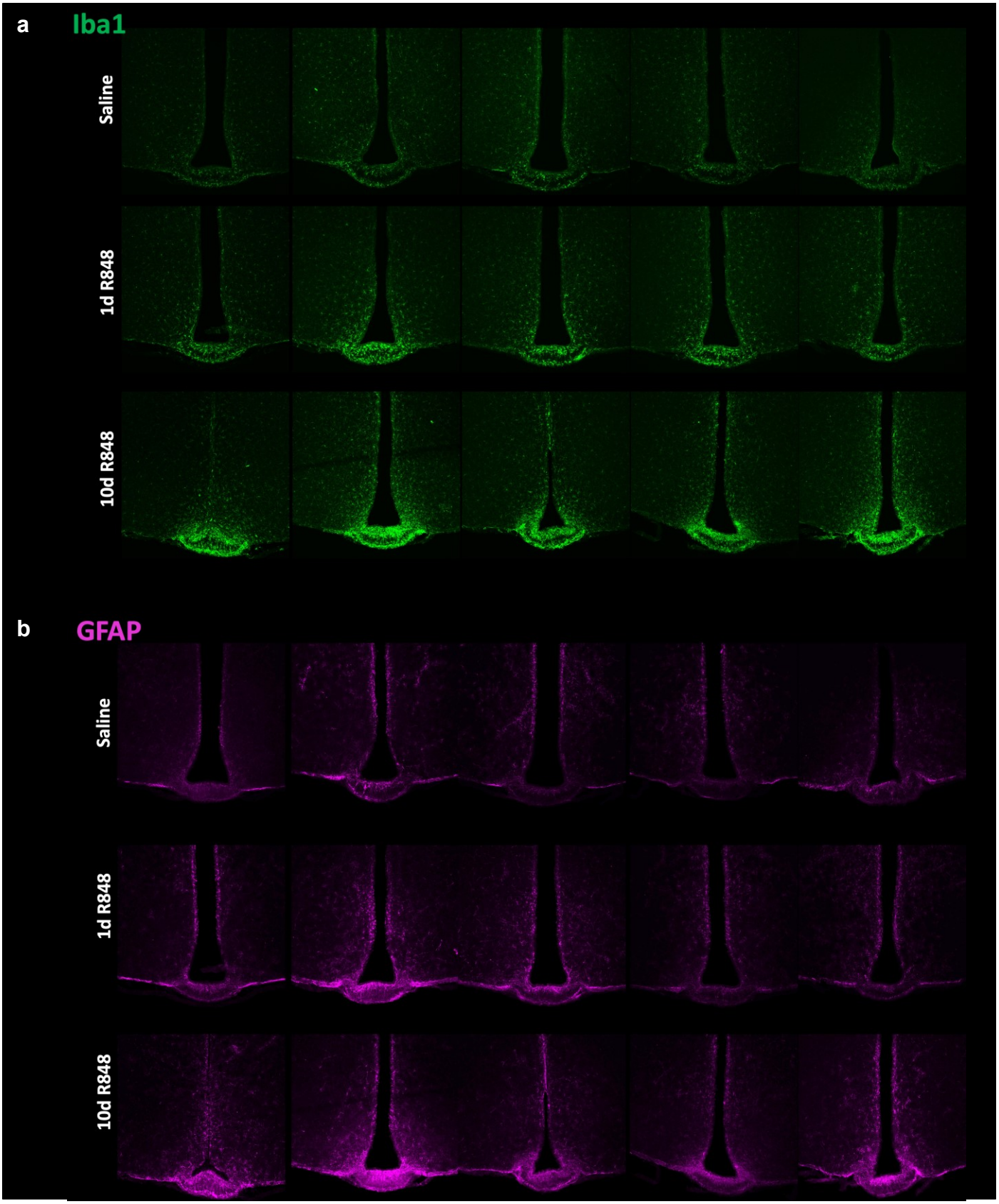
a
Iba1
Saline
1d R848
10d R848
b
GFAP
Saline
1d R848
10d R848

Figure S2. *Extended data: microglial and astrocytic adaptations to acute and chronic TLR7 stimulation*
Confocal microscopy images of the mediobasal hypothalamus following IP vehicle treatment, 24 hours following a single IP dose of 10μg R848, and 24 hours following 10 doses of daily 10μg R848. Images are displayed for all subjects (5/group), to demonstrate range of responses, with (a) Iba-1 in green to mark microglia and macrophages, and (b) GFAP in magenta to mark astrocytes.

---

single dose of therapy, as evidenced by increased Iba1 signal intensity particularly in the median eminence of the hypothalamus. Following the interval of behavioral tachyphylaxis and normalized inflammatory gene expression, brains from mice exposed to daily R848 for 10 days exhibited progressive changes to both astrocytic and microglial populations, especially in the median eminence of the hypothalamus.

To quantitate changes to microglia and astrocytes, confocal Z-stacks were obtained for the mediobasal hypothalamus in anatomically matched coronal planes across all subjects. Analyses were performed to query morphological and quantity changes to Iba1 (Figure 6a) and GFAP (Figure 6b) in three key appetite regulatory regions: the median eminence (ME), arcuate nucleus (ARC), and dorsomedial nucleus (DMH). Microglia demonstrated increasing morphological evidence of activation over the course of progressive TLR7 stimulation across all three regions of the hypothalamus, and underwent absolute increases in cell count in both the ME and ARC (Figure 6a-c, g). Astrocytes, however, only underwent morphological changes in the ME, and did not change in quantity over the course of prolonged TLR7 stimulation (Figure 6d-f, h).

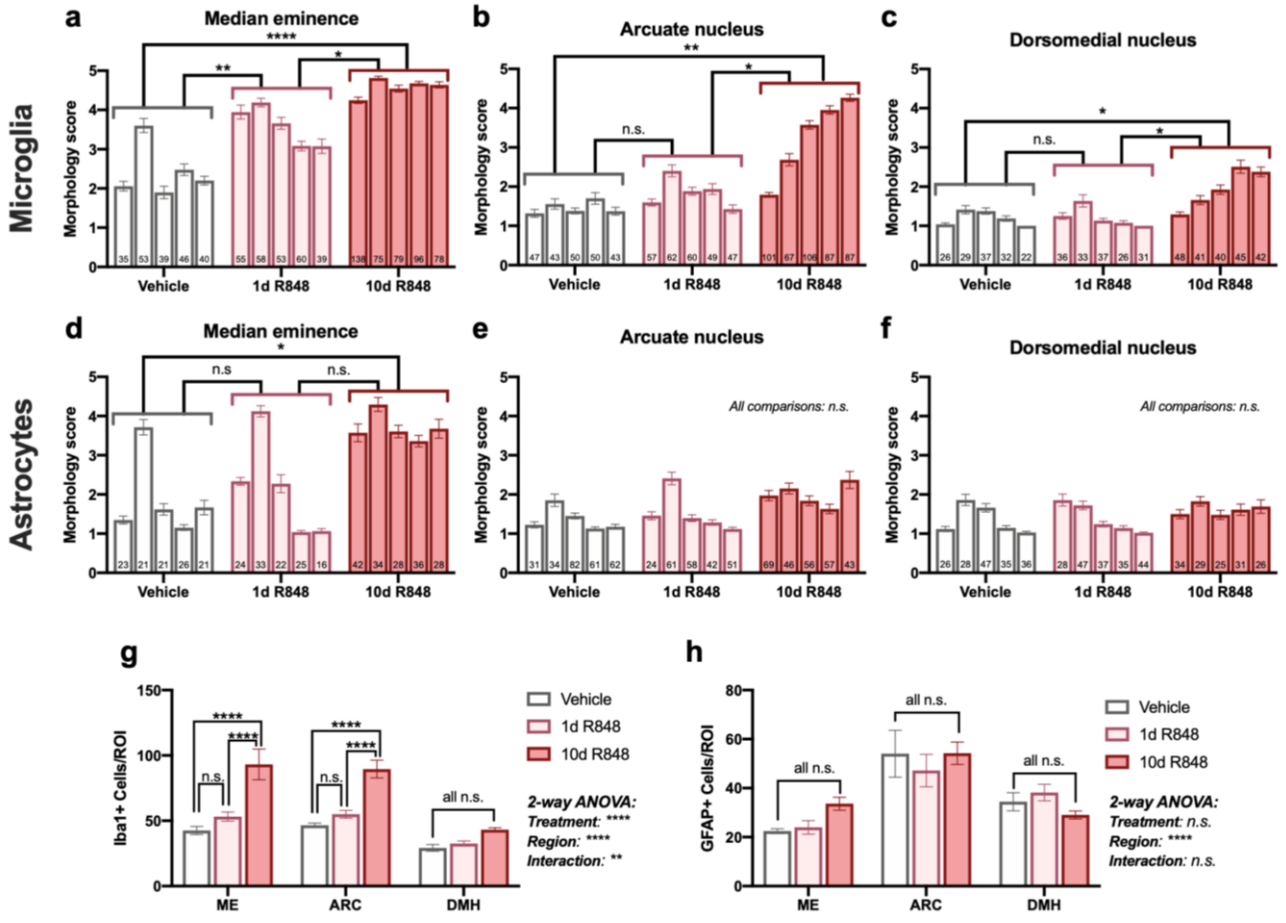

Figure 6. *Hypothalamic microglia demonstrate changes in morphology and quantity following chronic TLR7 stimulation, but astrocytes remain relatively unchanged*

Morphologic activation scores of microglia in the median eminence (a), arcuate nucleus (b), and dorsomedial nucleus (c) following 0, 1 day, and 10 days of pharmacologic stimulation of TLR7 with the agent R848. Astrocytic morphologic scores are shown in the median eminence (d), arcuate nucleus (e), and dorsomedial nucleus (f). In a-f, individual mice are displayed as bars, with the total number of cells counted in the region of interest displayed within each bar, with average morphology score across all counted cells on the y axis. The number of Iba1+ (g) and GFAP+ (h) cells per region of interest are shown based on mean +/- SEM per group. *, P<0.05; **, P<0.01; ***, P<0.001; ****, P<0.0001.

R848 administration results in homologous and heterologous PAMP tolerance in vitro

If microglia are the principal cells capable of TLR7 response in the CNS, their sensitivity to TLR7 agonists *in vitro* could predict the behavioral response to agonist *in vivo*. Therefore, SIM-A9 microglial cells were used to model the kinetics of repeated stimulation on inflammatory response. Given that *Tlr7* expression was not decreased following chronic R848 treatment (Figure 4d), we investigated other signaling proteins downstream of TLR7 to identify potential mediators of tolerance (Figure 7a). Microglia were initially pre-treated with R848 or saline for 1-6 days (Figure 7b). Gene expression profiling indicates that TLR7 stimulation results in self-tolerance, as indicated by decreased pro-inflammatory gene expression following repeated dosing of the same agonist (Figure 7c). In conjunction with progressive decreases in magnitude of R848-induced pro-inflammatory gene expression, we observed increased microglial gene expression of the negative regulators *A20* and *Irak3*. However, other TLR7 signaling transduction mediators such as *MyD88* and *Irak4*, and negative regulators such as *Peli1* and *Ship1*, were unchanged during this time.

Previous studies demonstrated that in peripheral macrophages, stimulation with PAMPS including imidazoquinolines and CpG can result in cross-tolerance to LPS. Therefore, following pre-treatment with R848 or vehicle, microglia were stimulated with a 24 hour pulse of 100ng/mL LPS or continued in their pretreatment condition (R848 or vehicle) (Figure 6b). To assess a variety of cytokines downstream of TLR7 activity, we performed gene expression assays on *Ccl2, Il1b, Il6,* and *Tnfa* (Figure 6d). Both *Ccl2* and *Il6* demonstrated synergistic effects of R848 and LPS exposure, while *Tnfa* primarily demonstrated an additive effect. However, *Il1b* demonstrated a clear pattern of R848-mediated tolerance to LPS, with suppression of LPS-induced gene expression apparent from day 3 onward. This pattern overall suggests that microglia undergo partial cross-tolerance following exposure to R848, particularly with cytokines such as *Il1b* important for induction of acute sickness responses.

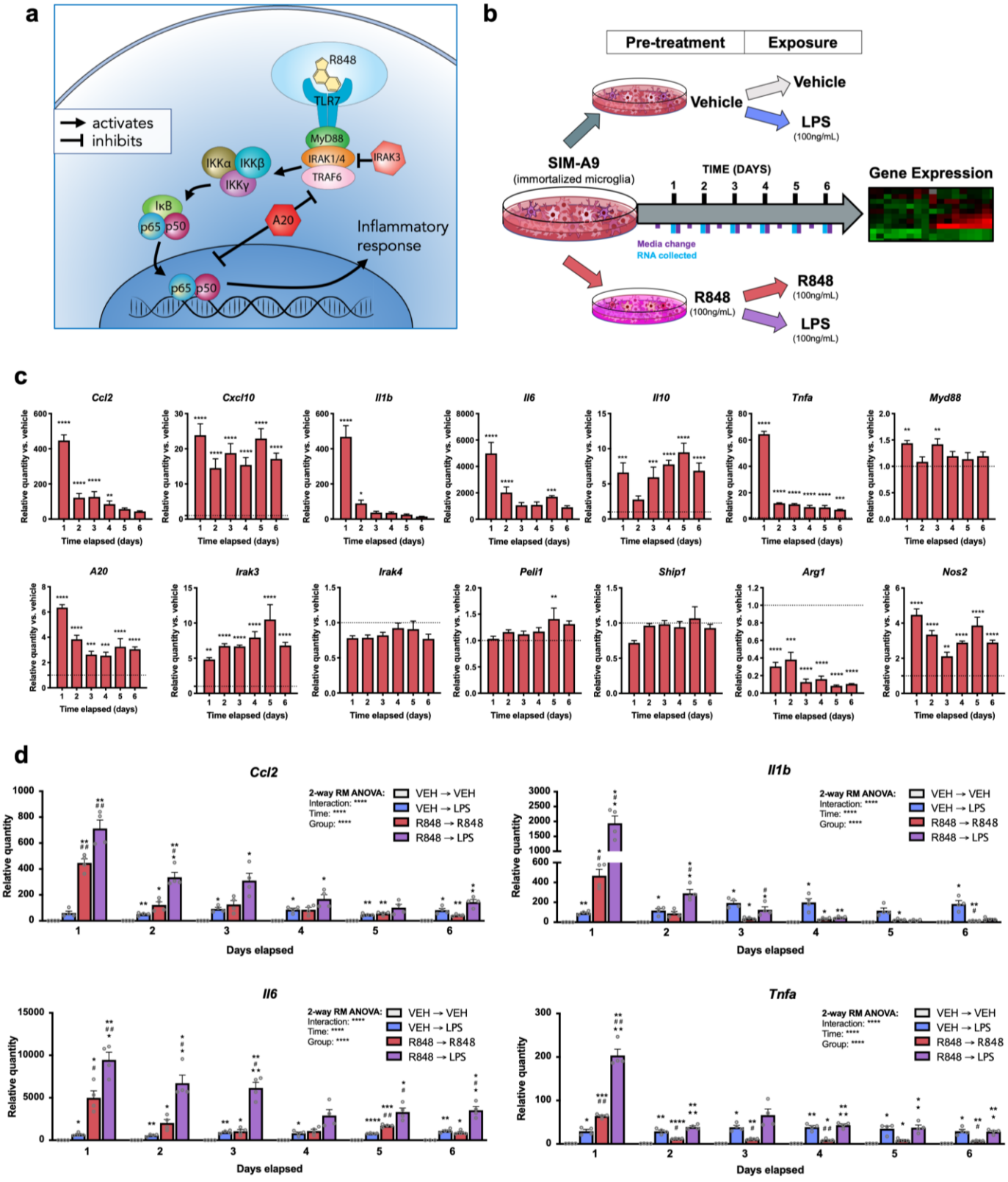
a
R848
TLR7
activates
inhibits
MyD88
IRAK1/4
IRAK3
TRAF6
IKKα
IKKβ
IKKγ
IκB
p65 p50
A20
Inflammatory response
p65 p50
b
Pre-treatment
Exposure
Vehicle
Vehicle
LPS
(100ng/mL)
SIM-A9
(immortalized microglia)
TIME (DAYS)
1 2 3 4 5 6
Gene Expression
Media change
RNA collected
R848
(100ng/mL)
R848
(100ng/mL)
LPS
(100ng/mL)
c
Ccl2
Cxcl10
Il1b
Il6
Il10
Tnfa
Myd88
A20
Irak3
Irak4
Peli1
Ship1
Arg1
Nos2
Relative quantity vs. vehicle
Time elapsed (days)
d
Ccl2
Il1b
Il6
Tnfa
Relative quantity
Days elapsed
2-way RM ANOVA:
Interaction: ****
Time: ****
Group: ****
VEH → VEH
VEH → LPS
R848 → R848
R848 → LPS

Figure 7. *Chronic stimulation of microglia with R848 results in self-tolerance and cross-tolerance to LPS in vitro* (a) Simplified pathway of TLR7 signaling to demonstrate key mediators of response downstream of R848. (b) Experimental design for assessing tolerance to repeated exposures of R848 and cross-tolerance to LPS in microglia. (c) Gene expression of microglia exposed to R848 for 1-6 days, relative to vehicle-treated controls (n=4/group). (d) Gene expression of microglia exposed to R848 or vehicle for 1-6 days, then continued in pre-treatment condition or pulsed with 24h LPS (n=4/group). Gene expression is displayed relative to vehicle pre-treated microglia in the vehicle exposure group. *, P<0.05; **, P<0.01; ***, P<0.001; ****, P<0.0001.

R848 induces behavioral and molecular cross-tolerance to endotoxin

Next, we aimed to elucidate whether the cross-tolerance phenotype observed in microglia extends to whole animal physiology. Mice were allocated to daily 10μg R848 or vehicle IP pre-treatment for a total of 7 days, then given either vehicle or LPS (Figure 8a). While R848 itself did not have any effect on food intake or body weight, R848 pre-treatment was protective against LPS-induced hypophagia (Figure 8b). In addition, animals pre-treated with R848 were protected against LPS-induced weight loss (Figure 8c). In conjunction with this behavioral finding, we confirmed molecular evidence of cross-tolerance in both hypothalamus and liver, which exhibited decreased LPS-stimulated induction of *Ccl2, Il1b,* and *Tnf* following pre-treatment with R848 (Figure 8d,e).

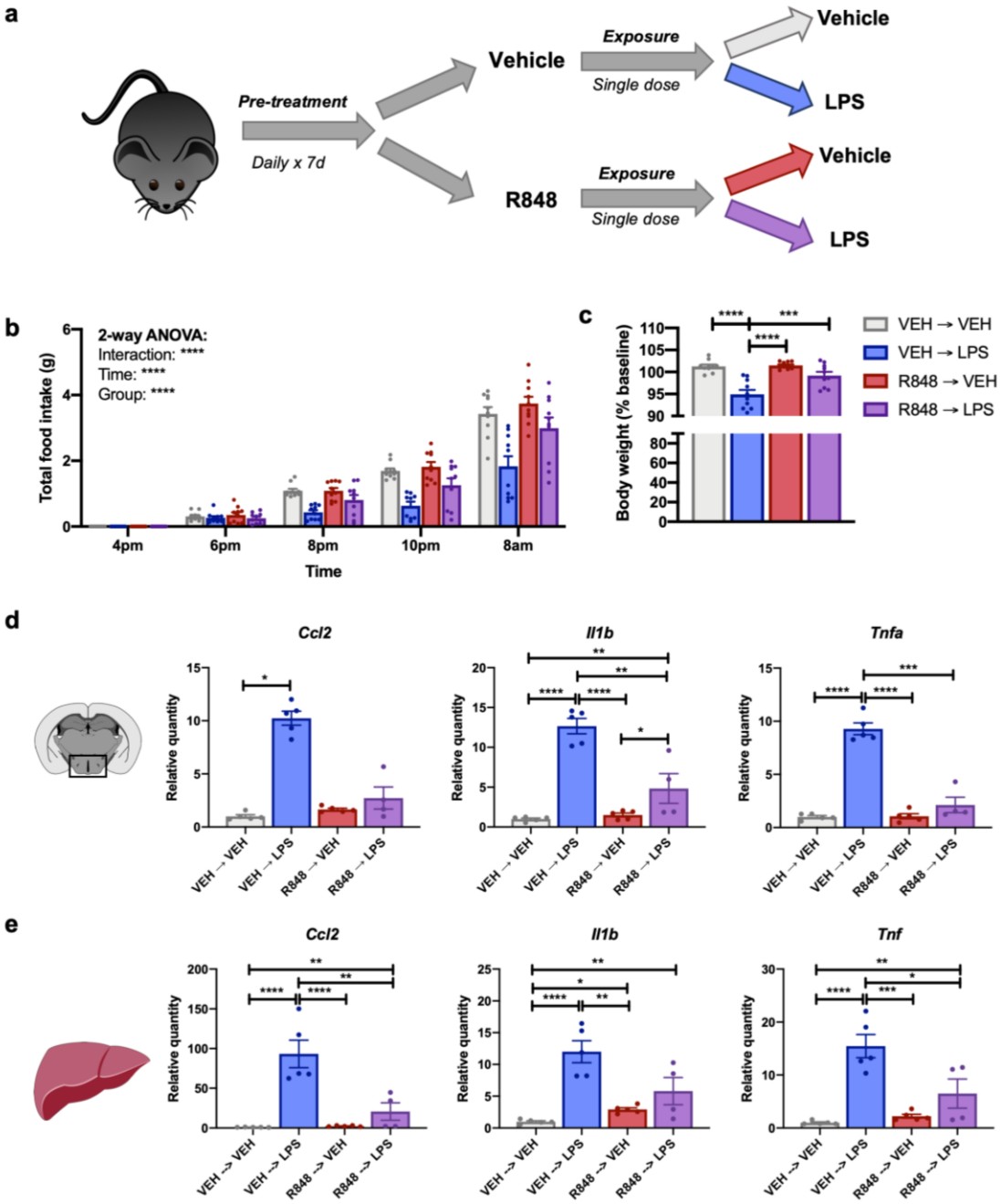

Figure 8. *Prolonged systemic dosing with R848 in vivo results in cross-tolerance to LPS*

(a) Experimental design diagram depicting allocation into a 7 day pretreatment of 10µg IP R848 or vehicle, with subsequent single exposure to vehicle or 100µg/kg LPS. (b) Food intake over 18 hours of exposure to LPS or vehicle in R848 or vehicle pre-treated groups. (c) Change in body weight from 1200h the day of injection – 0800h the subsequent morning. (d) Hypothalamic gene expression of pro-inflammatory cytokines following pretreatment and exposure. (e) Hepatic gene expression of pro-inflammatory cytokines following pretreatment and exposure. N=4-5 animals/group/experiment, with experiment repeated twice. ***, P<0.001; ****, P<0.0001.

Discussion

In this study, we confirmed that TLR7 is primarily expressed in immune cells, with central nervous system gene expression isolated specifically to microglia. Microglia both *in vitro* and *in vivo* respond robustly to R848 stimulation in a TLR7-dependent manner. Furthermore, animals develop classical acute sickness responses and systemic induction of NF-kB dependent inflammatory signaling pathways when drug is given either IP or ICV. However, behavioral tachyphylaxis is apparent by 48h, and is complete by 72h. The molecular data recapitulates the behavioral data by demonstrating acute inflammatory responses at early intervals, but virtually no residual inflammatory responses in by day 12 of treatment. In contrast to previous reports, TLR7 was not found to be expressed in central nervous system neurons. These data combined demonstrate that TLR7 stimulation induces acute behavioral and molecular evidence of sickness responses, but that these effects are self-limited and undergo rapid tachyphylaxis *in vivo.* This is reassuring for any applications, such as vaccine adjuvants, cancer immunotherapy, and asthma immunotherapy, in which TLR7 agonists show substantial therapeutic promise. Finally, we observe that in addition to promoting tolerance to TLR7-dependent signals, chronic R848 treatment results in cross-tolerance to LPS both in cultured microglia and *in vivo.*

Importantly, this study demonstrates that the brain undergoes immune tolerance following repeated exposure to TLR7 agonists, and that this process occurs at the level of microglia. These data provide evidence that in addition to immune cells of bone marrow origin, tissue resident macrophages of yolk sac origin such as microglia can develop immune tolerance [335]. The implications of this finding are particularly interesting in light of the immune privileged nature of the brain. Microglia are the key determinants of brain immune responses in the context of an intact blood-brain barrier. Their responses to stimuli therefore directly alter the activity of

inflammation-sensitive neuronal circuitry such as appetite- and activity-regulatory center of the hypothalamus. With repeated exposure to R848, we find that microglia cease to produce inflammatory signals, which results in a loss of sickness responses even when pattern recognition receptor ligands such as R848 or LPS are present. This therefore represents a novel and important manifestation of inducible immune tolerance, whereby the homeostatic setpoint for behavioral and metabolic sickness responses is globally altered.

A number of clinical trials with TLR7 agonists have observed manifestations associated with acute sickness responses, including fever and flu-like symptoms [336]. However, our study indicates that these sickness responses may be temporary in their nature and restricted to treatment induction: food intake and body weight both return to baseline levels even in the context of repeated dosing, and locomotor activity also returns to near-normal levels. Though both peripherally administered R848 results in marked increases in gene expression of inflammatory transcripts in the central nervous system, we found that continued dosing was associated with a return to basal levels of expression for most transcripts queried. While this study did not include comprehensive cognitive and behavioral assessments of chronic TLR7/8 stimulation, future studies to investigate these outcomes will be crucial in safety evaluations of this drug class for clinical applications.

Previous literature has simultaneously highlighted the potential for benefit and for harm following TLR7 stimulation. Therapeutic uses for TLR7 agonists include disease states driven by pathogenic Th2 responses, as well as vaccine adjuvants for infectious agents and cancer. As one example of clinical utility, TLR7 agonism demonstrates strong potential as a treatment for asthma and other allergic airway diseases. Synthetic agonists of TLR7, particularly imiquimod, decrease

airway hyperreactivity, and eosinophilic inflammation in the context of asthma, and shift CD4 T cell functional status from Th2 to Th1 [337]. A similar principle was explored as a cancer therapeutic, given that a common feature of established solid tumors is immunosuppression within the tumor microenvironment [338]. The TLR7 agonist imiquimod is FDA-approved as a monotherapy for basal cell carcinoma (since 2004), with cure rates ranging between 83-88% [339]. Beyond skin cancer, other investigations explored the use of TLR7 agonists for a large variety of malignancies. As one example, a recent study used nanoparticle delivery of R848 to CD8+ T cells, resulting in improved antitumor immunity and prolonged survival in the murine M38 model of colorectal cancer [340]. In addition, a purine-scaffolded TLR7 agonist known as GD5 was recently shown to augment doxorubicin's efficacy against T cell lymphoma [341]. In another example of TLR7 augmenting antitumor responses, a combinatorial therapy of imiquimod with bacillus Calemtte-Guérin (BCG) decreased tumorigenesis in the context of immunogenic nonmuscle-invasive bladder cancer [342]. At the time of this report, the database ClinicalTrials.gov lists 25 clinical trials for R848 and an additional 166 on the imidazoquinoline imiquimod. Indications for these studies include breast cancer, pediatric ependymoma, malignant glioma, ovarian cancer, lung cancer, and cervical cancer. Finally, TLR7 agonists have demonstrated substantial utility as an infectious disease vaccine adjuvant, particularly for influenza [343,344].

However, despite its multifaceted therapeutic potential, a variety of studies implicate TLR7 in the pathogenesis of systemic conditions such as autoimmune diseases, cancer, and cachexia. TLR7 agonists can be used to induce systemic and localized autoimmunity in mouse, and have been used as experimentally inducible models of lupus and psoriasis [345,346]. Furthermore, TLR7 activation is tied to accelerated pancreatic carcinogenesis in a mouse model of cerulean-induced pancreatitis, and was proposed as a mechanism of apoptotic muscular cell death in

cancer cachexia in an *in vitro* study using myoblasts. In this study, we did not find evidence for neurodegeneration with systemic administration of R848 at acute or chronic intervals. This may highlight differences between routes of administration, given that many previous studies finding deleterious effects have focused on topical and intradermal applications of imidazoquinolines [334]. To this effect, intraperitoneal administration of R848 is consistently associated with less severe autoimmunity and neuroinflammation than topical administration [333]. Furthermore, a number of studies implicating TLR7 in disease use different types of agonists than we did, including native ligands like ssRNA40 and microRNAs. It is highly possible that outcomes of TLR7 stimulation differ between different classes of agonist, particularly since TLR7 has many steps of regulation and co-receptors that could modify signaling dynamics [347,348].

In addition to the aforementioned peripheral and systemic adverse roles, TLR7 was investigated in the context of central nervous system processes and pathologies, including acute sickness responses, Alzheimer's disease, and alcoholism. Previous studies suggested that TLR7 is present in a variety of CNS cell types, particularly neurons, and proposed mechanisms in which TLR7 agonists act directly on neurons to induce apoptosis and altered dendritic arborization.[329,349-351] Using a meta-analysis of single-cell RNA sequencing, *in situ* hybridization, and RNAscope, we found that *in vivo* central nervous system gene expression of TLR7 is restricted specifically to microglia. In light of this data, it is possible that deleterious CNS findings that were previously reported following TLR7 agonists might not be direct neuronal responses, but instead could represent changes downstream of microglial activity. In agreement with previous studies using TLR7 agonists, we found that administration of R848 resulted in sickness responses including anorexia and weight loss, and in agreement with one group, a hypothermic response [333,352]. While we did observe changes in microglial and astrocytic morphology following treatment

with R848, further work must be done to determine whether this outcome is adaptive or harmful. Indeed, gliosis can be a protective outcome and is not necessarily indicative of neuropathology.

In physiological contexts, immune tolerance is a well-described phenomenon that can occur following major inflammatory stressors such as infection [353]. In sepsis, immune tolerance is a crucial defense strategy that maintains systemic homeostasis while still permitting host defense to occur [354]. However, the nature of the immune tolerance mechanism is important, and bioinformatics-derived studies have also associated immune tolerance gene signatures with end organ dysfunction in sepsis [355]. Indeed, certain viral infections such as influenza are known to cause increased risk of subsequent bacterial infections due to inappropriate immune tolerance [356]. Previous studies have shown that in the context of peritoneal macrophages, pre-treatment with imidazoquinoline compounds can prevent LPS-induced pro-inflammatory responses [357]. This study shows that microglia, the resident immune cells of the central nervous system, are also capable of undergoing a process of immune tolerance following TLR7 stimulation. While this property could be useful for disease states in which a primary mechanism of illness involves aberrant pro-inflammatory responses, it could be dangerous in the context of pathogen burden and risk of infectious disease. Further studies will be required to determine whether systemic pathogen response remains intact during and following R848 therapy, despite partial molecular hyporesponsiveness to LPS stimulation.

In summary, these studies provide evidence supporting further therapeutic investigation of combined TLR7/8 agonists, given that sickness responses are not protracted and do not result in cell death. While sickness responses do occur following initial dosing of TLR7/8 agonist, this drug class results in receptor tolerance thereafter and does not continue to provoke behavioral or

molecular evidence of inflammation. The lack of detected adverse outcomes in these studies further support the notion that TLR7 agonists could be used in both acute applications, such as vaccines, and in chronic applications, such as immunotherapies for cancer and Th2-associated illnesses.

Materials and methods

Study design

This study was designed to 1) query principal cell types involved in TLR7-mediated responses in the central nervous system, 2) explore molecular outcomes of acute and chronic TLR7 stimulation in microglia *in vitro*, 3) investigate physiological outcomes of acute and chronic TLR7 stimulation in mice, 4) perform tissue-specific analyses of the molecular underpinnings of physiological outcomes of TLR7 stimulation, and 5) determine whether sickness response tachyphylaxis was TLR7 intrinsic or extends to other pertinent pattern recognition receptors. These studies were performed in a combination of mouse models and *in vitro* systems. Array data included for the single-cell RNA-sequencing meta-analysis consisted of both male and female murine samples, and primary cell lines were derived from mixed-sex backgrounds. The immortalized microglial cell line SIM-A9 was derived from a female clone. Mouse studies used male animals of 8-10 weeks of age at study outset, with randomization performed for metrics pertinent to sickness response measurements (age, basal food intake, basal body weight). To determine appropriate sample size in mouse studies, power analyses were performed using food intake and body weight pilot data for single dose R848. Blinding was performed for all subjective analyses, including scoring of glia in histological sections.

Meta-analysis of published RNA-sequencing studies

Single-cell RNA sequencing studies performed in brain tissue isolated from mouse were included for analysis by the Oregon Health and Science University Bioinformatics Core. Datasets available on the Gene Expression Omnibus (GEO) were queried for studies pertaining to gene expression of central nervous system cell types during healthy states. A total of 8 studies meeting inclusion criteria were used. Platforms and citations for all studies within the meta-analyses are included in Supplemental Table 1. The following expression datasets were downloaded from the GEO website: GSE52564, GSE71585, GSE74672, GSE75246, GSE82187, GSE93374, GSE87544, GSE90806 (Supplemental Table 1). Given the differences in technology, processing/quantification and design across the datasets, expression was summarized based on the distribution within each GEO data set as follows. First, average quantification unit across each Cell Type for each gene of interest was computed. Second, each gene of interest was then assigned to one of four quartiles (1-4) based on its average quantification as compared to expression of all of the genes in that cell type. For all GEO data sets except GSE75246, Gene model annotation was provided and used to identify the genes of focus for this study. For GSE75246, NCBI Entrez Gene ID was provided and gene name was annotated using org.Mm.eg.db package from Bioconductor [358]. The heatmap was created using the pheatmap Bioconductor package [359]. The Cell Type annotation in the heatmap was hand-curated based on review of the GEO annotation. Cell types were pooled into broad categories of cell identity rather than functional state or subset.

Tissue culture

Primary mixed glia and primary microglia isolates were generated as previously described [360]. For further studies we used the spontaneously immortalized murine microglial cell line SIM-A9, which were provided generously as a gift by Dr. Kumi Nagamoto-Combs [332]. SIM-A9 were

maintained in DMEM/F12 supplemented with 10% heat-inactivated FBS, 5% normal horse serum, and 50 U/mL penicillin/streptomycin (Gibco), with incubators maintained at 37°C and 5% CO_2.

Animal studies

Male C57BL/6J mice (cat. #000664), TLR7KO mice (cat. # 008380), and MyD88KO mice (cat. #009088) were obtained from The Jackson Laboratory and maintained in standard housing at 26°C and 12h light / 12h dark cycles (0600h-1800h light). Animals were provided with *ad libitum* access to water and standard chow (Purina rodent diet 5001; Purina Mills, St. Louis, MO, USA). In the week prior to studies, animals were transitioned to individual housing to acclimate to experimental conditions. Animal food intake and body weight were monitored daily at designated timepoints for acute response studies, and from 0900-1000h for chronic response studies. All studies were conducted according to the National Institutes of Health Guide for the Care and Use of Laboratory Animals and approved by the Institutional Animal Care and Use Committee of Oregon Health & Science University.

Body temperature and locomotor activity measurement

Body temperature and voluntary home cage locomotor activity were measured via MiniMitter tracking devices (MiniMitter, Bend, OR, USA). Mice were implanted three days prior drug administration with MiniMitter transponders in the intrascapular subcutaneous space. Using these devices, body temperature and movement counts in x-, y- and z-axes were recorded in 5-minute intervals (Vital View, MiniMitter). To maximize signal-to-noise ratio while still capturing nuanced activity peaks and nadirs, movement data was binned into hourly averages per subject.

Tissue collection

At designated time points, animals were deeply anesthetized by ketamine cocktail. For gene expression analyses, tissues including hypothalamus, cortex, and liver were harvested and stored in RNAlater (Ambion). For *in situ* hybridization studies, whole brain was collected and immediately flash frozen, then sectioned on a cryostat. For histology, animals were perfused with cold PBS and 4% paraformaldehyde for tissue extraction. Whole brain tissue was post-fixed overnight in 4% PFA, cryoprotected in 20% sucrose, and stored at –80°C.

In situ hybridization and RNAscope

Age and sex matched mice from control, acute inflammatory conditions (LPS), or chronic inflammatory conditions (pancreatic cancer) were sacrificed and underwent transcaridal perfusion with PBS. Fresh frozen brains were subsequently and processed for *in situ* hybridization as previously described [361]. Antisense ^{33}P-labeled mouse TLR7 (*Tlr7*) riboprobe (corresponding to bases 123-518 of murine *Tlr7*; GenBank accession no. NM_ 013179) (0.1 pmol/ml) was denatured, dissolved in hybridization buffer along with tRNA (1.7 mg/ ml), and applied to slides. Slides were covered with glass coverslips, placed in a humidified chamber, and incubated overnight at 55°C. The following day, slides were treated with RNase A and washed under conditions of increasing stringency. Slides were dipped in 100% ethanol, air dried, and then dipped in NTB-2 liquid emulsion (Eastman Kodak Co., Rochester, NY). Slides were developed 17d later and coverslipped. RNAscope was performed with probes against *Tlr7* and *Tmem119*, a microglia-specific marker, according to manufacturer protocol (ACDBio, Newark, CA)

Intracerebroventricular and intraperitoneal injections

For placement of intracerebroventricular (ICV) cannulas, mice were anesthetized under isoflurane and placed on a stereotactic alignment instrument (Kopf Instruments). 26-gauge cannulas were placed at 1.0 mm X, –0.5 mm Y, and –2.25 mm Z relative to bregma, allowing placement in the lateral ventricular space. Mice were given one week for recovery after cannula placement, with repeated handling to acclimate to the injection protocol. Injections were given in 1 µl total volume infused over 1 minute. Intraperitoneal (IP) injections were performed in a volume of 200µL at the designated doses. R848 was obtained from Enzo Life Sciences (#NC9739083), lipopolysaccharide (LPS) was obtained from Sigma, and Poly I:C was obtained from Sigma.

Nocturnal feeding studies

Studies monitoring acute sickness responses were performed at night, in accordance with the feeding behavior and activity of mice. For all studies, mice were housed individually for one week prior to experiments, with Enviro-Dri and Nestlet enrichment. Baseline body weight was used to randomize groups to ensure equal distribution between experimental groups. For dose response and illness response studies, drug or vehicle were administered between 1200-1300h. Food was weighed at 7 time points following injection (4h, 6h, 8h, 10h, 20h, 22h, and 24h), and body weights were measured at 2 time points (20h and 24h).

Immunofluorescence immunohistochemistry

Following harvest and fixation in 4% paraformaldehyde, cryopreserved frozen brain tissue was sectioned at 30µm using a sliding microtome with a freezing stage (Leica). Sections were incubated in 5% normal horse serum in 0.01M PBS and 0.3% Triton X-100 for initial blocking. Next, sections were incubated for 24h in antibodies against Iba-1 (Wako, Rabbit, #NCNP24,

1:1000) and GFAP (EMD Millipore, mouse, #MAB360; 1:1000) to mark microglia and astrocytes respectively. For detection, secondary antibodies of goat origin were used as follows: anti-rabbit AF488 (1:500), anti-mouse AF647 (1:500), (Invitrogen). Confocal images were acquired with a Nikon Eclipse inverted microscope and processed with the Nikon A1 confocal image acquisition system (Nikon Instruments).

Quantitative reverse transcription PCR

RNA was extracted and purified with RNeasy Mini kits (Qiagen Inc., Valencia, CA), then reverse transcribed into cDNA with a High Capacity cDNA Reverse Transcription Kit (Life Technologies). qRT-PCR was performed using TaqMan reagents and primer-probes (Applied Biotechnologies). Inflammatory response genes in the brain (C-C motif chemokine ligand 2, *Ccl2,* C-X-C motif chemokine 10, *Cxcl10,* interleukin-1 beta, *Il-1β*; tumor necrosis factor α, *Tnfα*; interleukin 10, *Il10*; arginase 1, *Arg1*, nitric oxide synthase 2, *Nos2*; Intercellular adhesion molecule 1, *Icam1,* P-selectin, *Selp*; interleukin-6, *Il-6*; Toll-like receptor 7, *Tlr7*), innate immune signal transduction genes in microglia (Myeloid differentiation factor 88, *Myd88*; TNF alpha induced protein 3, *A20;* Interleukin 1 associated receptor associated kinase 3, *Irak3*; Interleukin 1 associated receptor kinase 4, *Irak4*; Pellino E3 ubiquitin protein ligase 1, *Peli1;* SH-2 containing inositol 5' polyphosphatase 1, *Ship1*) and inflammatory response genes in liver (amyloid P component, serum, *Apcs*; C-reactive protein, *Crp,* orosomucoid 1, *Orm1*) were compared between experimental groups by qRT-PCR and normalized to 18s using the ΔΔCT method.

Flow cytometry

SIMA9 cells transduced with a construct expressing luciferase under the control of an NF□B-binding consensus sequence were plated at 0.2 x 10^6 cells per well in 12-well tissue culture plates.

LPS (10 ng/ml), PBS (20µl), R848 (1µg/ml) or DMSO (0.1µl/ml) was added for 6, 24, or 48 hours and cells were collected for analysis. For flow cytometry, cells were fixed and permeabilized (Cytofix and Fix/Perm solution, BD Biosciences), blocked with 2% normal rat serum, and then stained with PE-labeled anti-mouse TNFa (BD 554419) and APC-Cy7-labeled mouse anti-CD45 (BioLegend 103115) mAbs for 1.5hr. Control cells were stained with a PE-labeled isotype control mAb (BD 557078) and APC-Cy7 mouse anti-CD45 mAb. Cells were washed and then analyzed on a FACS Canto II flow cytometer (BD Biosciences) collecting 40,000 events per sample. The data were processed using FlowJo analytical software version 10.1r7 (FlowJo LLC, Ashland, OR, USA).

Image analysis

Iba-1 and GFAP labeled images for each brain were imported as .nd2 format files into FIJI and converted to maximum projection Z-stacks for each channel. For each subject, coronal sections were selected to match as closely as possible on the rostral-caudal level. A blinded reviewer then used the FIJI Count Cells function to score individual microglia and astrocytes in the median eminence (ME), arcuate nucleus of the hypothalamus (ARC), and the dorsomedial hypothalamus (DMH) using a validated activation scale [362]. All visible cells were counted per region of interest, from which average microglial and astrocyte morphology scores and total count were obtained per region of interest per subject.

Statistical analysis

Throughout figures, data are expressed as mean ± SEM. Statistical analyses were performed with Prism 8.0 software (Graphpad Software Corp). For longitudinal comparisons and for 2x2 exposure designs, data were analyzed with a two-way ANOVA followed with *post hoc* Tukey's multiple comparisons test. For cross-sectional comparisons and for single exposure designs, data were

analyzed with a One-way ANOVA followed with Sidak *post hoc* test. For all analyses, significance was assigned at the level of $p< 0.05$, with specific P value ranges denoted throughout figures.

Supplemental Table 1

RNA-Seq studies used for comparing cell category gene expression of TLR7 in the murine central nervous system

GEO accession	Platform	Cell categories represented
GSE52564	Illumina HiSeq 2000 (Mus musculus).	Neurons, astrocytes, microglia, oligodendrocytes, endothelium
GSE52564	Illumina HiSeq 2000 (Mus musculus).	Neurons, astrocytes, microglia, oligodendrocytes, endothelium
GSE71585	Illumina HiSeq 2000, Illumina MiSeq, and Illumina HiSeq 2500	Neurons, astrocytes, microglia, oligodendrocytes, endothelium
GSE74672	Illumina HiSeq 2000 (Mus musculus)	Neurons, astrocytes, microglia, oligodendrocytes, endothelium
GSE79374	llumina HiSeq 2500 (Mus musculus).	Neurons, astrocytes, microglia, oligodendrocytes, endothelium
GSE82187	Illumina HiSeq 2000 and Illumina NextSeq 500 (Mus musculus)	Neurons, astrocytes, microglia, oligodendrocytes, endothelium (Within striatum)
GSE90806	Illumina NextSeq 500 (Mus musculus).	Neurons
GSE93374	Illumina NextSeq 500 (Mus musculus)	Neurons, astrocytes, microglia, oligodendrocytes, endothelium (Within arcuate and median eminence)
GSE106447	Ilumina NextSeq 500 (Mus musculus).	Astrocytes, microglia, oligodendrocytes, endothelium

Conflicts of interest

DLM declares that he is a paid consultant for Pfizer, Inc.

Acknowledgements

We are grateful for the help of many investigators, cores, and lab personnel, including Dr. Stephanie Krasnow, the OHSU Flow Cytometry Core, and the OHSU Advanced Light Microscopy Core. Funding for this work was provided by R01CA184324-01, R01CA217989-01, and Brenden-Colson Center for Pancreatic Care to DLM, and NCATS TL1TR002371 to KAM.

VII. The TLR7/8 agonist R848 remodels tumor and host immune responses to promote survival in pancreatic cancer

Katherine A. Michaelis, Mason A. Norgard, Xinxia Zhu, Peter R. Levasseur, Shamilene Sivagnanam, Shannon M. Liudahl, Kevin G. Burfeind, Brennan Olson, Katherine R. Pelz, Diana M. Angeles Ramos, H. Carlo Maurer, Kenneth P. Olive, Lisa M. Coussens, Terry K. Morgan, Daniel L. Marks

Fig S1. *Graphical abstract*

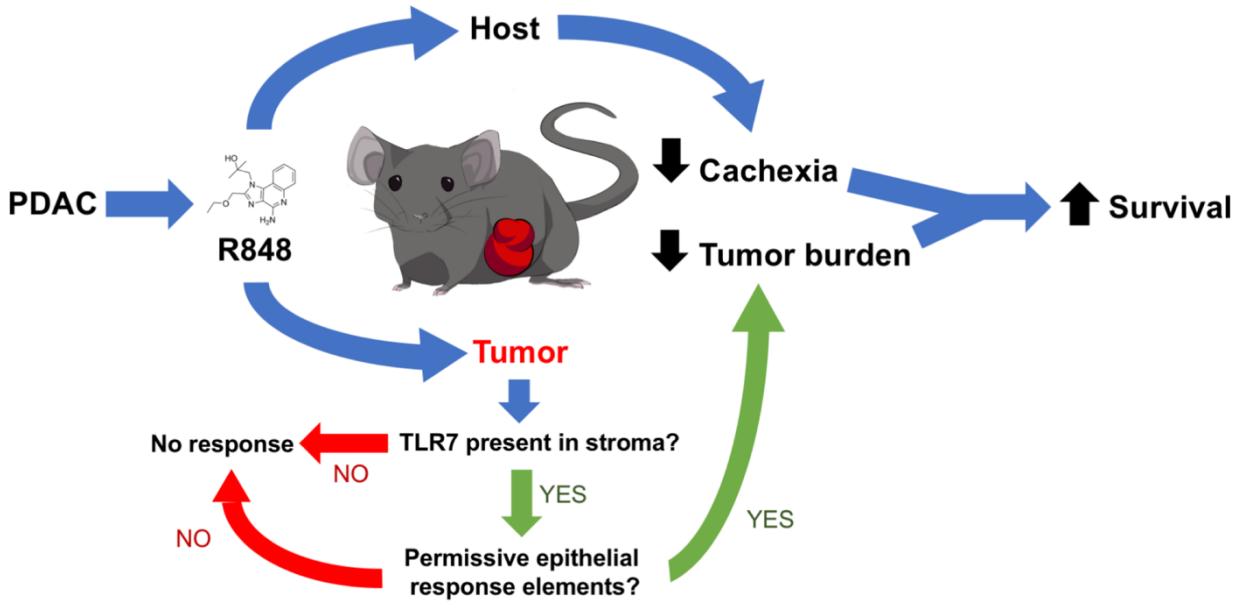

Abstract

A priority in cancer research is to innovate therapies that not only are effective against tumor progression, but address comorbidities such as cachexia that limit quality and quantity of life. We demonstrate that the TLR7/8 agonist R848 induces anti-tumor responses and attenuates cachexia in murine models of pancreatic ductal adenocarcinoma (PDAC). A majority of epithelial clones were sensitive to R848, as evidenced by smaller tumor mass, increased immune complexity, increased $CD8^+$ T cell infiltration and activity, and decreased Treg frequency. R848-treated mice demonstrated improvements in behavioral and molecular cachexia manifestations, resulting in a near-doubling of survival duration. Knockout mouse studies revealed that stromal, not epithelial, TLR7 is requisite for R848-mediated responses. In patient samples, we found *Tlr7* is ubiquitously expressed in stroma across all stages of pancreatic neoplasia, but epithelial *Tlr7* expression is relatively uncommon. These studies indicate immune-enhancing approaches including R848 may be useful in PDAC and cancer-associated cachexia.

Introduction

With recent advances in the field of cancer immunotherapy, a number of highly effective therapies have been developed to enhance anti-tumor immunity. Some of these approaches, such as immune checkpoint inhibitors and adoptive cell transfer, already demonstrate great benefit for a subset of cancer patients [363,364]. Unfortunately, despite these revolutionary advances for many forms of cancer, immune therapy approaches for patients with pancreatic ductal adenocarcinoma (PDAC) are lacking. With a median survival of 6 months and a 5-year survival rate of 8%, outcomes for PDAC remain dismal, and new therapies are urgently needed [365]. Numerous biological rationales have been hypothesized as underlying barriers for lack of effective immunotherapy responses in PDAC, including that the tumor microenvironment in PDAC is profoundly immunosuppressive. Not only are immune cell infiltrates sparse in pancreatic cancer, but abundant presence of myeloid cells harboring T cell-suppressive activities are thought to interfere with all stages of anti-tumor immune responses [366,367]. These factors make it clear that to create successful immunotherapy approaches in PDAC, it will be essential to modify the immune landscape of these tumors.

One promising strategy for remodeling tumor immune composition and functionality in PDAC is to inhibit tumor promoting inflammatory signaling pathways common to myeloid and lymphoid cells, including Toll-like receptors (TLRs). Stimulation of TLRs not only results in changes to myeloid cell activity in the tumor microenvironment, but augments the activity and specificity of adaptive immunity. For example, recent research highlights that stimulation of TLR7, an endosomal ssRNA receptor traditionally associated with viral response, lowers PD-1 (programmed cell death protein 1) expression on T cells and enhances $CD8^+$ T cell cytotoxic responses [368]. Small molecule TLR7 agonists have already demonstrated success in dermatologic

malignancies including basal cell carcinoma [339], but will require further optimization for other types of cancer. Despite how TLR7 is abundantly expressed in pancreatic cancer lesions [369], studies of therapeutic TLR7 stimulation in PDAC are lacking.

An additional unexplored question is how targeted immunotherapies compare to conventional chemotherapies in their effects on cachexia and treatment-associated toxicities. Cachexia is a common and devastating comorbidity of cancer that limits therapeutic options, decreases quality of life, and increases mortality risk [254,255]. This is a highly pertinent clinical problem for malignancies such as PDAC, in which up to 80% of patients suffer from cachexia [260,261]. Many chemotherapy agents induce or worsen cachexia by independently causing anorexia, weight loss, muscle wasting, and fatigue [370,371]. Acute systemic inflammatory responses, often elicited by various immunotherapies, result in adverse events such as fever and fatigue that are typically self-limited in healthy individuals [270]. In accordance with the idea that treatment outcomes are the sum of the treatment's effects on tumor and host, it is crucial to evaluate the effects immunotherapeutic strategies exert both on the tumor and on host physiology.

In this study, we investigated whether the TLR7/8 agonist R848 elicits anti-tumor responses in syngeneic orthotopic murine PDAC models, and whether this class of therapy is beneficial or harmful toward PDAC-associated cachexia. Moreover, we revealed how TLR7 agonists alter the tumor immune microenvironment using a combination of quantitative multiplex immunohistochemistry (mIHC) and flow cytometry. Behavioral and molecular phenotyping of cachexia status was performed for tumor-bearing animals to explore R848's efficacy, and on tumor-naïve animals to explore R848's safety. After establishing evidence of benefit for both tumor burden and cachexia severity, we determined whether the effects of R848

in the tumor microenvironment were dependent on stromal or epithelial TLR7. Finally, to explore therapeutic viability of R848 in human populations, we compared stromal and epithelial expression of *Tlr7* and related transcripts by RNA-seq in laser capture microdissected human lesions across stages of pancreatic neoplasia and carcinogenesis.

Results

R848 reduces PDAC tumor burden and alters the tumor immune microenvironment

TLR agonists have been employed for a variety of malignancies to induce anti-tumor immunity [339-342], which we hypothesized could occur in the context of PDAC. Further, we hypothesized this response may depend on epithelial cell factors regulating immune cell recruitment and neoantigen quality, both of which are necessary components of $CD8^+$ T cell mediated anti-tumor immunity. To assess efficacy of R848 for induction of anti-tumor responses, animals were implanted with one of three $KRAS^{LSL.G12D/+}$ $P53^{R172H/+}$ Pdx-Cre (KPC) derived epithelial clones (KxPxCx, FC1199, FC1242) or given sham surgery (Sham). Each epithelial clone was implanted into C57BL/6 mice using either atraumatic intraperitoneal (IP) or surgical orthotopic (OT) routes, as a means of querying the role of pancreatic inflammation in drug response. Two days post-implantation, mice were randomized on the covariates of weight, body composition, and basal food intake, then were allocated to receive daily R848 or vehicle until study endpoint. For tumor response studies, the experimental endpoint for all groups was onset of end-stage cachexia or exceeding maximum tumor burden in any experimental arm.

Significant reductions in tumor mass were evident at endpoint in two of three KPC-derived clones, without sensitivity differences on the basis of implantation method (Fig. 1A). In the most R848-sensitive clone, KxPxCx, anti-tumor response was more pronounced in IP

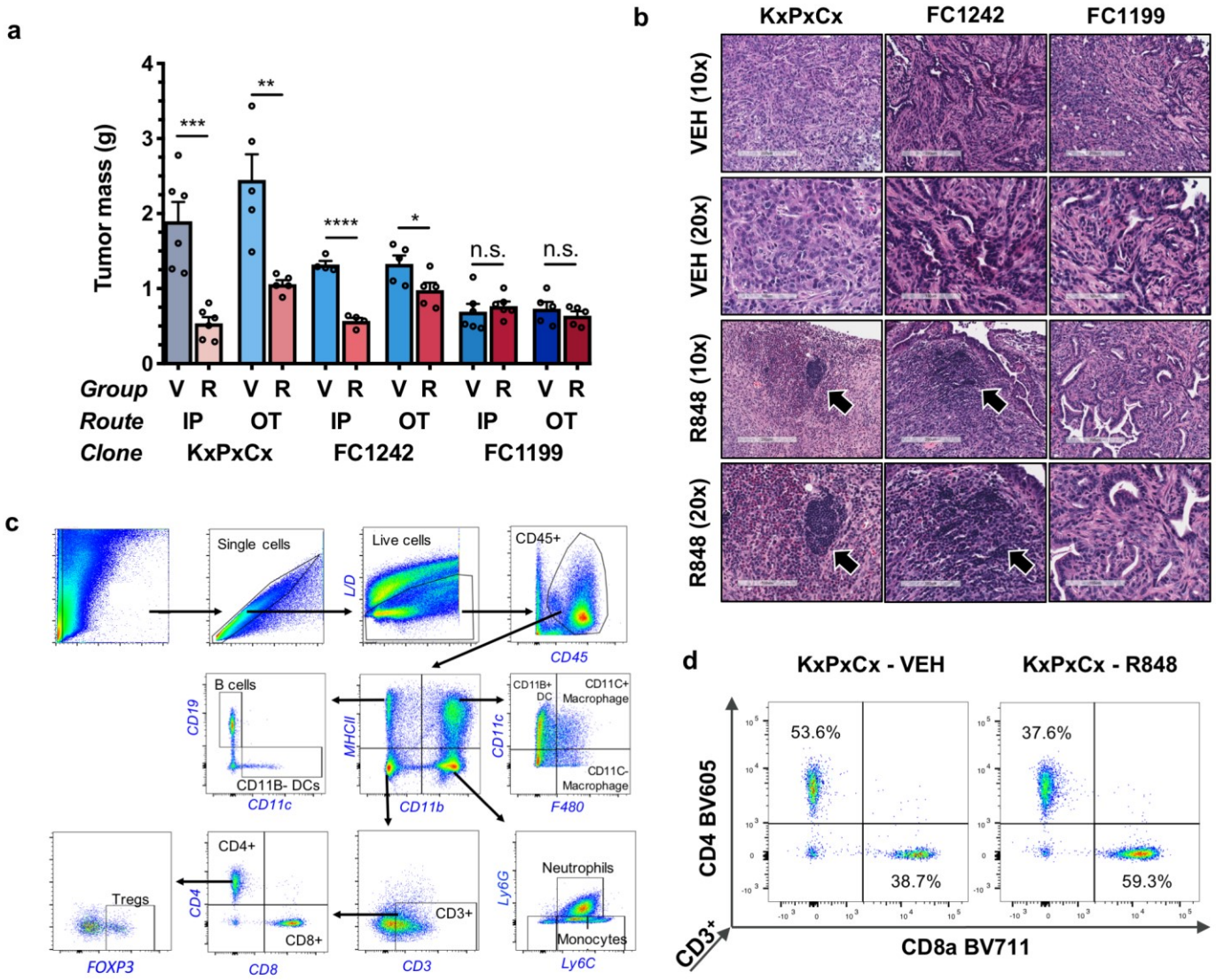
a
Tumor mass (g)
***
**
****
*
n.s.
n.s.
Group V R V R V R V R V R V R
Route IP OT IP OT IP OT
Clone KxPxCx FC1242 FC1199
b
KxPxCx
FC1242
FC1199
VEH (10x)
VEH (20x)
R848 (10x)
R848 (20x)
c
Single cells
Live cells
L/D
CD45+
CD45
B cells
CD19
CD11B- DCs
CD11c
MHCII
CD11b
CD11B+ DC
CD11C+ Macrophage
CD11C- Macrophage
CD11c
F480
CD4+
CD8+
CD4
CD8
Tregs
FOXP3
CD3+
CD3
Neutrophils
Monocytes
Ly6G
Ly6C
d
KxPxCx - VEH
KxPxCx - R848
53.6%
38.7%
37.6%
59.3%
CD4 BV605
CD3+
CD8a BV711
e
CD45+ (% Live)
F4/80+ Macrophages (% CD45+)
Total Dendritic Cells (% CD45+)
Monocytes (% CD45+)
Neutrophils (% CD45+)
T Cells (% CD45+)
CD8+ T Cells (% CD45+)
CD4+ T Cells (% CD45+)
Tregs (% CD4+)
B Cells (% CD45+)
VEH
R848

Fig. 1. *R848 remodels the tumor immune microenvironment and induces epithelium-dependent anti-tumor responses.*

A) Tumor size in epithelial clones KxPxCx, FC1242, and FC1199, implanted either intraperitoneally (IP) or orthotopically (OT), allocated to vehicle (V) or R848 (R) treatment groups. B) Representative H&E imaged at 10x and 20x magnification of KxPxCx, FC 1242, and FC1199 OT tumors with and without R848 (scale bars represent 200μm and 100μm respectively). Arrows indicate intratumoral lymphoid structures. C) Gating strategy for quantitation of immune cell complexity in tumors. D) Representative plots from KxPxCx-engrafted animals treated with vehicle and R848, depicting CD4 and CD8 populations on flow cytometry. E) Flow cytometry plots of R848 treated and untreated KxPxCx tumor immune cells. *n*=5-6/group, Comparisons were performed as Student's t-test. *, $P<0.05$; **, $P<0.01$; ***, $P<0.001$; ****, $P<0.0001$.

---

implantation (71.7% reduction, $P<0.005$) than OT implantation (56.6% reduction, $P<0.01$). In the second clone for which we observed an anti-tumor response, FC1242, R848 sensitivity was also greater for IP implantation (57.0% reduction, $P<0.0001$) than OT implantation (19.7% reduction, $P<0.05$). No tumor mass differences were observed between R848 and vehicle treatment for clone FC1199. with any method of implantation. For clone KxPxCx, R848 resulted in decreased extrapancreatic tumor growth, without gross evidence of invasion of lymph nodes, mesentery, liver, or other abdominal structures.

Histological analysis was performed on KPC-derived tumors at endpoint, with the goal of elucidating structural and cellular correlates for variations in R848 response. Orthotopic implantation of all cell lines produced pancreatic masses consistent with moderate-to-poorly differentiated PDAC (Fig. 1B). Tumors from KxPxCx and FC1242-implanted animals treated with

R848 were characterized by increased lymphocytic infiltration and formation of intratumoral lymphoid structures (Fig. 1B, arrow). In contrast, histological examination of tumors derived from FC1199 did not indicate formation of lymphoid structures or increased lymphocytic infiltrate in response to R848. These findings together indicated an epithelium-dependent role in immune cell recruitment and activity during R848 treatment.

To explore the immune cell changes observed on histology, flow cytometry was used to compare tumor immune population frequencies between vehicle- and R848-treated KxPxCx tumors after 10 days of treatment (Fig. 1C). The overall frequency of $CD45^+$ leukocytes was increased in R848-treated tumors, with widespread differences in both T lymphocyte and myeloid populations (Fig. 1D). The frequency of $CD3^+CD8^+$ T cells more than doubled following R848 treatment (Figs. 1D-E) (2.27% $CD45^+$ in vehicle vs. 5.23% $CD45^+$ in R848, $P<0.01$). In addition, $CD3^+CD4^+$ T cell frequency increased following R848 treatment (2.39% $CD45^+$ in vehicle vs. 4.17% of $CD45^+$ in R848, $P<0.01$). Among $CD3^+CD4^+$ cells, the proportion of $FOXP3^+$ regulatory T (Treg) cells significantly decreased following treatment with R848 (34.86% $CD4^+$ in vehicle vs. 25.07% in R848, $P<0.01$) (Fig. 1E). Despite the presence of intratumoral lymphoid structures on histology, no overall differences were observed in B cell frequency.

Among granulocytic populations, neutrophils were increased after treatment with R848 (21.48% of $CD45^+$ events vehicle vs. 31.53% R848, $P<0.05$). Both total macrophages ($CD45^+F4/80^+$) and $CD11c^-$ macrophages trended toward increases with R848, but did not reach the threshold of statistical significance. Following treatment with R848, both $CD11b^+$ and $CD11b^-$ dendritic cell ($CD45^+MHCII^+CD11c^+$) frequency decreased (combined; 3.75% $CD45^+$ events vehicle vs. 1.39%

a

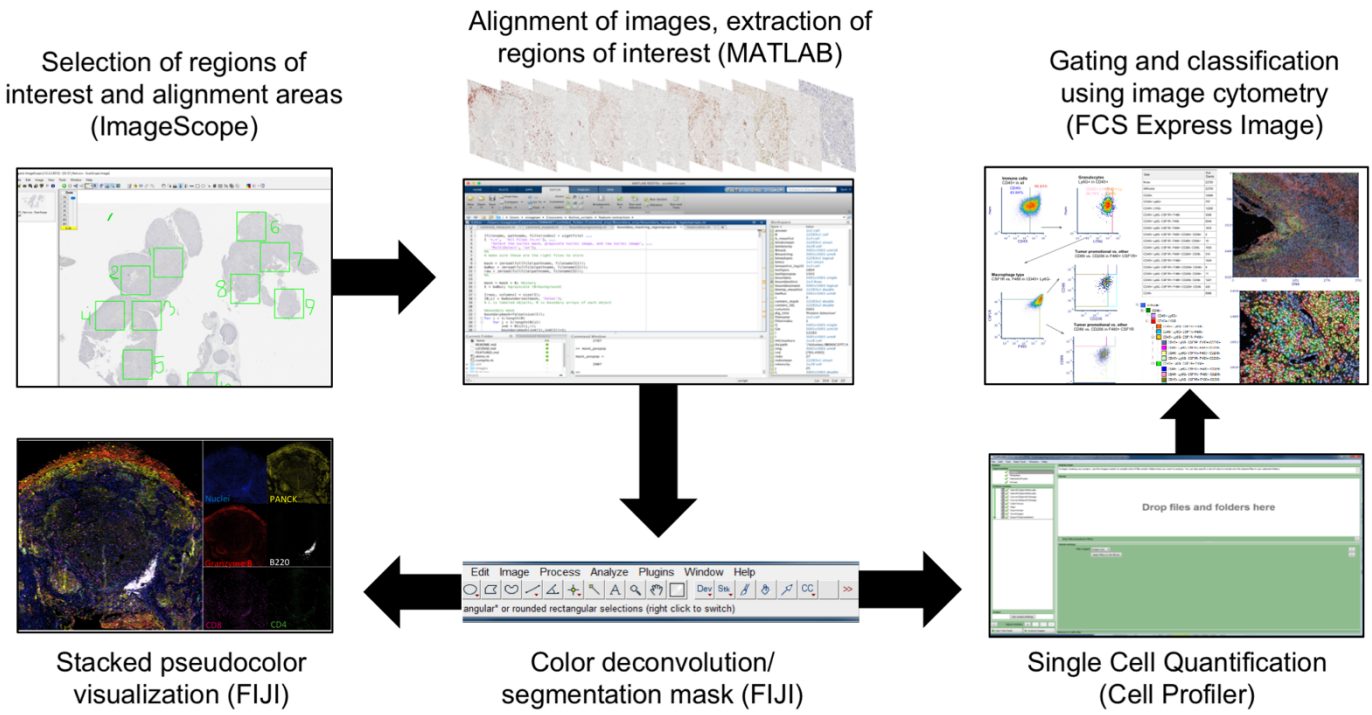

b

Type	Class	Identity	Subclass	Functional marker 1	Functional marker 2	Functional marker 3	Functional marker 4	Functional marker 5
Not Immune CD45-	Neoplastic PANCK+			PDL-1	Ki67			
	Fibroblasts/Other PANCK-			PDL-1	Ki67			
Immune CD45+	Lymphocytes	B Cells B220+		BTK	PDL-1	Ki67		
		CD4+ T Cell (CD3+ CD4+)	TH0/TH1 (Neg for all)	TIM3	TCF1	Granzyme B	Ki67	
			TH2 GATA3+	TIM3	TCF1	Granzyme B	Ki67	
			TH17 RORGT+	TIM3	TCF1	Granzyme B	Ki67	
			Treg FOXP3+	TIM3	TCF1	Granzyme B	Ki67	
		CD8+ T Cell	CD3+	EOMES	TIM3	TCF1	Granzyme B	Ki67
			CD3-	EOMES	TIM3	TCF1	Granzyme B	Ki67
		Other T Cell	CD4+ CD8+	EOMES	TIM3	TCF1	Granzyme B	Ki67
			CD4- CD8-	EOMES	TIM3	TCF1	Granzyme B	Ki67
	Myeloid cells CD11B+	Macrophages (F480+) CSF1R+ vs. CSF1R-	CD206+ / CD11C-	PDL-1	Ki67			
			CD206+ / CD11C+	PDL-1	Ki67			
			CD206- / CD11C-	PDL-1	Ki67			
			CD206- / CD11C+	PDL-1	Ki67			
		DCs (F480-)	CD206+ / CD11C+	PDL-1	Ki67			
			CD206- / CD11C+	PDL-1	Ki67			
		Granulocytes (Ly6G+)		PDL-1	Ki67			
		Other		PDL-1	Ki67			

Fig. S2. *Workflow of quantitative multiplex immunohistochemistry analysis.* A) Experimental pipeline of image acquisition, alignment, extraction of regions of interest, image assembly, cell quantitation, and image cytometry. B) Gating strategy used for image cytometry in mIHC studies.

R848, $P<0.0001$). Similarly, monocyte ($CD45^+MHCII^-CD11b^+$) frequency decreased following treatment (24.12% of $CD45^+$ vehicle vs. 7.98% of $CD45^+$ R848, $P<0.0001$).

For in-depth characterization of the tumor immune microenvironment, tissue sections from orthotopically implanted KxPxCx tumors treated with vehicle or R848 were analyzed *in situ* with 23-marker quantitative multiplex immunohistochemistry (mIHC) (experimental pipeline and gating strategy described in Fig. S2) [42]. This method permits quantitation of the cellular composition of tumors with simultaneous spatial localization. Utilizing this approach, we revealed that R848 resulted in overall increases in $CD45^+$ cells throughout both edges and core of tumors, with broad changes in both immune cell complexity and functional status (Fig. 2A-B, Fig. S3-S4).

In agreement with the flow cytometry analyses, R848 did not change relative proportions of B cells ($CD45^+CD3^-B220^+$) (2.83% $CD45^+$ in vehicle versus 2.82% in R848). However, while the majority of B cells were disseminated throughout tumor parenchyma in vehicle-treated tumors, R848-treated tumors revealed frequent formation of B cell aggregates (Fig. 2F). $CD3^+CD4^+$ T cells also evidenced generalized increases (0.27% total in vehicle versus 0.60% total in R848, $P<0.05$), with significant changes to $CD3^+CD4^+$ subset frequency (Fig. S3C). Consistent with the known mechanism of TLR7 agonists in promoting T_H1 differentiation [372], the most common $CD3^+CD4^+$ lineage in R848-treated tumors was $GATA3^-FOXP3^-RORGT^-$, collectively representing T_H0 and T_H1

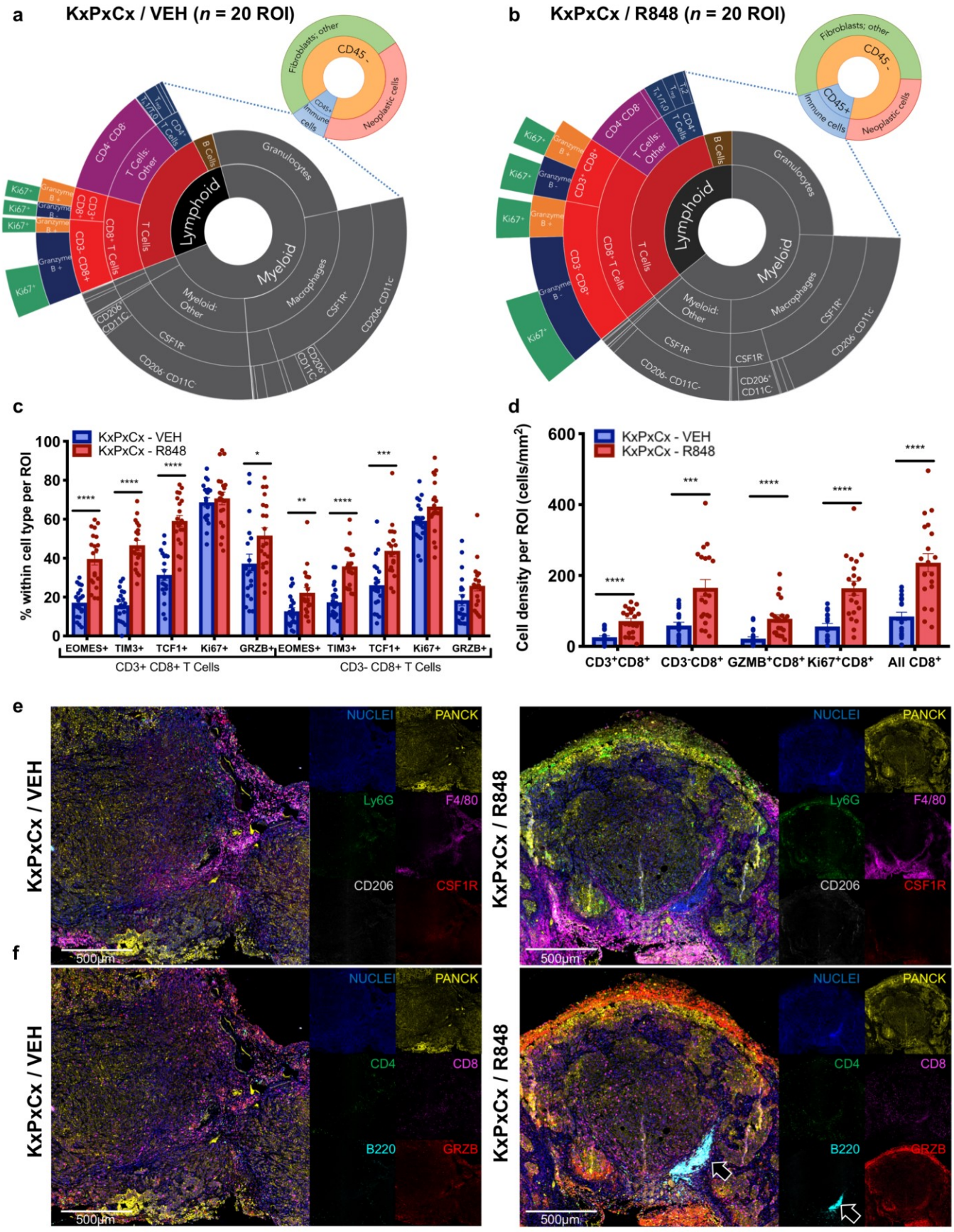
a
KxPxCx / VEH (n = 20 ROI)
b
KxPxCx / R848 (n = 20 ROI)
Fibroblasts; other
CD45-
CD45+ Immune cells
Neoplastic cells
Lymphoid
Myeloid
B Cells
T Cells
CD4+ T Cells
CD8+ T Cells
T Cells: Other
CD4- CD8-
CD3+ CD8+
CD3- CD8+
Granulocytes
Macrophages
Myeloid: Other
CSF1R+
CD206+ CD11C+
CD206- CD11C-
Ki67+
Granzyme B +
c
% within cell type per ROI
KxPxCx - VEH
KxPxCx - R848
EOMES+
TIM3+
TCF1+
Ki67+
GRZB+
CD3+ CD8+ T Cells
CD3- CD8+ T Cells
d
Cell density per ROI (cells/mm²)
CD3+CD8+
CD3-CD8+
GZMB+CD8+
Ki67+CD8+
All CD8+
e
KxPxCx / VEH
KxPxCx / R848
NUCLEI
PANCK
Ly6G
F4/80
CD206
CSF1R
500µm
f
CD4
CD8
B220
GRZB

Fig. 2. *Tumor immune microenvironment composition and functional status are enhanced by R848, promoting cytotoxic T cell responses.*

Sunburst plots depicting image cytometry quantitation of tumor immune subsets for KxPxCx-derived tumors treated with vehicle (A) and KxPxCx treated with R848 (B). Upper right plots depict overall immune versus non-immune composition within tumors, with lower left plots depicting immune composition and activation status. Plots represent 4 tumors per treatment group and 5 ROIs per tumor, representing a minimum of 50% of the tumor area. C) Functional status analysis for both $CD3^+CD8^+$ and $CD3^-CD8^+$ T cells, including EOMES, TIM3, memory T cell marker TCF1, proliferation and activity marker Ki67, and activity marker granzyme B (GRZB). D) Cell density of overall, proliferative, and cytotoxic $CD8^+$ T cell populations per ROI in vehicle and R848-treated KxPxCx derived tumors. E) Representative myeloid multiplex imaging for vehicle and R848 treated tumors, emphasizing PANCK (tumor cells), F4/80 (macrophages), CD206 (tumor promotional marker), colony stimulating factor 1 receptor (CSF1R; macrophage survival and differentiation), and Ly6G (granulocytes). F) Representative lymphoid multiplex imaging for vehicle and R848 treated tumors, emphasizing PANCK, B220 (B cell marker), CD4, CD8, and Granzyme B (cytotoxic activity marker). Scale bars represent 500μm. Arrow indicates intratumoral lymphoid structure. *, $P<0.05$; **, $P<0.01$; ***, $P<0.001$; ****, $P<0.0001$.

cells (34.11% $CD3^+CD4^+$ in vehicle vs. 41.86% in R848, $P<0.05$). In contrast, the most common $CD3^+CD4^+$ subset in vehicle-treated tumors were Tregs (35.97% $CD3^+CD4^+$ cells in vehicle versus 19.07% R848, $P=0.001$).

Of importance to anti-neoplastic immunity, $CD8^+$ T cells were more concentrated and distributed throughout the epithelial and stromal compartments following R848 treatment (Figs. 2C-D) (0.85% of total cells in vehicle vs. 2.5% R848, $P<0.0001$). $CD8^+$ T cell density increased from

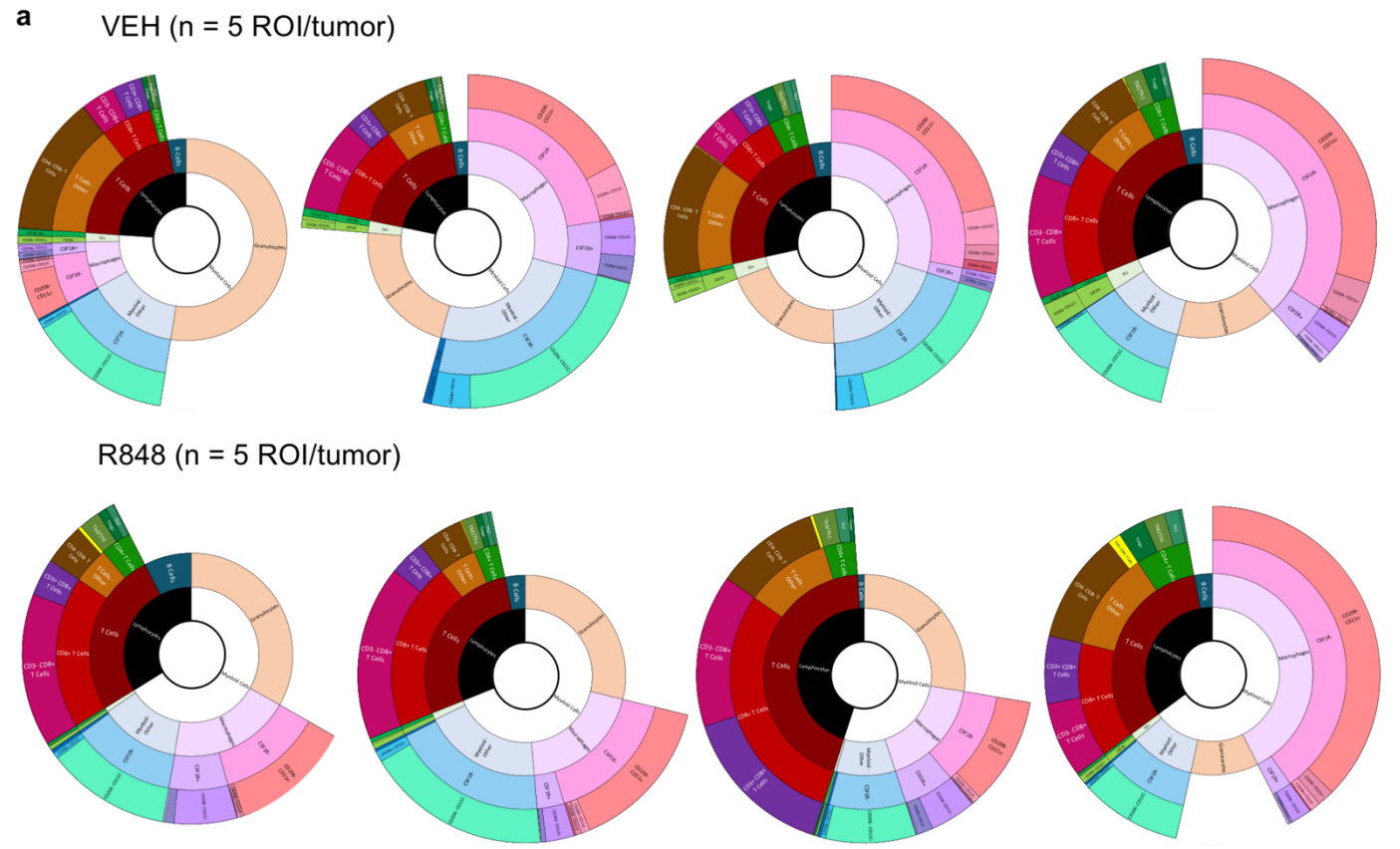
a
VEH (n = 5 ROI/tumor)
R848 (n = 5 ROI/tumor)
Lymphocytes
T Cells
CD4+ T Cells
CD8+ T Cells
T Cells - Other
B Cells
Th0/Th1
Th2
Tregs
Th17
CD3+CD8+
CD3-CD8+
CD4+CD8+
CD4-CD8-
Myeloid Cells
Myeloid - Other
CSF1R-
CSF1R+
CD206- CD11C-
CD206+ CD11C-
CD206- CD11C+
CD206+ CD11C+
Dendritic Cells (CD11C+)
Granulocytes (Ly6G+)
Macrophages (F4/80+)
b
% cells per ROI
KxPxCx - VEH
KxPxCx - R848
All
Ki67+ PDL1-
Ki67+ PDL1+
Ki67- PDL1-
Ki67- PDL1+
Neoplastic Cells
Fibroblasts/Other
c
% CD4 per ROI
Tregs
Th17
TH2
TH1/0

Fig. S3. *Immune complexity mIHC analyses within KxPxCx-derived tumors following R848 versus vehicle*
A) Sunburst plots depicting the immune composition of each tumor within the dataset, derived from 5 ROIs representing greater than 50% of total section area. B) Proportion of proliferating ($Ki67^+$) and exhaustion-promoting ($PDL1^+$) cells in neoplastic and fibroblast/other compartments of the tumor, depicted as % per ROI within treatment groups vehicle and R848. C) Proportions of CD4 subsets within vehicle and R848-treated KxPxCx tumors. *, $P<0.05$; **, $P<0.01$; ***, $P<0.001$; ****, $P<0.0001$

84.56 to 236.2 cells/mm² following treatment with R848 ($P<0.0001$) (Fig. 2D). In addition, granzyme B^+ $CD8^+$ T cells increased in density following treatment (21.62 cells/mm² vehicle versus 71.09 cells/mm² R848, $P<0.0001$), indicating improved cytotoxic effector function. Furthermore, R848 increased the cell density of proliferating $CD8^+$ T cells as assessed by Ki67 (55.87 cells/mm² vehicle versus 164.1 R848, $P<0.0001$). R848 also resulted in increased $CD8^+$ T cell expression of TIM3 (0.68% vehicle vs. 2.739% R848, $P=0.001$) and EOMES (0.47% vehicle vs. 1.43% R848, $P<0.01$), reflecting their varied differentiation and/or functional state. Within cell populations pertinent to T cell function, decreases in programmed cell death ligand-1 (PD-L1) were observed among $PANCK^+$ tumor cells (30.30% vehicle vs. 20.69% R848) and $CD11b^+$ cells (16.20% vehicle vs. 12.83% R848), however, these changes did not approach statistical significance.

A sub-analysis of myeloid cells in $CD45^+$ dense tumor regions demonstrated that in areas of immune cell enrichment, macrophages increased following R848 treatment from a mean of 0.55% to 8.08% of cells per region of interest ($P<0.01$, n=20 ROI/group, Fig. S4C). Macrophages following R848 treatment had relatively increased CSF1R positivity, but decreased CD206 positivity (Fig. S4C). In $CD45^+$ enriched regions, R848 also increased granulocyte infiltration from a mean of 1.93% to 4.41% ($P<0.01$). However, dendritic cells were decreased from a mean of 1.5% $CD45^+$ cells in vehicle-treated tumors to 0.54% $CD45^+$ cells in R848-treated tumors ($P<0.001$).

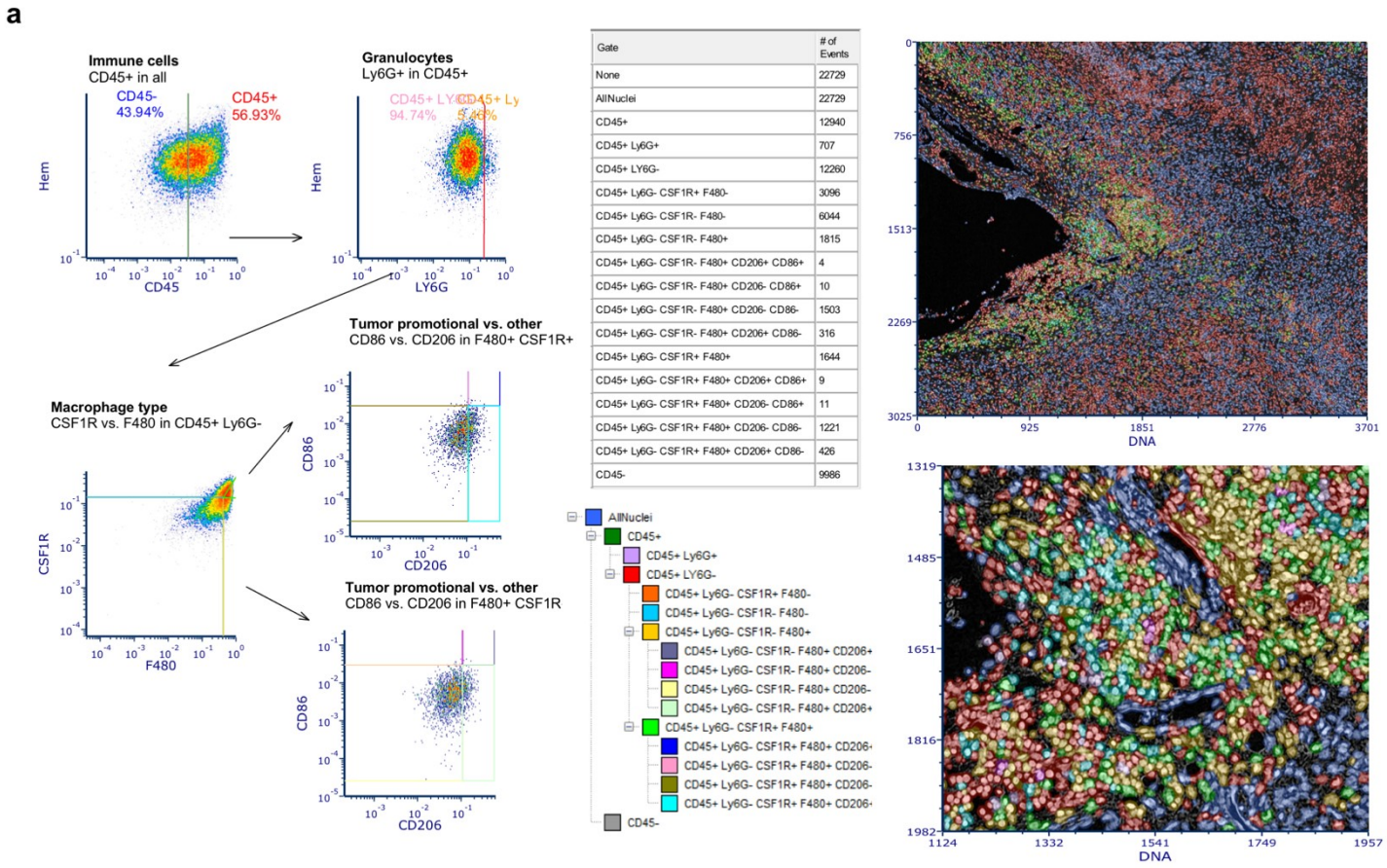
a
Immune cells
CD45+ in all
CD45- 43.94%
CD45+ 56.93%
Hem
CD45
Granulocytes
Ly6G+ in CD45+
CD45+ Ly6G+ 94.74%
CD45+ Ly 5.26%
LY6G
Tumor promotional vs. other
CD86 vs. CD206 in F480+ CSF1R+
Macrophage type
CSF1R vs. F480 in CD45+ Ly6G-
CSF1R
F480
CD86
CD206
Tumor promotional vs. other
CD86 vs. CD206 in F480+ CSF1R
Gate | # of Events
None | 22729
AllNuclei | 22729
CD45+ | 12940
CD45+ Ly6G+ | 707
CD45+ LY6G- | 12260
CD45+ Ly6G- CSF1R+ F480- | 3096
CD45+ Ly6G- CSF1R- F480- | 6044
CD45+ Ly6G- CSF1R- F480+ | 1815
CD45+ Ly6G- CSF1R- F480+ CD206+ CD86+ | 4
CD45+ Ly6G- CSF1R- F480+ CD206- CD86+ | 10
CD45+ Ly6G- CSF1R- F480+ CD206- CD86- | 1503
CD45+ Ly6G- CSF1R- F480+ CD206+ CD86- | 316
CD45+ Ly6G- CSF1R+ F480+ | 1644
CD45+ Ly6G- CSF1R+ F480+ CD206+ CD86+ | 9
CD45+ Ly6G- CSF1R+ F480+ CD206- CD86+ | 11
CD45+ Ly6G- CSF1R+ F480+ CD206- CD86- | 1221
CD45+ Ly6G- CSF1R+ F480+ CD206+ CD86- | 426
CD45- | 9986
AllNuclei
CD45+
CD45+ Ly6G+
CD45+ LY6G-
CD45+ Ly6G- CSF1R+ F480-
CD45+ Ly6G- CSF1R- F480-
CD45+ Ly6G- CSF1R- F480+
CD45+ Ly6G- CSF1R- F480+ CD206+
CD45+ Ly6G- CSF1R- F480+ CD206-
CD45+ Ly6G- CSF1R- F480+ CD206-
CD45+ Ly6G- CSF1R- F480+ CD206+
CD45+ Ly6G- CSF1R+ F480+
CD45+ Ly6G- CSF1R+ F480+ CD206-
CD45+ Ly6G- CSF1R+ F480+ CD206-
CD45+ Ly6G- CSF1R+ F480+ CD206-
CD45+ Ly6G- CSF1R+ F480+ CD206-
CD45-
DNA
DNA

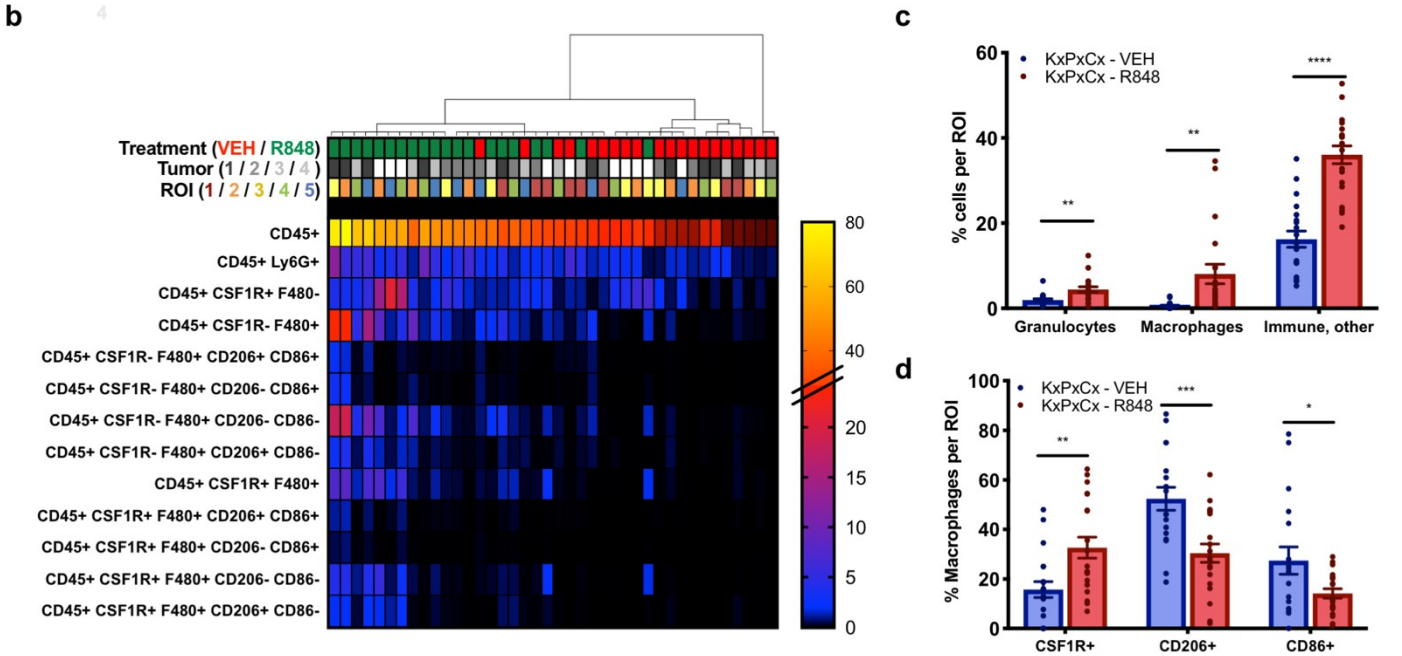
b
Treatment (VEH / R848)
Tumor (1 / 2 / 3 / 4)
ROI (1 / 2 / 3 / 4 / 5)
CD45+
CD45+ Ly6G+
CD45+ CSF1R+ F480-
CD45+ CSF1R- F480+
CD45+ CSF1R- F480+ CD206+ CD86+
CD45+ CSF1R- F480+ CD206- CD86+
CD45+ CSF1R- F480+ CD206- CD86-
CD45+ CSF1R- F480+ CD206+ CD86-
CD45+ CSF1R+ F480+
CD45+ CSF1R+ F480+ CD206+ CD86+
CD45+ CSF1R+ F480+ CD206- CD86+
CD45+ CSF1R+ F480+ CD206- CD86-
CD45+ CSF1R+ F480+ CD206+ CD86-
80
60
40
20
15
10
5
0
c
KxPxCx - VEH
KxPxCx - R848
% cells per ROI
Granulocytes
Macrophages
Immune, other
d
KxPxCx - VEH
KxPxCx - R848
% Macrophages per ROI
CSF1R+
CD206+
CD86+

R848 is well-tolerated and improves cachexia manifestations, including anorexia and lethargy, during PDAC

Despite their beneficial effects on tumor response, significant concerns exist about TLR agonists' potential systemic toxicities. Indeed, cancer cachexia is an often-deadly comorbidity and widely believed to be a disorder of inflammatory responses. Therefore, it is critical for cachexia-associated malignancies including PDAC to ensure cachexia is not worsened by immunotherapies that alter systemic inflammatory signaling. To assess tolerability, mice were orthotopically implanted with one of three KPC-derived epithelial clones (KxPxCx, FC1199, FC1242) or given sham surgery (Sham), allocated to R848 or vehicle treatment, then tracked for food intake, body weight, locomotor activity, and body temperature (Fig. 3). Consistent with known effects of TLR agonists, R848 treatment induction resulted in brief hypophagia and weight loss. Following this stage, R848-treated mice exhibited comparable food intake to vehicle-treated KPC-bearing mice in pre-cachexia stages of illness. However, ongoing R848 treatment increased cachexia stage food intake above that of vehicle-treated tumor-bearing animals in all three epithelial clones tested (Fig. 3A-C). KxPxCx-bearing mice treated with R848 initially developed significant weight gain and ascites relative to untreated KxPxCx-bearing animals, but underwent dramatic weight loss and regression of ascites as treatment progressed (Fig. 3D). In contrast, clones FC1242 and FC1199 did not produce ascites, and mice receiving R848 were modestly protected from weight loss during later stages of illness (Fig. 3E-F). During pre-cachexia stage, KxPxCx mice treated with R848 exhibited treatment-related decreases in locomotor activity, but in later stages of illness exhibited improvements in locomotor activity relative to vehicle-treated subjects (Fig. 3G).

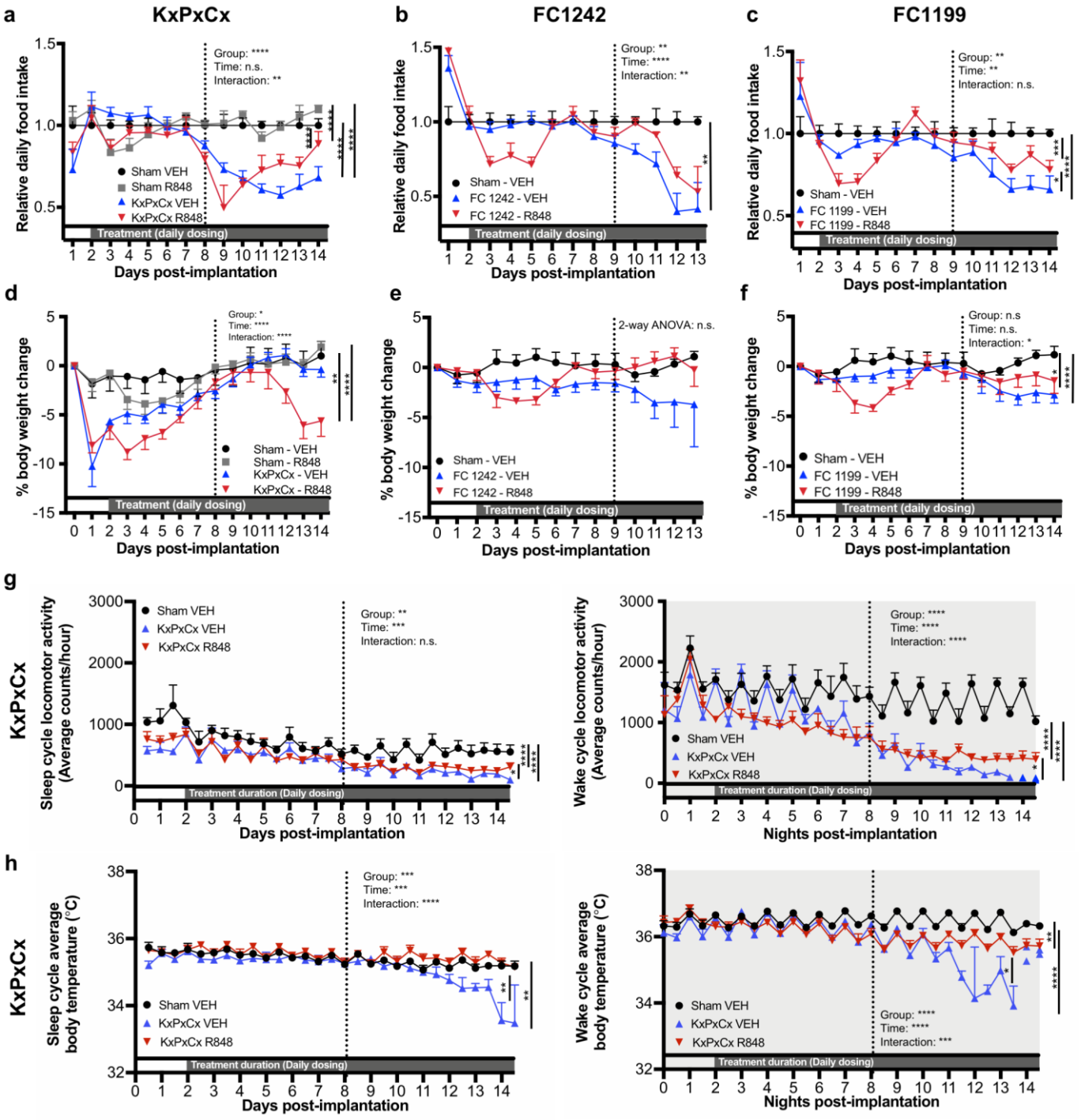

Fig. 3. *R848 improves cachexia manifestations, including appetite and voluntary locomotor activity, during PDAC.* Mice were orthotopically implanted with one of three distinct syngeneic KPC-derived clones: KxPxCx, FC1199, and FC1242. Vertical dotted lines denote the onset of cachexia as defined by consistent hypophagia exceeding 10% below control food intake. KxPxCx studies were (*continued on next page*…)

Fig. 3. *R848 improves cachexia manifestations, including appetite and voluntary locomotor activity, during PDAC.* (*continued from previous*)

[…] performed independently, while FC1242 and FC1199 studies were performed concurrently with a shared control group. A) Food intake relative to sham-operated vehicle-treated mice (Sham-VEH) for sham-operated R848-treated mice (Sham-R848), KxPxCx-engrafted mice receiving vehicle (KxPxCx-VEH), and KxPxCx-engrafted mice receiving R848 (KxPxCx-R848). B-C) Food intake relative to sham-operated vehicle-treated mice implanted for FC1242 (B) and FC1199 (C) treated with vehicle (VEH) or R848. D-F) Body weight relative to baseline for clones KxPxCx (D), FC1242 (E), and FC1199 (F) throughout treatment with R848 or vehicle. G/) Average locomotor activity during day/sleep and night/wake cycles for KxPxCx-implanted animals treated with R848 or vehicle, binned into six-hour intervals. H) Average body temperature during day/sleep and night/wake cycles for KxPxCx implanted animals treated with R848 or vehicle, binned into six-hour intervals. Data for all panels are displayed as mean ±SEM, unless fewer than 3 subjects were remaining in a group, in which case individual data points are plotted. Statistics were performed as two-way ANOVA during the cachexia stage to test for main effects of tumor and treatment, and the interaction thereof, with multiple comparisons to test for main column effects. *, $P<0.05$; **, $P<0.01$; ***, $P<0.001$; ****, $P<0.0001$.

While vehicle-treated KxPxCx mice became hypothermic during cachexia stages of illness, R848-treated KxPxCx mice were significantly less hypothermic throughout the study (Fig. 3H). Importantly, no fever or hypothermia was observed with R848 treatment alone. In sham-operated controls, R848 only resulted in transient decreases in body weight and appetite, suggesting that sickness responses to R848 are temporary and can be overcome with appropriate dosing kinetics (Fig. 3A, 3B). These findings combined indicate that R848 is tolerable, especially when delivered on a consistent repeated dosing schedule.

R848 decreases cardiac and lean mass catabolism from PDAC-associated cachexia

To assess the overall effects of tumor burden and R848 on body composition, lean mass and adiposity were measured using nuclear magnetic relaxometry immediately prior to tumor implantation and again prior to necropsy. Across all epithelial clones, tumor burden resulted in lean and adipose tissue wasting (Fig. 4A-B). For clone KxPxCx, R848-treated mice exhibited improvements in lean mass retention over vehicle-treated mice ($P<0.05$). No improvements were noted in fat mass retention in any epithelial clone tested.

At necropsy, R848 did not result in muscle catabolism in sham-operated animals, but did not rescue the muscle wasting phenotype resulting from KxPxCx engraftment (Fig. 4C). Nevertheless, skeletal muscle catabolic gene signatures were distinctly improved by treatment with R848. Compared to vehicle-treated KxPxCx-engrafted mice, R848-treated animals demonstrated decreases in the E3 ubiquitin ligases *Mafbx* and *Murf1,* as well as the transcription factor *Foxo1*. Targeted array profiling of skeletal muscle was performed for 84 transcripts related to myogenesis and myopathy, comparing sham-operated animals to KxPxCx-bearing animals with and without R848 (Fig. S5). Principle component analysis revealed that R848 modified the skeletal muscle transcriptome to become more similar to sham-operated animals than vehicle-treated tumor-bearing counterparts (Fig. 4D). Of these transcripts, 21 were found to differ significantly at a threshold of $\alpha=0.05$ with a fold change >2.0 versus one or more experimental groups (Fig. 4E). Skeletal muscle gene transcription more closely resembled sham-operated animals following R848, with the exception of the pro-inflammatory cytokine *Il1b* and muscle differentiation and repair transcription factor *Myod1*, which were upregulated in R848-treated KxPxCx-engrafted mice compared to vehicle-treated KxPxCx-engrafted mice and healthy controls.

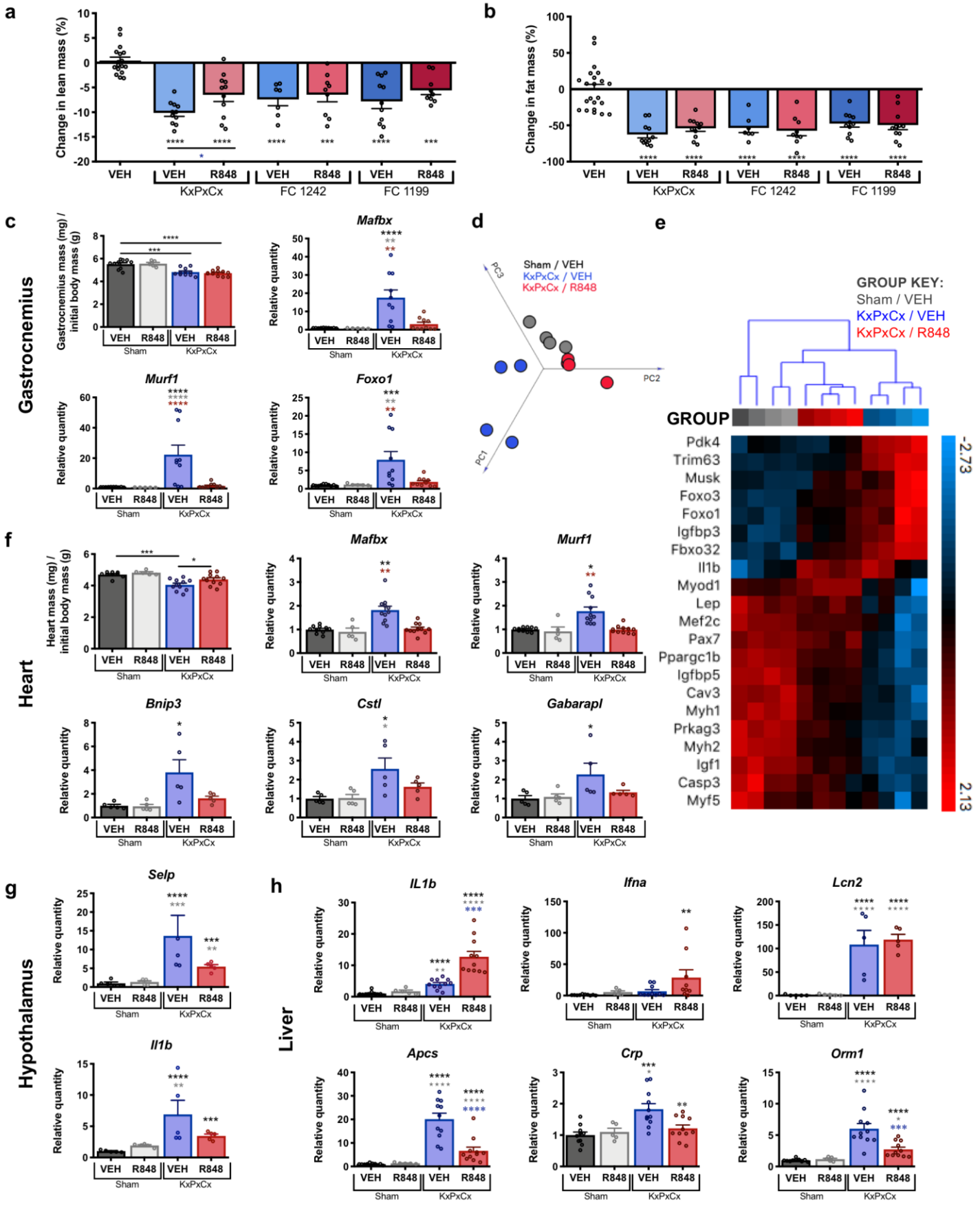
a
Change in lean mass (%)
b
Change in fat mass (%)
VEH
VEH
R848
KxPxCx
FC 1242
FC 1199
c
Gastrocnemius
Gastrocnemius mass (mg) / initial body mass (g)
Mafbx
Murf1
Foxo1
Relative quantity
Sham
KxPxCx
d
Sham / VEH
KxPxCx / VEH
KxPxCx / R848
PC1
PC2
PC3
e
GROUP KEY:
Sham / VEH
KxPxCx / VEH
KxPxCx / R848
GROUP
Pdk4
Trim63
Musk
Foxo3
Foxo1
Igfbp3
Fbxo32
Il1b
Myod1
Lep
Mef2c
Pax7
Ppargc1b
Igfbp5
Cav3
Myh1
Prkag3
Myh2
Igf1
Casp3
Myf5
-2.73
2.13
f
Heart
Heart mass (mg) / initial body mass (g)
Mafbx
Murf1
Bnip3
Cstl
Gabarapl
g
Hypothalamus
Selp
Il1b
h
Liver
IL1b
Ifna
Lcn2
Apcs
Crp
Orm1

Fig. 4. *R848 improves molecular physiology markers related to cachexia in skeletal muscle, cardiac muscle, hypothalamus, and liver.*

A) Lean mass changes assessed by nuclear magnetic resonance (NMR) relaxometry, comparing absolute lean mass prior to implantation with tumor-free lean mass at end of study. Clones include KxPxCx, FC1199, and FC1242. B) Fat mass changes assessed by NMR, comparing absolute quantity of fat mass prior to implantation with absolute quantity of fat mass at end of study. Statistics depict significance as compared to sham-operated vehicle treated mice unless otherwise designated, via one-way ANOVA with Sidak multiple comparison correction. C) Normalized gastrocnemius mass and gene expression of key catabolic transcripts for sham or KxPxCx-implanted animals treated with vehicle (VEH) or R848. D) Principle component analysis of all 84 myopathy and myogenesis related transcripts in sham vehicle, and KxPxCx allocated to vehicle or R848. E) Unsupervised clustering analysis of all myogenesis and myopathy related transcripts with a fold regulation greater than 2 and adjusted $P<0.05$ between groups. Expression values are normalized by standard deviation for each transcript to depict variance from the mean. F) Normalized heart mass and cardiac gene expression of catabolic and autophagy transcripts for sham or KxPxCx-implanted animals treated with vehicle (VEH) or R848. Gene expression for hypothalamus (G) and liver (H) are shown for sham-operated and KxPxCx-implanted mice treated with VEH or R848. *, $P<0.05$; **, $P<0.01$; ***, $P<0.001$; ****, $P<0.0001$, with the color of symbol matched to the relevant comparison group

---

In addition to improvements in the molecular physiology of skeletal muscle, KxPxCx-bearing animals treated with R848 demonstrated preserved heart mass ($P<0.05$ versus vehicle-treated KxPxCx, n.s. versus sham). qRT-PCR of cardiac muscle demonstrated that R848 decreased expression of *Mafbx* and *Murfi,* as well as autophagy-associated transcripts frequently upregulated in cardiac tissue during cachexia (*Bnip3, Ctsl, Gabarapl*) (Fig. 4F).

a

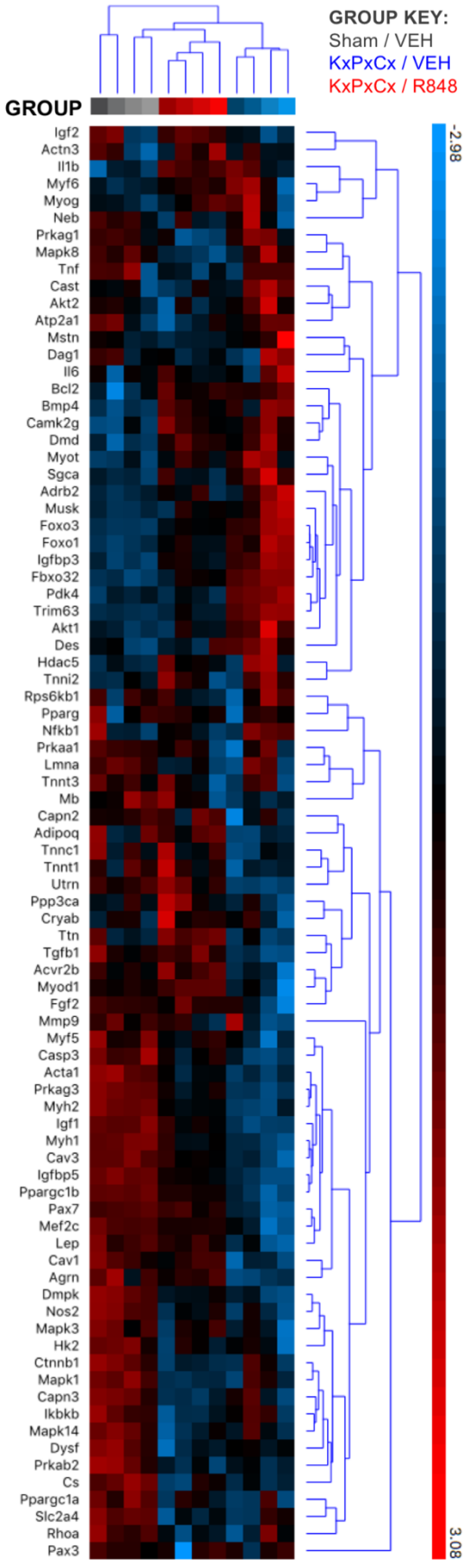

b

	KPC / VEH vs. SHAM / VEH (Fold change)	*p* value	KPC / R848 vs. SHAM / VEH (Fold change)	*p* value	KPC / VEH vs. KPC / R848 (Fold change)	*p* value
Acta1	0.612	0.0004	0.713	0.0024	0.858	0.0319
Actn3	1.036	0.7297	1.137	0.2882	0.911	0.2731
Acvr2b	0.705	0.0227	1.243	0.0843	0.567	0.0068
Adipoq	0.538	0.0945	1.035	0.8942	0.520	0.0053
Adrb2	2.422	0.0663	1.389	0.1148	1.744	0.1715
Agrn	0.657	0.0105	0.924	0.4619	0.711	0.0004
Akt1	2.750	0.0541	1.251	0.2479	2.198	0.0926
Akt2	1.161	0.1818	0.911	0.2804	1.275	0.0826
Atp2a1	1.061	0.5885	0.849	0.2256	1.250	0.0435
Bcl2	1.716	0.0117	1.619	0.0267	1.060	0.6199
Bmp4	1.765	0.0211	1.563	0.0039	1.129	0.4782
Camk2g	1.556	0.0241	1.543	0.0170	1.008	0.9546
Capn2	0.840	0.1073	1.019	0.7900	0.824	0.1344
Capn3	0.751	0.0602	0.622	0.0007	1.208	0.2192
Casp3	0.446	0.0036	0.648	0.0300	0.688	0.0251
Cast	1.351	0.0731	0.982	0.8714	1.375	0.0526
Cav1	0.600	0.0045	0.913	0.3557	0.657	0.0043
Cav3	0.412	0.0002	0.684	0.0025	0.602	0.0054
Cryab	0.966	0.8542	1.455	0.1754	0.664	0.1764
Cs	0.535	0.0007	0.569	0.0068	0.940	0.7242
Ctnnb1	0.800	0.0379	0.728	0.0012	1.098	0.3149
Dag1	1.075	0.7425	0.888	0.2223	1.210	0.4044
Des	1.413	0.0138	1.101	0.3921	1.283	0.0524
Dmd	1.297	0.0170	1.268	0.0028	1.023	0.7528
Dmpk	0.510	0.0008	0.635	0.0017	0.802	0.0528
Dysf	0.752	0.0087	0.631	0.0046	1.190	0.0829
Fbxo32	10.621	0.0016	2.880	0.0069	3.688	0.0052
Fgf2	0.615	0.0315	1.006	0.9554	0.611	0.0609
Foxo1	5.917	0.0326	2.038	0.0061	2.903	0.0736
Foxo3	3.178	0.0106	1.602	0.0001	1.983	0.0387
Hdac5	1.216	0.1834	1.162	0.0456	1.047	0.7349
Hk2	0.676	0.0255	0.704	0.0209	0.960	0.8073
Igf1	0.276	0.0001	0.582	0.0044	0.474	0.0014
Igf2	0.808	0.2901	1.148	0.3904	0.704	0.0017
Igfbp3	6.241	0.0117	2.209	0.0088	2.826	0.0351
Igfbp5	0.062	0.0001	0.247	0.0005	0.252	0.0003
Ikbkb	0.866	0.1464	0.721	0.0035	1.202	0.0895
Il1b	5.594	0.1111	6.421	0.0010	0.871	0.7600
Il6	2.395	0.2518	1.347	0.3791	1.777	0.3825
Lep	0.071	0.0417	0.441	0.1818	0.161	0.0132
Lmna	0.870	0.2989	0.790	0.0039	1.102	0.5158
Mapk1	0.812	0.0316	0.731	0.0001	1.110	0.2370
Mapk14	0.760	0.0365	0.648	0.0043	1.174	0.2850
Mapk3	0.792	0.0299	0.881	0.1377	0.899	0.2910
Mapk8	1.000	0.9976	0.797	0.0013	1.255	0.0476
Mb	0.487	0.0446	0.799	0.5444	0.609	0.2521
Mef2c	0.294	0.0011	0.644	0.0045	0.457	0.0078
Mmp9	0.792	0.4878	0.777	0.1419	1.018	0.9618
Mstn	2.108	0.2720	0.840	0.1379	2.511	0.2141
Musk	2.591	0.0422	1.395	0.0794	1.857	0.1122
Myf5	0.443	0.0265	0.673	0.1207	0.658	0.0667
Myf6	1.717	0.1777	1.441	0.0011	1.191	0.5796
Myh1	0.467	2.77E-05	0.674	0.0008	0.694	0.0078
Myh2	0.466	3.01E-05	0.640	3.81E-05	0.728	0.0038
Myod1	0.387	0.0133	2.357	0.0012	0.164	0.0004
Myog	1.748	0.1993	1.501	0.0759	1.165	0.6710
Myot	1.557	0.0230	1.283	0.0179	1.213	0.1953
Neb	0.967	0.8211	0.872	0.1255	1.109	0.5423
Nfkb1	1.099	0.4134	0.967	0.7458	1.136	0.1361
Nos2	0.524	0.0032	0.631	0.0059	0.831	0.2746
Pax3	0.854	0.4942	0.731	0.4566	1.168	0.6995
Pax7	0.310	0.0001	0.819	0.0704	0.378	0.0015
Pdk4	15.356	0.0084	1.181	0.6444	13.006	0.0090
Pparg	0.901	0.6325	1.009	0.9558	0.893	0.4004
Ppargc1a	0.629	0.0259	0.703	0.0231	0.895	0.5704
Ppargc1b	0.244	8.93E-06	0.585	0.0001	0.417	0.0004
Ppp3ca	0.886	0.2338	1.242	0.1534	0.713	0.0639
Prkaa1	0.870	0.2472	0.900	0.1548	0.967	0.8028
Prkab2	0.755	0.0049	0.727	0.0044	1.038	0.5163
Prkag1	1.049	0.4941	0.826	0.0220	1.269	0.0276
Prkag3	0.121	0.0002	0.324	0.0010	0.375	0.0048
Rhoa	0.891	0.1499	0.857	0.0116	1.040	0.6233
Rps6kb1	1.016	0.8931	0.960	0.5970	1.058	0.6229
Sgca	1.428	0.0212	1.119	0.1903	1.277	0.0911
Slc2a4	0.633	0.0087	0.563	0.0013	1.124	0.5298
Tgfb1	0.718	0.0114	1.036	0.6960	0.693	0.0011
Tnnc1	0.667	0.1066	1.068	0.7925	0.625	0.0930
Tnni2	1.302	0.1503	1.224	0.2906	1.064	0.7706
Tnnt1	0.666	0.0584	1.192	0.5074	0.559	0.0827
Tnnt3	0.935	0.3325	0.941	0.4062	0.993	0.9413
Trim63	20.389	0.0085	1.957	0.1026	10.417	0.0108
Ttn	0.924	0.2749	1.174	0.0222	0.787	0.0009
Utrn	0.782	4.96E-05	1.040	0.5110	0.752	0.0031

Fig. S5. *Targeted array of myopathy- and myogenesis-associated genes in skeletal muscle from control mice and tumor-bearing mice with and without R848 therapy.*

A) Unsupervised clustering analysis of all array transcripts, normalized to mean expression within transcript and scaled by standard deviation. B) Fold regulation values and P values for all transcripts, with ddCT values normalized to 5 control transcripts (*Actb, B2m, Gapdh, Gusb*, and *Hsp09ab1*).

Hypothalamic and systemic inflammation signatures in PDAC are modified by R848

Cancer cachexia is commonly understood to result from pathogenic crosstalk between the tumor and a variety of physiological systems. With successful reduction in tumor burden, abnormal inflammatory signaling in peripheral tissues could improve due to loss of tumor-derived mediators associated with cachexia. Because of the improvements noted in appetite and behavior, the hypothalamus was queried for changes in inflammatory transcripts associated with cachexia. Consistent with prior studies, KxPxCx allograft-induced cachexia resulted in hypothalamic inflammation in vehicle-treated animals, with increases in expression of *Selp, Il1b, Il1r1, Tlr7, Ccl2,* and *Icam1* (Fig. 4G, Fig. S6A). Treatment with R848 resulted in decreased hypothalamic inflammatory gene expression in a subset of these transcripts, including *Il1b* and *Selp*, but these changes did not approach statistical significance.

Given the liver's central role in processing inflammatory stimuli, we hypothesized that R848 and tumor burden would each exert influences on hepatic gene expression. Consistent with previous studies, we found that tumor burden resulted in elevated hepatic *Il1b, Ifna, Lcn2, Apcs, Crp,* and *Orm1* (Fig. 4H). No changes were observed in these transcripts when R848 was delivered to healthy sham-operated animals. However, livers from KxPxCx animals treated with R848 had a distinct inflammatory profile from other experimental groups. Two transcripts, the cytokines *Il1b*

and *Ifna*, were more elevated in tumor-bearing animals treated with R848 as compared to vehicle alone (P<0.0001 and P<0.01 respectively, ANOVA with Tukey test). One transcript, the acute stress response signal *Lcn2*, was equally increased in R848 and vehicle treated tumor-bearing animals (P<0.0001 versus sham-operated vehicle for both groups). However, three classical acute phase reactants, *Apcs, Orm1,* and *Crp*, were significantly decreased in tumor-bearing animals treated with R848 compared to vehicle, consistent with decreased tumor burden associated inflammatory responses.

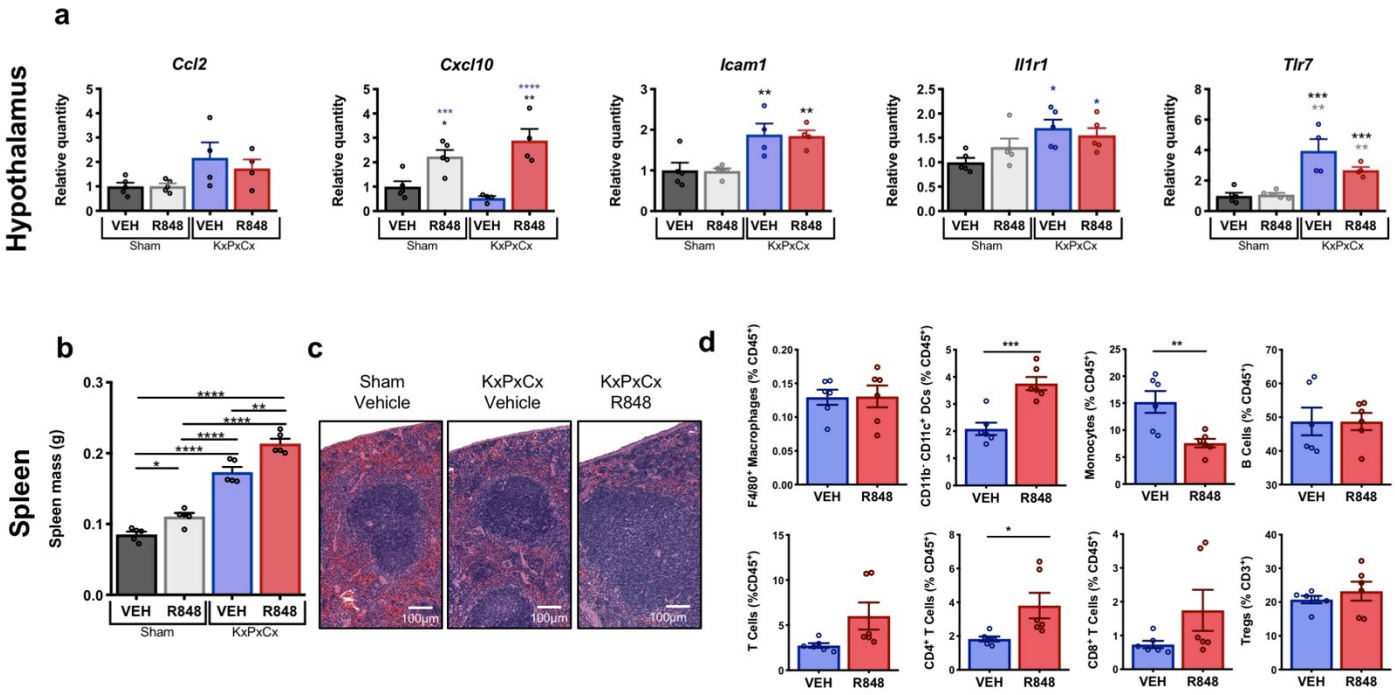

Fig. S6. *Extended data on cachexia molecular physiology.*

A) Hypothalamic gene expression of inflammatory transcripts *Ccl2, Cxcl10*, *Icam1*, *Il1r1*, and *Tlr7* (n=5/group). B) Spleen mass at necropsy for sham-operated and KxPxCx-engrafted mice treated with R848 or vehicle (n=5/group). C) Representative splenic H&E, imaged at 20x, demonstrating progressive inflammatory responses to tumor burden and reactive lymphoid hyperplasia following treatment with R848. D) Flow cytometric analysis of splenic immune populations in tumor-bearing animals allocated to vehicle (VEH) or R848 (n=6/group). *, P<0.05; **, P<0.01; ***, P<0.001.

As another means of assessing systemic immune responses during tumor progression and R848 therapy, the spleen was investigated for gross morphology, histology, and cell composition. Splenic mass at necropsy was markedly increased both due to KPC tumor burden and R848 treatment (Fig. S6B). Histological analysis of spleens from R848-treated tumor-bearing animals revealed expansion of the white pulp, compatible with reactive lymphoid hyperplasia (Fig. S6C). Flow cytometry performed on spleens from R848-treated KxPxCx-engrafted animals demonstrated, compared to vehicle-treated KxPxCx animals, an increase in $CD11b^{-}CD11c^{+}$ dendritic cells ($P<0.0001$), a decrease in monocytes ($P<0.01$), and an increase in $CD3^{+}CD4^{+}$ T cells ($P<0.05$) (Fig. S6D), suggestive of increased trafficking of dendritic cells to lymphoid tissue following R848.

Continuous, but not burst, R848 treatment extends survival in allografted PDAC

Since we observed that tumor burden and cachexia manifestations were decreased following R848, we next investigated whether these improvements translated to meaningful changes in survival. As a related question, we investigated how treatment duration affected the outcomes of anti-tumor response and survival. We therefore included two R848 treatment arms for survival analysis: a 5-dose "burst" dosing regimen and a continuous dosing regimen (Fig. 5A). Animals were compared for duration of survival while being tracked for food intake, body weight, and behavior. Continuous treatment with R848 resulted in a near doubling of survival duration in KxPxCx-engrafted animals and 12.5% survival at 35 days (median survival 15d vehicle versus 28d continuous-treated R848, Log-rank test $p<0.0001$) (Fig. 5B). In contrast, burst treatment with R848 modestly extended survival, but appeared to have a sustained response in only a small proportion of subjects (median survival 15d vehicle vs. 17d burst-treated R848, Log-rank test

P=0.056). Though mice remained hypophagic despite R848 therapy in later stages of illness, food intake was improved relative to vehicle-treated KxPxCx-bearing animals through most of the study (Fig. 5C). Body weight continued to decrease over the course of the study among R848-continuous treated mice, indicative of possible drug toxicity or the result of ongoing hypophagia (Fig. 5D). In addition to prolonged survival, mice treated with R848 exhibited normalized behavior for weeks following initiation of therapy, including decreased physical signs of illness (video data available by contact).

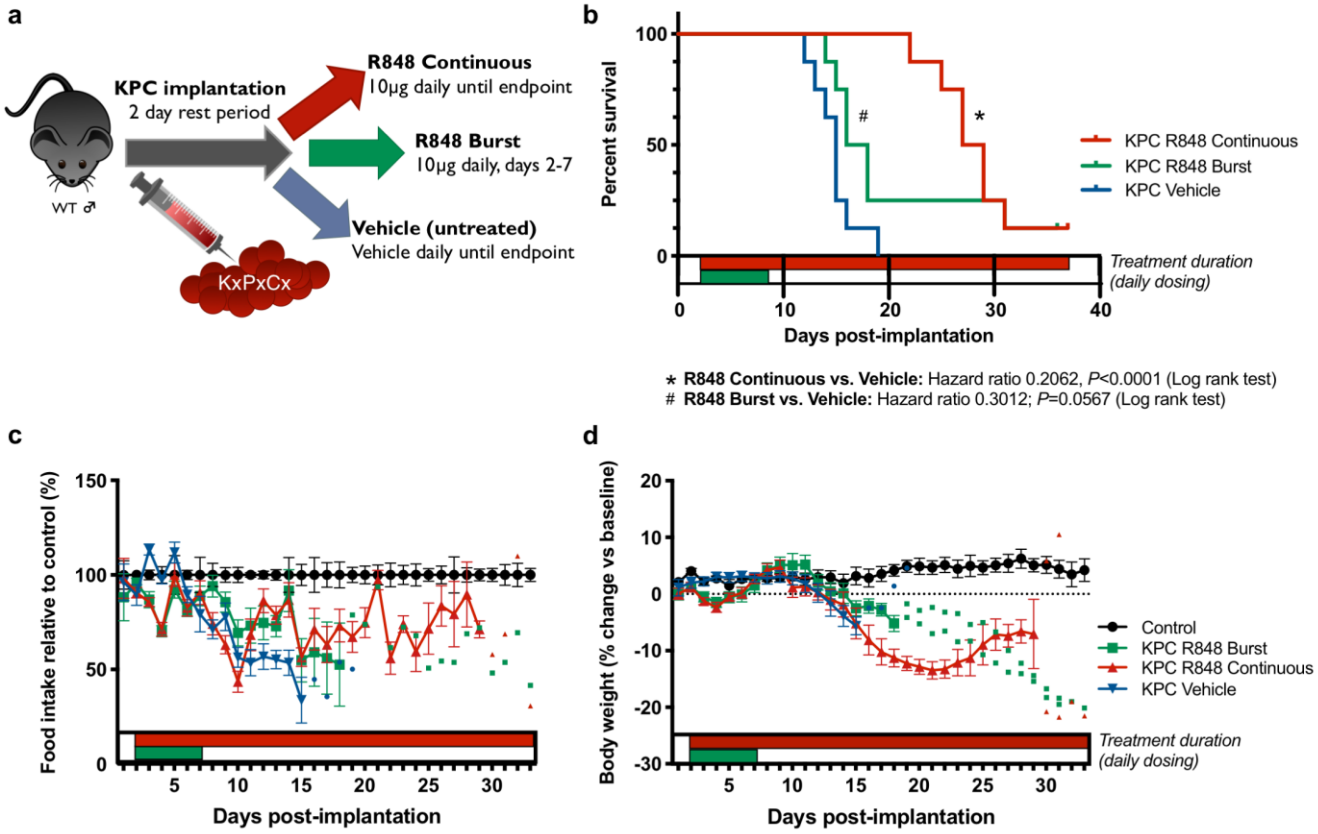

Fig. 5. *Continuous R848 monotherapy extends survival in allografted PDAC.*

Experimental design (a), Kaplan-Meier curve comparing sham-treated, burst-treated R848, and continuous-treated R848 KxPxCx-engrafted mice (b), food intake relative to sham controls (c), and body weight relative to initial measurement (d). *n*=8/group. Values are depicted as mean ± SEM, unless fewer than 3 subjects were remaining in a group, for which individual values are plotted.

The anti-tumor effects of R848 are mediated by stromal, not epithelial, TLR7 expression

The effects of TLR stimulating agents on tumor immunity could be attributed to actions on neoplastic cells, stromal elements, or a combination thereof. While our earlier results indicated that epithelial factors mediate R848 response, the changes in immune complexity of treated tumors led us to hypothesize that R848-induced tumor immunity also requires stromal TLR7. Mice harboring hemizygous null deletions in TLR7 (TLR7KO) were implanted with R848-responsive KxPxCx epithelial tumor cells and tracked for tumor growth and cachexia status (Fig. 6A). Contrary to the results in TLR7-proficient mice, KxPxCx-engrafted TLR7KO mice treated with R848 experienced increased tumor growth relative to vehicle-treated mice (Fig. 6B-C). While there was no decrease in food intake or body weight associated with treatment induction, due to the receptor specificity of R848 for TLR7 in mouse, treatment groups began to diverge significantly during the cachexia stage. KxPxCx-engrafted TLR7KO animals treated with R848 developed significantly worse anorexia and weight loss compared to vehicle-treated counterparts. (Fig. 6D-F) Simultaneously, KPC-bearing TLR7KO animals treated with R848 had substantially exacerbated lean mass loss (Fig. 6G), skeletal muscle catabolism (Fig. 6I), and cardiac atrophy (Fig. 6J). Combined, these results confirm that host rather than epithelial TLR7 is necessary for R848's beneficial effects, and substantiate caution that TLR7 activity may increase tumor burden if unchecked by immune response.

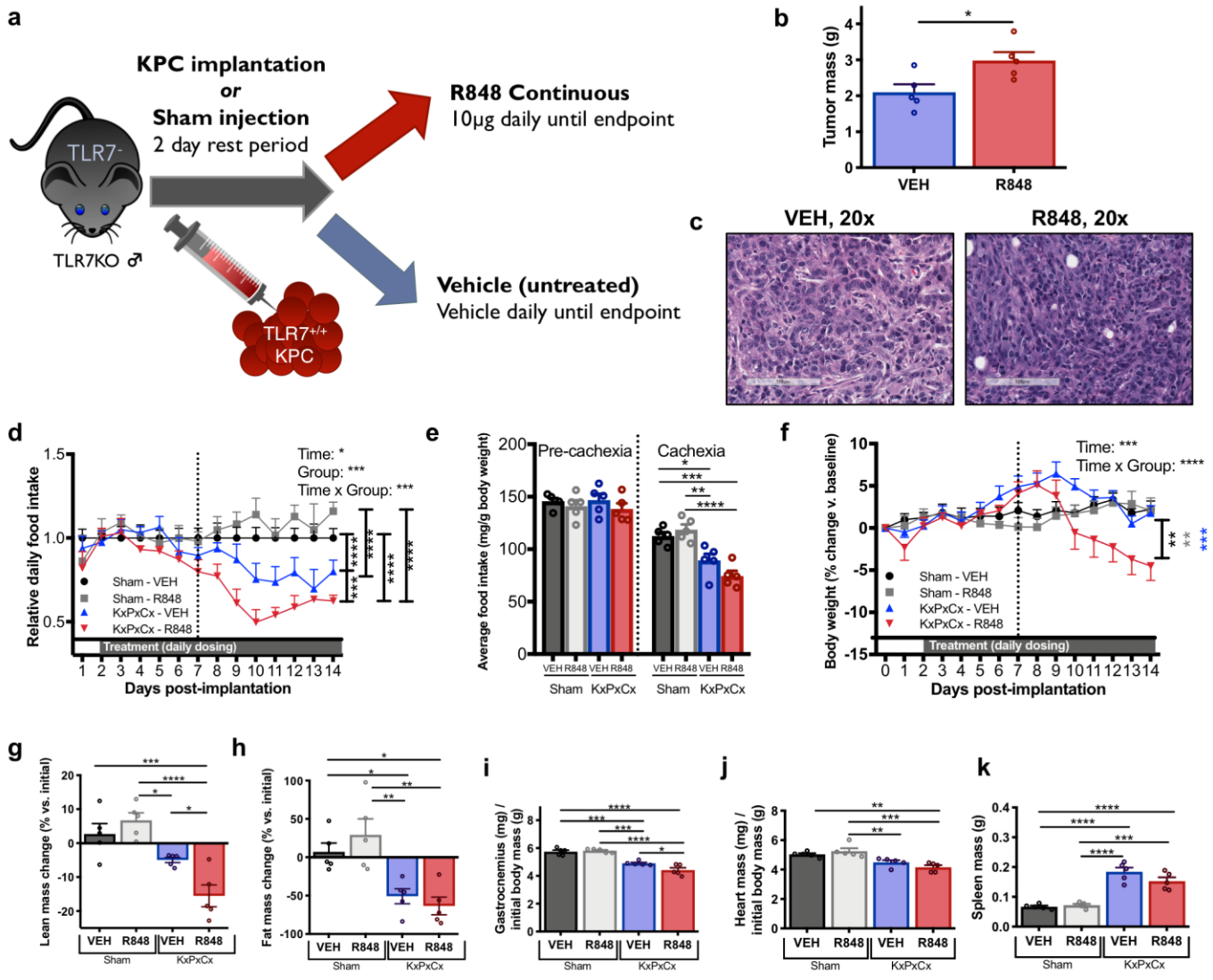

Fig. 6. *The anti-tumor and cachexia attenuating effects of R848 require stromal TLR7.*

TLR7 hemizygous null (TLR7^{-}) mice were implanted with TLR7 intact KxPxCx, then randomized to R848 or vehicle as previous (a). Tumor size (b) was increased following R848 in this context, with representative histology shown in (d). Food intake (plotted as a function of time in d and as cumulative averages in e) and body weight (f) were both more severely affected during cachexia stage R848 treatment when TLR7 was absent in host tissues but present in neoplastic cells. This was accompanied by lean mass loss (g), no further changes in adipose wasting (h), skeletal muscle catabolism (i), cardiac muscle catabolism (j), and lack of splenic response to treatment (k). Statistics were performed as two-way ANOVA during the cachexia stage to test for main effects of tumor and treatment, and the interaction thereof, with multiple comparisons tests for main column effects. Values represent mean ± SEM. *, P<0.05; **, P<0.01; ***, P<0.001; ****, P<0.0001.

Tlr7 is commonly expressed in stroma, but not epithelium, across all stages of human pancreatic neoplasia progression

Based on the differential effects we observed depending on whether TLR7 was present in tumor stroma, we investigated the frequency of R848-responsive genes in tumor compartments using an RNAseq library of laser-capture microdissected human pancreatic lesions. To determine whether expression differed over the course of disease development, we queried two types of precursor lesions, pancreatic intraepithelial neoplasia (PanIN) and intraductal papillary mucinous neoplasia (IPMN), and PDAC. The vast majority of samples expressed stromal *Tlr7*, including 12/12 IPMN samples, 23/23 PanIN samples, and 111/124 PDAC samples (Fig. 7A). *Tlr7* was far less abundant in epithelial samples, with at least 1 TPM in 8/19 IPMN samples, 7/26 PanIN samples, and 59/197 PDAC samples (Fig. 7B). While murine Toll-like receptor 8 (TLR8) is generally considered inactive, human TLR8 is abundantly expressed and responsive to ligands including ssRNAs and imidazoquinolines. We found *Tlr8* demonstrated a gene expression distribution similar to *Tlr7* across stages of pancreatic neoplasia, with a majority of stromal samples expressing at least 1 TPM, and only a minority of epithelial samples demonstrating positive *Tlr8* expression (Fig. 7C-D). The transcript encoding the obligate intracellular shuttle protein for TLR7, uncoordinated homolog 93 B1 (*Unc93b1)*, was typically present in both epithelium and in stroma, indicating the machinery to traffic TLR7 to its active signaling compartment was intact in both types of cell populations (Fig. 7E-F). These data collectively indicate that most patients with pancreatic neoplasms have tumor gene expression profiles compatible with therapeutic responses to TLR7 agonists.

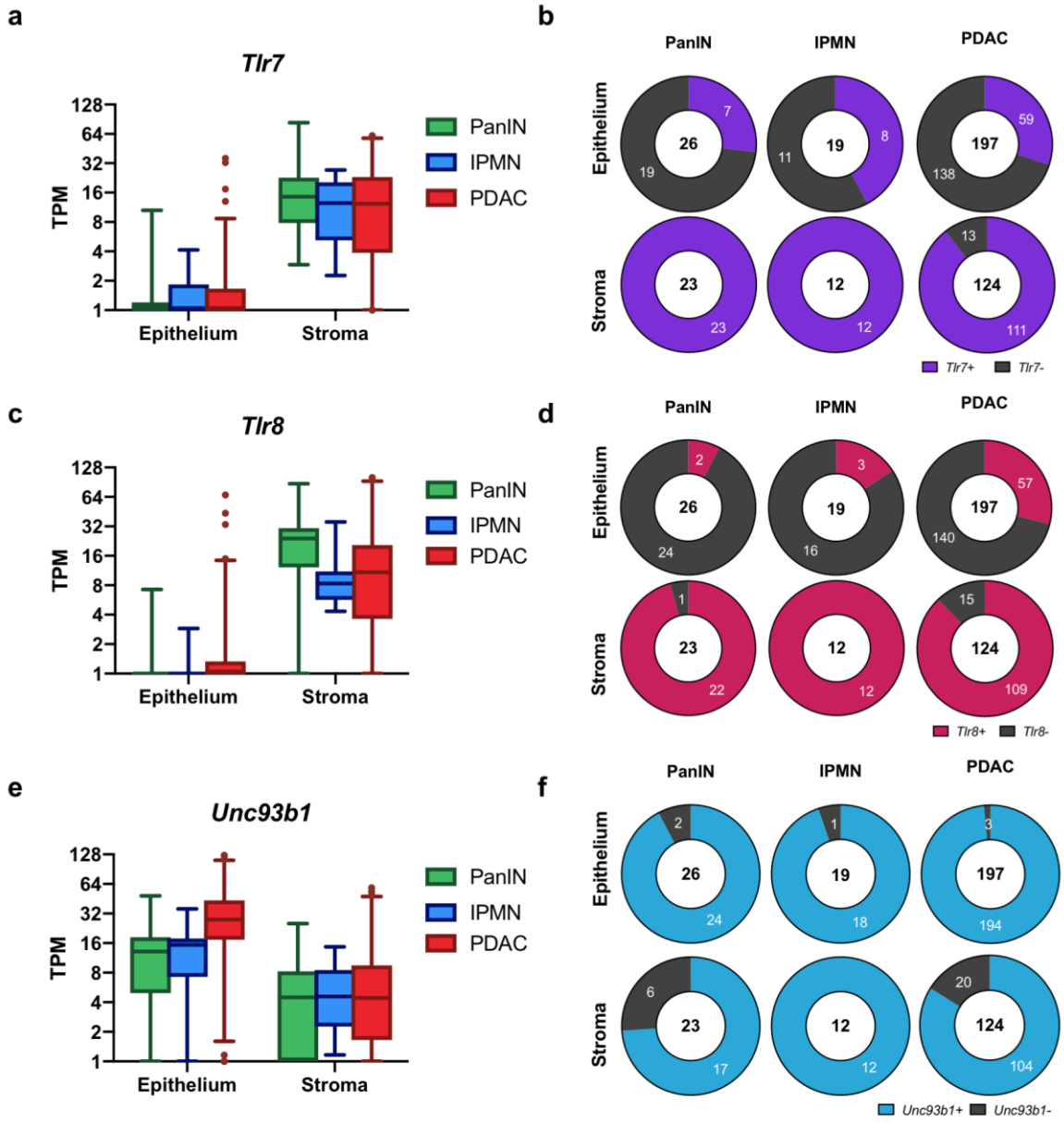

Fig. 7. *Tlr7 expression is ubiquitous among human PanIN, IPMN, and PDAC stroma, but not commonly expressed in tumor epithelium.* Left: Transcript count per million (TPM) from RNA-seq in epithelial and stromal laser capture microdissected samples from PanIN, IPMN, and PDAC samples for *Tlr7* (a), *Tlr8* (c), and *Unc93b1* (e). Data displayed as interquartile range, with whiskers depicting 2.5th-97.5th perecentile. Right: Proportions of samples positive and negative for *Tlr7* (b), *Tlr8* (d), and *Unc93b1* (f) based on the threshold of 1 TPM. Sample size for each category of neoplasm (PanIN, IPMN, and PDAC) and tumor compartment (epithelium and stroma) is shown in the center of the plot, with the outer values depicting absolute frequency of positive and negative expression.

Discussion

In this study, we demonstrate that R848 remodels the tumor immune microenvironment and host responses in PDAC, and is ultimately associated with improved survival. The anti-tumor response elicited by R848 is characterized by formation of tertiary lymphoid structures, increased $CD8^+$ T cell infiltration with evidence of increased activation and cytotoxicity, and decreases in Treg concentration, all of which are associated with improved prognosis in human malignancy [373-375]. Based on the lack of tumor reduction and exacerbation of cachexia in TLR7-deficient hosts, we report that the beneficial effects of R848 require stromal rather than epithelial TLR7. Given that not all epithelial PDAC tumor cell lines demonstrate tumor response to R848, we show that R848 sensitivity is additionally dependent on epithelial factors. This is consistent with recent work illustrating that tumor cell intrinsic factors dictate the extent of T cell infiltration and the ability to respond to combination immunotherapy during PDAC [376]. Surprisingly, though TLR7 agonists are classically associated with acute illness responses, we observed that ongoing therapy resulted in tachyphylaxis of sickness responses without diminution of therapeutic effect. The anti-tumor response coupled with the lack of persistent deleterious physiological effects resulted in improvements in cachexia status and decreases in tissue catabolism during the course of treatment. This represents a key difference from many cytotoxic chemotherapies, and suggests some classes of immunotherapy may be beneficial in the treatment of cachexia-associated malignancies.

A growing array of immunotherapy modalities, such as tumor vaccines, cytokines, monoclonal antibodies, and immunostimulatory small molecules, show considerable promise, yet crucial unknowns persist in their clinical application [377,378]. The first years of experience with T cell checkpoint inhibitors demonstrated that immune-related adverse events are common, including

new onset autoimmune disorders, exacerbation of underlying autoimmunity, and sequelae of cytokine release [379]. Immunotherapy optimization will likely become even more complex as other clinical variables, such as cachexia, are taken into account. Options for patients with cachexia often prove startlingly narrow, and specifically in PDAC, newer and more effective treatment regimens such as FOLFIRINOX are contraindicated for patients with poor performance status [380]. The presence of cachexia increases complications during cancer treatment, decreases therapeutic tolerance, and has been identified as a key determinant of survival duration in PDAC clinical trials [60,63,381]. However, with further optimization, it is possible that immune-based therapies could provide effective tumor responses without the same degree of systemic toxicity as cytotoxic chemotherapy, thereby providing new therapeutic avenues for patients with cachexia.

Several recent studies highlight the dual potential for benefit and harm of TLR7 agonists, which hold substantial promise as antitumor agents but are well-known to cause acute toxicities [333,382,383]. Indeed, we observed that treatment induction was associated with acute hypophagia, weight loss, and decreased locomotor activity. However, these effects desensitize over time, consistent with the tightly regulated role of TLR7 activity in immune responses. TLRs are evolutionarily conserved components of the innate immune system that respond to common molecular motifs in pathogens, including membrane components, lipoproteins, and nucleic acid species [384]. Both TLR7 and TLR8 are endosomal receptors that detect a variety of purine-rich ssRNA species [385]. In mouse, TLR7 is predominantly expressed in plasmacytoid dendritic cells and B cells, with context-dependent expression in subsets of macrophages and T cells [386]. Following inflammatory stimuli, TLR7 is ubiquitinated and packaged into COPII-coated vesicles by the ER-resident chaperone UNC93B1 [387,388]. Upon binding ssRNA, TLR7 dimerizes and initiates downstream signal transduction via myeloid differentiation primary response gene 88 (MyD88),

resulting in production of pro-inflammatory cytokines and type I interferon, T cell proliferation, and induction of T_H1 responses [389,390]. We observed many of these elements within PDAC tumors treated with R848, including $CD8^+$ T cell proliferation and effector function, as well as decreased T_H2 polarization among $CD4^+$ T cells. However, it is clear from the sweeping changes to immune populations with R848 that TLR7 agonists have widespread effects on numerous immune cell lineages during malignancy.

A cardinal feature of cancer is evasion of immune responses via immunosuppressive signaling within the tumor microenvironment [338]. This feature is particularly common in PDAC: both local immunosuppression and structural barriers, such as stromal desmoplasia, are key therapeutic challenges. The TLR7 agonist imiquimod is FDA-approved as a monotherapy for basal cell carcinoma, and the potential for TLR agonists is quickly expanding into numerous other malignancies [339]. In some cases, TLR7 stimulation of T cells alone is sufficient for anti-tumor responses: nanoparticle delivery of R848 to $CD8^+$ T-cells results in increased antitumor immunity and prolonged survival in the murine M38 model of colorectal cancer [340]. TLR7 agonists also demonstrate benefit in combination with doxorubicin in T cell lymphoma [341], with bacillus Calemtte-Guérin in non-muscle-invasive bladder cancer [342], and with radiotherapy against gastrointestinal tumors [391]. Recent work also demonstrates utility for short-burst strategies of TLR agonists in conjunction with T cell potentiating therapies, modifying both innate and adaptive arms of immune response. To this effect, a brief course of the TLR9 agonist CpG combined with agonistic anti-OX40 was recently demonstrated to be highly effective against a wide range of solid tumors [392]. However, in the monotherapy context, we found that short-regimen R848 was only weakly beneficial, and that continuous dosing was more effective in improving overall survival.

While we did not employ a combinatorial approach in this study, there is strong rationale for future studies investigating efficacy and tolerability of TLR7/8 agonists as part of a combination therapy. On monotherapy alone, KPC-derived mice treated with R848 eventually developed tumor progression leading to cachexia and mortality. Interestingly, adverse responses to R848 such as hypophagia and weight loss demonstrated relatively rapid desensitization kinetics, but anti-tumor responses were substantially more robust with long-term dosing. This suggests that R848's adverse systemic effects and anti-tumor responses are likely mediated by different cell types with functionally distinct signaling kinetics and receptor modulation. Similar uncoupling of central nervous system immune tolerance and anti-tumor responses has been observed with TNF, suggesting that this phenomenon may occur in a variety of contexts [162]. Indeed, most pathogen-associated molecular patterns and damage-associated molecular patterns demonstrate behavioral tachyphylaxis following repeated stimuli, and it is therefore not entirely surprising that R848's initial illness responses are limited in duration [270,393]. In contrast, the limited course of illness responses is not observed with cytotoxic chemotherapy, which induces dose-dependent deleterious effects [394], nor checkpoint inhibitors, which are associated with acute and chronic immune related adverse events [379]. It therefore remains possible that with use of TLR7/8 agonists, lower doses or shorter courses of other therapies can be used to attain effective tumor response without exacerbating cachexia.

Further studies will be crucial as this class of drug is evaluated for clinical use. We used syngeneic orthotopic models of pancreatic cancer to avoid the risk of global pancreatic dysfunction, which can occur in genetically engineered mouse models of pancreatic cancer and confounds assessment of cachexia. The ideal framework for studies combining cachexia evaluation with tumor response is both inducible, to avoid developmental effects on appetite and

metabolism, and arising from a limited number of transformed cells, to avoid distortion of the tumor biology. Given that genetically engineered mouse models provide the most accurate recapitulation of tumor biology, future work ought to evaluate TLR agonists in the transgenic context to determine how spontaneously arising tumors respond to treatment. In addition, it will be beneficial to evaluate other aspects of cachexia, including muscle strength, motor performance, stamina, as well as cognitive and affective components of behavior.

Finally, these results highlight the importance of evaluating immunotherapy effects using a whole animal physiology approach. Outcomes from PDAC can be thought of as the sum of two domains: the tumor itself, and the host in which the disease takes place. At the same level of tumor burden, a more resilient host will have improved outcomes relative to a weakened host, which is vividly illustrated by the increased morbidity and mortality seen in patients with cachexia. The most effective treatment paradigms for PDAC therefore should not only be effective against the primary tumor, but also serve neutral or beneficial roles systemically. Though not all forms of immunotherapy will necessarily have positive effects on host pathologies such as cachexia, agents like R848 that confer local and systemic benefits will be highly valuable as we strive to improve outcomes in pancreatic cancer.

Methods

Experimental Design

The primary objective of this study was to simultaneously evaluate tumor and cachexia responses to the immunotherapy R848 in preclinical models of PDAC. Furthermore, we aimed to uncover mechanistic data regarding the necessary components to observe anti-tumor immunity, including testing for the effects of epithelial heterogeneity and stromal immune receptor expression.

Finally, we sought to verify whether the mechanistic factors required for anti-tumor response in a large set of patient pancreatic neoplasia samples. To assess cachexia outcomes and tumor response, we used a murine PDAC-associated cachexia model recently developed in our laboratory [253]. Three distinct epithelial clones were used to account for neoplastic heterogeneity in drug response. Murine TLR7 knock-out mice were used to query the role of host biology in R848 response. Human data was used to perform clinical correlation for the gene expression pattern we found is required for favorable R848 response. Sample sizes were selected based on pilot data assessing tumor mass at endpoint and anorexia during cachexia stage. Blinding was performed for any qualitative analysis, including histology interpretation. Endpoints and data collection were designated *a priori* as described in subsections below.

Animals

Male C57BL6/J mice (JAX, cat. #000664) and TLR7^{-} mice backcrossed to the C57BL6/J background (JAX, cat. #008380) were maintained in standard housing at 26°C and 12h light / 12h dark cycles. Animals were provided *ad libitum* access to water and food (Rodent Diet 5001; Purina Mills). In the week prior to implantation, animals were transitioned to individual housing to acclimate to experimental conditions. Animal food intake and body weight were monitored daily at 0900-1000h. Treatment was delivered from 1200-1300h. All studies were performed in accordance with the NIH Guide for the Care and Use of Laboratory Animals.

KPC-derived epithelial clones

The KPC model expresses double heterozygous knock-in pancreas specific conditional alleles KRAS^{G12D} and TP53^{R172H} via the PDX-1-Cre driver, and is a preferred model of PDAC for its close recapitulation of human disease. To study KPC-derived tumors, we used an epithelial clone

derived from KPC mice back-crossed into the C57BL/6 background (here referred to as KxPxCx), kindly provided by Dr. Elizabeth Jaffee [268]. Additional cell lines from C57BL/6 KPC animals were generously provided by Dr. David Tuveson (FC1242 and FC1199). Cells were maintained in RPMI 1640 supplemented with 10% fetal bovine serum, 1% minimum essential medium non-essential amino acids, 1mM sodium pyruvate, and 50 U/mL penicillin/streptomycin (Gibco), with incubators maintained at 37°C and 5% CO_2.

Generation of PDAC model and treatment paradigm

8-week-old male C57BL/6J wildtype or $TLR7^-$ mice were orthotopically or intraperitoneally implanted with 10^6 KPC-derived epithelial cells or equivalent volume saline, then randomized two days later to daily IP R848 (10μg) or vehicle until sacrifice. R848 was obtained from Enzo Life Sciences (#NC9739083). In studies comparing cachexia status and tumor immune response, all animals were sacrificed when any study arm developed end-stage cachexia or tumor burden exceeding IACUC guidelines. In studies comparing survival duration, animals were sacrificed following onset of IACUC-designated signs of moribund behavior.

Tumor fixation and histology

Tumor samples were fixed in formalin and paraffin embedded, then sectioned for further analysis. H&E stains were interpreted by a board-certified pathologist blinded to experimental group (TKM).

Flow cytometry

At sacrifice, tumor-bearing mice were perfused with PBS to clear tissue of vascular immune cells. Tumors were harvested in DMEM on ice, then minced and enzymatically digested in DMEM

containing 1.0 mg/mL Collagenase IV (Gibco, #17104-019), 1.0 mg/mL Soybean Trypsin Inhibitor (Gibco; #17075-029), and 50 U/mL DNAse 1 (Roche; #10104159001). Samples were incubated for 30 minutes at 37°C with agitation at 125 rpm, filtered through 100µM cell strainers, centrifuged at 400g for 5 minutes at 4°C, then resuspended and immediately stained for flow cytometry. Antibodies and reagents to label cells can be found in Supplementary Methods. Flow cytometry was performed on a BD Fortessa and data was analyzed in FlowJo software.

Multiplex immunohistochemistry staining

Representative tumors from vehicle- and R848-treated KxPxCx-implanted animals were stained using a 23-marker mIHC panel, as previously described [42]. Briefly, tumors were fixed in PFA, paraffin-embedded, and sectioned immediately prior to staining. Antibodies used for sequential staining are described in Supplementary Methods. Histofine Simple Stain Max Reagents for anti-rat (Nichirei Biosciences, #414311F) and anti-rabbit (#414144F) were used for detection of primary antibodies, and final stain development performed with AEC (Vector Lab, SK-4200). Slides were coverslipped in water and scanned following each marker using a Leica Aperio. Hematoxylin stains were performed at cycle 2 and after the final cycle to identify cells and account for any tissue loss.

Analysis of multiplex immunohistochemistry

ImageScope software (Leica) was used to select 5 regions of interest (ROIs) of fixed size (5000x5000 pixels) per sample, collectively representing a minimum of 50% of the tumor cross-sectional area. On average, ROIs contained 42,200 cells (range: 28,236-61,573), with an average of 237,380 cells analyzed per tumor (range: 165,960-266,659). ROIs were registered for all markers using the SURF algorithm in MATLAB. Registered regions were imported into FIJI-ImageJ to

extract AEC signal from background with color deconvolution, and generate single cell segmentation masks, upon which merged pseudocolor images were generated for markers of interest. Cell Profiler was used to measure the mean intensity of each marker for each segmented cell. The output was imported into FCS Express 6.0 Image Cytometry, and manually gated with picture plots to visually validate the expression of each cell as true positive or true negative for each marker through the gating hierarchy. The hierarchical gating strategy for identification of cell types and functional markers is described in Fig. S2B. Results were exported into SPSS (IBM) and Orange (University of Ljubljana) to perform unsupervised clustering analysis, and to generate heat maps depicting cell identities and activation states. Statistical analysis was performed using Prism 8.0 software, with per-ROI or per-tumor analysis as specified.

Analysis of cachexia outcomes

Animal food intake and body weight were monitored daily, with bedding sieves to account for ort spillage. Body temperature and voluntary locomotor activity were measured via implanted Minimitter tracking devices on 5-minute recording intervals (MiniMitter, Bend, OR, USA). Body composition was assessed at designated timepoints using EchoMRI nuclear magnetic resonance relaxometry. Necropsies were performed to obtain mass measurements of tumor, heart, gastrocnemius, and spleen. Tumor, hypothalamus, heart, gastrocnemius, and liver were immediately stored in RNAlater for gene expression analysis (Ambion).

Gene expression assays

Following tissue homogenization, RNA was purified with the RNeasy Mini Kit (Qiagen), then reverse transcribed with the High Capacity cDNA Reverse Transcription Kit (Life Technologies). qRT-PCR was performed using TaqMan reagents and primer-probes listed in Supplementary

Methods, with normalization to 18S using the ddCT method. Gene expression analysis was performed on gastrocnemius with the Myogenesis and Myopathy RT2 Profiler Array (#PAMM-099Z, Qiagen). Log_2 transformed expression values were imported into Orange, normalized to standard deviations from mean for each transcript, and subjected to PCA and unsupervised clustering analysis.

RNA-seq of stromal and epithelial compartments in human pancreatic neoplasia

To compare gene expression in stromal and epithelial samples for key R848 response elements in human neoplasia, we queried a dataset of RNAseq using human cohorts of PanIN, IPMN, and PDAC, as previously described [395]. Samples were normalized to transcripts per million for analysis, and stratified for level of expression and overall positive rate for the transcripts *Tlr7*, *Tlr8*, and *Unc93b1*.

Statistics

Prism 8.0 software was used for statistical analyses. For cross-sectional analyses of two groups, we performed T-tests, and when greater than two groups, ANOVA with Tukey test for multiple comparisons between all experimental groups or Sidak test for comparisons against a single control group. For longitudinal comparisons of cachexia parameters, data were grouped into the bins of pre-cachexia and cachexia. Differences for these variables are only expected between groups during the cachexia stage, defined as persistently decreased food intake of 10% or more relative to control subjects. During cachexia stage, we performed two-way ANOVA for the main effects of experimental group and time, the interaction thereof, and Tukey test for multiple comparisons of main column effect. For interpretation of survival data, we did not expect the magnitude of effect to depend on duration of exposure, nor did we expect the differences to

emerge at relatively early time points, and therefore selected the Log rank test for comparison of groups with respect to median survival and hazard ratio. All statistical tests were performed as two-tailed analyses.

Materials used for flow cytometry

Target and conjugate	Name	Manufacturer	Catalog	FMO Prepared
CD11b FITC	Integrin alpha M	BioLegend	#101206	Yes
CD11c APC-Fluor780	Integrin, alpha X (complement component 3 receptor 4 subunit)	eBioscience	#47-0114-82	Yes
CD19 BV650	Cluster of differentiation 19	BioLegend	#115541	No
CD3 BV786	Cluster of differentiation 3	BD Horizon	#564010	Yes
CD4 BV605	T-cell surface glycoprotein CD4	BD Horizon	#563151	No
CD45 PE-Cy7	Protein tyrosine phosphatase, receptor type, C	BD Pharmingen	#552848	No
CD8a BV711	Cluster of differentiation 8a	BD Horizon	#563046	No
F4/80 APC	EGF-like module-containing mucin-like hormone receptor-like 1	BioLegend	#123116	Yes
FOXP3 PE	Forkhead box P3	eBioscience	#12-5773-82	Yes
Ly6C PerCP	Lymphocyte antigen 6 complex, locus C1	BioLegend	#128028	Yes
Ly6G Alexa Fluor 700	Lymphocyte antigen 6 complex locus G6D	BioLegend	#127622	Yes
MHCII eFluor450	MHC class II antigen	eBioscience	#48-5321-82	No
NK1.1 PE-Dazzle	Killer cell lectin-like receptor subfamily B, member 1	BioLegend	#108748	Yes
Live Dead Aqua	(N/A)	Invitrogen	#L34957	N/A

Antibodies used for mIHC

Target	Name	Manufacturer	Catalog
B220	Protein tyrosine phosphatase receptor type C isoform B220	BD Biosciences	#550286
BTK	Bruton's tyrosine kinase	LS Bio	#LS-C180161
CD11b	Integrin alpha M	Abcam	#133357
CD11c	Integrin, alpha X (complement component 3 receptor 4 subunit)	Cell Signaling	#97585
CD206	Cluster of Differentiation 206	Abcam	#64693
CD3	Cluster of differentiation 3	Thermo	#RM-9107-S
CD4	T-cell surface glycoprotein CD4	Cell Signaling	#25229
CD45	Protein tyrosine phosphatase, receptor type, C	BD Biosciences	#550539
CD8	Cluster of differentiation 8	eBioscience	#14-0808-82
CD86	Cluster of Differentiation 86	eBioscience	#14-0862-81
CSF-1R	Colony stimulating factor 1 receptor	Santa Cruz	#Sc-692
EOMES	Eomesodermin	Abcam	#183991
F4/80	EGF-like module-containing mucin-like hormone receptor-like 1	Serotec	#Cl:A3-1
FOXP3	Forkhead box P3	eBioscience	#14-5773-82
GATA3	GATA Binding Protein 3	Abcam	#199428
GZMB	Granzyme B	Abcam	#4059
Ki67	Marker of proliferation Ki-67	Abcam	#15580
Ly6G	Lymphocyte antigen 6 complex locus G6D	eBioscience	#551459
PANCK	Cytokeratin	Abcam	#ab27988
PDL-1	Programmed death-ligand 1	Cell Signaling	#13684
RORγt	RAR-related orphan receptor gamma	Abcam	#ab207082
TCF1	Transcription factor T-cell factor 1	Cell Signaling	#2203s
TIM3	T-cell immunoglobulin and mucin-domain containing-3	Cell Signaling	#83882

Primer-probes used for qRT-PCR

Gene	Name	Catalog	Tissue(s)
Mafbx	Muscle atrophy F-box	Mm00399518_m1	Gastrocnemius, heart
Murf1	Muscle ring finger 1	Mm01185221_m1	Gastrocnemius, heart
Foxo1	Forkhead box O1	Mm00490672_m1	Gastrocnemius
Bnip3	BCL2 Interacting Protein 3	Mm01275600_g1	Heart
Ctsl1	Cathespin L1	Mm00515597_m1	Heart
Gabarapl	GABA Type A Receptor Associated Protein Like	Mm00457880_m1	Heart
Il1b	Interleukin-1 beta	Mm01336189_m1	Hypothalamus, liver
Il1r1	Interleukin 1 receptor type 1	Mm00434237_m1	Hypothalamus
Selp	P-selectin	Mm00441295_m1	Hypothalamus
Tlr7	Toll-like receptor 7	Mm00446590_m1	Hypothalamus
Ccl2	C-C motif chemokine ligand 2	Mm00441242_m1	Hypothalamus
Cxcl10	C-X-C motif chemokine 10	Mm00445235_m1	Hypothalamus
Icam1	Intercellular adhesion molecule 1	Mm00516023_m1	Hypothalamus
Apcs	Amyloid P component, serum	Mm00488099_g1	Liver
Crp	C-reactive protein	Mm00432680_g1	Liver
Orm1	Orosomucoid 1	Mm00435456_g1	Liver
Lcn2	Lipocalin 2	Mm01324470_m1	Liver
Ifna	Interferon alpha-1	Mm03030145_gH	Liver
18s	18s ribosomal subunit	4352930E	All

VIII. Discussion

> *"Sometimes we can offer a cure, sometimes only a salve, sometimes not even that. But whatever we can offer, our interventions, and the risks and sacrifices they entail, are justified only if they serve the larger aims of a person's life. When we forget that, the suffering we inflict can be barbaric. When we remember it, the good we do can be breathtaking."*
>
> - Atul Gawande, *Being Mortal*

In these studies, I aimed to improve upon existing experimental methods to study cachexia, and to apply the improved methodology to a preclinical evaluation of the effects of TLR7 agonism on tumor and on systemic physiology. Accordingly, this work has provided evidence toward three main objectives. First, I have demonstrated that PDAC-associated cachexia can be modeled with high fidelity in the preclinical setting using a syngeneic KPC-derived mouse model. This model is useful not only for uncovering new mechanisms of cachexia, but is beneficial for testing therapies for their effects on cachexia manifestations and systemic biology. Next, using the PDAC cachexia mouse model, we evaluated the immune response modifier R848 for effects on tumor biology and systemic response. We found that a majority of KPC-derived epithelial clones responded to treatment with R848, and furthermore, that R848 was protective against a variety of cachexia manifestations regardless of tumor response. Finally, I performed experiments to understand the tumor-independent effects of R848 on sickness behavior and systemic immune responses. These studies unveiled that microglia are the primary recipients of TLR7 stimulatory signals in the central nervous system, and that despite initial sickness responses and pro-

inflammatory signaling cascades with R848 treatment induction, chronic treatment results in an induced state of immune tolerance.

Given that cachexia is thought to be driven by aberrant inflammatory signaling between tumor and host, the fact that R848 improves rather than exacerbates cachexia was initially surprising. Indeed, multiple papers cited throughout this dissertation have implicated TLR7 signaling in causing different elements of cachexia and sickness, particularly the muscle wasting phenotype. However, our work on chronic R848 treatment may provide an explanation why this therapy is beneficial in the context of cachexia. When thinking about the acute sickness response as compared to cachexia, two core differences are (1) the temporal nature of the underlying illness and (2) whether the response is beneficial or harmful toward survival. The acute sickness response is brought about as a coordinated, multi-system reaction to limit pathogen growth, mount an immune response, and shift metabolic outputs to defend the host from immediate danger. These are crucial and highly conserved evolutionary responses that allow survival in the face of the innumerable acute threats every organism encounters over the course of life. However, the components of the acute sickness response cease to be beneficial when continued over long-term intervals, particularly when the responses are ineffective against the threat at hand. This is the case with cancer, for which manifestations of the sickness response become a chronic maladaptive condition and contribute to cachexia pathogenesis. Just as cancer has been described in a cell biology context as a wound that does not heal [396], cachexia can be thought of as an acute sickness response that does not resolve. As an extension, achieving resolution of cachexia requires interference with the molecular and cellular pathways that generate and sustain sickness. If we assume cachexia is indeed a disorder of maladaptive inflammatory responses, one way to interfere with this etiology is to induce tolerance to inflammatory signals elaborated during cancer. In the

previous chapter, I demonstrated that R848 is capable of inducing tolerance to TLR7-independent inflammatory signals including LPS. It is possible that the mechanism of R848 in PDAC cachexia may operate by similar means to induce desensitization and move the homeostatic setpoint for innate immune signals triggering sickness responses. However, future studies will be required to investigate this mechanism in greater depth.

While we did find an immune tolerance phenotype in sickness responses, an interesting contradiction arises in light of my study on R848 in PDAC. It is clear that while the cells and tissues responsible for transduction of sickness responses undergo a process of desensitization to R848 over time, this does not apply to all immune cells and all tissues. In my work on R848 in KPC-derived models of cachexia, continuous treatment was associated with tremendous improvements in survival over a short course of treatment. Furthermore, my studies on tumor-bearing mice treated with R848 demonstrate that the benefit of treatment is related to a tumor-extrinsic cell population. I believe that this is evidence that TLR7 is differentially regulated between different immune cells following stimulation with imidazoquinolines. Given that response to LPS is diminished as well, and that pattern recognition receptor expression is not different before and after tolerance induction, this is likely due to changes in a shared innate immune intracellular signaling cascade. Our preliminary work has suggested that this may be through A20 or IRAK-M, but further work will need to be done to establish whether these are indeed responsible for R848-induced immune induction. If so, differences in the expression of these mediators may explain why some tissues develop tolerance to R848 and others retain sensitivity despite repeated exposures.

Even if the R848-evoked immune tolerance is of benefit for the purpose of cachexia, the next steps should necessarily focus on safety profile. Cancer patients are frequently immunocompromised at baseline and can suffer from cytopenia in cell lineages critical for immune response, and infection remains a major cause of morbidity and mortality in the oncology setting. If the hyporesponsiveness to PAMPs we observe following R848 portends a decreased ability to detect and neutralize infectious threats, systemic R848 may be a risky drug to add into PDAC treatment regimens. Further work should include tests to evaluate the ability of chronically R848-treated mice to neutralize and survive pathogen load, especially of bacterial origin.

Future directions

There are numerous future studies that would improve upon and strengthen the findings described in this dissertation. The model we used throughout the PDAC studies may recapitulate many aspects of cachexia, but would be strengthened by a few additional features. To allow the highest fidelity model of PDAC tumorigenesis and progression, and to create a model better recapitulating the heterogeneity of true pancreatic cancer, an inducible genetically engineered mouse model would likely be the best preclinical platform for modeling cancer-associated cachexia. This would also provide a longer window of time to model the evolution of the cachexia disease process in all of its phases.

For the evaluation of R848 in PDAC and cancer-associated cachexia, it would be ideal to test the R848 intervention in a genetically engineered mouse model to ensure that it is still effective in spontaneously arising tumors. In addition, to test the therapy in a similar pattern to the oncology setting, it will be beneficial to examine the effects of R848 in animals with advanced

pre-existing tumor burden. Next, recent studies in CCR2 inhibitors and hyaluronidase PEGPH20 in PDAC have highlighted the crucial and not-always-intuitive choice of chemotherapy backbone in treatment [397,398]. R848 ought to be evaluated in conjunction with common chemotherapeutics such as gemcitabine, FOLFIRINOX, and nab-paclitaxel to assess for anti-neoplastic response and systemic toxicities, given that it is unlikely to work long-term in the monotherapy context. Other beneficial studies would include evaluation of R848 as an adjuvant to a tumor vaccine treatment strategy, or in combination with checkpoint inhibitors and other immunotherapeutics.

Next, while we demonstrated benefits to food intake and some elements of behavior in R848-treated PDAC-engrafted mice, these studies were still preliminary in their nature. Future experiments should include more in-depth characterization of behavior, cognition, and affect during and after R848 treatment. These should include tests of memory, complex task-solving, motivated behavior, anxiety and depressive behaviors, and social behaviors, all of which can be impacted by chemotherapy and could potentially be impacted by R848.

Ultimately, this dissertation demonstrates the benefit and utility of a systems-based oncology approach. While the current outlook for those diagnosed with pancreatic cancer is bleak, the continued efforts in this field are making crucial headway toward changing the fate of patients with this illness. With more knowledge of the tumor and systemic responses to cancer, we will move closer to a therapeutic ideal that not only extends survival, but upholds the dignity, strength, autonomy, and quality of life all cancer patients deserve.

References

1. Rahib, L., *et al.* Projecting cancer incidence and deaths to 2030: the unexpected burden of thyroid, liver, and pancreas cancers in the United States. *Cancer Res* **74**, 2913-2921 (2014).
2. Kleeff, J., *et al.* Pancreatic cancer. *Nat Rev Dis Primers* **2**, 16022 (2016).
3. Noone AM, H.N., Krapcho M, Miller D, Brest A, Yu M, Ruhl J, Tatalovich Z, Mariotto A, Lewis DR, Chen HS, Feuer EJ, Cronin KA SEER Cancer Statistics Review, 1975-2015, National Cancer Institute. *https://seer.cancer.gov/csr/1975_2015/*, (2018).
4. Michaud, D.S., *et al.* Physical activity, obesity, height, and the risk of pancreatic cancer. *JAMA* **286**, 921-929 (2001).
5. Bracci, P.M. Obesity and pancreatic cancer: overview of epidemiologic evidence and biologic mechanisms. *Mol Carcinog* **51**, 53-63 (2012).
6. Raimondi, S., Lowenfels, A.B., Morselli-Labate, A.M., Maisonneuve, P. & Pezzilli, R. Pancreatic cancer in chronic pancreatitis; aetiology, incidence, and early detection. *Best Pract Res Clin Gastroenterol* **24**, 349-358 (2010).
7. Stevens, R.J., Roddam, A.W. & Beral, V. Pancreatic cancer in type 1 and young-onset diabetes: systematic review and meta-analysis. *Br J Cancer* **96**, 507-509 (2007).
8. Huxley, R., Ansary-Moghaddam, A., Berrington de Gonzalez, A., Barzi, F. & Woodward, M. Type-II diabetes and pancreatic cancer: a meta-analysis of 36 studies. *Br J Cancer* **92**, 2076-2083 (2005).
9. Sharma, A., *et al.* Model to Determine Risk of Pancreatic Cancer in Patients With New-Onset Diabetes. *Gastroenterology* **155**, 730-739 e733 (2018).
10. Turati, F., *et al.* Family history of cancer and the risk of cancer: a network of case-control studies. *Ann Oncol* **24**, 2651-2656 (2013).

11. Vasen, H.*, et al.* Benefit of Surveillance for Pancreatic Cancer in High-Risk Individuals: Outcome of Long-Term Prospective Follow-Up Studies From Three European Expert Centers. *J Clin Oncol* **34**, 2010-2019 (2016).

12. Tempero, M.A.*, et al.* Pancreatic Adenocarcinoma, Version 1.2019. *J Natl Compr Canc Netw* **17**, 202-210 (2019).

13. Conroy, T.*, et al.* FOLFIRINOX or Gemcitabine as Adjuvant Therapy for Pancreatic Cancer. *N Engl J Med* **379**, 2395-2406 (2018).

14. Conroy, T.*, et al.* FOLFIRINOX versus gemcitabine for metastatic pancreatic cancer. *N Engl J Med* **364**, 1817-1825 (2011).

15. Prigerson, H.G.*, et al.* Chemotherapy Use, Performance Status, and Quality of Life at the End of Life. *JAMA Oncol* **1**, 778-784 (2015).

16. DuFort, C.C.*, et al.* Interstitial Pressure in Pancreatic Ductal Adenocarcinoma Is Dominated by a Gel-Fluid Phase. *Biophys J* **110**, 2106-2119 (2016).

17. PEGPH20 May Improve Standard-of-Care Therapy in Pancreatic Cancer. *Cancer Discov* **8**, 136 (2018).

18. Naing, A.*, et al.* PEGylated IL-10 (Pegilodecakin) Induces Systemic Immune Activation, CD8(+) T Cell Invigoration and Polyclonal T Cell Expansion in Cancer Patients. *Cancer Cell* **34**, 775-791 e773 (2018).

19. Lutz, E.R.*, et al.* Immunotherapy converts nonimmunogenic pancreatic tumors into immunogenic foci of immune regulation. *Cancer Immunol Res* **2**, 616-631 (2014).

20. Rosenberg, A. & Mahalingam, D. Immunotherapy in pancreatic adenocarcinoma-overcoming barriers to response. *J Gastrointest Oncol* **9**, 143-159 (2018).

21. Hezel, A.F., Kimmelman, A.C., Stanger, B.Z., Bardeesy, N. & Depinho, R.A. Genetics and biology of pancreatic ductal adenocarcinoma. *Genes Dev* **20**, 1218-1249 (2006).

22. Moffitt, R.A.*, et al.* Virtual microdissection identifies distinct tumor- and stroma-specific subtypes of pancreatic ductal adenocarcinoma. *Nat Genet* **47**, 1168-1178 (2015).

23. Collisson, E.A.*, et al.* Subtypes of pancreatic ductal adenocarcinoma and their differing responses to therapy. *Nat Med* **17**, 500-503 (2011).

24. Bailey, P.*, et al.* Genomic analyses identify molecular subtypes of pancreatic cancer. *Nature* **531**, 47-52 (2016).

25. Omary, M.B., Lugea, A., Lowe, A.W. & Pandol, S.J. The pancreatic stellate cell: a star on the rise in pancreatic diseases. *J Clin Invest* **117**, 50-59 (2007).

26. Tsuchida, T. & Friedman, S.L. Mechanisms of hepatic stellate cell activation. *Nat Rev Gastroenterol Hepatol* **14**, 397-411 (2017).

27. Sherman, M.H. Stellate Cells in Tissue Repair, Inflammation, and Cancer. *Annu Rev Cell Dev Biol* **34**, 333-355 (2018).

28. Sherman, M.H.*, et al.* Stromal cues regulate the pancreatic cancer epigenome and metabolome. *Proc Natl Acad Sci U S A* **114**, 1129-1134 (2017).

29. Sousa, C.M.*, et al.* Pancreatic stellate cells support tumour metabolism through autophagic alanine secretion. *Nature* **536**, 479-483 (2016).

30. Ohlund, D.*, et al.* Distinct populations of inflammatory fibroblasts and myofibroblasts in pancreatic cancer. *J Exp Med* **214**, 579-596 (2017).

31. Biffi, G.*, et al.* IL1-Induced JAK/STAT Signaling Is Antagonized by TGFbeta to Shape CAF Heterogeneity in Pancreatic Ductal Adenocarcinoma. *Cancer Discov* **9**, 282-301 (2019).

32. Ozdemir, B.C.*, et al.* Depletion of Carcinoma-Associated Fibroblasts and Fibrosis Induces Immunosuppression and Accelerates Pancreas Cancer with Reduced Survival. *Cancer Cell* **28**, 831-833 (2015).

33. Olive, K.P.*, et al.* Inhibition of Hedgehog signaling enhances delivery of chemotherapy in a mouse model of pancreatic cancer. *Science* **324**, 1457-1461 (2009).

34. Lee, J.J.*, et al.* Stromal response to Hedgehog signaling restrains pancreatic cancer progression. *Proc Natl Acad Sci U S A* **111**, E3091-3100 (2014).

35. Love, J.A., Yi, E. & Smith, T.G. Autonomic pathways regulating pancreatic exocrine secretion. *Auton Neurosci* **133**, 19-34 (2007).

36. Babic, T., Browning, K.N., Kawaguchi, Y., Tang, X. & Travagli, R.A. Pancreatic insulin and exocrine secretion are under the modulatory control of distinct subpopulations of vagal motoneurones in the rat. *J Physiol* **590**, 3611-3622 (2012).

37. De Oliveira, T.*, et al.* Syndecan-2 promotes perineural invasion and cooperates with K-ras to induce an invasive pancreatic cancer cell phenotype. *Mol Cancer* **11**, 19 (2012).

38. Renz, B.W.*, et al.* Cholinergic Signaling via Muscarinic Receptors Directly and Indirectly Suppresses Pancreatic Tumorigenesis and Cancer Stemness. *Cancer Discov* **8**, 1458-1473 (2018).

39. Renz, B.W.*, et al.* beta2 Adrenergic-Neurotrophin Feedforward Loop Promotes Pancreatic Cancer. *Cancer Cell* **33**, 75-90 e77 (2018).

40. Clark, C.E.*, et al.* Dynamics of the immune reaction to pancreatic cancer from inception to invasion. *Cancer Res* **67**, 9518-9527 (2007).

41. Mills, C.D. M1 and M2 Macrophages: Oracles of Health and Disease. *Crit Rev Immunol* **32**, 463-488 (2012).

42. Tsujikawa, T.*, et al.* Quantitative Multiplex Immunohistochemistry Reveals Myeloid-Inflamed Tumor-Immune Complexity Associated with Poor Prognosis. *Cell Rep* **19**, 203-217 (2017).

43. Balachandran, V.P., *et al.* Identification of unique neoantigen qualities in long-term survivors of pancreatic cancer. *Nature* **551**, 512-516 (2017).

44. Sanford, D.E., *et al.* Inflammatory monocyte mobilization decreases patient survival in pancreatic cancer: a role for targeting the CCL2/CCR2 axis. *Clin Cancer Res* **19**, 3404-3415 (2013).

45. Delitto, D., Wallet, S.M. & Hughes, S.J. Targeting tumor tolerance: A new hope for pancreatic cancer therapy? *Pharmacol Ther* **166**, 9-29 (2016).

46. Hendifar, A.E., *et al.* Pancreas Cancer-Associated Weight Loss. *Oncologist* (2018).

47. Kalantar-Zadeh, K., *et al.* Why cachexia kills: examining the causality of poor outcomes in wasting conditions. *J Cachexia Sarcopenia Muscle* **4**, 89-94 (2013).

48. Tas, F., *et al.* Performance status of patients is the major prognostic factor at all stages of pancreatic cancer. *Int J Clin Oncol* **18**, 839-846 (2013).

49. Bachmann, J.H., M.;Krakowski-Roosen, H.;Buchler, M. W.;Friess, H.;Martignoni, M. E. Cachexia worsens prognosis in patients with resectable pancreatic cancer. *J Gastrointest Surg* **12**, 1193-1201 (2008).

50. Pausch, T., *et al.* Cachexia but not obesity worsens the postoperative outcome after pancreatoduodenectomy in pancreatic cancer. *Surgery* **152**, S81-88 (2012).

51. Hendifar, A., *et al.* Influence of Body Mass Index and Albumin on Perioperative Morbidity and Clinical Outcomes in Resected Pancreatic Adenocarcinoma. *PLoS One* **11**, e0152172 (2016).

52. Peng, P., *et al.* Impact of sarcopenia on outcomes following resection of pancreatic adenocarcinoma. *J Gastrointest Surg* **16**, 1478-1486 (2012).

53. Kazemi-Bajestani, S.M.M., V. C.;Baracos, V. Computed tomography-defined muscle and fat wasting are associated with cancer clinical outcomes. *Semin Cell Dev Biol* **54**, 2-10 (2016).

54. Ali, R.*, et al.* Lean body mass as an independent determinant of dose-limiting toxicity and neuropathy in patients with colon cancer treated with FOLFOX regimens. *Cancer Med* **5**, 607-616 (2016).

55. Cousin, S.*, et al.* Low skeletal muscle is associated with toxicity in patients included in phase I trials. *Invest New Drugs* **32**, 382-387 (2014).

56. Di Sebastiano, K.M.*, et al.* Accelerated muscle and adipose tissue loss may predict survival in pancreatic cancer patients: the relationship with diabetes and anaemia. *Br J Nutr* **109**, 302-312 (2013).

57. Hubbard, T.J., Lawson-McLean, A. & Fearon, K.C. Nutritional predictors of postoperative outcome in pancreatic cancer (Br J Surg 2011; 98: 268-274). *Br J Surg* **98**, 1032; author reply 1032-1033 (2011).

58. Kanda, M.*, et al.* Nutritional predictors of postoperative outcome in pancreatic cancer. *Br J Surg* **98**, 268-274 (2011).

59. Dalal, S.*, et al.* Relationships among body mass index, longitudinal body composition alterations, and survival in patients with locally advanced pancreatic cancer receiving chemoradiation: a pilot study. *J Pain Symptom Manage* **44**, 181-191 (2012).

60. Kindler, H.L.*, et al.* Gemcitabine plus bevacizumab compared with gemcitabine plus placebo in patients with advanced pancreatic cancer: phase III trial of the Cancer and Leukemia Group B (CALGB 80303). *J Clin Oncol* **28**, 3617-3622 (2010).

61. Falconer, J.S., Fearon, K.C., Plester, C.E., Ross, J.A. & Carter, D.C. Cytokines, the acute-phase response, and resting energy expenditure in cachectic patients with pancreatic cancer. *Ann Surg* **219**, 325-331 (1994).

62. Tisdale, M.J. Biology of cachexia. *J Natl Cancer Inst* **89**, 1763-1773 (1997).

63. Kays, J.K.*, et al.* Three cachexia phenotypes and the impact of fat-only loss on survival in FOLFIRINOX therapy for pancreatic cancer. *J Cachexia Sarcopenia Muscle* **9**, 673-684 (2018).

64. Mintziras, I.*, et al.* Sarcopenia and sarcopenic obesity are significantly associated with poorer overall survival in patients with pancreatic cancer: Systematic review and meta-analysis. *Int J Surg* **59**, 19-26 (2018).

65. Bodnar, R.J.*, et al.* Mediation of anorexia by human recombinant tumor necrosis factor through a peripheral action in the rat. *Cancer research* **49**, 6280-6284 (1989).

66. Grossberg, A.J.*, et al.* Arcuate nucleus proopiomelanocortin neurons mediate the acute anorectic actions of leukemia inhibitory factor via gp130. *Endocrinology* **151**, 606-616 (2010).

67. Lawrence, C.B. & Rothwell, N.J. Anorexic but not pyrogenic actions of interleukin-1 are modulated by central melanocortin-3/4 receptors in the rat. *J Neuroendocrinol* **13**, 490-495 (2001).

68. Sonti, G., Ilyin, S.E. & Plata-Salaman, C.R. Anorexia induced by cytokine interactions at pathophysiological concentrations. *Am J Physiol* **270**, R1394-1402 (1996).

69. Cone, R.D.*, et al.* The arcuate nucleus as a conduit for diverse signals relevant to energy homeostasis. *Int J Obes Relat Metab Disord* **25 Suppl 5**, S63-67 (2001).

70. Morton, G.J., Cummings, D.E., Baskin, D.G., Barsh, G.S. & Schwartz, M.W. Central nervous system control of food intake and body weight. *Nature* **443**, 289-295 (2006).

71. Millington, G.W. The role of proopiomelanocortin (POMC) neurones in feeding behaviour. *Nutr Metab (Lond)* **4**, 18 (2007).

72. Murphy, K.G. Dissecting the role of cocaine- and amphetamine-regulated transcript (CART) in the control of appetite. *Brief Funct Genomic Proteomic* **4**, 95-111 (2005).

73. Ollmann, M.M., Lamoreux, M.L., Wilson, B.D. & Barsh, G.S. Interaction of Agouti protein with the melanocortin 1 receptor in vitro and in vivo. *Genes Dev* **12**, 316-330 (1998).

74. Cowley, M.A., *et al.* Integration of NPY, AGRP, and melanocortin signals in the hypothalamic paraventricular nucleus: evidence of a cellular basis for the adipostat. *Neuron* **24**, 155-163 (1999).

75. Pritchard, L.E., *et al.* Agouti-related protein (83-132) is a competitive antagonist at the human melanocortin-4 receptor: no evidence for differential interactions with pro-opiomelanocortin-derived ligands. *J Endocrinol* **180**, 183-191 (2004).

76. Tatemoto, K., Carlquist, M. & Mutt, V. Neuropeptide Y--a novel brain peptide with structural similarities to peptide YY and pancreatic polypeptide. *Nature* **296**, 659-660 (1982).

77. Kuo, L.E., *et al.* Neuropeptide Y acts directly in the periphery on fat tissue and mediates stress-induced obesity and metabolic syndrome. *Nat Med* **13**, 803-811 (2007).

78. McCusker, R.H. & Kelley, K.W. Immune-neural connections: how the immune system's response to infectious agents influences behavior. *The Journal of experimental biology* **216**, 84-98 (2013).

79. Marks, D.L., Ling, N. & Cone, R.D. Role of the Central Melanocortin System in Cachexia. *Cancer research* **61**, 1432-1438 (2001).

80. Scarlett, J.M., *et al.* Regulation of central melanocortin signaling by interleukin-1 beta. *Endocrinology* **148**, 4217-4225 (2007).

81. Scarlett, J.M., *et al.* Regulation of agouti-related protein messenger ribonucleic acid transcription and peptide secretion by acute and chronic inflammation. *Endocrinology* **149**, 4837-4845 (2008).

82. Wisse, B.E., Frayo, R.S., Schwartz, M.W. & Cummings, D.E. Reversal of cancer anorexia by blockade of central melanocortin receptors in rats. *Endocrinology* **142**, 3292-3301 (2001).

83. Wisse, B.E., *et al.* Evidence that lipopolysaccharide-induced anorexia depends upon central, rather than peripheral, inflammatory signals. *Endocrinology* **148**, 5230-5237 (2007).

84. Mitch, W.E. & Goldberg, A.L. Mechanisms of Muscle Wasting — The Role of the Ubiquitin–Proteasome Pathway. *New England Journal of Medicine* **335**, 1897-1905 (1996).

85. Reid, M.B. & Li, Y.P. Cytokines and oxidative signalling in skeletal muscle. *Acta Physiologica Scandinavica* **171**, 225-232 (2001).

86. Frost, R.A. & Lang, C.H. Skeletal muscle cytokines: regulation by pathogen-associated molecules and catabolic hormones. *Current Opinion in Clinical Nutrition & Metabolic Care* **8**, 255-263 (2005).

87. Braun, T.P. & Marks, D.L. The regulation of muscle mass by endogenous glucocorticoids. *Front Physiol* **6**, 12 (2015).

88. Braun, T.P., *et al.* Muscle atrophy in response to cytotoxic chemotherapy is dependent on intact glucocorticoid signaling in skeletal muscle. *PLoS One* **9**, e106489 (2014).

89. Johns, N., Stephens, N.A. & Fearon, K.C. Muscle wasting in cancer. *Int J Biochem Cell Biol* **45**, 2215-2229 (2013).

90. Braun, T.P., *et al.* Central nervous system inflammation induces muscle atrophy via activation of the hypothalamic-pituitary-adrenal axis. *J Exp Med* **208**, 2449-2463 (2011).

91. Braun, T.P., *et al.* Cancer- and endotoxin-induced cachexia require intact glucocorticoid signaling in skeletal muscle. *FASEB J* **27**, 3572-3582 (2013).

92. Febbraio, M.A. & Pedersen, B.K. Muscle-derived interleukin-6: mechanisms for activation and possible biological roles. *FASEB J* **16**, 1335-1347 (2002).

93. Munoz-Canoves, P., Scheele, C., Pedersen, B.K. & Serrano, A.L. Interleukin-6 myokine signaling in skeletal muscle: a double-edged sword? *FEBS J* **280**, 4131-4148 (2013).

94. Senaris, R.M.*, et al.* Interleukin-6 regulates the expression of hypothalamic neuropeptides involved in body weight in a gender-dependent way. *J Neuroendocrinol* **23**, 675-686 (2011).

95. Li, Y.-P. & Reid, M.B. *NF-κB mediates the protein loss induced by TNF-α in differentiated skeletal muscle myotubes*, (2000).

96. Glass, D.J. Signaling pathways perturbing muscle mass. *Curr Opin Clin Nutr Metab Care* **13**, 225-229 (2010).

97. Dalla Libera, L.*, et al.* Apoptosis in the Skeletal Muscle of Rats with Heart Failure is Associated with Increased Serum Levels of TNF-α and Sphingosine. *Journal of Molecular and Cellular Cardiology* **33**, 1871-1878 (2001).

98. Arruda, A.P.*, et al.* Hypothalamic actions of tumor necrosis factor alpha provide the thermogenic core for the wastage syndrome in cachexia. *Endocrinology* **151**, 683-694 (2010).

99. Ramos, E.J.*, et al.* Cancer anorexia-cachexia syndrome: cytokines and neuropeptides. *Curr Opin Clin Nutr Metab Care* **7**, 427-434 (2004).

100. Tsigos, C. & Chrousos, G.P. Hypothalamic-pituitary-adrenal axis, neuroendocrine factors and stress. *J Psychosom Res* **53**, 865-871 (2002).

101. Lecker, S.H.*, et al.* Multiple types of skeletal muscle atrophy involve a common program of changes in gene expression. *FASEB J* **18**, 39-51 (2004).

102. Bodine, S.C.*, et al.* Identification of ubiquitin ligases required for skeletal muscle atrophy. *Science* **294**, 1704-1708 (2001).

103. Shimizu, N., *et al.* Crosstalk between glucocorticoid receptor and nutritional sensor mTOR in skeletal muscle. *Cell Metab* **13**, 170-182 (2011).

104. Pleasure, D.E., Walsh, G.O. & Engel, W.K. Atrophy of skeletal muscle in patients with Cushing's syndrome. *Arch Neurol* **22**, 118-125 (1970).

105. Hu, Z., Wang, H., Lee, I.H., Du, J. & Mitch, W.E. Endogenous glucocorticoids and impaired insulin signaling are both required to stimulate muscle wasting under pathophysiological conditions in mice. *J Clin Invest* **119**, 3059-3069 (2009).

106. Thaler, J.P., *et al.* Obesity is associated with hypothalamic injury in rodents and humans. *J Clin Invest* **122**, 153-162 (2012).

107. Fuente-Martin, E., *et al.* Hypothalamic inflammation without astrogliosis in response to high sucrose intake is modulated by neonatal nutrition in male rats. *Endocrinology* **154**, 2318-2330 (2013).

108. Pimentel, G.D., *et al.* High-fat fish oil diet prevents hypothalamic inflammatory profile in rats. *ISRN Inflamm* **2013**, 419823 (2013).

109. Guyenet, S.J., *et al.* High-fat diet feeding causes rapid, non-apoptotic cleavage of caspase-3 in astrocytes. *Brain Res* **1512**, 97-105 (2013).

110. Valdearcos, M., *et al.* Microglia dictate the impact of saturated fat consumption on hypothalamic inflammation and neuronal function. *Cell Rep* **9**, 2124-2138 (2014).

111. Zhang, X., *et al.* Hypothalamic IKKbeta/NF-kappaB and ER stress link overnutrition to energy imbalance and obesity. *Cell* **135**, 61-73 (2008).

112. Benzler, J., *et al.* Central inhibition of IKKbeta/NF-kappaB signaling attenuates high-fat diet-induced obesity and glucose intolerance. *Diabetes* **64**, 2015-2027 (2015).

113. Cheng, L., *et al.* Palmitic acid induces central leptin resistance and impairs hepatic glucose and lipid metabolism in male mice. *J Nutr Biochem* **26**, 541-548 (2015).

114. Milanski, M., *et al.* Inhibition of hypothalamic inflammation reverses diet-induced insulin resistance in the liver. *Diabetes* **61**, 1455-1462 (2012).

115. Elmquist, J.K., Scammell, T.E., Jacobsen, C.D. & Saper, C.B. Distribution of Fos-like immunoreactivity in the rat brain following intravenous lipopolysaccharide administration. *J Comp Neurol* **371**, 85-103 (1996).

116. Matsuwaki, T., Eskilsson, A., Kugelberg, U., Jonsson, J.I. & Blomqvist, A. Interleukin-1beta induced activation of the hypothalamus-pituitary-adrenal axis is dependent on interleukin-1 receptors on non-hematopoietic cells. *Brain Behav Immun* **40**, 166-173 (2014).

117. Tolchard, S., Hare, A.S., Nutt, D.J. & Clarke, G. TNF alpha mimics the endocrine but not the thermoregulatory responses of bacterial lipopolysaccharide (LPS): correlation with FOS-expression in the brain. *Neuropharmacology* **35**, 243-248 (1996).

118. von Meyenburg, C., *et al.* Role for CD14, TLR2, and TLR4 in bacterial product-induced anorexia. *Am J Physiol Regul Integr Comp Physiol* **287**, R298-305 (2004).

119. Sergeyev, V., Broberger, C. & Hokfelt, T. Effect of LPS administration on the expression of POMC, NPY, galanin, CART and MCH mRNAs in the rat hypothalamus. *Brain Res Mol Brain Res* **90**, 93-100 (2001).

120. Borges, B.C., *et al.* Leptin resistance and desensitization of hypophagia during prolonged inflammatory challenge. *Am J Physiol Endocrinol Metab* **300**, E858-869 (2011).

121. Jang, P.G., *et al.* NF-kappaB activation in hypothalamic pro-opiomelanocortin neurons is essential in illness- and leptin-induced anorexia. *J Biol Chem* **285**, 9706-9715 (2010).

122. Sartin, J.L., *et al.* Central role of the melanocortin-4 receptors in appetite regulation after endotoxin. *J Anim Sci* **86**, 2557-2567 (2008).

123. Huang, Q.H., Hruby, V.J. & Tatro, J.B. Role of central melanocortins in endotoxin-induced anorexia. *Am J Physiol* **276**, R864-871 (1999).

124. Denis, R.G.*, et al.* TNF-alpha transiently induces endoplasmic reticulum stress and an incomplete unfolded protein response in the hypothalamus. *Neuroscience* **170**, 1035-1044 (2010).

125. Ogimoto, K., Harris, M.K., Jr. & Wisse, B.E. MyD88 is a key mediator of anorexia, but not weight loss, induced by lipopolysaccharide and interleukin-1 beta. *Endocrinology* **147**, 4445-4453 (2006).

126. Thaler, J.P.*, et al.* Atypical protein kinase C activity in the hypothalamus is required for lipopolysaccharide-mediated sickness responses. *Endocrinology* **150**, 5362-5372 (2009).

127. Riediger, T., Cordani, C., Potes, C.S. & Lutz, T.A. Involvement of nitric oxide in lipopolysaccharide induced anorexia. *Pharmacol Biochem Behav* **97**, 112-120 (2010).

128. Borner, T., Pinkernell, S., Lutz, T.A. & Riediger, T. Lipopolysaccharide inhibits ghrelin-excited neurons of the arcuate nucleus and reduces food intake via central nitric oxide signaling. *Brain Behav Immun* **26**, 867-879 (2012).

129. Fortier, M.-E.*, et al. The viral mimic, polyinosinic:polycytidylic acid, induces fever in rats via an interleukin-1-dependent mechanism*, (2004).

130. Cunningham, C., Campion, S., Teeling, J., Felton, L. & Perry, V.H. The sickness behaviour and CNS inflammatory mediator profile induced by systemic challenge of mice with synthetic double-stranded RNA (poly I:C). *Brain Behav Immun* **21**, 490-502 (2007).

131. Traynor, T.R., Majde, J.A., Bohnet, S.G. & Krueger, J.M. Sleep and body temperature responses in an acute viral infection model are altered in interferon type I receptor-deficient mice. *Brain Behav Immun* **20**, 290-299 (2006).

132. Murray, C.*, et al.* Interdependent and independent roles of type I interferons and IL-6 in innate immune, neuroinflammatory and sickness behaviour responses to systemic poly I:C. *Brain Behav Immun* **48**, 274-286 (2015).

133. Milton, N.G., Self, C.H. & Hillhouse, E.W. Effects of pyrogenic immunomodulators on the release of corticotrophin-releasing factor-41 and prostaglandin E2 from the intact rat hypothalamus in vitro. *Br J Pharmacol* **109**, 88-93 (1993).

134. del Rey, A., Randolf, A., Wildmann, J., Besedovsky, H.O. & Jessop, D.S. Re-exposure to endotoxin induces differential cytokine gene expression in the rat hypothalamus and spleen. *Brain Behav Immun* **23**, 776-783 (2009).

135. Yamawaki, Y., Kimura, H., Hosoi, T. & Ozawa, K. MyD88 plays a key role in LPS-induced Stat3 activation in the hypothalamus. *Am J Physiol Regul Integr Comp Physiol* **298**, R403-410 (2010).

136. Ginhoux, F., Lim, S., Hoeffel, G., Low, D. & Huber, T. Origin and differentiation of microglia. *Front Cell Neurosci* **7**, 45 (2013).

137. Yona, S.*, et al.* Fate mapping reveals origins and dynamics of monocytes and tissue macrophages under homeostasis. *Immunity* **38**, 79-91 (2013).

138. Seelaender, M., Batista, M., Jr., Lira, F., Silverio, R. & Rossi-Fanelli, F. Inflammation in cancer cachexia: to resolve or not to resolve (is that the question?). *Clin Nutr* **31**, 562-566 (2012).

139. Anker, S.D.*, et al.* Cytokines and neurohormones relating to body composition alterations in the wasting syndrome of chronic heart failure. *Eur Heart J* **20**, 683-693 (1999).

140. Levine, B., Kalman, J., Mayer, L., Fillit, H.M. & Packer, M. Elevated circulating levels of tumor necrosis factor in severe chronic heart failure. *N Engl J Med* **323**, 236-241 (1990).

141. Argiles, J.M., Busquets, S., Stemmler, B. & Lopez-Soriano, F.J. Cancer cachexia: understanding the molecular basis. *Nat Rev Cancer* **14**, 754-762 (2014).

142. Grossberg, A.J., Scarlett, J.M. & Marks, D.L. Hypothalamic mechanisms in cachexia. *Physiol Behav* **100**, 478-489 (2010).

143. Vitkovic, L.*, et al.* Cytokine signals propagate through the brain. *Mol Psychiatry* **5**, 604-615 (2000).

144. Banks, W.A., Kastin, A.J. & Gutierrez, E.G. Penetration of interleukin-6 across the murine blood-brain barrier. *Neurosci Lett* **179**, 53-56 (1994).

145. Gutierrez, E.G., Banks, W.A. & Kastin, A.J. Murine tumor necrosis factor alpha is transported from blood to brain in the mouse. *J Neuroimmunol* **47**, 169-176 (1993).

146. Banks, W.A., Ortiz, L., Plotkin, S.R. & Kastin, A.J. Human interleukin (IL) 1 alpha, murine IL-1 alpha and murine IL-1 beta are transported from blood to brain in the mouse by a shared saturable mechanism. *J Pharmacol Exp Ther* **259**, 988-996 (1991).

147. Quan, N., Whiteside, M. & Herkenham, M. Time course and localization patterns of interleukin-1beta messenger RNA expression in brain and pituitary after peripheral administration of lipopolysaccharide. *Neuroscience* **83**, 281-293 (1998).

148. Dantzer, R., O'Connor, J.C., Freund, G.G., Johnson, R.W. & Kelley, K.W. From inflammation to sickness and depression: when the immune system subjugates the brain. *Nature reviews. Neuroscience* **9**, 46-56 (2008).

149. Duan, K.*, et al.* Endotoxemia-induced muscle wasting is associated with the change of hypothalamic neuropeptides in rats. *Neuropeptides* **48**, 379-386 (2014).

150. Cawthorn, W.P. & Sethi, J.K. TNF-alpha and adipocyte biology. *FEBS Lett* **582**, 117-131 (2008).

151. Jackman, R.W. & Kandarian, S.C. The molecular basis of skeletal muscle atrophy. *Am J Physiol Cell Physiol* **287**, C834-843 (2004).

152. Bernardini, R.*, et al.* Interactions between tumor necrosis factor-alpha, hypothalamic corticotropin-releasing hormone, and adrenocorticotropin secretion in the rat. *Endocrinology* **126**, 2876-2881 (1990).

153. Romanatto, T.*, et al.* TNF-alpha acts in the hypothalamus inhibiting food intake and increasing the respiratory quotient--effects on leptin and insulin signaling pathways. *Peptides* **28**, 1050-1058 (2007).

154. Katafuchi, T., Motomura, K., Baba, S., Ota, K. & Hori, T. Differential effects of tumor necrosis factor-alpha and -beta on rat ventromedial hypothalamic neurons in vitro. *Am J Physiol* **272**, R1966-1971 (1997).

155. Ericsson, A., Liu, C., Hart, R.P. & Sawchenko, P.E. Type 1 interleukin-1 receptor in the rat brain: Distribution, regulation, and relationship to sites of IL-1-induced cellular activation. *Journal of Comparative Neurology* **361**, 681-698 (1995).

156. Ching, S.*, et al.* Endothelial-specific knockdown of interleukin-1 (IL-1) type 1 receptor differentially alters CNS responses to IL-1 depending on its route of administration. *J Neurosci* **27**, 10476-10486 (2007).

157. Quan, N., He, L. & Lai, W. Endothelial activation is an intermediate step for peripheral lipopolysaccharide induced activation of paraventricular nucleus. *Brain Res Bull* **59**, 447-452 (2003).

158. Wohleb, E.S.*, et al.* Knockdown of interleukin-1 receptor type-1 on endothelial cells attenuated stress-induced neuroinflammation and prevented anxiety-like behavior. *J Neurosci* **34**, 2583-2591 (2014).

159. Hill, A.G.*, et al.* Chronic central nervous system exposure to interleukin-1 beta causes catabolism in the rat. *Am J Physiol* **271**, R1142-1148 (1996).

160. Schafers, M., Lee, D.H., Brors, D., Yaksh, T.L. & Sorkin, L.S. Increased sensitivity of injured and adjacent uninjured rat primary sensory neurons to exogenous tumor necrosis factor-alpha after spinal nerve ligation. *J Neurosci* **23**, 3028-3038 (2003).

161. van Riemsdijk, I.C.*, et al.* T cells activate the tumor necrosis factor-alpha system during hemodialysis, resulting in tachyphylaxis. *Kidney Int* **59**, 883-892 (2001).

162. Takahashi, N., Brouckaert, P. & Fiers, W. Induction of tolerance allows separation of lethal and antitumor activities of tumor necrosis factor in mice. *Cancer Res* **51**, 2366-2372 (1991).

163. Carlson, C.D., Bai, Y., Jonakait, G.M. & Hart, R.P. Interleukin-1 beta increases leukemia inhibitory factor mRNA levels through transient stimulation of transcription rate. *Glia* **18**, 141-151 (1996).

164. Gayle, D., Ilyin, S.E., Flynn, M.C. & Plata-Salaman, C.R. Lipopolysaccharide (LPS)- and muramyl dipeptide (MDP)-induced anorexia during refeeding following acute fasting: characterization of brain cytokine and neuropeptide systems mRNAs. *Brain Res* **795**, 77-86 (1998).

165. Beretta, E., Dhillon, H., Kalra, P.S. & Kalra, S.P. Central LIF gene therapy suppresses food intake, body weight, serum leptin and insulin for extended periods. *Peptides* **23**, 975-984 (2002).

166. Metcalf, D. & Gearing, D.P. Fatal syndrome in mice engrafted with cells producing high levels of the leukemia inhibitory factor. *Proc Natl Acad Sci U S A* **86**, 5948-5952 (1989).

167. Mori, M.*, et al.* Cancer cachexia syndrome developed in nude mice bearing melanoma cells producing leukemia-inhibitory factor. *Cancer Res* **51**, 6656-6659 (1991).

168. Nicola, N.A. & Babon, J.J. Leukemia inhibitory factor (LIF). *Cytokine & Growth Factor Reviews*.

169. Kalaria, R.N. The blood-brain barrier and cerebral microcirculation in Alzheimer disease. *Cerebrovasc Brain Metab Rev* **4**, 226-260 (1992).

170. Whitton, P.S. Inflammation as a causative factor in the aetiology of Parkinson's disease. *Br J Pharmacol* **150**, 963-976 (2007).

171. Popescu, B.O.*, et al.* Blood-brain barrier alterations in ageing and dementia. *Journal of the Neurological Sciences* **283**, 99-106 (2009).

172. Wardlaw, J.M., Sandercock, P.A., Dennis, M.S. & Starr, J. Is breakdown of the blood-brain barrier responsible for lacunar stroke, leukoaraiosis, and dementia? *Stroke* **34**, 806-812 (2003).

173. Minagar, A. & Alexander, J.S. Blood-brain barrier disruption in multiple sclerosis. *Mult Scler* **9**, 540-549 (2003).

174. Puhlmann, M.*, et al.* Interleukin-1beta induced vascular permeability is dependent on induction of endothelial tissue factor (TF) activity. *J Transl Med* **3**, 37 (2005).

175. Samad, T.A.*, et al.* Interleukin-1[beta]-mediated induction of Cox-2 in the CNS contributes to inflammatory pain hypersensitivity. *Nature* **410**, 471-475 (2001).

176. Kim, Y.-J., Hwang, S.-Y., Oh, E.-S., Oh, S. & Han, I.-O. IL-1β, an immediate early protein secreted by activated microglia, induces iNOS/NO in C6 astrocytoma cells through p38 MAPK and NF-κB pathways. *Journal of Neuroscience Research* **84**, 1037-1046 (2006).

177. Peng, J., He, F., Zhang, C., Deng, X. & Yin, F. Protein kinase C-α signals P115RhoGEF phosphorylation and RhoA activation in TNF-α-induced mouse brain microvascular endothelial cell barrier dysfunction. *Journal of Neuroinflammation* **8**, 28-28 (2011).

178. Fabry, Z.*, et al.* Production of the cytokines interleukin 1 and 6 by murine brain microvessel endothelium and smooth muscle pericytes. *J Neuroimmunol* **47**, 23-34 (1993).

179. Katerina, D.-Z. & Alexander, E. Inflammatory Mediators and the Blood-Brain Barrier. in *The Blood-Brain Barrier in Health and Disease, Volume One* 239-288 (CRC Press, 2015).

180. Kastin, A.J., Akerstrom, V. & Pan, W. Circulating TGF-beta1 does not cross the intact blood-brain barrier. *J Mol Neurosci* **21**, 43-48 (2003).

181. Pan, W., Vallance, K. & Kastin, A.J. TGFalpha and the blood-brain barrier: accumulation in cerebral vasculature. *Exp Neurol* **160**, 454-459 (1999).

182. Ronaldson, P.T., Demarco, K.M., Sanchez-Covarrubias, L., Solinsky, C.M. & Davis, T.P. Transforming growth factor-beta signaling alters substrate permeability and tight junction protein expression at the blood-brain barrier during inflammatory pain. *J Cereb Blood Flow Metab* **29**, 1084-1098 (2009).

183. Rodriguez, E.M., Blazquez, J.L. & Guerra, M. The design of barriers in the hypothalamus allows the median eminence and the arcuate nucleus to enjoy private milieus: the former opens to the portal blood and the latter to the cerebrospinal fluid. *Peptides* **31**, 757-776 (2010).

184. Langlet, F. Tanycytes: a gateway to the metabolic hypothalamus. *J Neuroendocrinol* **26**, 753-760 (2014).

185. Nadeau, S. & Rivest, S. Effects of circulating tumor necrosis factor on the neuronal activity and expression of the genes encoding the tumor necrosis factor receptors (p55 and p75) in the rat brain: a view from the blood-brain barrier. *Neuroscience* **93**, 1449-1464 (1999).

186. Utsuyama, M. & Hirokawa, K. Differential expression of various cytokine receptors in the brain after stimulation with LPS in young and old mice. *Experimental Gerontology* **37**, 411-420 (2002).

187. Yamakuni, H., Minami, M. & Satoh, M. Localization of mRNA for leukemia inhibitory factor receptor in the adult rat brain. *Journal of Neuroimmunology* **70**, 45-53 (1996).

188. Rossi, B., Angiari, S., Zenaro, E., Budui, S.L. & Constantin, G. Vascular inflammation in central nervous system diseases: adhesion receptors controlling leukocyte-endothelial interactions. *J Leukoc Biol* **89**, 539-556 (2011).

189. Collins, T.*, et al.* Transcriptional regulation of endothelial cell adhesion molecules: NF-kappa B and cytokine-inducible enhancers. *The FASEB Journal* **9**, 899-909 (1995).

190. Davies, M.J.*, et al.* The expression of the adhesion molecules ICAM-1, VCAM-1, PECAM, and E-selectin in human atherosclerosis. *J Pathol* **171**, 223-229 (1993).

191. Chung, I., Choudhury, A., Patel, J. & Lip, G.Y. Soluble, platelet-bound, and total P-selectin as indices of platelet activation in congestive heart failure. *Ann Med* **41**, 45-51 (2009).

192. Arijs, I.*, et al.* Mucosal gene expression of cell adhesion molecules, chemokines, and chemokine receptors in patients with inflammatory bowel disease before and after infliximab treatment. *Am J Gastroenterol* **106**, 748-761 (2011).

193. Amin, K. The role of mast cells in allergic inflammation. *Respir Med* **106**, 9-14 (2012).

194. Rabelink, T.J., de Boer, H.C. & van Zonneveld, A.J. Endothelial activation and circulating markers of endothelial activation in kidney disease. *Nat Rev Nephrol* **6**, 404-414 (2010).

195. Romano, S.J. Selectin antagonists : therapeutic potential in asthma and COPD. *Treat Respir Med* **4**, 85-94 (2005).

196. Hoesel, B. & Schmid, J.A. The complexity of NF-kappaB signaling in inflammation and cancer. *Mol Cancer* **12**, 86 (2013).

197. Tan, B.H.*, et al.* P-selectin genotype is associated with the development of cancer cachexia. *EMBO Mol Med* **4**, 462-471 (2012).

198. Avan, A.*, et al.* AKT1 and SELP polymorphisms predict the risk of developing cachexia in pancreatic cancer patients. *PLoS One* **9**, e108057 (2014).

199. Love, S. & Barber, R. Expression of P-selectin and intercellular adhesion molecule-1 in human brain after focal infarction or cardiac arrest. *Neuropathol Appl Neurobiol* **27**, 465-473 (2001).

200. Kerfoot, S.M.*, et al.* TNF-alpha-secreting monocytes are recruited into the brain of cholestatic mice. *Hepatology* **43**, 154-162 (2006).

201. D'Mello, C., Le, T. & Swain, M.G. Cerebral microglia recruit monocytes into the brain in response to tumor necrosis factoralpha signaling during peripheral organ inflammation. *J Neurosci* **29**, 2089-2102 (2009).

202. D'Mello, C. & Swain, M.G. Liver-brain interactions in inflammatory liver diseases: implications for fatigue and mood disorders. *Brain Behav Immun* **35**, 9-20 (2014).

203. Cayrol, R.*, et al.* Activated leukocyte cell adhesion molecule promotes leukocyte trafficking into the central nervous system. *Nat Immunol* **9**, 137-145 (2008).

204. Liu, G.*, et al.* Cell adhesion molecules contribute to Alzheimer's disease: multiple pathway analyses of two genome-wide association studies. *J Neurochem* **120**, 190-198 (2012).

205. Yilmaz, G. & Granger, D.N. Cell adhesion molecules and ischemic stroke. *Neurol Res* **30**, 783-793 (2008).

206. Christensen, J.E., de Lemos, C., Moos, T., Christensen, J.P. & Thomsen, A.R. CXCL10 is the key ligand for CXCR3 on CD8+ effector T cells involved in immune surveillance of the lymphocytic choriomeningitis virus-infected central nervous system. *J Immunol* **176**, 4235-4243 (2006).

207. Christensen, J.E.*, et al.* Fulminant lymphocytic choriomeningitis virus-induced inflammation of the CNS involves a cytokine-chemokine-cytokine-chemokine cascade. *J Immunol* **182**, 1079-1087 (2009).

208. Ransohoff, R.M.*, et al.* Astrocyte expression of mRNA encoding cytokines IP-10 and JE/MCP-1 in experimental autoimmune encephalomyelitis. *FASEB J* **7**, 592-600 (1993).

209. Biber, K., Neumann, H., Inoue, K. & Boddeke, H.W. Neuronal 'On' and 'Off' signals control microglia. *Trends Neurosci* **30**, 596-602 (2007).

210. Banisadr, G., Rostene, W., Kitabgi, P. & Parsadaniantz, S.M. Chemokines and brain functions. *Curr Drug Targets Inflamm Allergy* **4**, 387-399 (2005).

211. Rostene, W.*, et al.* Chemokines and chemokine receptors: new actors in neuroendocrine regulations. *Front Neuroendocrinol* **32**, 10-24 (2011).

212. Plata-Salaman, C.R. & Borkoski, J.P. Chemokines/intercrines and central regulation of feeding. *Am J Physiol* **266**, R1711-1715 (1994).

213. Licinio, J., Wong, M.L. & Gold, P.W. Neutrophil-activating peptide-1/interleukin-8 mRNA is localized in rat hypothalamus and hippocampus. *Neuroreport* **3**, 753-756 (1992).

214. Wu, F.*, et al.* CXCR2 is essential for cerebral endothelial activation and leukocyte recruitment during neuroinflammation. *J Neuroinflammation* **12**, 98 (2015).

215. Klein, R.S.*, et al.* Neuronal CXCL10 directs CD8+ T-cell recruitment and control of West Nile virus encephalitis. *J Virol* **79**, 11457-11466 (2005).

216. Mills Ko, E.*, et al.* Deletion of astroglial CXCL10 delays clinical onset but does not affect progressive axon loss in a murine autoimmune multiple sclerosis model. *J Neuroinflammation* **11**, 105 (2014).

217. Amin, D.N.*, et al.* Expression and role of CXCL10 during the encephalitic stage of experimental and clinical African trypanosomiasis. *J Infect Dis* **200**, 1556-1565 (2009).

218. Doherty, P.C., Hou, S. & Southern, P.J. Lymphocytic choriomeningitis virus induces a chronic wasting disease in mice lacking class I major histocompatibility complex glycoproteins. *J Neuroimmunol* **46**, 11-17 (1993).

219. Lin, A.A., Tripathi, P.K., Sholl, A., Jordan, M.B. & Hildeman, D.A. Gamma interferon signaling in macrophage lineage cells regulates central nervous system inflammation and chemokine production. *J Virol* **83**, 8604-8615 (2009).

220. Stamm, A., Valentine, L., Potts, R. & Premenko-Lanier, M. An intermediate dose of LCMV clone 13 causes prolonged morbidity that is maintained by CD4+ T cells. *Virology* **425**, 122-132 (2012).

221. Mahic, M., Kalland, M.E., Aandahl, E.M., Torgersen, K.M. & Tasken, K. Human naturally occurring and adaptive regulatory T cells secrete high levels of leukaemia inhibitory factor upon activation. *Scandinavian journal of immunology* **68**, 391-396 (2008).

222. Vanderlocht, J., Hendriks, J.J., Venken, K., Stinissen, P. & Hellings, N. Effects of IFN-beta, leptin and simvastatin on LIF secretion by T lymphocytes of MS patients and healthy controls. *J Neuroimmunol* **177**, 189-200 (2006).

223. Kamperschroer, C. & Quinn, D.G. The role of proinflammatory cytokines in wasting disease during lymphocytic choriomeningitis virus infection. *J Immunol* **169**, 340-349 (2002).

224. Wohleb, E.S.*, et al.* beta-Adrenergic receptor antagonism prevents anxiety-like behavior and microglial reactivity induced by repeated social defeat. *J Neurosci* **31**, 6277-6288 (2011).

225. Sugihara, A.Q., Rolle, C.E. & Lesniak, M.S. Regulatory T cells actively infiltrate metastatic brain tumors. *Int J Oncol* **34**, 1533-1540 (2009).

226. Sandri, M. Protein breakdown in cancer cachexia. *Semin Cell Dev Biol* **54**, 11-19 (2016).

227. Talbert, E.E. & Guttridge, D.C. Impaired regeneration: A role for the muscle microenvironment in cancer cachexia. *Semin Cell Dev Biol* **54**, 82-91 (2016).

228. Zhou, X.*, et al.* Reversal of cancer cachexia and muscle wasting by ActRIIB antagonism leads to prolonged survival. *Cell* **142**, 531-543 (2010).

229. Narsale, A.A. & Carson, J.A. Role of interleukin-6 in cachexia: therapeutic implications. *Curr Opin Support Palliat Care* **8**, 321-327 (2014).

230. Schaap, L.A., Pluijm, S.M., Deeg, D.J. & Visser, M. Inflammatory markers and loss of muscle mass (sarcopenia) and strength. *Am J Med* **119**, 526 e529-517 (2006).

231. Zimmers, T.A., Fishel, M.L. & Bonetto, A. STAT3 in the systemic inflammation of cancer cachexia. *Semin Cell Dev Biol* **54**, 28-41 (2016).

232. Wakefield, L.M. & Hill, C.S. Beyond TGFbeta: roles of other TGFbeta superfamily members in cancer. *Nat Rev Cancer* **13**, 328-341 (2013).

233. Awad, S.*, et al.* Marked changes in body composition following neoadjuvant chemotherapy for oesophagogastric cancer. *Clin Nutr* **31**, 74-77 (2012).

234. Sandri, M.*, et al.* Foxo transcription factors induce the atrophy-related ubiquitin ligase atrogin-1 and cause skeletal muscle atrophy. *Cell* **117**, 399-412 (2004).

235. Sartori, R.*, et al.* BMP signaling controls muscle mass. *Nat Genet* **45**, 1309-1318 (2013).

236. Johns, N.*, et al.* Clinical classification of cancer cachexia: phenotypic correlates in human skeletal muscle. *PLoS One* **9**, e83618 (2014).

237. Baracos, V.E., Martin, L., Korc, M., Guttridge, D.C. & Fearon, K.C.H. Cancer-associated cachexia. *Nat Rev Dis Primers* **4**, 17105 (2018).

238. Femia, R.A. & Goyette, R.E. The science of megestrol acetate delivery: potential to improve outcomes in cachexia. *BioDrugs* **19**, 179-187 (2005).

239. Goodwin, J.W.*, et al.* Phase III randomized placebo-controlled trial of two doses of megestrol acetate as treatment for menopausal symptoms in women with breast cancer: Southwest Oncology Group Study 9626. *J Clin Oncol* **26**, 1650-1656 (2008).

240. Ruiz Garcia, V., Lopez-Briz, E., Carbonell Sanchis, R., Gonzalvez Perales, J.L. & Bort-Marti, S. Megestrol acetate for treatment of anorexia-cachexia syndrome. *Cochrane Database Syst Rev* **3**, CD004310 (2013).

241. Ruiz Garcia, V., Lopez-Briz, E., Carbonell Sanchis, R., Gonzalvez Perales, J.L. & Bort-Marti, S. Megestrol acetate for treatment of anorexia-cachexia syndrome. *Cochrane Database Syst Rev*, CD004310 (2013).

242. Bruera, E., Roca, E., Cedaro, L., Carraro, S. & Chacon, R. Action of oral methylprednisolone in terminal cancer patients: a prospective randomized double-blind study. *Cancer Treat Rep* **69**, 751-754 (1985).

243. Akamizu, T. & Kangawa, K. Ghrelin for cachexia. *J Cachexia Sarcopenia Muscle* **1**, 169-176 (2010).

244. Argilés, J.M., López-Soriano, F.J., Stemmler, B. & Busquets, S. Novel targeted therapies for cancer cachexia. *Biochemical Journal* **474**, 2663-2678 (2017).

245. Temel, J.S.*, et al.* Anamorelin in patients with non-small-cell lung cancer and cachexia (ROMANA 1 and ROMANA 2): results from two randomised, double-blind, phase 3 trials. *The Lancet Oncology* **17**, 519-531 (2016).

246. Breit, S.N., Tsai, V.W. & Brown, D.A. Targeting Obesity and Cachexia: Identification of the GFRAL Receptor-MIC-1/GDF15 Pathway. *Trends Mol Med* **23**, 1065-1067 (2017).

247. Ratnam, N.M.*, et al.* NF-kappaB regulates GDF-15 to suppress macrophage surveillance during early tumor development. *J Clin Invest* **127**, 3796-3809 (2017).

248. Stewart Coats, A.J.*, et al.* Espindolol for the treatment and prevention of cachexia in patients with stage III/IV non-small cell lung cancer or colorectal cancer: a randomized, double-blind, placebo-controlled, international multicentre phase II study (the ACT-ONE trial). *J Cachexia Sarcopenia Muscle* **7**, 355-365 (2016).

249. Goldberg, R.M.*, et al.* Pentoxifylline for treatment of cancer anorexia and cachexia? A randomized, double-blind, placebo-controlled trial. *J Clin Oncol* **13**, 2856-2859 (1995).

250. Jatoi, A., *et al.* A placebo-controlled double blind trial of etanercept for the cancer anorexia/weight loss syndrome: results from N00C1 from the North Central Cancer Treatment Group. *Cancer* **110**, 1396-1403 (2007).

251. Jatoi, A., *et al.* A placebo-controlled, double-blind trial of infliximab for cancer-associated weight loss in elderly and/or poor performance non-small cell lung cancer patients (N01C9). *Lung Cancer* **68**, 234-239 (2010).

252. Hingorani, S.R., *et al.* Trp53R172H and KrasG12D cooperate to promote chromosomal instability and widely metastatic pancreatic ductal adenocarcinoma in mice. *Cancer Cell* **7**, 469-483 (2005).

253. Michaelis, K.A., *et al.* Establishment and characterization of a novel murine model of pancreatic cancer cachexia. *J Cachexia Sarcopenia Muscle* **8**, 824-838 (2017).

254. von Haehling, S. & Anker, S.D. Cachexia as a major underestimated and unmet medical need: facts and numbers. *J Cachexia Sarcopenia Muscle* **1**, 1-5 (2010).

255. von Haehling, S., Anker, M.S. & Anker, S.D. Prevalence and clinical impact of cachexia in chronic illness in Europe, USA, and Japan: facts and numbers update 2016. *J Cachexia Sarcopenia Muscle* **7**, 507-509 (2016).

256. Fearon, K., *et al.* Definition and classification of cancer cachexia: an international consensus. *The lancet oncology* **12**, 489-495 (2011).

257. Fearon, K.C., Glass, D.J. & Guttridge, D.C. Cancer cachexia: mediators, signaling, and metabolic pathways. *Cell metabolism* **16**, 153-166 (2012).

258. Tisdale, M.J. Cachexia in cancer patients. *Nat Rev Cancer* **2**, 862-871 (2002).

259. Aoyagi, T., Terracina, K.P., Raza, A., Matsubara, H. & Takabe, K. Cancer cachexia, mechanism and treatment. *World J Gastrointest Oncol* **7**, 17-29 (2015).

260. Fearon, K., Arends, J. & Baracos, V. Understanding the mechanisms and treatment options in cancer cachexia. *Nat Rev Clin Oncol* **10**, 90-99 (2013).

261. Mueller, T.C., Burmeister, M.A., Bachmann, J. & Martignoni, M.E. Cachexia and pancreatic cancer: are there treatment options? *World J Gastroenterol* **20**, 9361-9373 (2014).

262. Fearon, K.C., Voss, A.C., Hustead, D.S. & Cancer Cachexia Study, G. Definition of cancer cachexia: effect of weight loss, reduced food intake, and systemic inflammation on functional status and prognosis. *Am J Clin Nutr* **83**, 1345-1350 (2006).

263. Prado, C.M.*, et al.* Body composition as an independent determinant of 5-fluorouracil-based chemotherapy toxicity. *Clin Cancer Res* **13**, 3264-3268 (2007).

264. Prado, C.M.*, et al.* Sarcopenia as a determinant of chemotherapy toxicity and time to tumor progression in metastatic breast cancer patients receiving capecitabine treatment. *Clin Cancer Res* **15**, 2920-2926 (2009).

265. Ross, P.J.*, et al.* Do patients with weight loss have a worse outcome when undergoing chemotherapy for lung cancers? *Br J Cancer* **90**, 1905-1911 (2004).

266. Stewart, G.D., Skipworth, R.J. & Fearon, K.C. Cancer cachexia and fatigue. *Clin Med (Lond)* **6**, 140-143 (2006).

267. Sun, Y.*, et al.* The Acute-Phase Protein Orosomucoid Regulates Food Intake and Energy Homeostasis via Leptin Receptor Signaling Pathway. *Diabetes* **65**, 1630-1641 (2016).

268. Foley, K.*, et al.* Semaphorin 3D autocrine signaling mediates the metastatic role of annexin A2 in pancreatic cancer. *Sci Signal* **8**, ra77 (2015).

269. Guerra, C. & Barbacid, M. Genetically engineered mouse models of pancreatic adenocarcinoma. *Mol Oncol* **7**, 232-247 (2013).

270. Burfeind, K.G., Michaelis, K.A. & Marks, D.L. The central role of hypothalamic inflammation in the acute illness response and cachexia. *Semin Cell Dev Biol* **54**, 42-52 (2016).

271. Ezeoke, C.C. & Morley, J.E. Pathophysiology of anorexia in the cancer cachexia syndrome. *J Cachexia Sarcopenia Muscle* **6**, 287-302 (2015).

272. Mendes, M.C., Pimentel, G.D., Costa, F.O. & Carvalheira, J.B. Molecular and neuroendocrine mechanisms of cancer cachexia. *J Endocrinol* **226**, R29-43 (2015).

273. Ansar, W. & Ghosh, S. C-reactive protein and the biology of disease. *Immunol Res* **56**, 131-142 (2013).

274. Pepys, M.B. & Hirschfield, G.M. C-reactive protein: a critical update. *J Clin Invest* **111**, 1805-1812 (2003).

275. Maccio, A.*, et al.* The role of inflammation, iron, and nutritional status in cancer-related anemia: results of a large, prospective, observational study. *Haematologica* **100**, 124-132 (2015).

276. Theurl, M.*, et al.* Hepcidin as a predictive factor and therapeutic target in erythropoiesis-stimulating agent treatment for anemia of chronic disease in rats. *Haematologica* **99**, 1516-1524 (2014).

277. Dev, R. The assessment and management of cancer cachexia: hypogonadism and hypermetabolism among supportive and palliative care patients. *Curr Opin Support Palliat Care* **8**, 279-285 (2014).

278. Burney, B.O. & Garcia, J.M. Hypogonadism in male cancer patients. *J Cachexia Sarcopenia Muscle* **3**, 149-155 (2012).

279. Bachmann, J., Buchler, M.W., Friess, H. & Martignoni, M.E. Cachexia in patients with chronic pancreatitis and pancreatic cancer: impact on survival and outcome. *Nutr Cancer* **65**, 827-833 (2013).

280. Bachmann, J.*, et al.* Cachexia worsens prognosis in patients with resectable pancreatic cancer. *Journal of gastrointestinal surgery : official journal of the Society for Surgery of the Alimentary Tract* **12**, 1193-1201 (2008).

281. Bachmann, J.*, et al.* Pancreatic cancer related cachexia: influence on metabolism and correlation to weight loss and pulmonary function. *BMC Cancer* **9**, 255 (2009).

282. Uomo, G., Gallucci, F. & Rabitti, P.G. Anorexia-cachexia syndrome in pancreatic cancer: recent development in research and management. *JOP* **7**, 157-162 (2006).

283. Von Hoff, D.D.*, et al.* Increased survival in pancreatic cancer with nab-paclitaxel plus gemcitabine. *N Engl J Med* **369**, 1691-1703 (2013).

284. Paulson, A.S., Tran Cao, H.S., Tempero, M.A. & Lowy, A.M. Therapeutic advances in pancreatic cancer. *Gastroenterology* **144**, 1316-1326 (2013).

285. Del Fabbro, E. Current and future care of patients with the cancer anorexia-cachexia syndrome. *Am Soc Clin Oncol Educ Book*, e229-237 (2015).

286. Dewys, W.D.*, et al.* Prognostic effect of weight loss prior to chemotherapy in cancer patients. Eastern Cooperative Oncology Group. *Am J Med* **69**, 491-497 (1980).

287. Tan, B.H.*, et al.* P-selectin genotype is associated with the development of cancer cachexia. *EMBO molecular medicine* **4**, 462-471 (2012).

288. Aversa, Z.*, et al.* Autophagy is induced in the skeletal muscle of cachectic cancer patients. *Sci Rep* **6**, 30340 (2016).

289. Xu, H.*, et al.* Myocardial dysfunction in an animal model of cancer cachexia. *Life Sci* **88**, 406-410 (2011).

290. Olivan, M.*, et al.* Theophylline is able to partially revert cachexia in tumour-bearing rats. *Nutr Metab (Lond)* **9**, 76 (2012).

291. Der-Torossian, H., Gourin, C.G. & Couch, M.E. Translational implications of novel findings in cancer cachexia: the use of metabolomics and the potential of cardiac malfunction. *Current opinion in supportive and palliative care* **6**, 446-450 (2012).

292. Cosper, P.F. & Leinwand, L.A. Cancer causes cardiac atrophy and autophagy in a sexually dimorphic manner. *Cancer research* **71**, 1710-1720 (2011).

293. Hinch, E.C., Sullivan-Gunn, M.J., Vaughan, V.C., McGlynn, M.A. & Lewandowski, P.A. Disruption of pro-oxidant and antioxidant systems with elevated expression of the ubiquitin proteosome system in the cachectic heart muscle of nude mice. *J Cachexia Sarcopenia Muscle* **4**, 287-293 (2013).

294. Musolino, V.*, et al.* Megestrol acetate improves cardiac function in a model of cancer cachexia-induced cardiomyopathy by autophagic modulation. *J Cachexia Sarcopenia Muscle* **7**, 555-566 (2016).

295. Potsch, M.S.*, et al.* The anabolic catabolic transforming agent (ACTA) espindolol increases muscle mass and decreases fat mass in old rats. *J Cachexia Sarcopenia Muscle* **5**, 149-158 (2014).

296. Petruzzelli, M.*, et al.* A switch from white to brown fat increases energy expenditure in cancer-associated cachexia. *Cell Metab* **20**, 433-447 (2014).

297. Kir, S.*, et al.* Tumour-derived PTH-related protein triggers adipose tissue browning and cancer cachexia. *Nature* **513**, 100-104 (2014).

298. Tanaka, Y.*, et al.* Experimental cancer cachexia induced by transplantable colon 26 adenocarcinoma in mice. *Cancer Res* **50**, 2290-2295 (1990).

299. Simpson-Herren, L., Sanford, A.H. & Holmquist, J.P. Cell population kinetics of transplanted and metastatic Lewis lung carcinoma. *Cell Tissue Kinet* **7**, 349-361 (1974).

300. van Lamsweerde, A.L., Henry, N. & Vaes, G. Metastatic heterogeneity of cells from Lewis lung carcinoma. *Cancer Res* **43**, 5314-5320 (1983).

301. Bonetto, A.*, et al.* JAK/STAT3 pathway inhibition blocks skeletal muscle wasting downstream of IL-6 and in experimental cancer cachexia. *Am J Physiol Endocrinol Metab* **303**, E410-421 (2012).

302. Seto, D.N., Kandarian, S.C. & Jackman, R.W. A Key Role for Leukemia Inhibitory Factor in C26 Cancer Cachexia. *J Biol Chem* **290**, 19976-19986 (2015).

303. Ando, K.*, et al.* Possible role for tocilizumab, an anti-interleukin-6 receptor antibody, in treating cancer cachexia. *J Clin Oncol* **31**, e69-72 (2013).

304. Berti, A., Boccalatte, F., Sabbadini, M.G. & Dagna, L. Assessment of tocilizumab in the treatment of cancer cachexia. *J Clin Oncol* **31**, 2970 (2013).

305. Ishida, J.*, et al.* Animal models of cachexia and sarcopenia in chronic illness: Cardiac function, body composition changes and therapeutic results. *Int J Cardiol* (2017).

306. Bonetto, A., Rupert, J.E., Barreto, R. & Zimmers, T.A. The Colon-26 Carcinoma Tumor-bearing Mouse as a Model for the Study of Cancer Cachexia. *J Vis Exp* (2016).

307. Gaskill, B.N.*, et al.* Heat or insulation: behavioral titration of mouse preference for warmth or access to a nest. *PLoS One* **7**, e32799 (2012).

308. Gordon, C.J. *Temperature Regulation in Laboratory Rodents*, (Cambridge University Press, Cambridge, 1993).

309. Karp, C.L. Unstressing intemperate models: how cold stress undermines mouse modeling. *J Exp Med* **209**, 1069-1074 (2012).

310. Rudaya, A.Y., Steiner, A.A., Robbins, J.R., Dragic, A.S. & Romanovsky, A.A. Thermoregulatory responses to lipopolysaccharide in the mouse: dependence on the dose and ambient temperature. *Am J Physiol Regul Integr Comp Physiol* **289**, R1244-1252 (2005).

311. Kokolus, K.M.*, et al.* Baseline tumor growth and immune control in laboratory mice are significantly influenced by subthermoneutral housing temperature. *Proc Natl Acad Sci U S A* **110**, 20176-20181 (2013).

312. Gaskill, B.N., Karas, A.Z., Garner, J.P. & Pritchett-Corning, K.R. Nest building as an indicator of health and welfare in laboratory mice. *J Vis Exp*, 51012 (2013).

313. Donohoe, C.L., Ryan, A.M. & Reynolds, J.V. Cancer cachexia: mechanisms and clinical implications. *Gastroenterol Res Pract* **2011**, 601434 (2011).

314. Hendifar, A.*, et al.* Gender disparities in metastatic colorectal cancer survival. *Clin Cancer Res* **15**, 6391-6397 (2009).

315. Palomares, M.R., Sayre, J.W., Shekar, K.C., Lillington, L.M. & Chlebowski, R.T. Gender influence on weight-loss pattern and survival of nonsmall cell lung carcinoma patients. *Cancer* **78**, 2119-2126 (1996).

316. Baracos, V.E., Reiman, T., Mourtzakis, M., Gioulbasanis, I. & Antoun, S. Body composition in patients with non-small cell lung cancer: a contemporary view of cancer cachexia with the use of computed tomography image analysis. *Am J Clin Nutr* **91**, 1133S-1137S (2010).

317. Chai, M.G., Kim-Fuchs, C., Angst, E. & Sloan, E.K. Bioluminescent orthotopic model of pancreatic cancer progression. *J Vis Exp* (2013).

318. Takeuchi, O. & Akira, S. Pattern recognition receptors and inflammation. *Cell* **140**, 805-820 (2010).

319. Ulich, T.R., Guo, K.Z., Irwin, B., Remick, D.G. & Davatelis, G.N. Endotoxin-induced cytokine gene expression in vivo. II. Regulation of tumor necrosis factor and interleukin-1 alpha/beta expression and suppression. *Am J Pathol* **137**, 1173-1185 (1990).

320. Duncan, J.R.*, et al.* White matter injury after repeated endotoxin exposure in the preterm ovine fetus. *Pediatr Res* **52**, 941-949 (2002).

321. Diebold, S.S., Kaisho, T., Hemmi, H., Akira, S. & Reis e Sousa, C. Innate antiviral responses by means of TLR7-mediated recognition of single-stranded RNA. *Science* **303**, 1529-1531 (2004).

322. Chen, X., Liang, H., Zhang, J., Zen, K. & Zhang, C.Y. microRNAs are ligands of Toll-like receptors. *RNA* **19**, 737-739 (2013).

323. Fabbri, M., Paone, A., Calore, F., Galli, R. & Croce, C.M. A new role for microRNAs, as ligands of Toll-like receptors. *RNA Biol* **10**, 169-174 (2013).

324. Shay, T. & Kang, J. Immunological Genome Project and systems immunology. *Trends in immunology* **34**, 602-609 (2013).

325. Cervantes, J.L., Weinerman, B., Basole, C. & Salazar, J.C. TLR8: the forgotten relative revindicated. *Cell Mol Immunol* **9**, 434-438 (2012).

326. Jurk, M.*, et al.* Human TLR7 or TLR8 independently confer responsiveness to the antiviral compound R-848. *Nat Immunol* **3**, 499 (2002).

327. Deane, J.A.*, et al.* Control of toll-like receptor 7 expression is essential to restrict autoimmunity and dendritic cell proliferation. *Immunity* **27**, 801-810 (2007).

328. Griffith, A.D.*, et al.* A requirement for slc15a4 in imiquimod-induced systemic inflammation and psoriasiform inflammation in mice. *Sci Rep* **8**, 14451 (2018).

329. Coleman, L.G., Jr., Zou, J. & Crews, F.T. Microglial-derived miRNA let-7 and HMGB1 contribute to ethanol-induced neurotoxicity via TLR7. *J Neuroinflammation* **14**, 22 (2017).

330. Ochi, A.*, et al.* Toll-like receptor 7 regulates pancreatic carcinogenesis in mice and humans. *J Clin Invest* **122**, 4118-4129 (2012).

331. He, W.A.*, et al.* Microvesicles containing miRNAs promote muscle cell death in cancer cachexia via TLR7. *Proc Natl Acad Sci U S A* **111**, 4525-4529 (2014).

332. Nagamoto-Combs, K., Kulas, J. & Combs, C.K. A novel cell line from spontaneously immortalized murine microglia. *J Neurosci Methods* **233**, 187-198 (2014).

333. Damm, J.*, et al.* Fever, sickness behavior, and expression of inflammatory genes in the hypothalamus after systemic and localized subcutaneous stimulation of rats with the Toll-like receptor 7 agonist imiquimod. *Neuroscience* **201**, 166-183 (2012).

334. Nerurkar, L., McColl, A., Graham, G. & Cavanagh, J. The Systemic Response to Topical Aldara Treatment is Mediated Through Direct TLR7 Stimulation as Imiquimod Enters the Circulation. *Sci Rep* **7**, 16570 (2017).

335. Ginhoux, F.*, et al.* Fate mapping analysis reveals that adult microglia derive from primitive macrophages. *Science* **330**, 841-845 (2010).

336. Sauder, D.N., Smith, M.H., Senta-McMillian, T., Soria, I. & Meng, T.C. Randomized, single-blind, placebo-controlled study of topical application of the immune response modulator resiquimod in healthy adults. *Antimicrob Agents Chemother* **47**, 3846-3852 (2003).

337. Lebold, K.M., Jacoby, D.B. & Drake, M.G. Toll-Like Receptor 7-Targeted Therapy in Respiratory Disease. *Transfus Med Hemother* **43**, 114-119 (2016).

338. Schon, M.P. & Schon, M. TLR7 and TLR8 as targets in cancer therapy. *Oncogene* **27**, 190-199 (2008).

339. Bath-Hextall, F.*, et al.* Surgical excision versus imiquimod 5% cream for nodular and superficial basal-cell carcinoma (SINS): a multicentre, non-inferiority, randomised controlled trial. *Lancet Oncol* **15**, 96-105 (2014).

340. Schmid, D.*, et al.* T cell-targeting nanoparticles focus delivery of immunotherapy to improve antitumor immunity. *Nat Commun* **8**, 1747 (2017).

341. Gao, D.*, et al.* Synergy of purine-scaffold TLR7 agonist with doxorubicin on systemic inhibition of lymphoma in mouse model. *J Cancer* **8**, 3183-3189 (2017).

342. Camargo, J.A.*, et al.* Intravesical Immunomodulatory Imiquimod Enhances Bacillus Calmette-Guerin Downregulation of Nonmuscle-invasive Bladder Cancer. *Clin Genitourin Cancer* (2017).

343. Weldon, W.C.*, et al.* Effect of adjuvants on responses to skin immunization by microneedles coated with influenza subunit vaccine. *PLoS One* **7**, e41501 (2012).

344. Hung, I.F.*, et al.* Topical imiquimod before intradermal trivalent influenza vaccine for protection against heterologous non-vaccine and antigenically drifted viruses: a single-centre, double-blind, randomised, controlled phase 2b/3 trial. *Lancet Infect Dis* **16**, 209-218 (2016).

345. Yokogawa, M.*, et al.* Epicutaneous application of toll-like receptor 7 agonists leads to systemic autoimmunity in wild-type mice: a new model of systemic Lupus erythematosus. *Arthritis Rheumatol* **66**, 694-706 (2014).

346. Gilliet, M.*, et al.* Psoriasis triggered by toll-like receptor 7 agonist imiquimod in the presence of dermal plasmacytoid dendritic cell precursors. *Arch Dermatol* **140**, 1490-1495 (2004).

347. Fukui, R.*, et al.* Unc93B1 restricts systemic lethal inflammation by orchestrating Toll-like receptor 7 and 9 trafficking. *Immunity* **35**, 69-81 (2011).

348. Baumann, C.L.*, et al.* CD14 is a coreceptor of Toll-like receptors 7 and 9. *J Exp Med* **207**, 2689-2701 (2010).

349. Liu, H.Y., Huang, C.M., Hung, Y.F. & Hsueh, Y.P. The microRNAs Let7c and miR21 are recognized by neuronal Toll-like receptor 7 to restrict dendritic growth of neurons. *Exp Neurol* **269**, 202-212 (2015).

350. Lehmann, S.M.*, et al.* Extracellularly delivered single-stranded viral RNA causes neurodegeneration dependent on TLR7. *J Immunol* **189**, 1448-1458 (2012).

351. Lehmann, S.M.*, et al.* An unconventional role for miRNA: let-7 activates Toll-like receptor 7 and causes neurodegeneration. *Nat Neurosci* **15**, 827-835 (2012).

352. Hayashi, T.*, et al.* Mast cell-dependent anorexia and hypothermia induced by mucosal activation of Toll-like receptor 7. *Am J Physiol Regul Integr Comp Physiol* **295**, R123-132 (2008).

353. Medzhitov, R., Schneider, D.S. & Soares, M.P. Disease tolerance as a defense strategy. *Science* **335**, 936-941 (2012).

354. Weis, S.*, et al.* Metabolic Adaptation Establishes Disease Tolerance to Sepsis. *Cell* **169**, 1263-1275 e1214 (2017).

355. Pena, O.M.*, et al.* An Endotoxin Tolerance Signature Predicts Sepsis and Organ Dysfunction at Initial Clinical Presentation. *EBioMedicine* **1**, 64-71 (2014).

356. van der Sluijs, K.F., van der Poll, T., Lutter, R., Juffermans, N.P. & Schultz, M.J. Bench-to-bedside review: bacterial pneumonia with influenza - pathogenesis and clinical implications. *Crit Care* **14**, 219 (2010).

357. Sato, S.*, et al.* A variety of microbial components induce tolerance to lipopolysaccharide by differentially affecting MyD88-dependent and -independent pathways. *Int Immunol* **14**, 783-791 (2002).

358. Carlson, M. Genome wide annotation for Mouse., Vol. R package version 3.5.0. (org.Mm.eg.db, 2017).

359. Kolde, R. pheatmap: Pretty Heatmaps. Vol. R package version 1.0.8. (R-Project, 2015).

360. Zhu, X., Levasseur, P.R., Michaelis, K.A., Burfeind, K.G. & Marks, D.L. A distinct brain pathway links viral RNA exposure to sickness behavior. *Sci Rep* **6**, 29885 (2016).

361. Grossberg, A.J.*, et al.* Inflammation-induced lethargy is mediated by suppression of orexin neuron activity. *J Neurosci* **31**, 11376-11386 (2011).

362. Harrison, L., Pfuhlmann, K., Schriever, S.C. & Pfluger, P.T. Profound weight loss induces reactive astrogliosis in the arcuate nucleus of obese mice. *Molecular metabolism* (2019).

363. Tumeh, P.C.*, et al.* PD-1 blockade induces responses by inhibiting adaptive immune resistance. *Nature* **515**, 568-571 (2014).

364. Sharma, P., Wagner, K., Wolchok, J.D. & Allison, J.P. Novel cancer immunotherapy agents with survival benefit: recent successes and next steps. *Nat Rev Cancer* **11**, 805-812 (2011).

365. Siegel, R.L., Miller, K.D. & Jemal, A. Cancer statistics, 2018. *CA Cancer J Clin* **68**, 7-30 (2018).

366. Corrales, L., Matson, V., Flood, B., Spranger, S. & Gajewski, T.F. Innate immune signaling and regulation in cancer immunotherapy. *Cell Res* **27**, 96-108 (2017).

367. Foley, K., Kim, V., Jaffee, E. & Zheng, L. Current progress in immunotherapy for pancreatic cancer. *Cancer Lett* **381**, 244-251 (2016).

368. Zahm, C.D., Colluru, V.T., McIlwain, S.J., Ong, I.M. & McNeel, D.G. TLR Stimulation during T-cell Activation Lowers PD-1 Expression on CD8(+) T Cells. *Cancer Immunol Res* **6**, 1364-1374 (2018).

369. Pushalkar, S.*, et al.* The Pancreatic Cancer Microbiome Promotes Oncogenesis by Induction of Innate and Adaptive Immune Suppression. *Cancer Discov* **8**, 403-416 (2018).

370. Caillet, P.*, et al.* Association between cachexia, chemotherapy and outcomes in older cancer patients: A systematic review. *Clin Nutr* **36**, 1473-1482 (2017).

371. Damrauer, J.S.*, et al.* Chemotherapy-induced muscle wasting: association with NF-kappaB and cancer cachexia. *Eur J Transl Myol* **28**, 7590 (2018).

372. Wagner, T.L.*, et al.* Modulation of TH1 and TH2 cytokine production with the immune response modifiers, R-848 and imiquimod. *Cell Immunol* **191**, 10-19 (1999).

373. Hiraoka, N.*, et al.* Intratumoral tertiary lymphoid organ is a favourable prognosticator in patients with pancreatic cancer. *Br J Cancer* **112**, 1782-1790 (2015).

374. De Monte, L.*, et al.* Intratumor T helper type 2 cell infiltrate correlates with cancer-associated fibroblast thymic stromal lymphopoietin production and reduced survival in pancreatic cancer. *J Exp Med* **208**, 469-478 (2011).

375. Fukunaga, A.*, et al.* CD8+ tumor-infiltrating lymphocytes together with CD4+ tumor-infiltrating lymphocytes and dendritic cells improve the prognosis of patients with pancreatic adenocarcinoma. *Pancreas* **28**, e26-31 (2004).

376. Li, J.*, et al.* Tumor Cell-Intrinsic Factors Underlie Heterogeneity of Immune Cell Infiltration and Response to Immunotherapy. *Immunity* **49**, 178-193 e177 (2018).

377. Gotwals, P.*, et al.* Prospects for combining targeted and conventional cancer therapy with immunotherapy. *Nat Rev Cancer* **17**, 286-301 (2017).

378. Nagarsheth, N., Wicha, M.S. & Zou, W. Chemokines in the cancer microenvironment and their relevance in cancer immunotherapy. *Nat Rev Immunol* **17**, 559-572 (2017).

379. Postow, M.A., Sidlow, R. & Hellmann, M.D. Immune-Related Adverse Events Associated with Immune Checkpoint Blockade. *N Engl J Med* **378**, 158-168 (2018).

380. Peixoto, R.D.*, et al.* Eligibility of Metastatic Pancreatic Cancer Patients for First-Line Palliative Intent nab-Paclitaxel Plus Gemcitabine Versus FOLFIRINOX. *Am J Clin Oncol* **40**, 507-511 (2017).

381. Hendifar, A.E., Chang, J.I., Huang, B.Z., Tuli, R. & Wu, B.U. Cachexia, and not obesity, prior to pancreatic cancer diagnosis worsens survival and is negated by chemotherapy. *J Gastrointest Oncol* **9**, 17-23 (2018).

382. Dovedi, S.J.*, et al.* Intravenous administration of the selective toll-like receptor 7 agonist DSR-29133 leads to anti-tumor efficacy in murine solid tumor models which can be potentiated by combination with fractionated radiotherapy. *Oncotarget* **7**, 17035-17046 (2016).

383. Hosoya, T.*, et al.* Induction of oligoclonal CD8 T cell responses against pulmonary metastatic cancer by a phospholipid-conjugated TLR7 agonist. *Proc Natl Acad Sci U S A* **115**, E6836-E6844 (2018).

384. Pandey, S., Kawai, T. & Akira, S. Microbial sensing by Toll-like receptors and intracellular nucleic acid sensors. *Cold Spring Harb Perspect Biol* **7**, a016246 (2014).

385. Hemmi, H.*, et al.* Small anti-viral compounds activate immune cells via the TLR7 MyD88-dependent signaling pathway. *Nat Immunol* **3**, 196-200 (2002).

386. Heng, T.S., Painter, M.W. & Immunological Genome Project, C. The Immunological Genome Project: networks of gene expression in immune cells. *Nat Immunol* **9**, 1091-1094 (2008).

387. Kim, Y.M., Brinkmann, M.M., Paquet, M.E. & Ploegh, H.L. UNC93B1 delivers nucleotide-sensing toll-like receptors to endolysosomes. *Nature* **452**, 234-238 (2008).

388. Lee, B.L.*, et al.* UNC93B1 mediates differential trafficking of endosomal TLRs. *Elife* **2**, e00291 (2013).

389. Petes, C., Odoardi, N. & Gee, K. The Toll for Trafficking: Toll-Like Receptor 7 Delivery to the Endosome. *Front Immunol* **8**, 1075 (2017).

390. Manavalan, B., Basith, S. & Choi, S. Similar Structures but Different Roles - An Updated Perspective on TLR Structures. *Front Physiol* **2**, 41 (2011).

391. Scholch, S.*, et al.* Radiotherapy combined with TLR7/8 activation induces strong immune responses against gastrointestinal tumors. *Oncotarget* **6**, 4663-4676 (2015).

392. Sagiv-Barfi, I.*, et al.* Eradication of spontaneous malignancy by local immunotherapy. *Sci Transl Med* **10**(2018).

393. Borges, B.C.*, et al.* Expression of hypothalamic neuropeptides and the desensitization of pituitary-adrenal axis and hypophagia in the endotoxin tolerance. *Horm Behav* **52**, 508-519 (2007).

394. Garcia, J.M.*, et al.* Inhibition of cisplatin-induced lipid catabolism and weight loss by ghrelin in male mice. *Endocrinology* **154**, 3118-3129 (2013).

395. He, J.*, et al.* Transcriptional deconvolution reveals consistent functional subtypes of pancreatic cancer epithelium and stroma. (2018).

396. Dvorak, H.F. Tumors: wounds that do not heal-redux. *Cancer Immunol Res* **3**, 1-11 (2015).

397. Ramanathan, R.K.*, et al.* Phase IB/II Randomized Study of FOLFIRINOX Plus Pegylated Recombinant Human Hyaluronidase Versus FOLFIRINOX Alone in Patients With Metastatic Pancreatic Adenocarcinoma: SWOG S1313. *J Clin Oncol*, JCO1801295 (2019).

398. Nywening, T.M.*, et al.* Targeting tumour-associated macrophages with CCR2 inhibition in combination with FOLFIRINOX in patients with borderline resectable and locally advanced pancreatic cancer: a single-centre, open-label, dose-finding, non-randomised, phase 1b trial. *Lancet Oncol* **17**, 651-662 (2016).